Understanding the effect of ultra-low nanofiller loadings on optically transparent polycarbonate

Siân Higlett
Department of Materials
Loughborough University

A thesis submitted in partial fulfilment of the requirements for the award of

Doctor of Philosophy

Supervisors
Professor Mo Song
Professor Stephen Shaw
Mr Phillip Duke

Sponsors
EPSRC
DSTL

Acknowledgements

My gratitude and respect goes to my project supervisors Professor Mo Song, Professor Stephen Shaw and Phillip Duke for their time, knowledge, encouragement and inspiration.

Thank you to my colleagues and friends in the department for all their support and expertise. Their willingness to help has amazed me. Thank you to my family and friends for keeping me grounded. I would also like to acknowledge the positive impact that Loughborough University, its ethos and sporting facilities have had on my life by inspiring me to be the best that I can be. I've learnt that I can do anything if I put my mind to it and I'm grateful to have met so many fantastic people here during my PhD.

And lastly but certainly not the least, a big thank you to Andrew McInnes for his continuous and unwavering support, motivational pep talks, honesty, wisdom and for being the voice of reason and my rock through our journey together. Also, my cat Tonks for always making me smile!

Abstract

The use of fillers in materials engineering has long been used to improve material properties such as strength, stiffness and toughness. However, these enhancements tend to occur at the detriment to optical transparency in transparent polymeric materials. Nano-sized fillers or nanofillers are thought to maintain the transparency of such materials due to their small size. Moreover because of their smaller size, nanofillers have larger interfacial areas and can therefore provide increased interaction sites (providing fine dispersion in the medium).

In this work, the nanofiller trisilanol-phenyl polyhedral oligomeric silsesquioxane (TSP-POSS) was added to polycarbonate (PC) to create a series of polymer nanocomposites for the intended use in transparent, lightweight armour. A variety of techniques were used to characterise the structural, morphological, viscoelastic, optical and mechanical properties of the polymer nanocomposites. A preliminary study into the effect of TSP-POSS on the physical aging behaviour of polycarbonate was also carried out.

The effect of TSP-POSS on polycarbonate depended on its loading in the matrix and the type of strain it was subjected to. Increases in toughness were seen in the nanocomposites in comparison to the unmodified polymer and is thought to be due to the formation of a stretchy hydrogen bonded network between TSP-POSS and the polycarbonate chains. Spectroscopy and microscopy techniques suggest TSP-POSS is uniformly dispersed at the nano- or molecular-scale within the polymer matrix, and therefore indicative of high compatibility between the nanofiller and the polymer. Moreover, TSP-POSS can induce one of two toughening mechanisms in the polymer matrix; at low loadings (0.1-0.3wt%) ductility of the matrix increases to form stretched fibrils, at higher loadings (0.5-1wt%), potential nanoscale TSP-POSS aggregates are observed, which appear to be involved in plastic void growth. Both changes increase the energy absorbing capabilities of the polymer matrix. Crucially, it was found that the optical transparency was maintained at all nanofiller loadings.

However, at higher strain rates the toughness enhancements of TSP-POSS disappear. This could be due to the higher impact energy which overcomes the interactions between TSP-POSS and the polymer chains, particularly if these involve weak bonds e.g. hydrogen. Therefore, the TSP-POSS/PC nanocomposite studied in this work would be more suitable for

protective applications involving low velocity projectiles or even as lightweight, backing materials for energy absorbing applications.

Contents

List of Figures

Chapter 1

Introduction

Chapter 1 Introduction

1.1. Polymers in Defence

By utilising their energy absorbing capabilities, polymers can provide increased ballistic protection to modern armour systems at a much lower weight [1].

Polymers can be used as trauma attenuating backings which help to protect the wearer from blunt force trauma caused by deformation to the armour. Polymers are also used in laminate structures e.g. bullet resistant glass, which are constructed from multiple layers of tempered glass and an optically transparent polymer such as polycarbonate. Figure 1b contains an example of a multi-layered bullet resistant glass. The tempered glass flattens and erodes the projectile whilst the softer polymer absorbs and dissipates the impact energy [2]. Additionally, transparent polymers such as polycarbonate can be used in ballistic eyewear protection, shields and bulletproof glass applications [3].

In the event of armour perforation, polymers can also be used as spall liners which act to catch the fragments, known as spall, and prevent them from causing damage to personnel [2]. Figure 1a shows a typical impact resulting in spall. As the projectile impacts the armour plate, energy is lost in deforming the armour plate. The polymer liner is placed behind the armour plate in order to catch the spall and absorb the remaining momentum carried by the spall.

Another notable polymer is Kevlar© which is used extensively in modern body armour to reduce damage caused by physical, ballistic, stab and slash attacks. Kevlar fibres are made up of highly oriented polymer molecules and have a high tensile strength which is over eight times greater than that of steel wire. The fibres are tightly woven into a dense but lightweight fabric which is able to resist large forces .When a bullet hits a Kevlar vest it will try to force the fibres apart however the fibres are able to resist the motion of the bullet, stretch slightly and absorb the kinetic energy of the bullet instead [4]. Figure 2 contains defence systems where polymers have been applied.

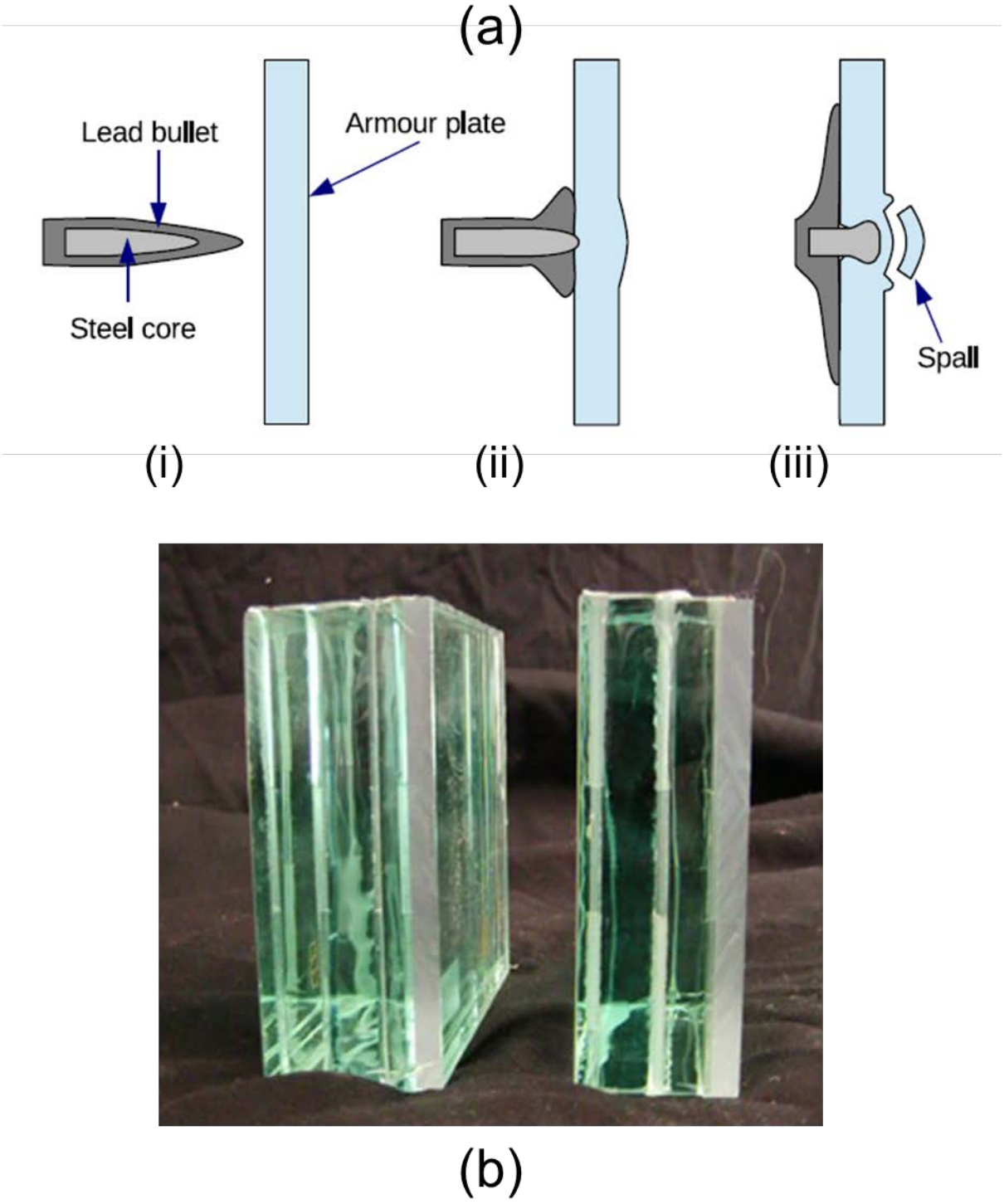

Figure 1 (a) (i) an armour piercing bullet with a full metal jacket bullet prior to impact, (ii) the lead outer deforms to absorb the majority of the impact energy which allows the hard steel core to continue to move fast enough to penetrate the armour and (ii) the steel core deforms and becomes blunt which results in spall [2] **and (b) examples of bullet-resistant glass** [5]

Figure 2 Examples of polymers applications in defence: (a) Police riot shields, (b) military armour, (c) visors and (d) armoured vehicles [6–9]

1.2. Nanotechnology in Defence

Within the last decade research into nanotechnology has flourished, bringing with it potential advancements to current defence technologies.

Nanotechnology offers the ability to work at the molecular scale to create structures with novel and improved properties. Naturally, nanotechnology offers novel and exciting opportunities in the development of military equipment with new properties, improved performance and functionality and reduced costs.

Defence technology that could benefit from nanotechnology includes medical and sensory devices, advanced materials and communication and weapons systems [10]. Moreover, better protection from ballistic and blast impact is always needed; the increased number of threats and increasingly sophisticated weapons mean that combat survivability is of the utmost importance. Personnel protection is vital to reduce the threats encountered by individuals who work in hostile situations such as soldiers, police and aid workers. Yet necessary advancements of the impact resistance of armour materials can introduce

shortcomings similar to those of ancient armour; modern armour is heavy, bulky and rigid and can therefore restrict the wearer's movement and have a detrimental effect on their performance. Research into the development of advanced armour from more lightweight and flexible materials is currently of major interest [10–13].

Fillers can be used to enhance the strength of polymers however they can have a detrimental effect on the optical transparency of transparent polymers.

1.3. Nanofillers

Nano-sized fillers have at least one dimension in the nanoscale. Consequently, nanofillers have (i) larger interfacial areas and therefore more interaction sites than conventional micron-sized fillers and (ii) unique size dependent properties which differ from the bulk material. As a result of nanofiller addition, materials with improved and/or new characteristics can be created. Moreover less filler material is required when using nano-sized fillers due to their larger interfacial areas and they can therefore maintain the mass/density of materials [14–16].

By incorporating nanofillers into polymer matrices, desirable properties of polymeric materials can be enhanced whilst maintaining the advantageous properties of polymers such as optical transparency, ductility, ease of processing, low mass and low cost. These nanostructured materials are known as polymer nanocomposites and are a relatively new class of material which have attracted considerable attention in a wide variety of fields, including the defence sector. Polymer nanocomposites have been found to possess enhanced mechanical properties and improved energy absorption and dissipation capabilities in comparison to the original polymer [17,18].

Research has shown that the energy dissipation capabilities of polymers can be enhanced by the addition of nanofillers [18]. Energy dissipation mechanisms include crack pinning, crack deflection, debonding, void nucleation, shear banding, micro-cracking and bond formation. As nanofillers have larger surface areas than their conventional micron sized counterparts and therefore increased potential to interact with the polymer matrix, these energy mechanisms may occur to a higher degree [1].

It has also been shown that energy absorption by fibre pull-out and fibre fracture is higher for carbon nanotubes than for the corresponding macro fibre, carbon fibres [19].

Moreover, it is proposed that because of their small size, nanofillers can maintain the good optical properties of transparent polymers compared to their micron-sized counterparts [20]. From a transparent armour viewpoint this is a highly desirable result.

1.4. Aims of the Project

The main aim of this project is to understand the effect that the nanofiller trisilanol phenyl polyhedral silsesquioxane (TSP-POSS) has on various physical properties of polycarbonate and how it is able to maintain the good optical transparency of the polycarbonate matrix, for the use in transparent armour applications. This will involve:

- **1) Synthesis of polymer nanocomposites – Chapter 3**
  A multi-step process involving melt blending will be used to promote good nanofiller dispersion within the polycarbonate matrix;
- **2) Characterisation of the nanocomposites – Chapter 4**
  The dispersion state of the nanofiller and any effect it has on the overall morphology and structure of the polycarbonate matrix will be investigated using techniques such as x-ray diffraction (XRD), scanning electron microscopy (SEM) and transmission electron microscopy (TEM). The effect of TSP-POSS on the viscoelastic properties and chain dynamics of polycarbonate will be studied using dynamic mechanical analysis (DMA). UV-vis will be used to assess the optical transparency of the nanocomposites;
- **3) Measurement of the mechanical properties of the nanocomposites at various strain rates – Chapter 5**
  The influence of TSP-POSS on the mechanical properties will be investigated using tensile tests, falling weight impact tests and split-Hopkinson pressure bar tests;
- **4) Preliminary investigation into the physical aging behaviour of the nanocomposites – Chapter 6**
  Modulated differential scanning calorimetry (MDSC) will be used to study the phenomena of physical aging in the nanocomposites. Physical aging causes the properties of polymers to change and can result in reduced mechanical performance and brittleness. Physical aging can be accelerated in polymers subjected to extreme

environments, which can very well be the case in combat zones. It is important therefore, to study the effect of TSP-POSS on the physical aging of the polycarbonate.

Chapter 2

Literature Review

Chapter 2 Literature review

2.1. Introduction

Polymer nanocomposites are a relatively new class of material which have attracted considerable interest in a wide variety of fields [21]. By incorporating nano-sized fillers such as graphene, carbon nanotubes, nanoclays and inorganic particles, e.g. polyhedral oligomeric silsesquioxane (POSS), into polymer matrices, desirable properties of the host polymer can be improved.

Nano-sized fillers, or nanofillers, have a large surface area to volume ratio which results in a large interfacial area and therefore increased interaction overall between the nanofiller and the host polymer. Moreover, as at least one dimension is nanoscale in size, nanofiller materials have unique, size dependent properties which differ to the properties of the bulk material [18]. Additionally, traditional micrometric fillers must be added in large quantities in order to properly function, however this often leads to a deterioration of properties e.g. density increase, brittleness, opacity, workability etc. Nanofillers can help to maintain the mass or density of polymers as less nanofiller is required to change the polymer properties due to their larger interfacial area [14–16]. Providing good nanofiller dispersion, the increased interactivity between nanofiller and polymer allows the unique properties of the nanofiller to be better imparted to the polymer matrix in order to promote maximal enhancement of properties; clearly, if the nanofiller particles form aggregates rather than existing as single particles in the matrix, less nanoparticle surface is exposed resulting in a decrease in the number of interaction sites.

Depending on the type of nanofiller chosen, improvements in physical properties such as tensile strength, stiffness, toughness, thermal stability and electrical conductivity have been reported [17,18]. The physical properties of polymer nanocomposites and the degree to which such properties are improved depend on a variety of factors. For example, the individual chemistry of both the polymer and nanofiller will determine the compatibility between polymer matrix and the ability of the nanofiller to disperse uniformly in the polymer matrix [16]. Again, fine, uniform dispersion is crucial to maximise the degree of interaction between filler and the polymer matrix. The preparation method can also influence these aspects. Some specific examples that also affect the physical properties of

polymer nanocomposites include the length of carbon nanotubes and the cage structure and type of POSS [1], [2].

Moreover, optical transparency can be maintained with the addition of nano-sized fillers; due to their smaller size and finer dispersion in the polymer matrix in comparison to conventional micron-sized fillers, nanofillers are less likely to scatter light and cause a reduction in optical properties [7–9].

2.2. Polymer Nanocomposite Preparation Methods

There are four primary processing methods that can be used to synthesise polymer nanocomposites: (i) melt mixing, (ii) *in-situ* polymerisation, (iii) solution mixing and, (iv) template (or sol-gel) method [22].

2.2.1. Melt Mixing

Melt mixing is the typical method used to synthesise thermoplastic polymer nanocomposites containing inorganic nanoparticles and carbon nanotubes. Melt mixing involves the annealing of the polymer and nanofiller above the softening point of the polymer. The mixture is subjected to high shear stress during the melting process e.g. by rotating screws in an extruder, in order to promote dispersion of the nanofiller in the polymer melt and break up any aggregates. In nanoclay-based nanocomposite systems, the shear force contributes to the delamination of silicate layers. During annealing, intercalation of the polymer chains can then occur more easily to form intercalated or exfoliated polymer-clay nanocomposites.

Melt mixing is the most commercially attractive method as it is environmentally friendly in the sense that it does not require large amounts of solvents such as *in-situ* polymerisation and solution mixing (discussed in section 2.2.2 and 2.2.3, respectively), it is fast, simple and capable of producing large volumes of sample. Moreover, melt mixing is more compatible with existing industrial processes such as injection moulding, extrusion and internal mixing than other methods, thus minimising costs. However, nanofiller dispersion is harder to control in this method and is generally less effective at dispersing nanofillers. Filler-filler interactions can lead to agglomeration. As a result, melt mixing is limited by nanofiller dispersion. As well as this, higher viscosities cause processing difficulties.

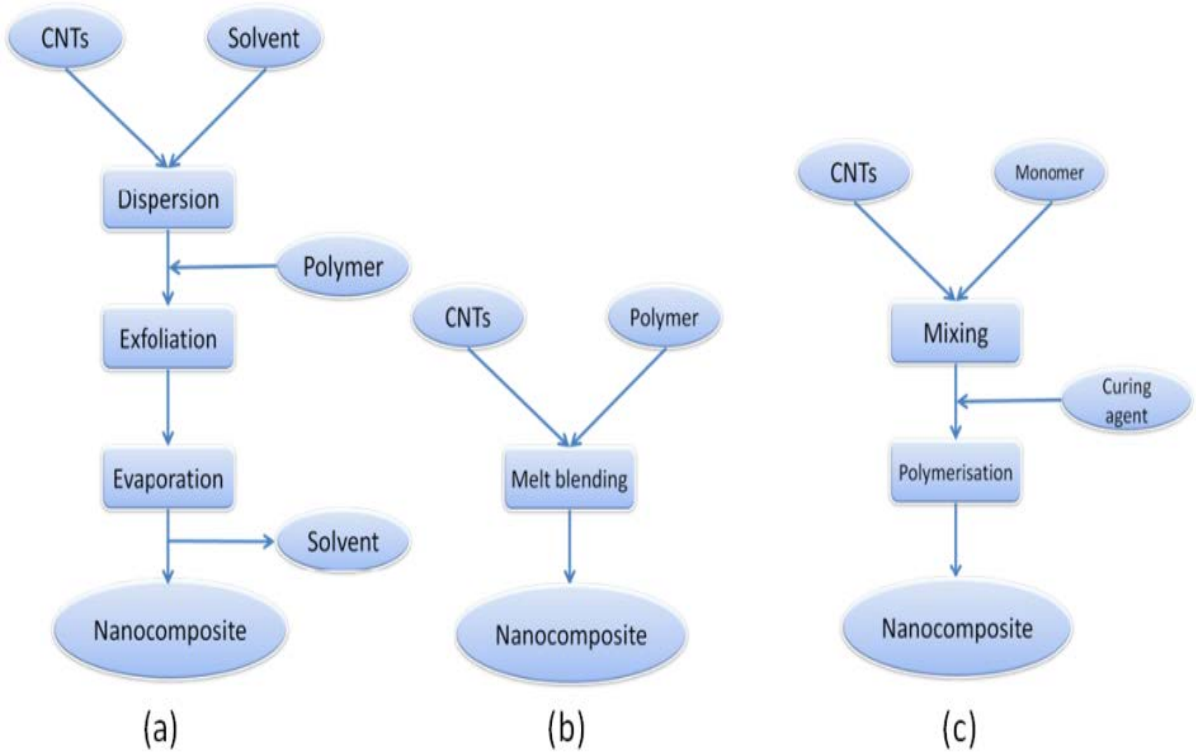

Figure 3 Flow charts of the most common preparation methods for synthesising CNT-based polymer nanocomposites: (a) solution mixing, (b) melt blending and (c) *in-situ* polymerisation [23]

Additionally, polymer and/or nanofiller degradation can occur due to the high temperatures and high shear rates involved in the process. For example, the high shear forces are necessary to overcome the strong van der Waals forces between CNTs and avoid aggregation, however they can fracture CNTs and decrease the aspect ratio of carbon nanotubes, and the high temperature can degrade the surface modification of organoclays [16,22,24,25].

Factors such as equipment type and design, processing conditions, compatibility of polymer and filler, filler surface modifications and polymer type and molecular weight can all affect the dispersion that will be achieved [16,22,24,25]. Ishafani et al. studied the effect of using either a Haake internal mixer or a co-rotating twin screw extruder on the tensile properties of organoclay/HIPS nanocomposites. They found that greater exfoliation of nanoclay occurred in the extruded samples, creating a better quality sample that exhibited better mechanical properties than the Haake mixed samples. Moreover, it was found that increasing rotor speed during mixing caused the tensile modulus to increase. However, it may also contribute to degradation as samples may experience greater shear rates which result in an increase in shear heating [26]. It has also been reported that excessive shear

force causes poor delamination and dispersion but increasing the mean residence time generally promotes exfoliation, [16].

2.2.2. *In-situ* Polymerisation

In-situ polymerisation is where polymerisation occurs in the presence of the nanofiller, thus removing the difficulty of intercalating large polymer chains between nanofiller layers. In CNT-based polymer nanocomposites, nanotubes are simply added to a monomer solution prior to polymerisation. Polymerisation can be initiated by heat, radiation or other methods utilising a suitable initiator or catalyst. In nanoclay systems, the layered silicate is swollen by the migration of a liquid monomer or monomer solution into its galleries, where polymerisation then occurs to form intercalated or exfoliated nanocomposites. The degree of clay exfoliation will depend on the nature of the organoclays and the balance between intra- and extra- gallery polymerisation rates; if the intra-gallery polymerisation occurs with a rate comparable to the extra-gallery polymerisation, the attractive forces between layers will be exceeded to produce a disordered exfoliated nanocomposite structure. If the intra-gallery polymerisation is slower than the extra-gallery polymerisation, the nanoclay will not be exfoliated. Graphene-based polymer nanocomposites can also be synthesised using *in-situ* polymerisation.

This method is most suitable for polymer nanocomposite systems which contain two-dimensional nanofillers; the dispersion of two-dimensional nanofillers is enhanced by this method due to the swelling of the nanofiller which causes an increase in the interlayer distance and impedes aggregation. Advantages of this method also include the ability to graft the polymers onto the surface of the filler, which can lead to increased interactivity between nanofiller and polymer, as well as providing an approach to synthesise both thermoset- and thermoplastic based polymer nanocomposites which are susceptible to thermal degradation and would otherwise be unsuitable for melt methods. However, the implementation of this method is limited as there is not always a suitable monomer or compatible polymer-silicate system available. Melt mixing can overcome this problem [16,24].

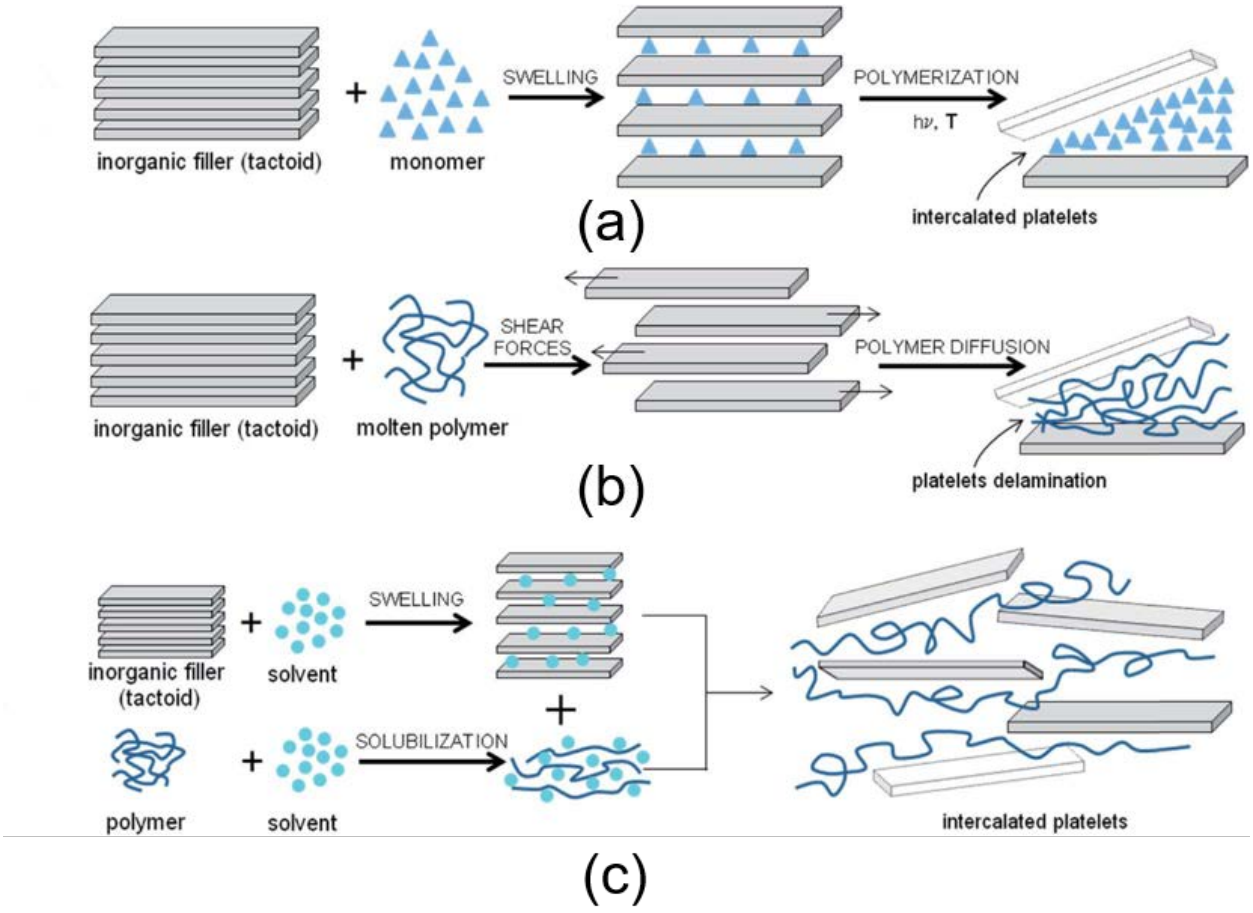

Figure 4 Schematic representation of the common processing methods used to synthesise nanoclay-based polymer nanocomposites: (a) *in-situ* polymerisation, (b) melt mixing and (c) solution mixing [27]

2.2.3. Solution mixing

Solution mixing, or exfoliation adsorption is another multi-step, intercalative process which involves: (i) dispersing (exfoliating in the case of layered silicates) the nanofiller in a solvent by mechanical mixing, magnetic agitation or ultrasonication, (ii) mixing the nanofiller solution with the polymer matrix/monomeric precursors either at ambient or elevated temperatures where the polymer chains will intercalate and lastly, (iii) controlled removal of the solvent either by evaporation or precipitation to obtain the nanocomposite, which is usually in the form of a cast film. This method is utilised mostly in the case of polymer nanocomposites based on carbon nanotubes, graphene or nanoclays.

This method is useful in the case of polymers which have either low or no polarity such as PVA, poly (ethylene oxide), poly (vinylpyrrolidone) and poly (acrylic acid). However, the

agitation methods used to disperse the nanofiller can again lead to defects or shortening of CNTs, damaging the properties of the nanotubes. Furthermore, like *in-situ* polymerisation, because of the large quantities of solvents used in this method it is difficult to apply this method in industry.

2.2.4. Template Synthesis

The template, or sol-gel, method involves the formation of the inorganic filler within the polymer matrix using an aqueous solution (or gel) containing the polymer and the filler precursors. The polymer serves as a nucleating agent and aids the growth of the inorganic filler. During the formation of the filler, the polymer chains become trapped within the filler layers to form the nanocomposite. Theoretically, the template method is advantageous as it is a one-step process, however it has serious disadvantages; the synthesis of clay minerals requires high temperatures which can lead to polymer degradation and moreover, layered silicate layers have a tendency to aggregate. It follows that this process is not commonly used [22,24].

2.3. Properties of Polymer Nanocomposites

2.3.1. Mechanical Properties

2.3.1.1. Graphene-based Polymer Nanocomposites

In the literature it was found that the addition of graphene sheets into a polymer matrix can have significant effects on the mechanical properties of the polymer matrix. In many cases, properties such as Young's modulus, yield strength and tensile strength were higher in the resulting graphene-based polymer nanocomposites than in the neat polymer sample [28–38]. The mechanical properties depended highly on the dispersion of the graphene sheets in the polymer matrix. Poor dispersion leads to decreases in mechanical properties such as elongation at break. Brittle behaviour was mostly found at higher nanofiller loadings where aggregation and restacking of graphene sheets was more likely to occur [31–33,35]. Aggregation results in a decrease in contact area between the graphene and the polymer matrix. Less contact reduces the degree to which the graphene can impart its unique mechanical properties to the polymer. Moreover, the graphene aggregates act as stress concentrators in the matrix, increasing the likelihood of brittle failure.

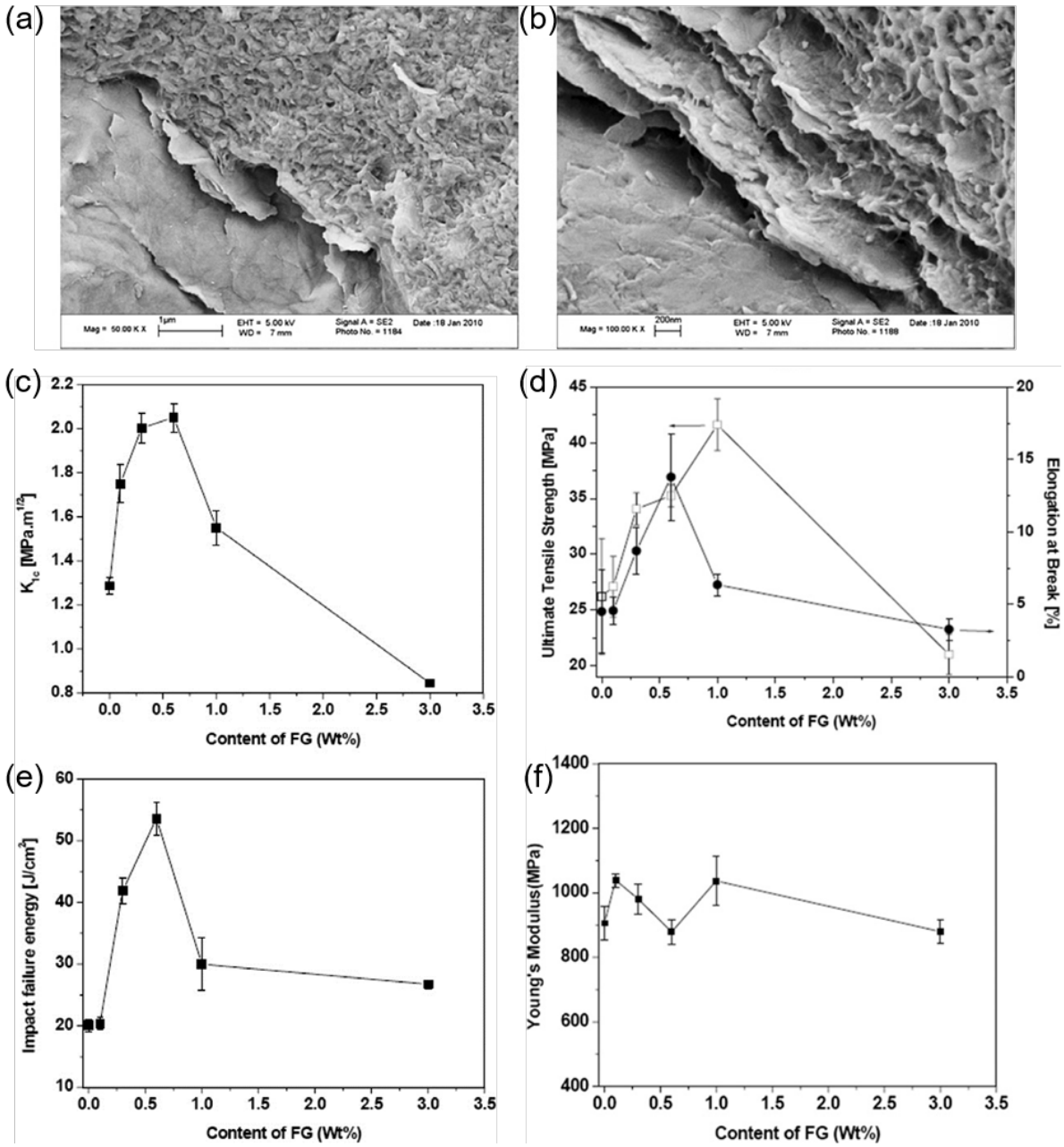

Figure 5 (a-b) SEM micrographs showing the fracture surface of functionalised nylon 12 composites created by Rafiq et al. at magnification (a) 50k x and (b) 100k and (c-f) The mechanical properties of functionalised nylon 12 composites: (c) K_{1C} measurements, (d) ultimate tensile strength, (e) impact failure energy and (f) Young's modulus [39]

The dispersion of graphene is affected by many factors such as the synthesis method used, whether the graphene is functionalised, the loading level of graphene in the polymer matrix and the formation of any bonds between the graphene and the polymer matrix, all of which can be used to control the compatibility and interfacial adhesion between filler and matrix

[28–32,34,35]. Figure 5 shows how functionalised graphene can improve the properties of nylon 12.

2.3.1.2. Carbon Nanotube-based Polymer Nanocomposites

In the literature it was found that the addition of carbon nanotube structures into a polymer matrix resulted in many changes in the polymeric material. Enhancements in mechanical properties of the resulting nanocomposites, such as increased tensile strength, increased elastic modulus and increased hardness were reported [40–45]. Structural changes to the polymer, such as increased crystallinity upon incorporation of CNTs suggest that the nanostructures can act as nucleating agents which can benefit the polymer [40,41]. However, CNTs can also cause a reduction in mechanical behaviour of the polymer. In most cases this is due to the formation of agglomerates at higher CNT loadings, resulting in poor dispersion throughout the matrix [46]. Other factors that can affect the final properties of the polymer nanocomposites include whether the CNTs are functionalised prior to their addition into the matrix, the length of the CNTs used, nanotube helical angle and orientation, processing method and conditions used, such as sonication time and choice of dispersing medium [41,42,44–51]. Many of these factors affect the dispersion of CNTs in the polymer matrix. Therefore, they can be manipulated to control and improve the CNT dispersion, which in turn will affect the final properties of the resulting material.

Jia el al. showed how functionalised CNTs were involved in the toughening of polyimide (PI) in PI/CNT nanocomposites. The found that upon deformation, tapered fibrils were formed at the fracture edges (see figure 6). They proposed that upon deformation, the polymer chains are stretched and aligned along the axis of the stiffer CNTs to form tapered fibrils. The CNTs are tightly packed with the PI macromolecules and they suggest that the CNTs effectively act as stress concentrators. This long-range creep increases the energy dissipation capabilities of the polymer matrix and allows it to withstand larger deformations and thus increase its strength [52].

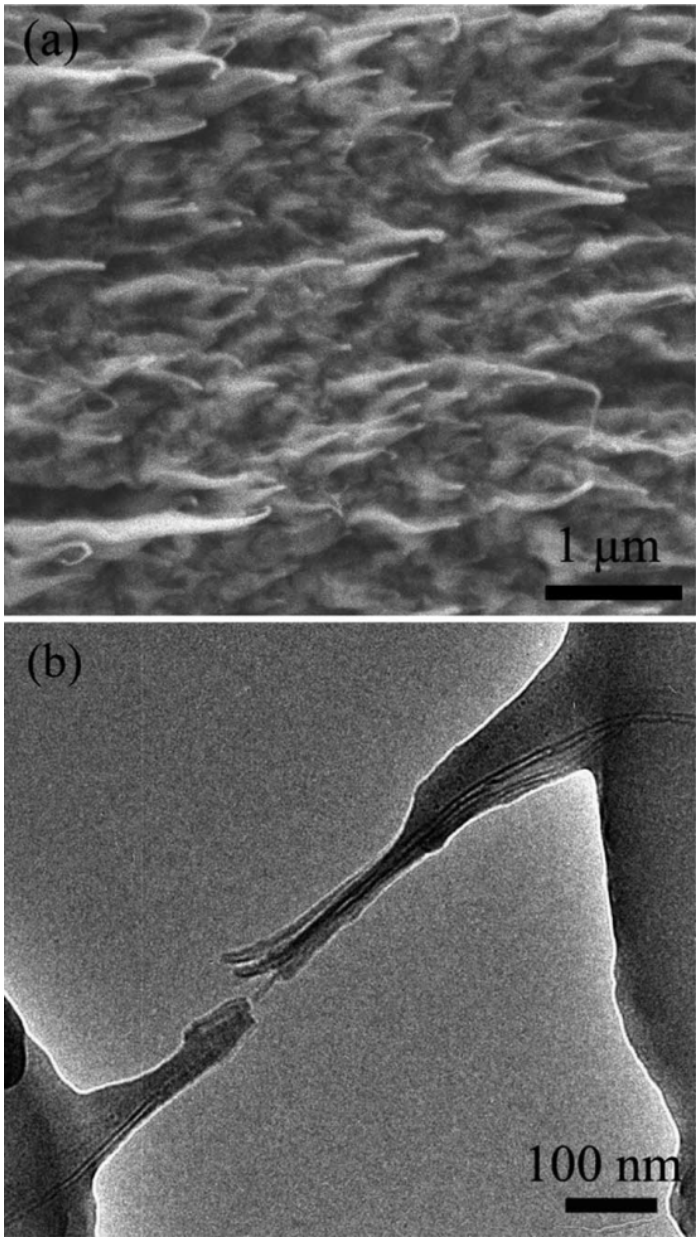

Figure 6 (a) SEM micrograph of the fracture surface morphology of long CNT/PI nanocomposites after ~150% deformation, clearly showing the tapered fibril structure formed around the carbon nanotube caused by long-range creep of the PI matrix and (b) TEM micrographs of the tapered fibrils [52]

2.3.1.3. Nanoclay-based Polymer Nanocomposites

Addition of clay nanoparticles into polymeric materials has been found to alter the mechanical properties of the polymer matrix. The incorporation of these rigid, inorganic nanoparticles can help to enhance polymer properties such as elastic modulus, hardness, scratch resistance, tensile strength and strain at break [53–63].

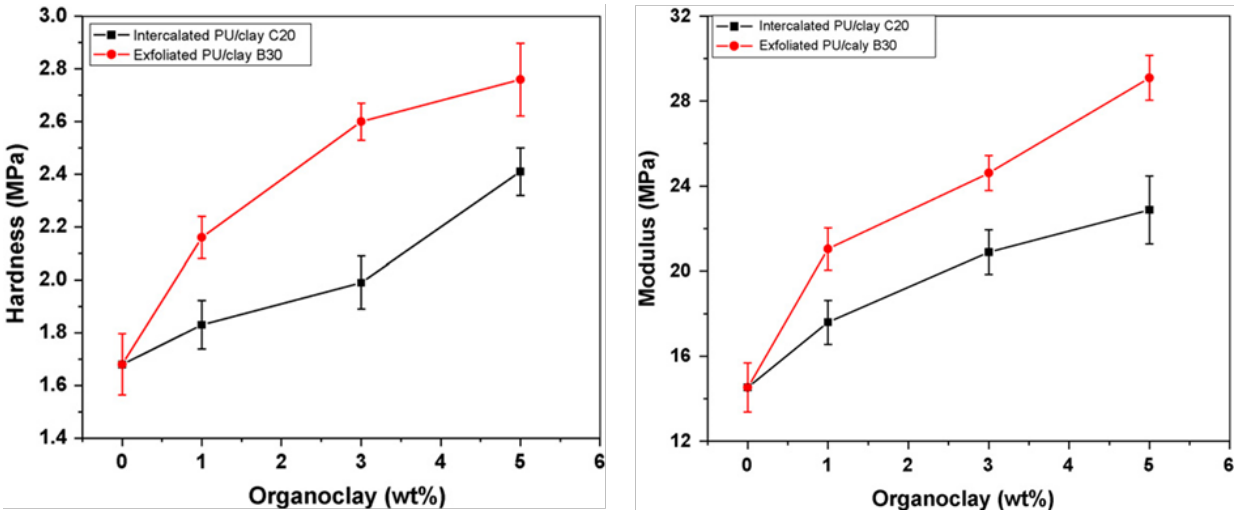

Figure 7 The variation in hardness and elastic modulus values of intercalated and exfoliated PU/organoclay films synthesised by Yusoh et al. [61]

However, the improvement of mechanical properties depended on the amount of clay loading. Typically, positive effects on the performance of polymer nanocomposites are seen at low clay loadings. Higher clay loadings can lead to poor dispersion and agglomeration within the polymer matrix and can even cause decreases in the mechanical properties mentioned above that were seen to improve in the literature [53–55,64,65]. Many other factors that can affect the mechanical properties of clay-based polymer nanocomposites are the processing methods and conditions used, type of clay nanofiller, distribution of nanofiller and the degree of compatibility between the clay and polymer materials [54,55,63,64]. Compatibilisers can be used to treat the clay surface by creating loops and tails to increase its interaction with the polymer. By cation exchange, the hydrophilic surface of the clay is converted to one that is hydrophobic, like polymers, to create organoclays [17]. As a result of improved compatibility, clay particles will be better dispersed within the matrix and will increase their effectiveness in reinforcing the polymer matrix. Organoclays, surface modified nanoclays, were reported to improve the mechanical properties of polymers beyond that of regular nanoclays. This is because of improved dispersion and enhanced interfacial adhesion between the matrix and the clay nanofiller [58]. Increased interfacial adhesion improves the effectiveness of load transfer from the polymer matrix to the clay nanofiller. The behaviour of clay-based nanocomposites is also directly related to their hierarchical microstructures; intercalated and exfoliated clay-based nanocomposites are seen as superior in mechanical properties with an exfoliated clay structure being the most desired [17,57,61]. Figure 7 illustrates this.

In the literature it was found that the incorporation of nanofillers such as POSS, clay, graphene and CNTs can have an effect on the impact properties of polymers. For each of the above nanofillers, improvements were seen in toughness, creep resistance, crack resistance and impact strength of the polymer nanocomposites containing them [126–143]. Some polymer nanocomposites even exhibited super tough behaviour [126]. The effect of the introduction of nanofillers on the impact performance and the degree of any improvements of a polymeric material depended on a variety of factors such as the processing methods and conditions involved, functionalisation and compatibilisation of the nanofillers, degree of nanofiller dispersion and presence of aggregates, annealing of nanocomposite samples, the size of the nanofiller and its alignment in the polymer matrix and in the case of CNTs, chirality [86,123,126,128,131,132,134,135,137–139,141,142,144–147]. Mechanisms such as crack pinning and crack deflection by nanofillers and pull-out of nanofillers and/or polymer matrix can help to reinforce polymers and enhance their impact performance by increasing the fracture surface area and thus the energy required for crack propagation [126,134,136,141–143]. The formation of a cross-linked nanostructure within the polymer matrix can also act as a toughening mechanism [148]. By modelling nanocomposite behaviour, the effect of nanofillers can be investigated and compared to experimental results. Differences between theoretical and experimental results can help to identify important factors which affect the performance of nanocomposites, such as processing methods that can then help towards optimising the nanocomposite [139].

2.3.2. High Strain Rate Properties

Polymers are highly rate-sensitive materials. In different frequency and/or temperature regimes, the nature of the rate-sensitivity will change as various primary (α) and secondary (β) molecular mobility mechanisms are accessed. The α-transition, or the glass transition as it is more commonly known as, involves increased polymer segmental motion which results in the polymer changing from a glassy to a rubbery state. In lower temperature/higher strain rate conditions, additional stress is required to activate the β process in order for the sample to yield. The motions associated with the β-transition are more local than those of the α-transition and involve movement of small groups along the polymer chain. It is believed that nanoparticles can alter the local molecular level structure by influencing these molecular motions as their dimensions are comparable to polymer chain segments. High

strain-rate testing ($<10^2$ s^{-1}) and ballistic tests have been carried out on various types of polymer nanocomposites to assess their suitability for applications involving large impacts.

Carbon nanotubes have the potential to improve behaviour at high strain rates through mechanisms such as nanotube pull out from the matrix, crack bridging and simply structural reinforcement due to their higher stiffness [66–68]. These work by increasing the energy absorbing capability of the polymer and distributing the stresses inside the matrix by crack deflection. However, above a critical loading, aggregation of nanotubes tends to occur. Aggregates can have a detrimental effect on the impact behaviour as they act as stress concentrators in the matrix causing premature failure [69]. As mentioned previously, carbon nanotubes can be functionalised to increase their compatibility with the host material in order to improve their processability and dispersion in the matrix, thus decreasing the degree of aggregation. Hosur et al. [70] found that nanocomposites containing amine functionalised MWNTs exhibited better properties during quasi-static compressions tests and split-Hopkinson pressure bar tests than those containing unmodified MWNTs due to better dispersion and improved interfacial interaction which increased the crosslinking density of the matrix. Rahman et al. [67] reported decreased damage area and increased energy absorption capabilities and ballistic limit of E-glass fibre/epoxy modified with functionalised MWNTs due to nanotube pull out and increased crosslinking density (figures 8 and 9). However, Jindal et al. [68] found that due to their shorter length, functionalised MWNTs decreased the impact energy absorption capabilities of polycarbonate.

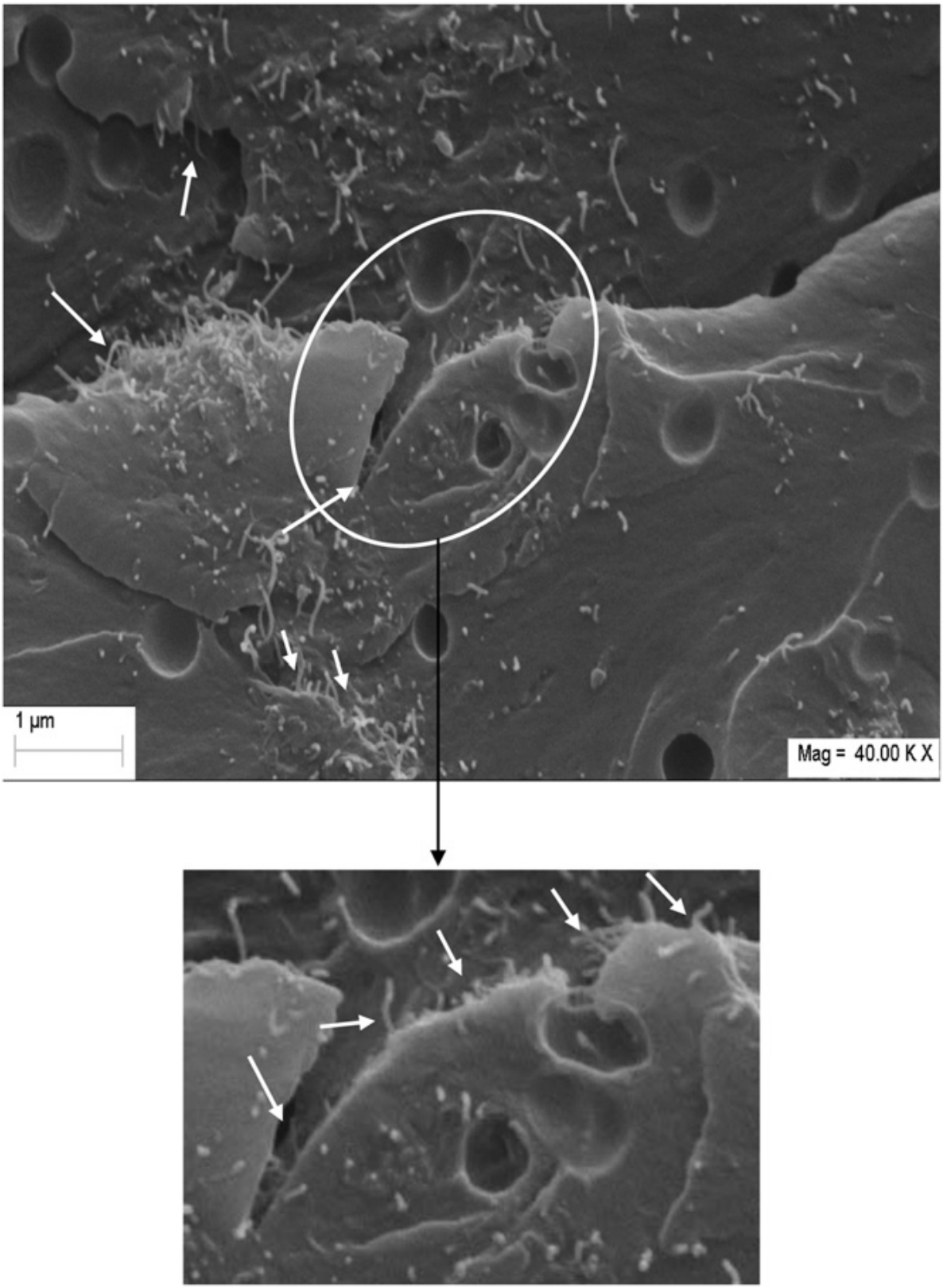

Figure 8 SEM micrograph showing CNT pull-out in the epoxy matrix of the nanocomposites created by Rahman et al. [67]

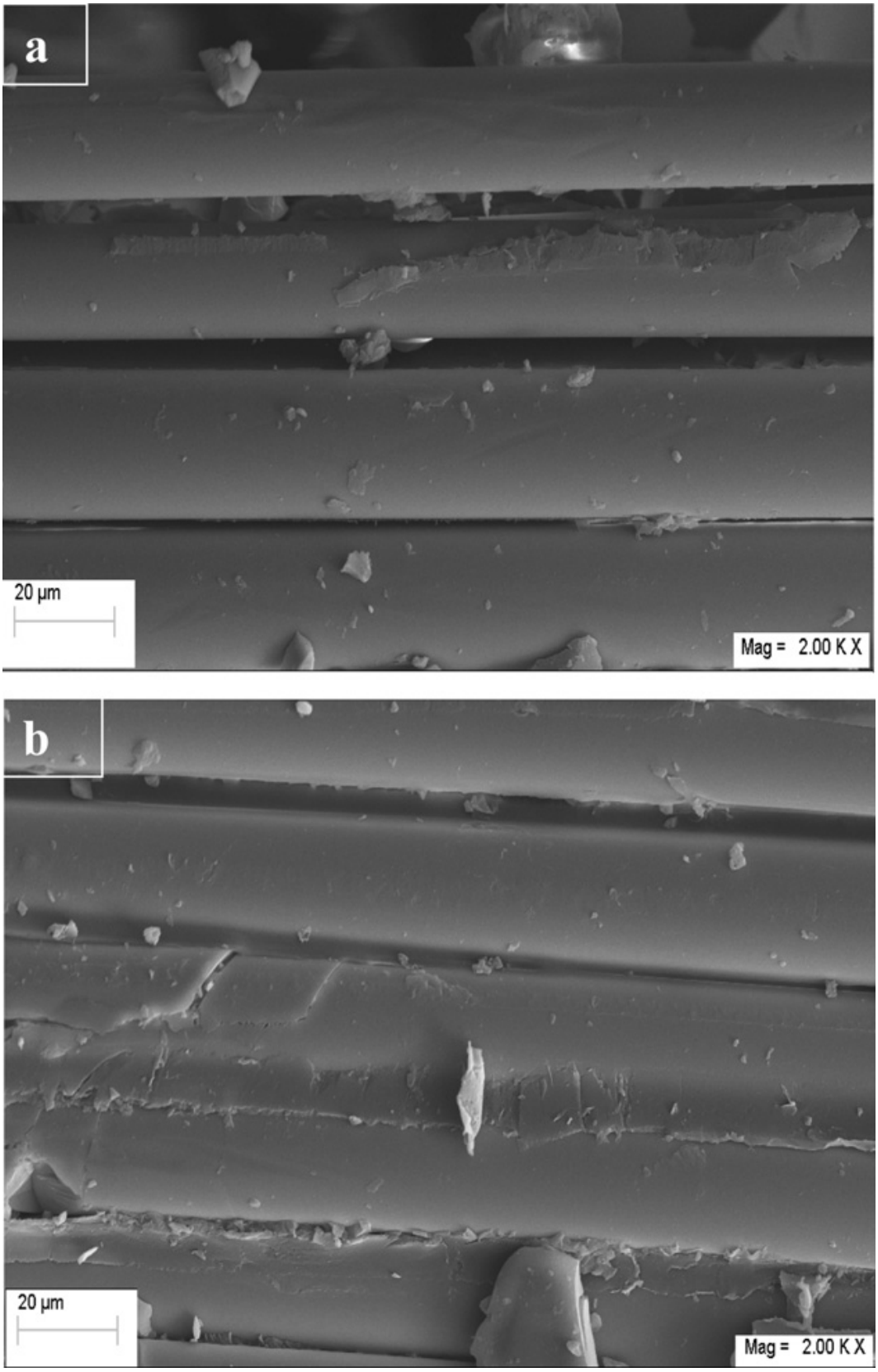

Figure 9 Interfacial bonding between fibre and matrix in a) neat sample and b) 0.3wt% NH_2-MWCNTs nanocomposite sample synthesised by Rahman et al. [67]

As discussed, the properties of nanoclay based polymer nanocomposites is highly dependent on the degree of the exfoliation of the clay platelets. The effect on the high strain-rate behaviour of polymers is no exception. Matadi Boumbimba et al. [71] showed that the yield stress of polypropylene is significantly affected by the extent of clay exfoliation as well as strain rate, temperature and organoclay content. The yield stress increased monotonically with increasing clay content (figure 10). At lower concentrations (<1wt%) the increase was more significant than at higher loadings (>1wt%) due to a mainly exfoliated morphology. At higher loadings, the morphology was a mixture of exfoliated-intercalated. No debonding was observed in samples before or after split-Hopkinson pressure bar (SHPB) tests implying good interfacial strength between filler and matrix.

Balaganesan et al. [72] also found that the addition of nanoclay had a positive effect on the high strain rate properties of a polymer, in this case glass/epoxy composite. Energy absorption during a gas gun experiment increased with increasing nanoclay content for laminates comprised of a varying number of layers. Moreover, the residual projectile velocity in an eight-layer laminate decreased monotonically with nanoclay concentration. High speed camera images revealed an increase in delamination area with increasing nanoclay loading. Hossein Pol et al. also tested glass/epoxy/nanoclay composites, however the nanocomposites were woven in this research. Ballistic tests were carried out using a flat-ended projectile at two different velocities, 134 m/s and 169 m/s. It was found that the optimum nanoclay loading depended on the projectile velocity; the nanocomposite containing 3wt% nanoclay performed best when the lower velocity was used, and 10wt% nanoclay was the optimum loading for the higher projectile velocity. This was shown by decreases in residual velocity and damage area involving energy absorbing mechanisms such as the tensile failure of primary yarns, the deformation of secondary yarns, formation of a cone on the back face of the target, delamination of layers and matrix cracking, all of which work to increase the perforation time.

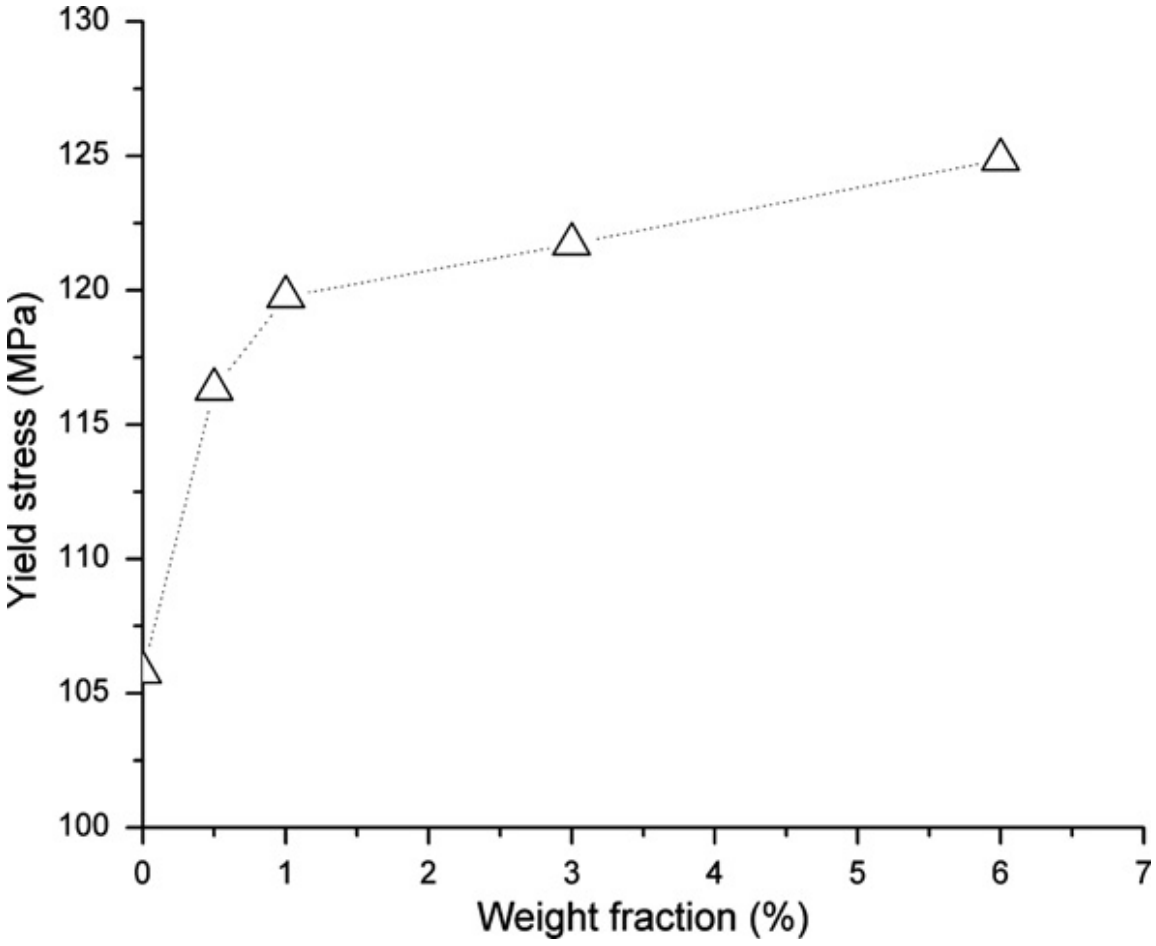

Figure 10 Variation of compressive yield stress with organoclay loading of organoclay-based polypropylene nanocomposites created by Matadi Boumbimba et al. [71]

Other types of nanofillers have been used in the enhancement of high strain-rate properties of polymers. Haro et al. [13] created hybrid composite laminates consisting of epoxy, aluminium sheets and woven Kevlar fibre fabric, the latter being impregnated with micro and nanofillers in powdered form such as aluminium, gamma alumina, silicon carbide, colloidal silica and potato flour. These were then subjected to ballistic tests complying with NATO standards and the ballistic impact resistance and energy absorption measured. SEM suggested that the nanopowder filled and coated gaps/voids existing between the fibres and provided extra reinforcement, facilitated stronger bonding of layers which lead to increased energy absorption capabilities. Fibre pull-out decreased as a result due to better fibre adhesion which led to increased elongation and impact resistance. The potato flour was an exception as it weakly bonded to the Kevlar.

2.3.3. Optical Properties

The transparency of polymers is determined by three factors; light transmittance, haze and clarity [73]. Incorporation of nanofiller into the matrix of a transparent polymer generally improved the mechanical properties of the polymer but tended to cause a decrease in transparency [73–77]. Factors affecting the transparency of a polymer nanocomposite include nanofiller dispersion, size and loading, the presence and size of nanofiller aggregates, the difference between polymer and nanofiller refractive indices, the presence of any degradation products and the use of any treatment products [73,75,76,78].

2.3.4. Physical Aging

Below the T_g, polymers are in a non-equilibrium state which is characterised by a larger free volume than that of the equilibrium state (see section 3.3.6 for a more detailed explanation). There is a very small amount of chain mobility and over time the chains move closer together to reduce the excess free volume and thus the enthalpy of the system in order to recover the thermodynamically stable state. This phenomenon is known as physical aging and is why such polymers tend to become brittle with age; a decrease in free volume results in an increase in intermolecular interactions and therefore a reduction in freedom of movement of the polymer chains [79]. Understanding the physical aging of polymers and the change in their properties is an important aspect when considering their long-term performance. It is therefore important to understand the effect that nanofillers have on the physical aging of the host polymers of such materials.

In the literature study it was found that the presence of nanoparticles can have contradictory effects on the physical aging of a polymer matrix. In some polymer nanocomposites systems, the physical aging was accelerated [80–82] whereas in other systems physical aging was suppressed [83–85] and depended on factors such as the proposed mechanism involved in the physical aging process and the nanofiller content [80]. In their review paper on the physical aging of polymer nanocomposites Cangialosi et al. emphasised two main aspects on how the presence of nanofillers affect the rate of physical aging: (i) the modification of the polymer segmental dynamics in proximity to the nanofiller surface; (ii) geometric factors [86].

Cangialosi et al. [80] studied the physical aging process of two polymer nanocomposite systems modified by silica nanoparticles. The time evolution of the enthalpy of PMMA/silica and PS/silica was monitored by DSC. It was found that in both systems, the presence of silica nanoparticles resulted in a decrease in the glass transition of the polymer via increased chain mobility and that the degree of reduction increased with increasing nanoparticle content. The results also indicated accelerated physical aging in the nanocomposites in comparison to the control polymers and again, are generally more pronounced in nanocomposites containing higher amounts of silica nanoparticles. Figure 11 shows how the structural relaxation function, Φ_H is reduced with the addition of nanoparticles. The structural relaxation function describes the enthalpic relaxation and so from figure 11 it could be inferred that the nanoparticles accelerate the physical aging process of both polymer systems, despite lower recoverable enthalpy values. It was suggested by Cangialosi et al. that the acceleration of the physical aging could therefore not be solely attributed to differences between the molecular mobility of the polymers in the nanocomposites and the control samples and that their results raise questions on the idea that physical aging is exclusively controlled by the molecular mobility and the distance from equilibrium of the polymer. Instead, they proposed a physical aging mechanism involving the diffusion of free volume holes to the polymer/nanoparticle interface which leads to densification of the glassy polymers.

Ramakrishnan et al. also investigated a silica-based polymer nanocomposite and found that the physical aging of polycarbonate was also increased [81]. However, Rittigstein and Torkelson found that addition of silica to PS, PMMA and poly(2-vinyl pyridine) suppressed the physical aging of the polymers which correlated to increases in the glass transition temperature [85].

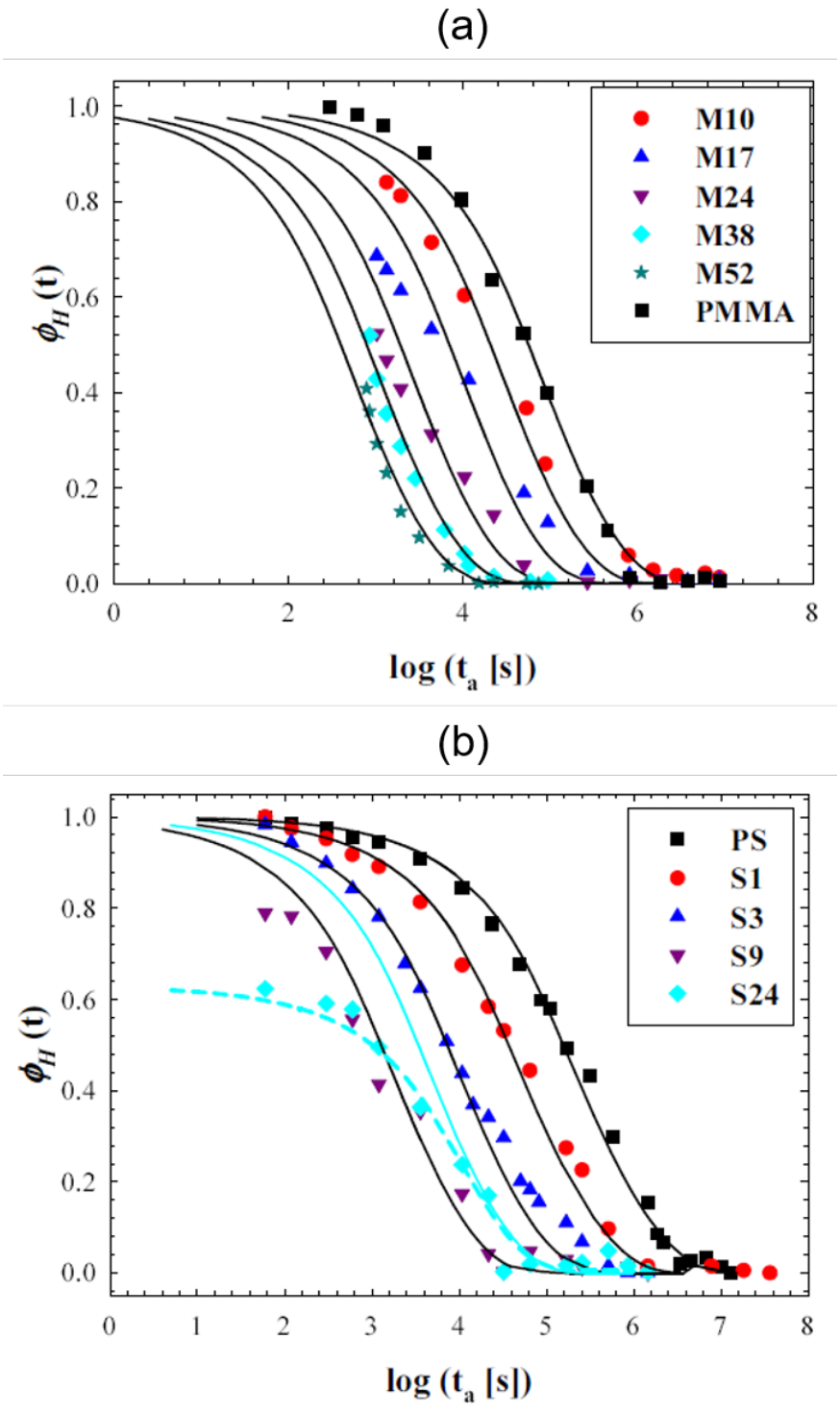

Figure 11 The structural relaxation function, $\Phi_H(t)$, which describes the enthalpic relaxation, as a function of aging time, t_a for (a) PMMA-POSS and (b) PS-POSS based nanocomposite systems (*S1*, *S3* etc. represents the weight percentage of silica nanoparticles in PS and *M10*, *M17* represents the weight percentage of silica nanoparticles in PMMA. It is shown here that the silica nanoparticles decreases the relaxation function in both polymer systems, suggesting the addition of nanosilica accelerates the physical aging process [80]

The effect of carbon nanotubes on the physical aging of PMMA and the role of functionalisation was investigated by Flory et al. [84]. DSC was used to study the physical aging of PMMA with 1wt% of either unmodified SWNT or amino-functionalised CNTs (a-SWNT). It was hoped that functionalisation of the SWNTs would promote better interaction with the polymer. It was found that T_g of PMMA was unchanged by the addition of unmodified SWNTs however it increased by 17 °C with the incorporation of the functionalised SWNTs. Flory et al. stated that the presence of a-SWNTs restricts the segmental motion of the PMMA chains. No significant change was found in the activation energy of enthalpy relaxation of PMMA/a-SWNT in comparison to the pure PMMA however a broadening of the enthalpy peak was observed with the addition of unmodified SWNTs implying poorer dispersion of the CNTs which result in areas of low and high polymer mobility and a distribution of temperatures. The restrictive environment created by the CNTs decrease the rate of enthalpy recovery implying that the present of nanotubes suppresses physical aging.

2.4. POSS-based Polymer Nanocomposites

2.4.1. Polyhedral Oligomeric Silsesquioxane

Polyhedral oligomeric silsesquioxanes (POSS) are a class of inorganic-organic hybrid molecules. POSS is most often referred to as a nanofiller, however it is more appropriate to consider POSS as a set of chemicals which are characterised by defined structures and possess their own intrinsic properties [87]. POSS molecules are rigid and inert like inorganic nanofillers and are 1-3 nm sized individual molecules possessing zero dimensionality or sphere-like structure. Yet unlike conventional particulate nanofillers POSS has the potential to be soluble in the matrix of the host polymer to provide true molecular dispersion [15,88,89]. Strictly speaking then when POSS is soluble in a matrix and exists as molecules, structurally the resulting material is not considered a nanocomposite as the POSS does not form a second phase within the polymer. However, for simplicity's sake, the term "polymer nanocomposite" shall be used in this work to describe both a system where POSS is molecularly dissolved and where it exists as a secondary phase (aggregates) in the polymer matrix.

At the core of a POSS molecule is a rigid and inert organosilicon compound known as a silsesquioxane, which is what gives POSS its overall cage-like form. Depending on whether the cage structure is open or closed, the flexibility of the POSS molecule will change [90]. Silsesquioxanes are organosilicon compounds with an empirical formula $RSiO_{1.5}$ i.e. they possess a chemical composition between that of silica and silicon with organic functional (R) groups attached to the corners of the cage, which can be almost any chemical group [91]. The ability to customise these R groups to such an extent makes POSS unique and highly versatile. For good compatibility between POSS and the polymer it is vital that the appropriate organic groups are chosen so that they match the polarity of the polymer. This will promote fine, homogeneous dispersion and increase the degree of enhancement of the polymer as well as potential retention of optical transparency [15,87]. Incompatibility can lead to poor dispersion and phase separation in the form of POSS aggregates [92,93]. As POSS molecules are 1-3 nm in diameter they are comparable in size to that of polymer chains and segments. A consequence of this similarity in size is that POSS molecules have the ability to control the motions of the polymer without compromising the workability nor the mechanical properties of the polymer matrix [87,94,95]. To control the motions of polymers would allow control over the extent to which a polymer under deformation is sensitive to strain-rate and temperature.

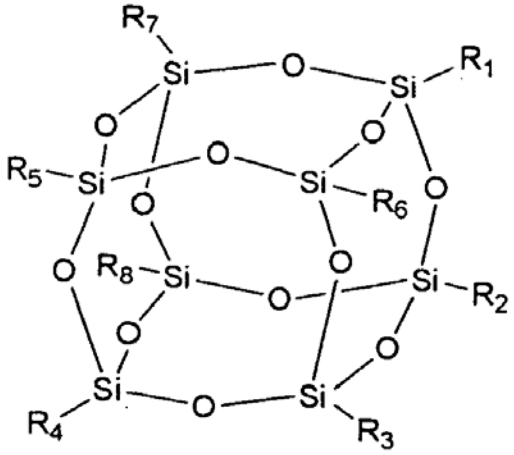

Figure 12 General chemical structure of a POSS molecule [96]

As previously discussed, the motion of a polymer chain involves various primary and secondary molecular mobility mechanisms and when a particular motion is restricted, the viscoelastic behaviour of the polymer will undergo a transition. The α-transition occurs at the glass transition temperature of an amorphous polymer and involves long-chain segmental translation or rotation relative to one another. At the *β*-transition, motion of side chains or branches occurs which are dubbed *β*-motions. Under the conditions of high strain-rate or low temperature some amorphous polymers exhibit a restriction in these secondary motions. It is the restriction of these motions that are believed to result in an increase in resistance of a polymer to deformation, achieved by the enhancement in stiffness, yield strength, post-yield strength and rate-sensitivity of yield [97,98]. It has been documented that incorporating POSS nanomaterials into polymer matrices can lead to enhancements of mechanical properties, reduction in flammability, surface hardening and much more. Combining these improvements with its versatility, POSS has become one of the principal nanomaterials in nanotechnology research and applications [89,95].

2.4.2. POSS-based Polymer Nanocomposite Preparation Methods

POSS-based polymer nanocomposites are typically synthesised either by physical blending (melt blending) or through chemical linking methods such as polymerisation or crosslinking.

As discussed in section 2.2.1, melt blending is considered an inexpensive, versatile, fast and environmentally friendly method. Moreover, standard polymer compounding equipment is generally suitable in the preparation of POSS-based polymer nanocomposites with limited modification. The miscibility of POSS with polymers can be utilised by this method however, successful dispersion depends on the surface interaction of POSS e.g. van der Waals forces, hydrogen bonding, with the polymer matrix which must be strong enough to overcome the POSS-POSS interactions that often lead to aggregation. Fine dispersion at the molecular- or nano-scale is necessary to utilise the full potential of POSS. Due to its tuneable miscibility via various available functional groups, the dispersion of POSS can be controlled to enhance the compatibility between POSS and the host matrix. Despite this, achieving optimum dispersion is still challenging. Fina et al. [87] discussed the use of melt reactive blending which involves the use of a chemical reaction between POSS and the polymer during melt blending to drive dispersion by increasing the interfacial interactions between the two

materials. Mixing conditions, such as temperature, time, shear force and mixing energy will also play a role in the final dispersion of POSS [87,99,100].

Chemical linking methods can be used to overcome phase separation of POSS from the polymer by covalent bonds however, as previously mentioned, these methods involve synthetic procedures and therefore are not as commercially viable due to their toxicity and harmful effects on the environment [99].

2.4.3. Properties of POSS-based Polymer Nanocomposites

2.4.3.1. Effect of POSS type

The ability to customise POSS makes it a unique and highly versatile class of nanofiller dispersant. Organic groups can be attached to the cage structure of POSS to increase the compatibility of the nanofiller to the host polymer. The polarity and chemical composition of the R groups will affect the solubility of the POSS dispersant in the polymer matrix and consequently the final properties of the resulting polymer nanocomposites. Therefore, to maximise enhancement of the host polymer, the R groups must be chosen so that the POSS and the polymer have a similar solubility parameter [90]. This frequently results in a more homogeneous nanofiller dispersion which promotes interaction between POSS and the host polymer. The length of the R groups and type of cage structure present will also change the effect that POSS has on a polymeric material.

Dintcheva [90] investigated the effect of structural and chemical differences on polystyrene (PS) nanocomposites by using five different types of POSS, either with open or closed cages and different organic groups. They found that cage structure affects the rheological properties of the polymer and POSS dispersability; open cage structures have a more pronounced plasticising effect than closed cage structured POSS types as they are more flexible. It was proposed by the authors that the plasticising effect is due to 1) an increase in free volume, 2) a reduction in entanglement density or 3) a reduction in frictional effects between matrix macromolecules. Additionally, open cage structures tended to have more similar solubility parameters to that of PS and therefore better dispersability in PS than those POSS types possessing a closed cage structure, as evidenced by SEM. Rheological behaviour was also affected by the length of the organic groups; longer organic R-groups increase the free volume more as they are bulkier in size.

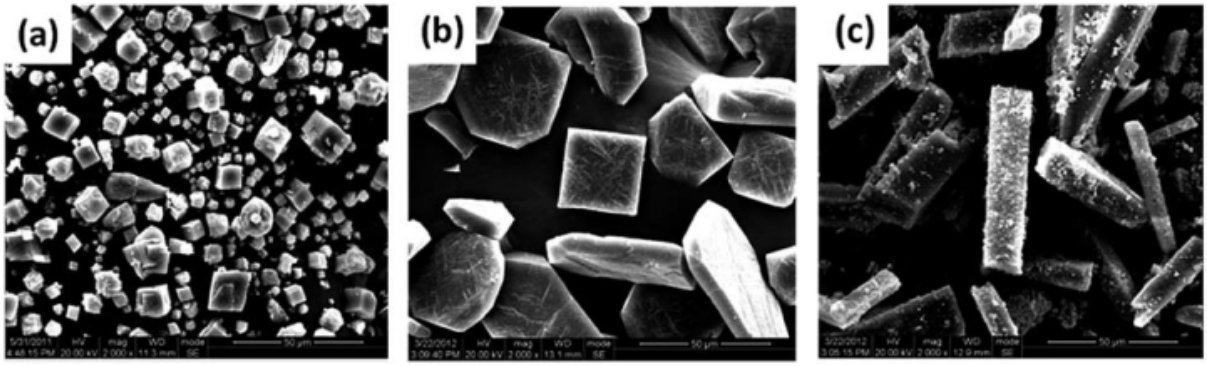

Figure 13 SEM micrographs showing the morphology of a) OMS-, b) OPS- and c) H-POSS crystals used by Zhang et al. to modify the mechanical properties of PDMS [101]

Longer R-groups can also have a shielding effect whereby the interaction between POSS and the polymer matrix is less pronounced. Mechanical properties were found to be influenced more by the type of chemical group. Regardless of good dispersion, there needs to be some interaction between the R-groups and the macromolecules of the matrix.

The nature of the POSS molecule also influences the crystallisation and melting behaviour of the host polymers [101–105]. Zhang et al. [101] investigated three types of POSS in polydimethylsiloxane (PDMS). The morphology of the three types of POSS nanofiller used can be found in figure 13. Octamethylsilsesquioxane (OMS) was found to have no nucleation effect on the crystallisation process. At high loadings, small crystals were shown to form due to weak POSS-POSS interactions. These small crystals were then shown to form small aggregates that pack together and thus prevent PDMS chains from interacting. Conversely, octaphenylsilsesquioxane (OPS) and heptaphenylhydrogensilsesquioxane (H-POSS) were shown to enhance the crystallisation rate of PDMS but by different nucleating mechanisms to that of OMS. OPS formed large flake-like crystals at high loadings which provided large surface areas for PDMS crystals to grow i.e. OPS increased the crystallinity of PDMS at these loadings. At low loadings, OPS did not form flakes and tended to inhibit the regular arrangement of PDMS. Conversely, small loadings of H-POSS were shown to increase the crystallisation rate of PDMS by physical crosslinking but did not increase the overall crystallinity of the polymer. As loading is increased, the H-POSS that could not graft to the polymer, due to saturation, actually impeded the crystallisation of PDMS.

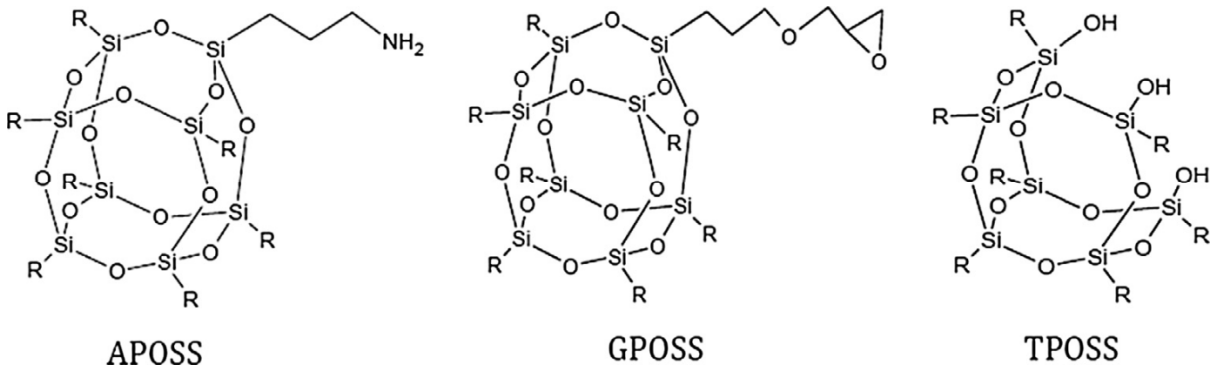

Figure 14 The chemical structures of the different types of POSS used by Sirin et al. to create PET/POSS nanocomposites [103]

Sirin et al. [103] investigated three types of POSS in polyethylene terephthalate polymers (PET) to create injection moulded samples and melt-spun fibres. They used epoxy, hydroxyl and amine functional POSS, noted as GPOSS, TPOSS and APOSS, respectively. Figure 14 shows the chemical structure of the POSS used. The mechanical properties of injection moulded composites were not affected by POSS which the authors stated was due to the low loading levels used (0.1 wt%, 0.5 wt% and 1 wt%). For drawn fibres containing 1 wt% TPOSS, Young's modulus of PET increased by about five times the value of the neat polymer. TPOSS/PET drawn fibres also had the highest breaking strength and lowest elongation at break which depended on the loading in the matrix. This suggests that drawing the TPOSS-PET into fibres enables the TPOSS to affect the mechanical properties of PET by perhaps more oriented domains, and therefore increased interaction between POSS and PET, which hinders the mobility of the amorphous chains. Since TPOSS has three functional groups it is thought to form a networked structure where three individual PET chains can attach to the same POSS molecule. The high crystalline content of TPOSS-PET fibres is also thought to explain the enhanced mechanical properties. GPOSS also increased the tensile modulus of PET fibres whereas APOSS did not produce any significant trend.

Sirin et al. proposed that with the help of longer alkyl chains APOSS and GPOSS are able to form bonds with the polymer more easily and as they are more flexible they allow the polymer to relax more under stress. This results in the decrease in Young's moduli of GPOSS- and APOSS-PET composites. However, as TPOSS possesses three hydroxyl groups close to its core, there will be some steric hindrance resulting in less interaction with the polymer. As a result, TPOSS will more likely be present in the matrix by itself, allowing more time for the

PET chains to crystallise and form longer chains. Thus the mechanical properties of PET composites with TPOSS were the most improved.

2.4.3.2. Viscoelastic Properties

POSS can be used to modify the viscoelastic properties of polymeric materials. The effect that POSS molecules have on the thermo-mechanical properties will depend on the type of polymer; bulky POSS cages can increase the free volume of polymers and is generally the dominant effect when incorporated into stiff, glassy polymers. In the case of rubbery polymers the rigidity of POSS helps to reinforce the polymer by restricting chain movement and reducing chain flexibility [106]. The precise nature of the polymer under modification will also have an effect [107]. In the literature it was found that POSS can either increase thermo-mechanical properties such as glass transition temperature and storage modulus, usually by forming crosslinks or reinforcement by other types of bonding e.g. hydrogen, covalent, or by restriction of chains due its bulky nature [108–122]. Alternatively, POSS can decrease such properties by acting as a plasticiser [123–130]. The manner in which POSS influences the viscoelastic properties of a polymer can depend on factors such as POSS loading [131–136] and the type of POSS used [104,112,113,137–140]. Additionally, the preparation method used to synthesise the nanocomposites can affect how POSS influences the viscoelastic properties; for example, when POSS is chemically grafted to the polymer chains via a method such as polymerisation, an increase in T_g is observed whereas physically mixed nanocomposites tend to cause a decrease in T_g usually due to aggregation [101,141,142].

Florea et al. [113] studied epoxy resin/epoxy-functionalised polydimethylsiloxane reinforced with epoxy-POSS. Two types of POSS were used, mono- and octa-epoxy POSS (MEP-POSS and OEP-POSS, respectively) with either one or eight epoxy groups, respectively. It was found that OEP-POSS increased glass transition temperature, storage modulus and hardness of the polymer whereas MEP-POSS had a decreasing effect on the glass transition temperature. It was found that MEP-POSS was heterogeneously dispersed in the polymer matrix as aggregates which were suggested to increase the free volume and thus lower T_g. The eight epoxy groups of OEP-POSS on the other hand help it to covalently bond with the polymer, improving its dispersion in the matrix but also facilitating crosslinking. Moreover,

possessing eight epoxy groups gives OEP-POSS a bulky and rigid structure which can restrict chain motion, as shown by a shorter and broader *tanδ* peak.

Iyer and Schiraldi studied the effects of trisilanol phenyl POSS on polycarbonate (PC) and phenoxy resin (PKFE) [107]. Nanocomposites containing between 5% and 25% POSS were synthesised via melt blending and compression moulding. It was proposed that the POSS would interact differently with the two polymers; PKFE contains hydroxyl groups which are capable of forming hydrogen bonds which is typically not available for PC as it contains carbonyl groups. The results from this work showed that POSS increased the T_g of PKFE along with room temperature and rubbery modulus whereas for the PC/POSS system these values decreased below that of the control sample. It was found that significant interactions occurred between POSS and PKFE which resulted in enhancement of the mechanical properties of the polymer. However poor compatibility was observed by SEM (fig. 15) between PKFE and POSS as evidenced by spherical POSS aggregates, which occur even at the lowest POSS loading (5%) and suggest the solubility limit is less than 5%, and an increase in void spacing between the two phases which increases the overall free volume. The free volume of PC/POSS stays constant however and is thought to be because of significant solubility of POSS in the polycarbonate matrix and/or improved adhesion between the phases i.e. POSS acts as an internal molecular lubricant with little to no interactions at low loadings. This is further supported by the lack of POSS aggregates up to 10% loading, and even then they are less numerous than the PKFE/POSS system. Moreover, the DSC heating scans showed an absence of melting peak for POSS in the PC/POSS system, indicative of nanoscale- or molecular-distribution of filler in the matrix. At higher loadings, POSS addition resulted in the embrittlement of the polycarbonate (anti-plasticisation).

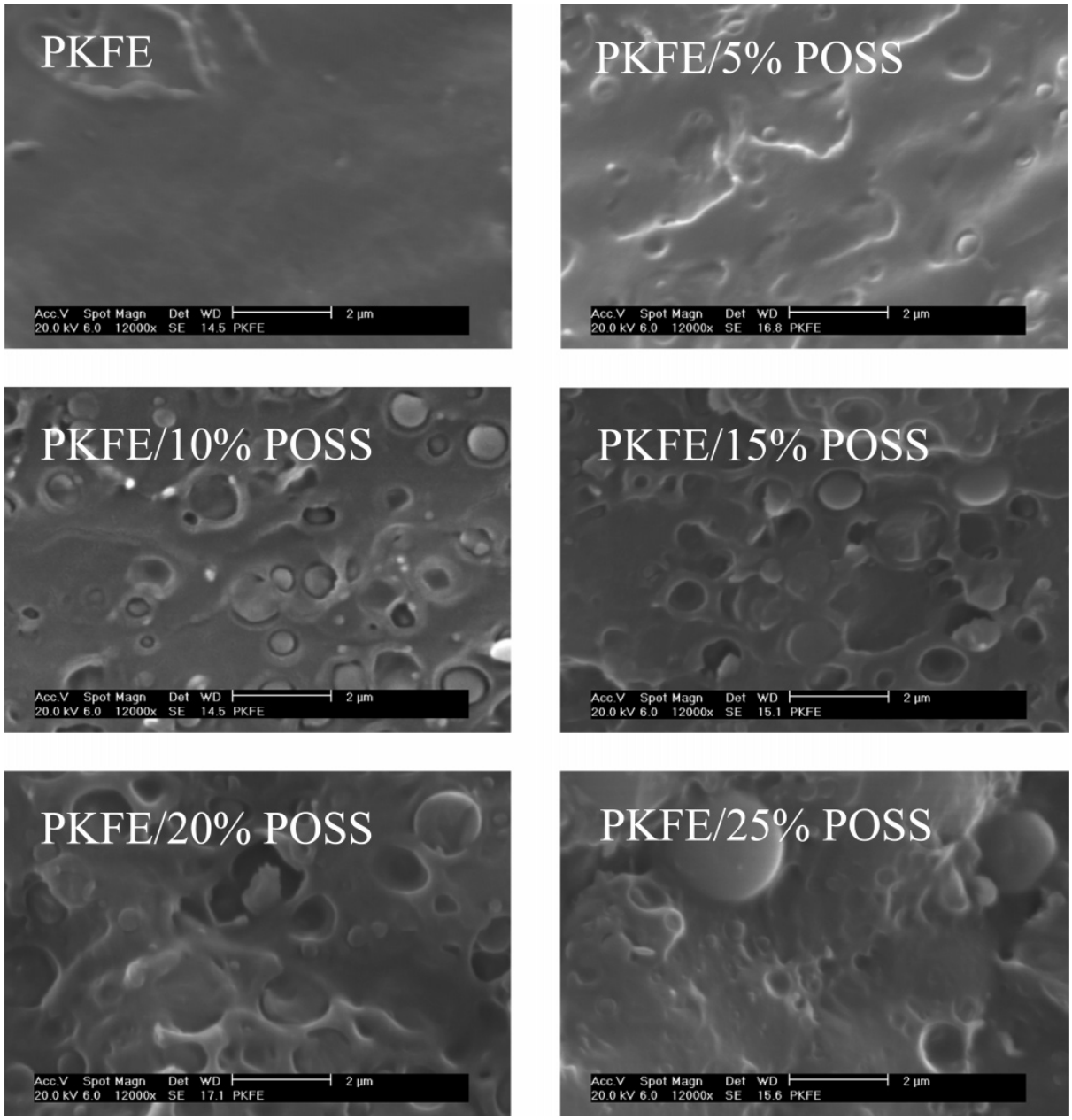

Figure 15 SEM micrographs of PKFE/POSS nanocomposites synthesised by Iyer and Schiraldi [107]

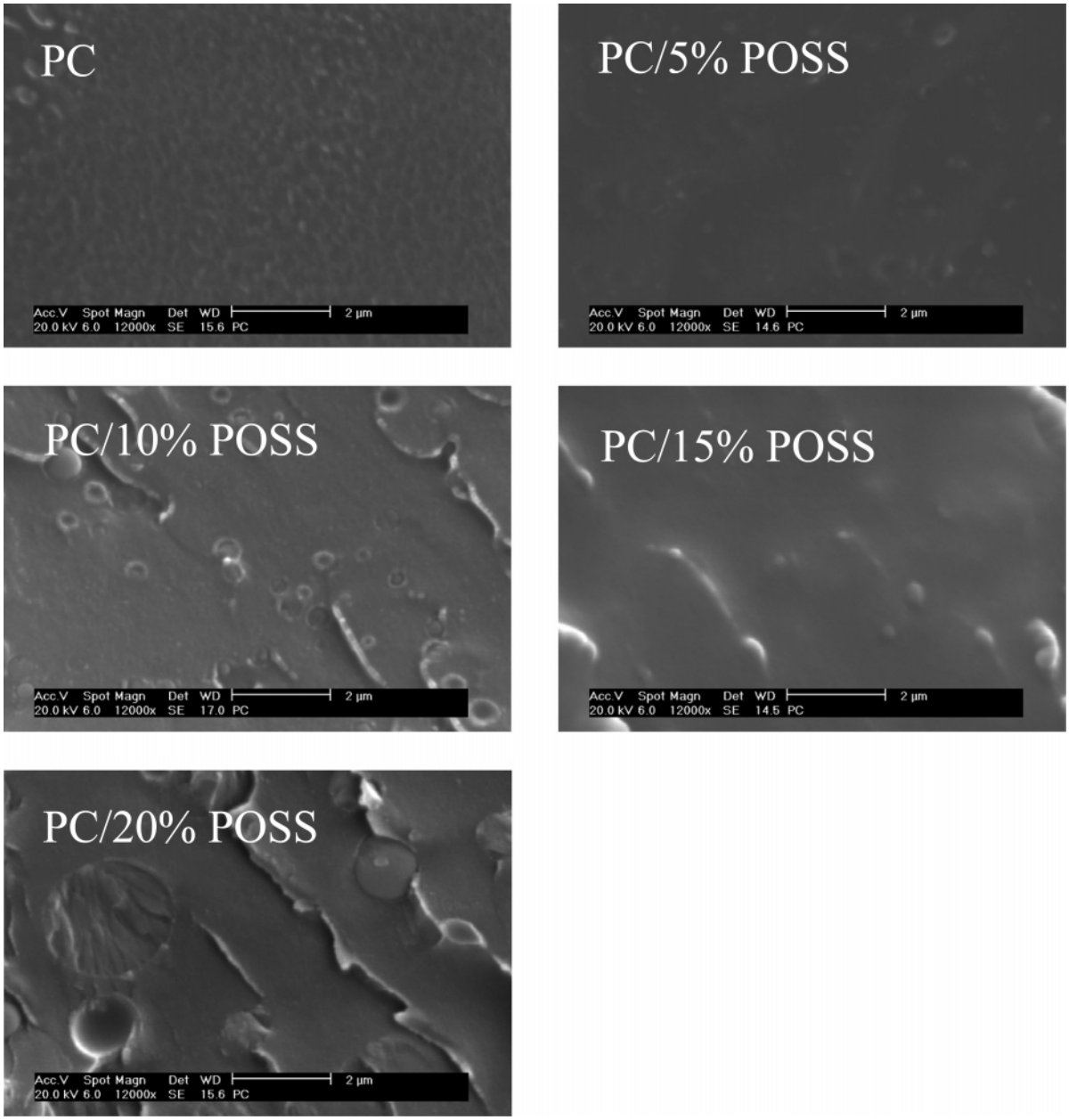

Figure 16 SEM micrographs of PC/POSS nanocomposites synthesised by Iyer and Schiraldi [107]

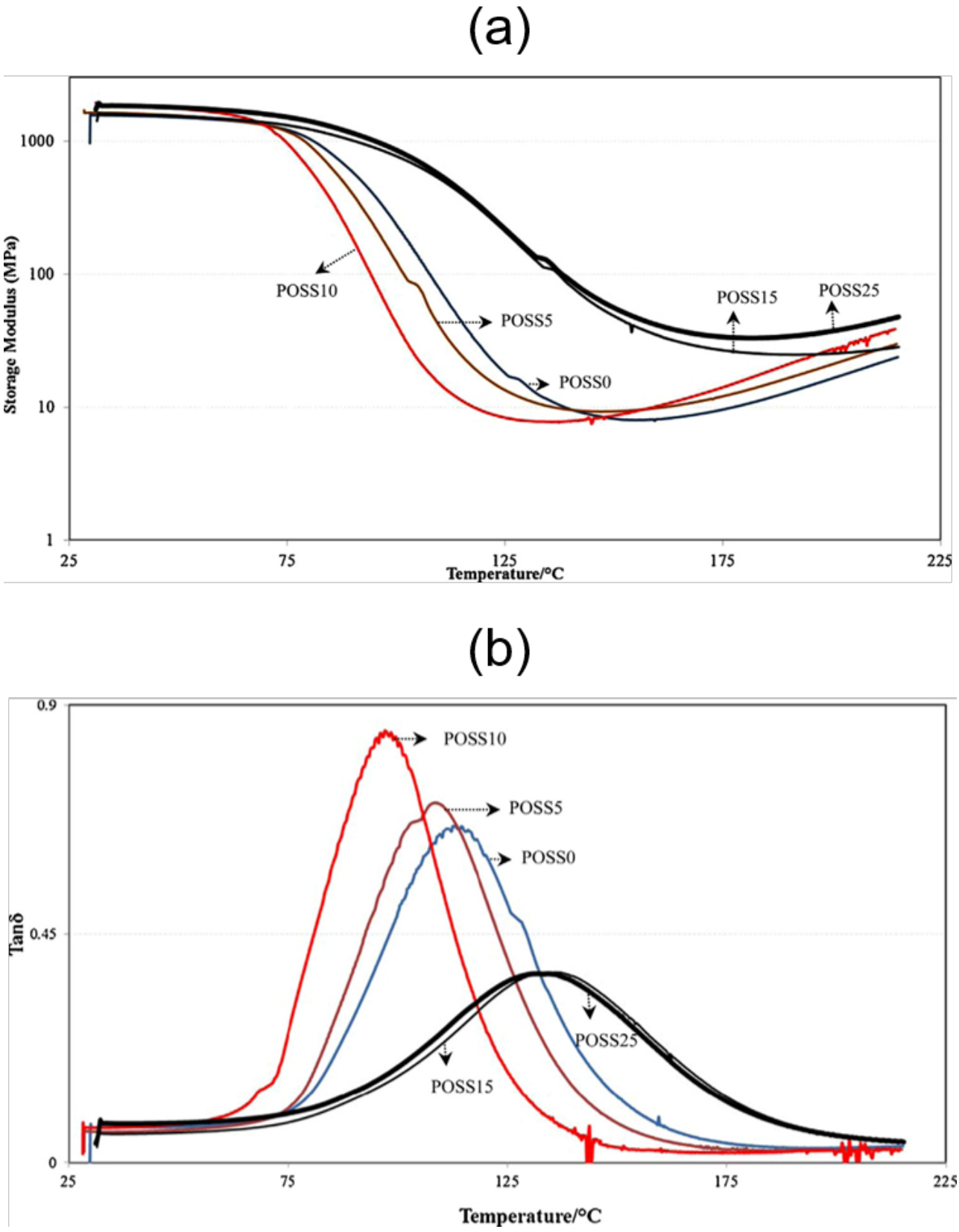

Figure 17 The variation of storage modulus (top) and tan*δ* (bottom) with temperature and POSS loading of an acrylic/melamine clearcoat nanocomposite created by Yari and Mohseni [126]

Yari and Mohseni investigated the effect that a hydroxyl functional polyhedral silsesquioxane had on the thermo-mechanical properties of an acrylic/melamine clearcoat. At low POSS loadings, the glass transition temperature of the clearcoat decreased due a more flexible structure. POSS acted as a chain substitute; it is able to locate between chains where it decreases entanglement due its more compact structure. This leads to a higher level of chain mobility and reduction in viscosity. At higher loadings, chain entanglement decreases. This has the effect of increasing crosslinking which outweighs the effect of lowered entanglement. As a result, viscosity rises and T_g increases. The $tan\delta$ peak width represents homogeneity of a network; at lower POSS loadings the width of the peak decreases whereas it increases for higher loadings, representing decreased entanglement and increased entanglement, respectively. Figure 17 demonstrates this effect as well as the effect on the storage modulus. FTIR confirms the presence of a highly cross-linked network at higher POSS loadings [126].

2.4.3.3. Mechanical Properties

The addition of POSS into a polymer matrix can enhance the mechanical properties of the polymer. Improvements in polymer ductility, strength, stiffness, toughness and impact resistance after incorporation of POSS have been reported [91,93,116,120,143–163]. The amount of improvement depends greatly on the dispersion of POSS in the polymer matrix, which in itself is influenced by a variety of factors such as the amount and type of POSS used and processing method employed. Both of these factors will influence whether bond formation occurs, the solubility of POSS in the matrix and therefore its distribution in the polymer and the resultant structure and morphology of the nanocomposite. Properties may also vary due to conversion of POSS moieties into new substances during polymer processing [164]. The formation of bonds between the polymer and POSS is one mechanism that can allow POSS to reinforce a polymer matrix [117,137,146,147,152,153,165,166]. This manifests as increases in strength and stiffness, but a decrease in ductility. The opposite occurs when POSS is able to molecularly dissolve in the matrix, whereby it typically acts as a plasticiser and can also have the possibility of toughening the polymer matrix [93,129,134,143,150,167]. In some cases, both gains in strength and toughness arise from the addition of POSS without a decrease in the polymer ductility [119,132,141,168]. POSS can also be used in the creation of self-healing polymers and shape memory polymers

[119,131,169]. For example, Lee et al. [170] prepared poly(ε-caprolactone)/trisilanol-phenyl POSS (PCL/TspPOSS) nanocomposites via solution blending. FTIR confirmed the formation of hydrogen bonds between the silanol groups of POSS and the carbonyl oxygen of PCL. Tensile properties of the polymer were found to increase with the addition of TspPOSS and were thought to be a consequence of the hydrogen bonding. Another interesting consequence of the hydrogen bonding was the thermally activated shape memory behaviour demonstrated by the nanocomposites. After heating, the deformed PCL/POSS samples shrank and regained their original shape with the degree of recovery increasing with increasing POSS; PC/10% TspPOSS recovered 97% of its original shape. The authors deduced that two structural features must be present in the nanocomposites for shape memory behaviour to occur; crosslinks (POSS nanocrystals) which determine the permanent shape of the material and reversible segments (crystalline segments of PCL) that act as switching phases.

Yari et al. [131] studied the effect of an OH-functionalised POSS on a typical acrylic melamine clearcoat. POSS enhanced the scratch resistance and hardness of the clearcoats. It was also suggested that POSS enhanced the healing ability of the clearcoats after being exposed to a thermal healing process. It was revealed that scratch depth profiles were lowered further for clearcoats containing up to 10% POSS. The enhanced healing ability was attributed to the physical hydrogen bonding interactions between POSS nanocages and the polymer and the creation of a more flexible structure. DMA results indicated at low loadings that the presence of POSS decreased T_g and potentially increased the homogeneity of the network by reducing the crosslinking density and its innate compact structure. The nature of POSS can promote the formation of strong hydrogen dipole-dipole bonds with components in the clearcoat due to its Si-O-Si linkages and hydroxyl groups. The authors propose that these interactions can be considered as physical cross-links which are thermally sensitive and can be broken at higher temperatures. Moreover, it is proposed that the loss of these bonds at elevated temperatures facilitate the segmental motion of polymeric chains and thus the greater chance of rearrangement of mechanically deformed chains.

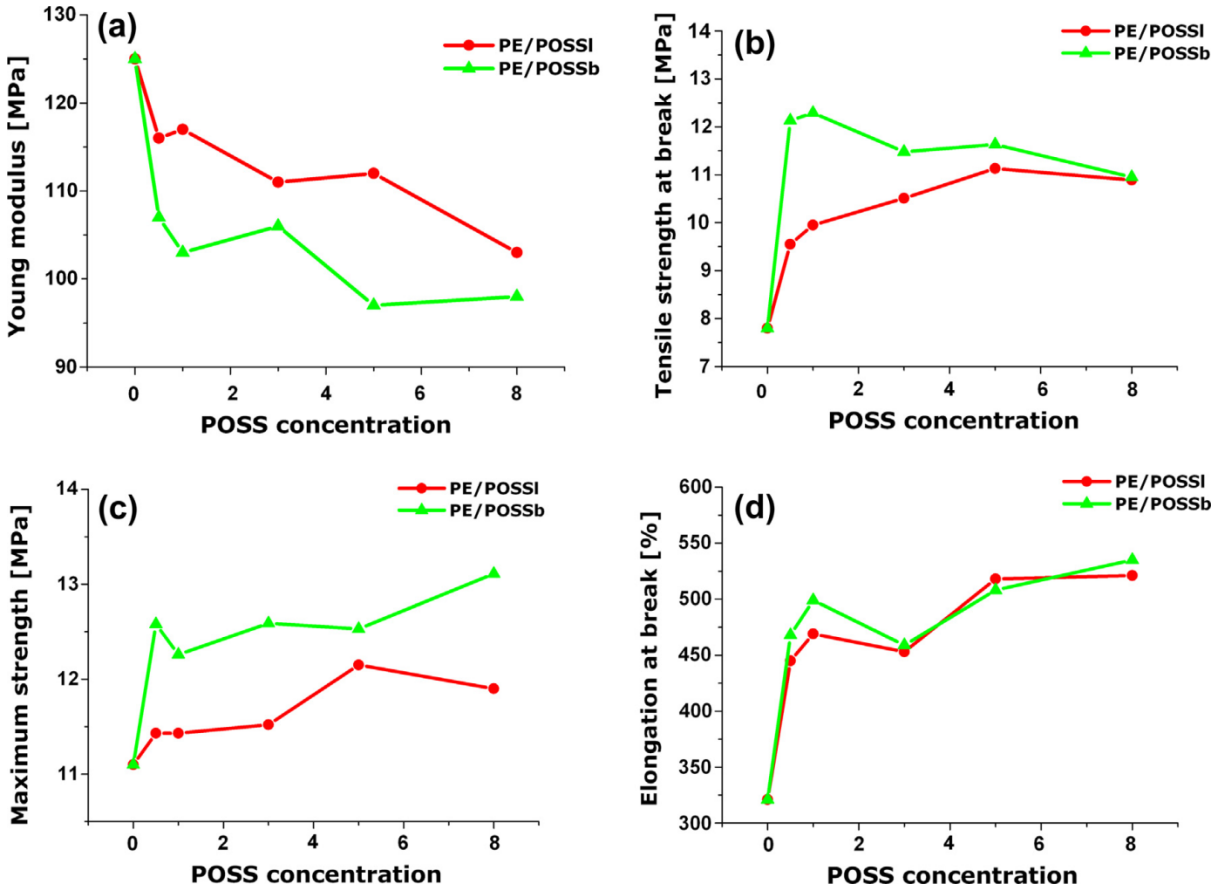

Figure 18 The tensile properties of PE and its POSS-based nanocomposites: (a) Young's modulus, (b) Tensile strength, (c) Maximum strength (Ultimate tensile strength) and (d) Elongation at break, synthesised by Frone et al. [171]

Frone et al. [171] investigated the effect of branching in the alkyl group of POSS particles on low density polyethylene. A significant improvement was found in tensile strength and ductility of PE for both types of POSS used, however this was particularly the case for the branched POSS, POSSb. Branching appears to have a more positive effect on mechanical properties and could be due to a stronger interaction between nanofiller and polymer. In this research POSS did not behave as a typical plasticiser; despite an increase in elongation at break, tensile strength is also increased and Young's modulus is slightly decreased, specifically when using low concentrations of the branched POSS. Increasing the POSS content beyond 1wt% resulted in a tendency for the POSS to aggregate. Figure 18 contains the tensile properties of PE and its POSS-based nanocomposites.

Liu et al. [141] prepared via in-situ polymerisation POSS-based (poly[2, 2'-(p-oxidiphenylene)-5, 5'-bibenzimidazole]) (OPBI) nanocomposites. For comparison, OPBI-POSS

composites were prepared via physical blending. NMR, XPS and XRD suggested that the phenyl groups of POSS had successfully attached to the OPBI chains through a Friedel-Crafts (F-C) reaction. SEM of the fracture surfaces suggests homogeneous dispersion as a result of the F-C reaction as no discernible phase separation or aggregation of POSS could be observed. Young's modulus increased for both the blended and F-C prepared composites however the OPBI-POSS nanocomposites with POSS grafted to the polymer chain saw a more enhanced improvement in Young's modulus. Moreover, tensile properties such as tensile strength, ultimate strain and toughness decreased in the blended composites but increased in the F-C prepared nanocomposites along with the ductility. It is thought that POSS is tightly embedded in the OPBI matrix by covalent bonding with OPBI acting as effective cross-linking sites. This resulted in improved mechanical properties due to a more efficient stress transfer from the matrix to POSS. DMA revealed a decrease in glass transition temperature, implying that POSS increases free volume which facilitates the movement of the polymer chains. These differ to traditional composites where incorporation of inorganic fillers increases the polymer strength at the expense of its ductility and toughness. The optical transparency of the polymer was also maintained.

Yari et al. [132] fabricated an acrylic/melamine thermosetting system modified by an OH-functional POSS to create toughened clear coats. SEM, XRD and TEM were used to assess the dispersion of POSS in the matrix. SEM of fracture surfaces revealed an increase in the surface roughness of the nanocomposites. This is suggested to be due to a greater deformation of polymer chains which is able to dissipate more energy. At higher POSS loadings, sharper edges were observed implying a more brittle fracture. EDS shows that POSS has a tendency to remain in the bulk and, by assessing silicon content POSS is uniformly dispersed within the matrix. XRD and TEM suggest POSS is well-dispersed at the molecular scale due to a lack of evidence of POSS aggregation. This is thought to be due to the compatibility between OH-functional POSS groups and the acrylic/melamine matrix in addition to covalent bonding. The XRD spectra can be found in figure 19. Tensile experiments show that the control sample breaks before experiencing any yield point. However, with the addition of low amounts of POSS an extension in deformation occurs and strain at break increases.

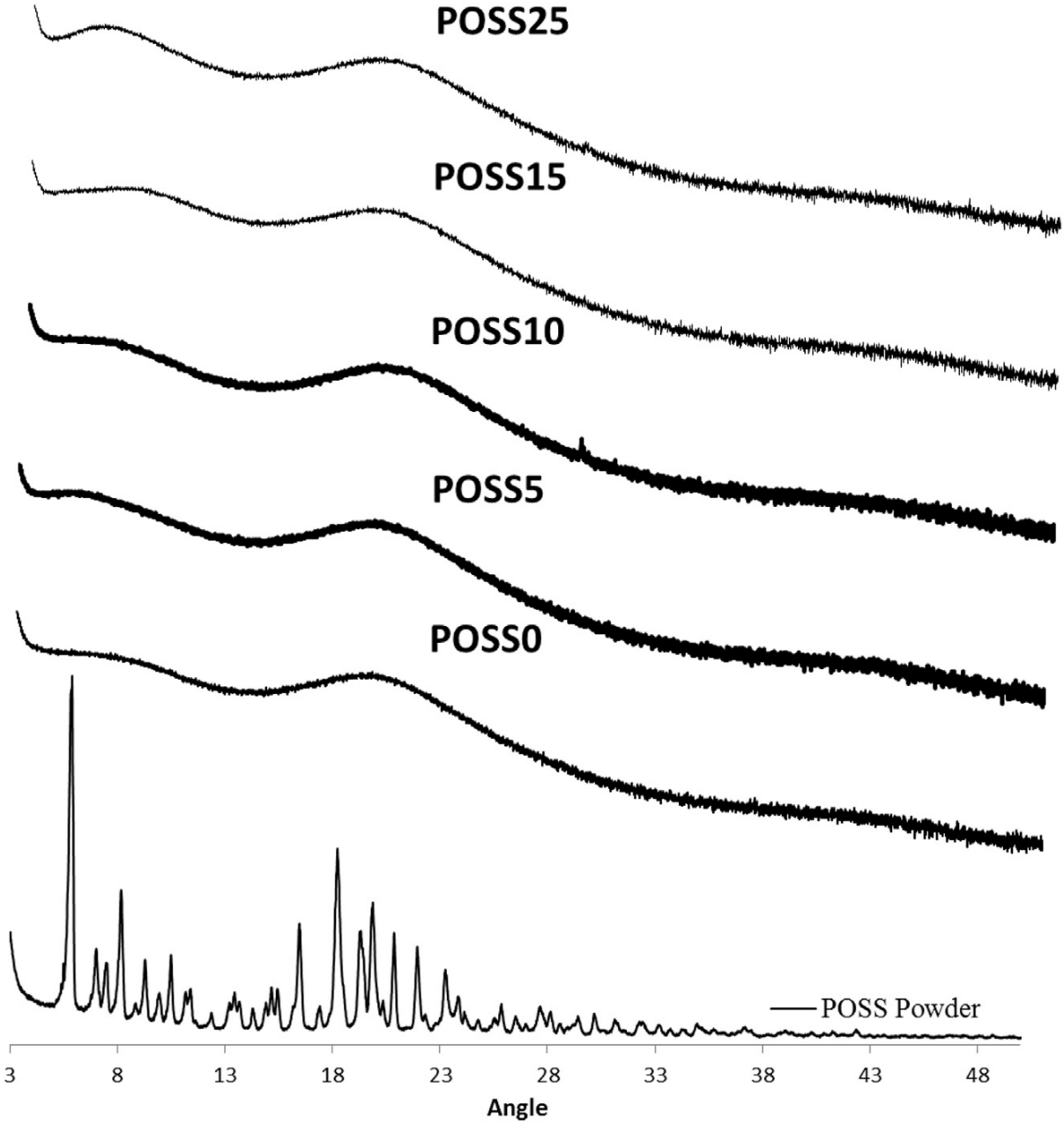

Figure 19 XRD spectra of POSS, control clearcoat and the POSS-based nanocomposite clear coats fabricated by Yari et al. [132]

At higher loadings however, brittle behaviour is once again observed. Young's modulus and toughness display a similar trend; an increase is seen up until a certain POSS loading beyond which the addition of POSS has a detrimental effect on the tensile properties. A simultaneous toughening and reinforcement is seen in this research. Considering the decrease in glass transition temperatures by POSS as measured by DMA, the toughening mechanism is thought to be due to an increase in free volume and flexibility of polymer chains. The authors propose that through the potential molecular dispersion and covalent

bonding, POSS is able to modify the polymer at the nanoscale and provide efficient stress transfer in order to reinforce the matrix.

2.4.3.4. High Strain Rate Properties

The influence of POSS on the behaviour of polymers at high-strain rates has also been studied [97,162,172–175]. Much like section 2.3.2 factors such as the type, loading and dispersion state of POSS can affect the final properties of the nanocomposite system. POSS can also be combined with other additives to form a synergistic system; Thitsartarn et al. [173] created a filler comprising of a rigid inner core (POSS) which was firmly bonded to a soft, ductile middle layer (rubber) with active functional groups to enable strong bonding to the epoxy matrix. TEM shows that the POSS-rubber particles were homogeneously distributed and that potential covalent linkages between POSS and rubber avoided phase separation, promoted better interaction and allowed synergising effects which led to mechanical enhancement. A loading of 1wt% POSS-rubber was found to be the optimum amount and resulted in increases in impact resistance, K_{IC}, tensile strength and elongation at break by ≈ 80%, 20%, 50% and more than 100%, respectively. SAXS suggested crazing and crack pinning as a result of rubber and POSS, respectively, which perhaps enabled more energy dissipation, as suggested by SEM images.

Mulliken and Boyce tested polycarbonate and a polycarbonate-POSS nanocomposite at high strain rates using aluminium SHPB. They concluded that POSS has little influence on the *α*-/glass transition but affects the *β*-motions which results in a reduction in resistance to high rate elastic and plastic deformation. DMA showed that below 15°C where the *β*-motions are restricted, the storage modulus of the neat polymer is higher and therefore the polycarbonate control sample is stiffer than the nanocomposite sample (figure 20). It was also found that the *α* contribution to the overall modulus is the same in the two systems but the *β* contribution is always less for the polymer nanocomposite, and the difference increases with increasing strain rate/decreasing temperature. Moreover, the yield stress of the nanocomposite containing 5wt% TSP-POSS is 10% less than the control sample (figure 20). This suggests that POSS locally interacts with the polymer molecules, alleviating *β* restrictions but does not create enough additional free volume to increase the mobility of large chain segments as opposed to a typical plasticiser [97].

Interestingly, Soong et al. [174] found that the addition of methacryl-POSS to PVC decreased both the α-transition temperature and the β-transition temperature i.e. POSS acted as a plasticiser and enhanced the mobility of both of these processes. This led to a decrease in yield stress with increasing POSS loading at high strain rates during compressive SHPB testing.

Kopesky et al. [162] investigated the effects of three different types of POSS: cyclohexyl, methacryl and trisilanol phenyl on PMMA, the first being a crystallisable type and the latter two both miscible at the molecular scale. Each of the three blends were able to toughen the polymer matrix in slow-speed tension tests but it was the ternary blend combining 2.5wt% cyclohexyl- and methacryl-POSS that showed the greatest increase in tensile toughness; the toughness was increased by a factor of 4 whilst maintaining the modulus of PMMA. Trisilanol phenyl POSS retained yield stress and modulus values of PMMA more than methacryl-POSS did, and is probably due to hydrogen bonding between pendant hydroxyl groups on trisilanol phenyl POSS and ester groups of PMMA. These multiple active sites are said to prevent trisilanol phenyl POSS acting as a simple plasticiser. However, both trisilanol phenyl POSS and methacryl POSS decrease T_g. The authors suggest that the increase in tensile toughness was due to a lowering of flow stress through the sample. SEM showed extensive particle-matrix debonding in cyclohexyl modified PMMA but an absence of aggregates in the miscible type POSS nanocomposites. SHPB tests showed that unfilled PMMA did not pass through its yield point before fracturing however some of the POSS/PMMA nanocomposite samples deformed well past the yield point without fracturing and that these samples exhibited reduced values of yield stress. It was only the ternary blend that demonstrated complete reproducibility of the enhanced yield behaviour. It was proposed that this was due to the synergistic mechanisms of both types of POSS that resulted in a large amount of plastic deformation necessary to form the distinct crack structure in these ternary blends, which lead to reduced flaw sensitivity.

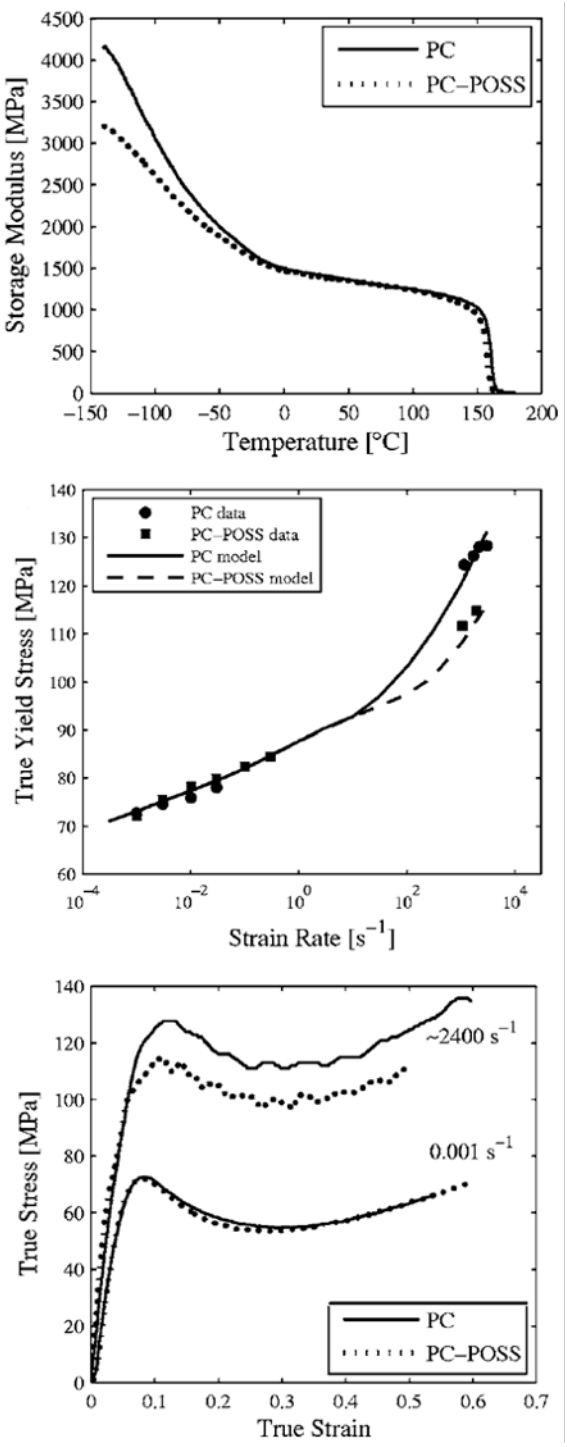

Figure 20 (a) Storage modulus of PC and PC-POSS at 1Hz, (b) true stress-strain behaviour of PC and PC-POSS and (c) True yield stress of PC and PC-POSS as measured by Mulliken and Boyce [97]

2.4.3.5. Optical Properties

Nano-sized fillers are thought to maintain the optical properties of transparent polymers due to their small size. However, this will depend on a number of factors. The dispersion of POSS greatly depends on the compatibility between polymer and nanofiller and whether the

solubility parameter of both materials matches. If POSS is well-dispersed within the polymer matrix as molecules or nano-sized aggregates, it will not have a detrimental effect on the light transmission of the polymer matrix. On the other hand, poor dispersion results in light scattering from large POSS aggregates, domains or phases, which results in a decrease in optical transparency and clarity [92,120,176–178]. Scattering can be reduced by reducing the size of POSS agglomerates to below the wavelength range of visible light (400 - 700nm) [120]. The type of POSS incorporated will also have an effect as it directly influences its dispersion within the polymer matrix [20,179–182]. Optical transparency can be measured either qualitatively (by eye) [20,92,178,181–184] or quantitatively (UV-Vis, haze meter etc.) [176,179,180,185,186]. Measuring the optical transparency qualitatively is less accurate than quantitative methods.

Zhao and Schiraldi synthesised POSS-based nanocomposites by incorporating various types of POSS into polycarbonate via melt blending. They proposed that the high compatibility between trisilanolphenyl POSS and polycarbonate resulted in transparent nanocomposites up to 5wt% POSS loading which exhibit transparency similar to that of the polymer control. However, the addition of octaphenyl-, trisilanoloctyl-, and two types of aluminium based-POSS resulted in translucent or even opaque films due to the presence of bubbles or degradation of the nanofiller. It was proposed that the silanol groups of trisilanolphenyl-POSS create particle-polymer interactions such as polar or covalent bonds which contribute to the enhanced compatibility and good dispersion. The optical properties in this study were assessed visually [92].

Tripropargyl poly(L-lactic acid) was modified by addition of N_3-POSS to create TriPOSS-PLLA nanocomposites by Cheng et al. [185]. Electron microscopy revealed the resultant nanocomposite containing N_3-POSS to have a homogeneous morphology, suggesting POSS was well dispersed within the polymer matrix. The tri-POSS nanocomposites possessed a high optical transmission (over 90%) at a wavelength of 600nm. This result is probably due to the good dispersion of POSS.

Figure 21 Appearance of control PLLA, i-POSS/PLLA and TriPOSS-PLLA/PLLA nanocomposites synthesised by Cheng et al. [185]

However, the films had a slight yellow tint to them, as shown in figure 21. PLLA nanocomposites containing octa-isobutyl POSS (i-POSS) however was white in appearance and had a light transmission of only 32%. XRD revealed characteristic diffraction peaks of i-POSS, indicating that i-POSS exists as a separate phase and tends to form aggregates within the polymer matrix due to poor compatibility between the nanofiller and polymer. Evidence of typical POSS-aggregate morphology was revealed by electron microscopy.

2.4.3.6. Physical Aging

The literature study revealed a limited amount of research into the physical aging behaviour of POSS-based polymer nanocomposites. Lee and Lichtenhan studied the thermal and viscoelastic properties as well as the physical aging process of a POSS-epoxy nanocomposite. It was found that POSS influences the motion of the molecular junctions within the epoxy matrix but not the overall deformation of the polymer chains or the crosslinking density due to the dimensions of POSS being comparable to polymeric segments. They found that the molecular level reinforcement provided by the POSS cages increased the glass transition temperature and impeded the physical aging of the polymer, as evidenced by increases in the characteristic relaxation time, τ_s, for all annealing times (0.5-64 hr) and loadings (5wt% and 10wt%) in comparison to the epoxy control (figure 22). Furthermore, it was found that after 64 hours of isothermal aging the sample had not yet reached its equilibrium point. It was noted that the width of the endothermic transition over the glass transition was unaffected by the addition of POSS suggesting that the nanofiller did not form macroscopic phase-separated domains [187].

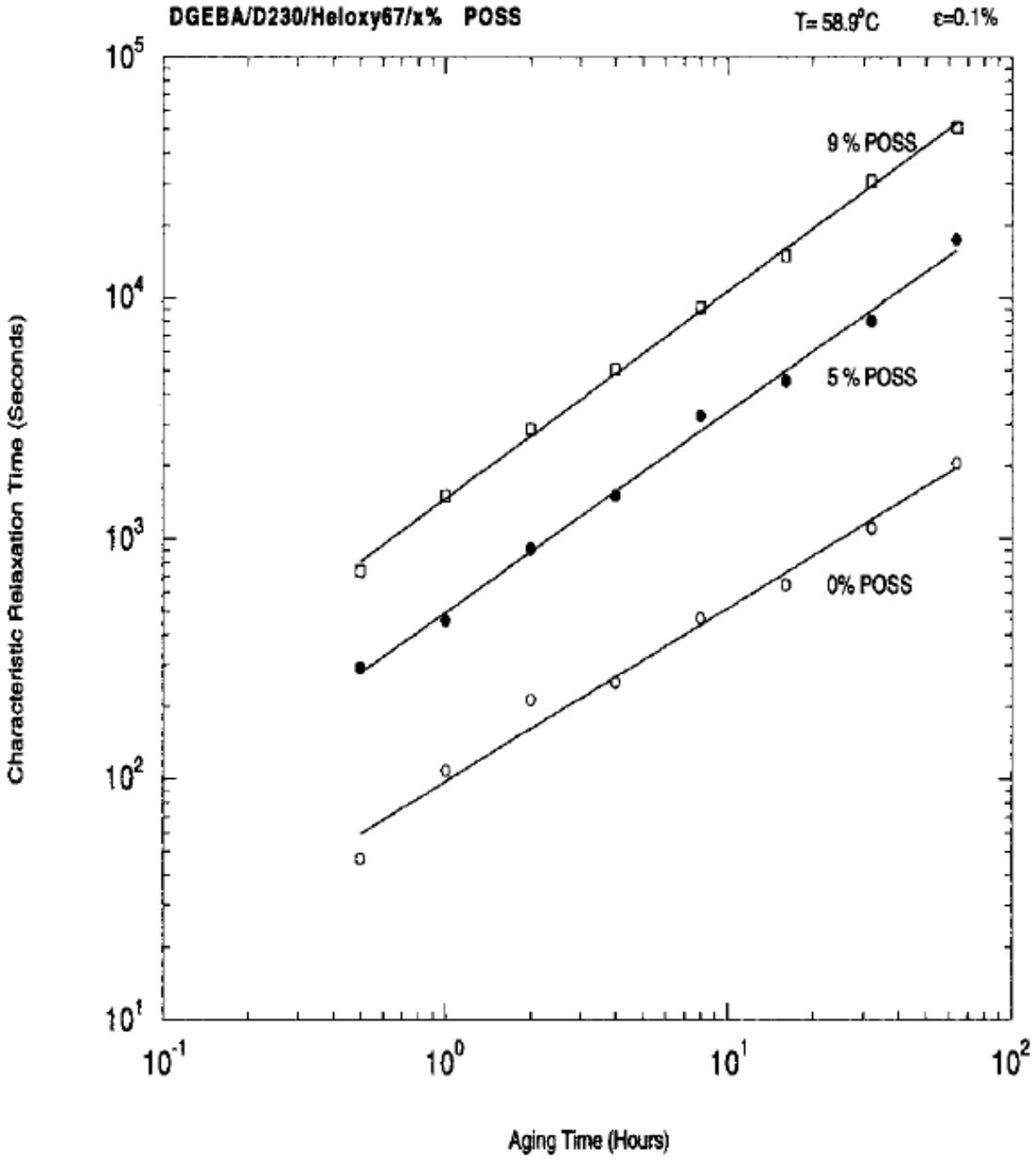

Figure 22 Characteristic relaxation time versus aging time at a testing temperature of 58.9°C for POSS-based epoxy glass fabricated by Lee et al. [187]

Yong et al. studied the effects of POSS on the physical aging and plasticisation of a polymer of intrinsic microporosity, PIM-1. Physical aging and plasticisation reduced gas permeability of polymers and therefore their suitability for gas separation membranes. Samples were aged for 120 days. It was found that the effect that POSS had on the polymer depended on its concentration in the matrix; at low loadings (0.5wt%-2wt%) POSS nanoparticles enhanced gas diffusivity by disrupting chain packing and increasing free volume while at higher loadings (≤5wt%) POSS increased chain rigidity, increasing selectivity and enhancing

gas separation performance, as indicated by PALS (positron annihilation lifetime spectroscopy). SEM-EDX revealed a uniform dispersion of silicon in the polymer matrix when POSS loading was less than or equal to 10wt%. At 20wt% the results suggested POSS agglomeration. XRD indicated that when POSS loading increases from 2wt% to 10wt%, the polymer packing and chain structure may become denser. It was found that the addition of POSS nanoparticles suppressed physical aging and that the embedded rigid POSS nanoparticles may slow down segmental motion of polymeric chains [188].

2.5. Summary and Further Research

Since polymer nanocomposites were first created, research into these novel and unique materials has flourished. Due to their large interfacial area, nanofillers have the potential to modify polymeric materials at the nano- and molecular-scale, resulting in more efficient enhancement by increased interaction sites. Polymer nanocomposites have potential in many applications and areas of research such as aerospace, defence, medical and many other fields.

It has been found that many factors affect the final properties of polymer nanocomposites, the key element being the dispersion state of the nanofiller within the polymer matrix. Good dispersion is vital for maximal enhancement of the polymer and can be enhanced by a variety of methods such as functionalisation of the nanofillers and mechanical mixing. Presence of aggregates in a polymer matrix can have a detrimental effect on the overall properties of the polymer. The processing method and polymer type must also be taken into account when fabricating polymer nanocomposites.

A more detailed literature review was conducted to explore the area of research of POSS-based polymer nanocomposites and their physical properties. Polyhedral oligomeric silsesquioxane (POSS) is a distinctive nanofiller. Conceptually, it can be considered as either a filler or a molecule; it is rigid and inert like an organic filler yet it has the potential to molecularly dissolve in a polymer matrix as 1-3nm sized molecules. Moreover, it can be tailored accordingly to the polymer system and the function it is required to improve. This makes it a highly versatile nanofiller with many applications.

POSS generally affects the mechanical performance of polymers by either plasticisation or reinforcement of the matrix. The bulky, rigid structure of POSS modifies the polymer matrix

by one of two mechanisms; it can increase the free volume of a polymer by locating itself between the polymer chains, thus reducing their entanglement and increasing their mobility, which is evidenced by a decrease in glass transition and an increase in ductility, at the detriment of strength (plasticisation). Alternatively, POSS can restrict chain movement and reinforce the matrix which results in increases in stiffness and tensile strength but a reduction in flexibility. In some cases, the addition of POSS can simultaneously improve strength and ductility of a polymer to create a toughened material. The type of the original polymer matrix can dictate which mechanism is dominant; glassy polymers will generally experience a plasticising effect whereas in rubbery systems, the prevalent effect is reinforcement. To aid in achieving good dispersion, the polarity of both the POSS and polymer systems must be matched. Compatibility between the two is necessary in overcoming POSS-POSS interactions and avoiding the formation of large POSS aggregates. By selecting the most suitable POSS molecule depending on its R groups, dimensions and cage structure, good dispersion can be achieved and may even result in dispersion at the nanoscale. For transparent polymer nanocomposites in personnel applications this is desirable to maintain good optical transparency whilst improving mechanical properties.

Overall, polymer nanocomposites show promise in many applications. The unique properties and versatility of nanofillers provide many ways to enhance polymeric materials, whilst utilising and maintaining the desirable properties of polymers such as low mass, low cost and flexibility.

Further research is still required to fully understand POSS-based polymer nanocomposites and determine their potential applications. Below are several areas that have been identified which could benefit from further research:

- **The preparation method and processing techniques used to create POSS-based polymer nanocomposites:**

A deeper understanding of how the preparation methods and processing techniques affects the final properties of the polymer nanocomposites is necessary to understand how the many factors involved in synthesis affect the final properties of the polymer nanocomposite system. Some studies show that physical mixing is a less superior method of preparing POSS-based polymer nanocomposites than methods such as polymerisation as chemical

bonding between the two materials is less likely to occur [50]. However, this is not always the case and chemical bonding is not always necessary to create an effective nanocomposite if good compatibility exists between filler and polymer [54];

- **Polymer-POSS compatibility:**

A more comprehensive understanding of the compatibility between different types of POSS and different polymers would also be useful in order to better understand the resultant nanocomposite system. To gain such an understanding would promote uniform dispersion and maximise the enhancement of the polymer and/or achieve the desired results;

- **Effect of POSS on optical properties:**

Further research is required to broaden our understanding of the effect that POSS has on the optical properties of transparent polymers;

- **Multi-technique studies of POSS-based polymer nanocomposites:**

It would also be useful to have more extensive studies involving various techniques providing results on for example, the optical, and mechanical and viscoelastic properties of one specific polymer/POSS system. This would be useful in determining the possible applications of such a system;

- **High strain-rate performance of POSS-based polymer nanocomposites:**

The mechanical properties of polymer nanocomposites have been substantially researched; however, there are not nearly as many publications on the performance of such nanocomposites at high strain rates/frequencies.

Our research will involve the modification of a transparent polycarbonate by trisilanol phenyl POSS for the intended use in transparent armour applications for personnel. This will involve characterising several physical aspects of the system by assessing the effect that POSS has on the optical, mechanical and thermal properties of polycarbonate as well as its impact performance at high-strain rate. A preliminary investigation into the physical aging behaviour of the nanocomposites will also be carried out to provide some information on how the nanocomposite would fare in extreme environments.

Chapter 3

Experimental Methods

Chapter 3 Experimental methods

3.1. Materials

Three linear, high-flow polycarbonate homopolymer resin of the same molecular weight, M_w were used as the polymer matrix. The nanofiller trisilanol-phenyl polyhedral oligomeric silsesquioxane (TSP-POSS) was incorporated into the polymer matrix at different loadings. Figure 23 shows the chemical structure of the polymer and the nanofiller; TSP-POSS possesses an open-cage structure and phenyl R-groups. Both materials are white powders in appearance.

3.2. Preparation procedures

3.2.1. Synthesis of polymer nanocomposites

TSP-POSS-based polycarbonate nanocomposites containing 0.05wt%, 0.1wt%, 0.3wt%, 0.5wt% and 1wt% TSP-POSS were fabricated via a multi-step process. Firstly, a pre-dispersion technique was used to combine the polymer and nanofiller prior to extrusion which involves: 1) Measuring 100 g polycarbonate powder and pouring it into a tray covered with tinfoil, 2) dissolving 0.05 g – 1 g TSP-POSS in 40 ml of ethanol using a magnetic stirrer and hot plate at approximately 40°C, 3) spraying the ethanol/TSP-POSS solution onto the polycarbonate powder using a generic spray bottle and 4) transferring the powder mixture into a plastic beaker and placing in an oven at 40 °C for three weeks to evaporate the ethanol and dry the mixture. Following this, the polymer-nanofiller mix was extruded using a Rondol Technology 10 mm microlab co-rotating twin screw extruder with a 20:1 L/D ratio which is a typical L/D ratio used in many extruders. Figure 24 contains an image and a schematic of the mini-extruder. (A) is the hopper where the polymer/nanofiller mixture is poured, (B) contains the feeder screw which introduces the mixture into the barrel of the extruder (C) which contains the twin screws, (D) is the die and is where the extruded material exits the extruder, where it is then fed into a granulator (E) which cuts the material into pellets. The speed of the feeder screw and twin screws can be controlled and the conditions can be found in table 1, alongside the temperature profile of the extruder barrel. The barrel of the mini-extruder contains fives zones. Each zone was set at a different temperature, with the temperature increasing with ascending zone number to ensure that the material is thoroughly melted before passing through the die.

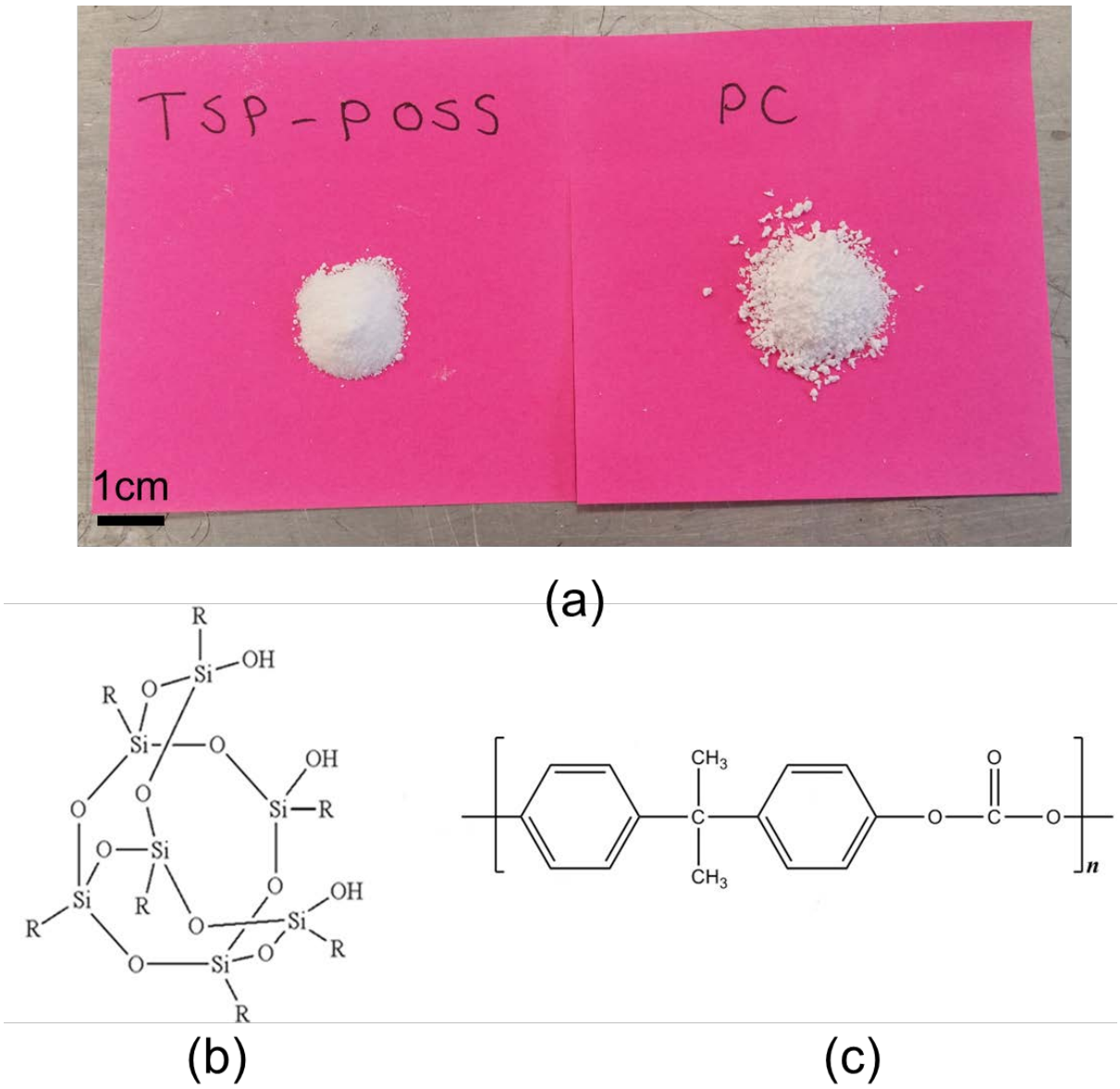

Figure 23 (a) Polycarbonate resin and POSS powder, and the chemical structure of (b) trisilanol-phenyl POSS [189] **and (c) polycarbonate**

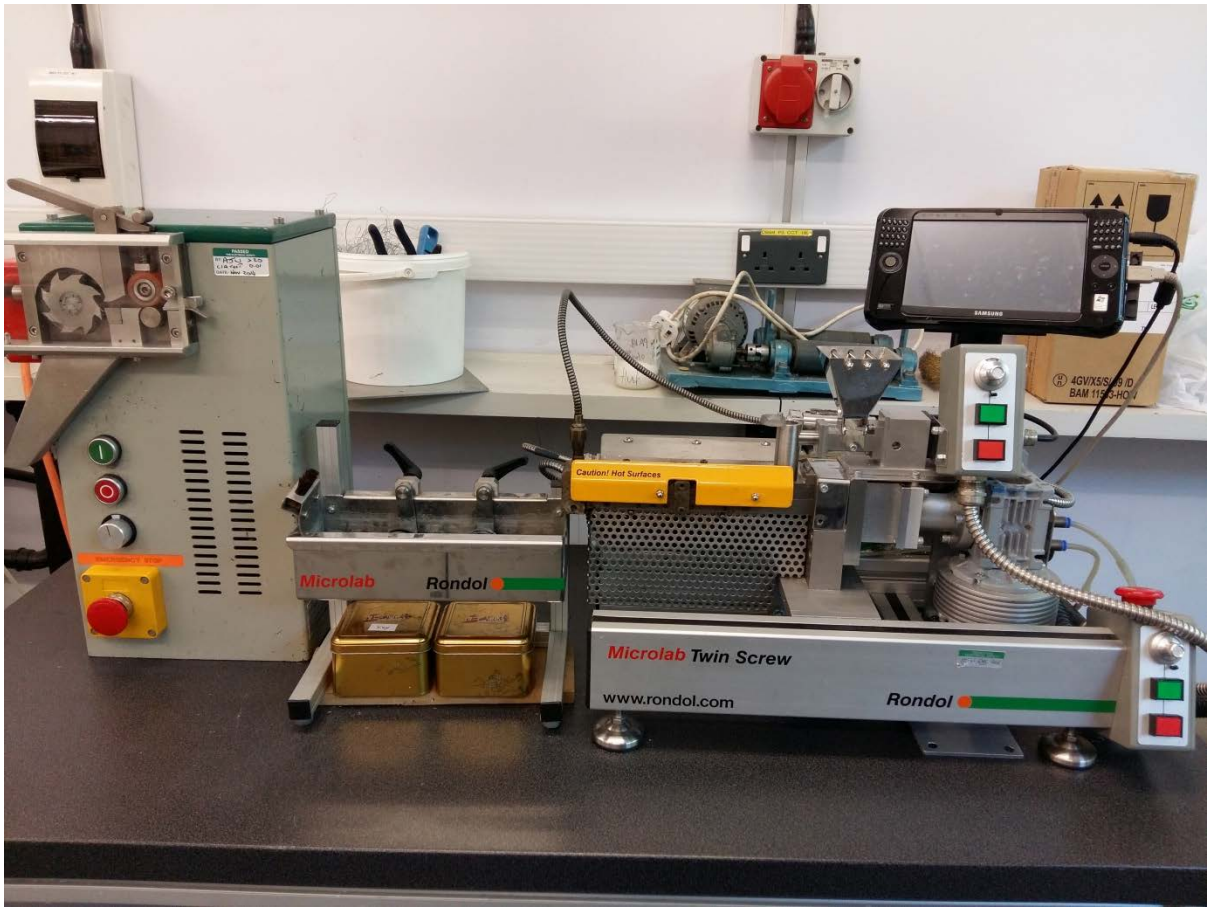

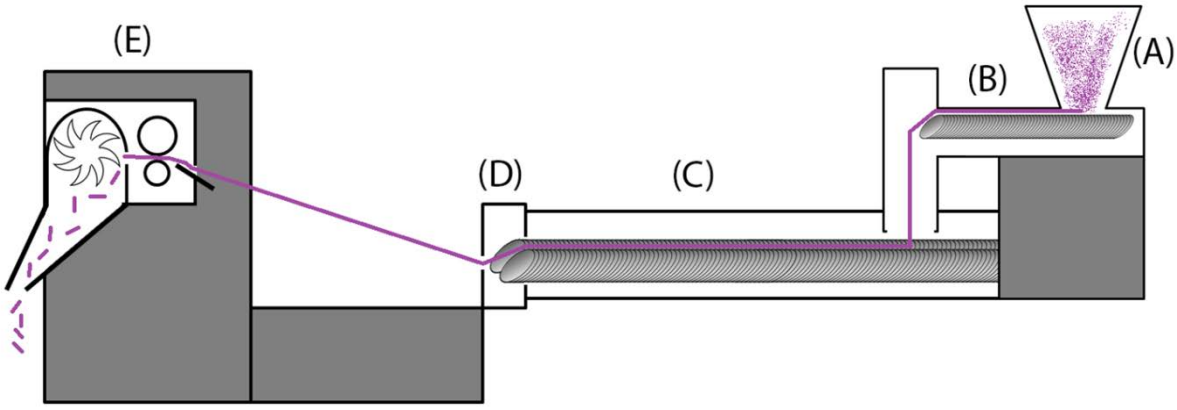

Figure 24 The mini-extruder: (a) hopper, (b) feeder screw, (c) twin mixing screws, (d) die and € granulator

Zone	Temperature (°C)
1	185
2	230
3	240
4	250
5 (Die)	260

Feeder screw speed	Twin screw speed (rpm)
7	80

Table 1 The temperature and screw speed conditions used in the extrusion of polymer nanocomposites

The extruded material was drawn out of the barrel and cut into fine pellets by a granulator. The pellets could then be moulded to produce samples of various shapes and sizes (see figure 26). A flow chart of the whole preparation process can be found in figure 25.

3.2.2. Sample preparation for characterisation and testing

A Collins hydraulic press (fig. 27) was used to compression mould the pellets at a temperature of 270 °C and a maximum pressure of 200 bars. Before applying the pressure, the material was pre-melted under the top plate of the press. Pre-melting was found to reduce the presence of bubbles in the final product. The pre-melted material was then sandwiched between two metal plates and placed in the press. Kapton film was used between the material and the plates. An initial pressure of around 40 bar was applied prior to 200 bars for three minutes and released to allow any trapped air to escape.

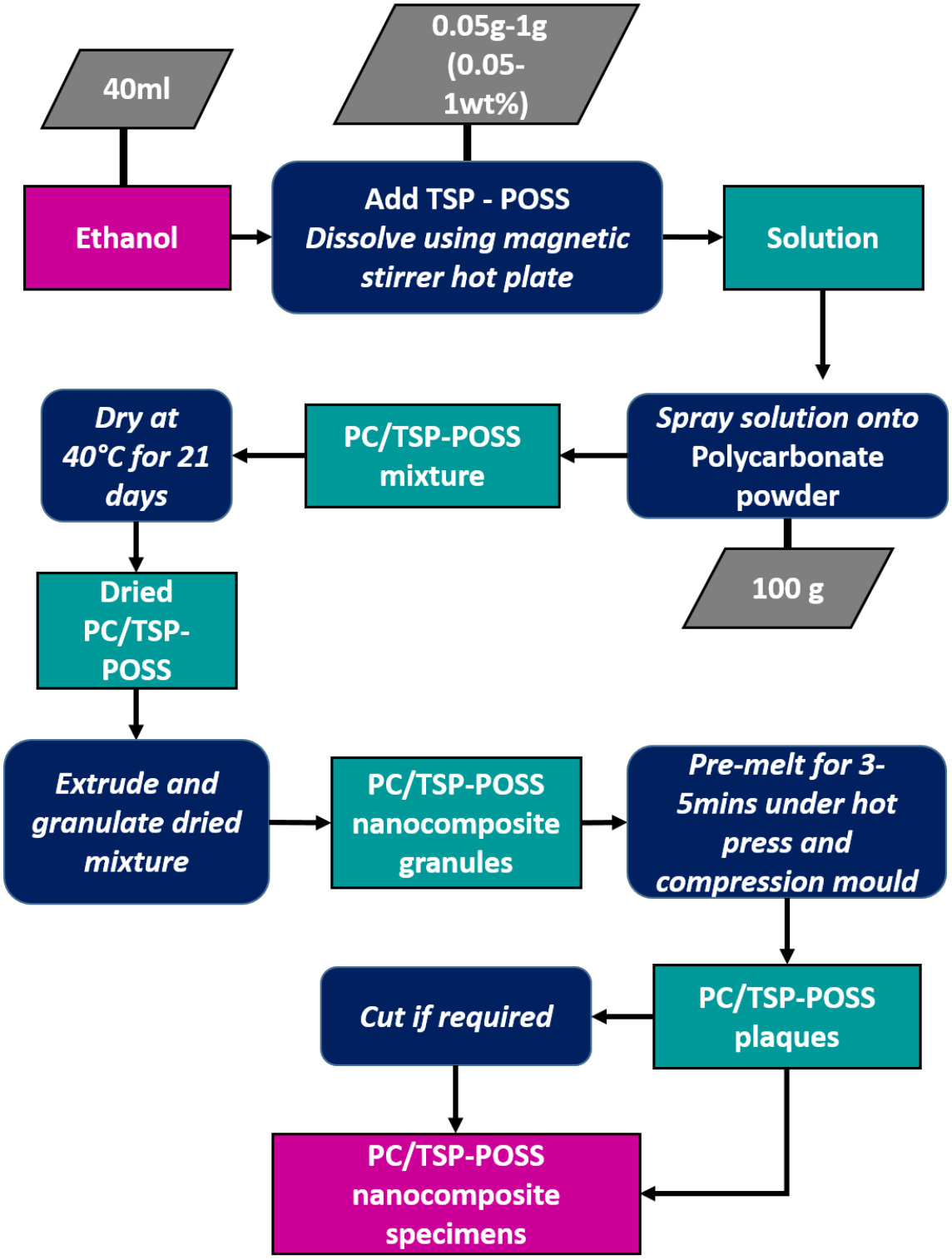

Figure 25 Flow chart of nanocomposite preparation method

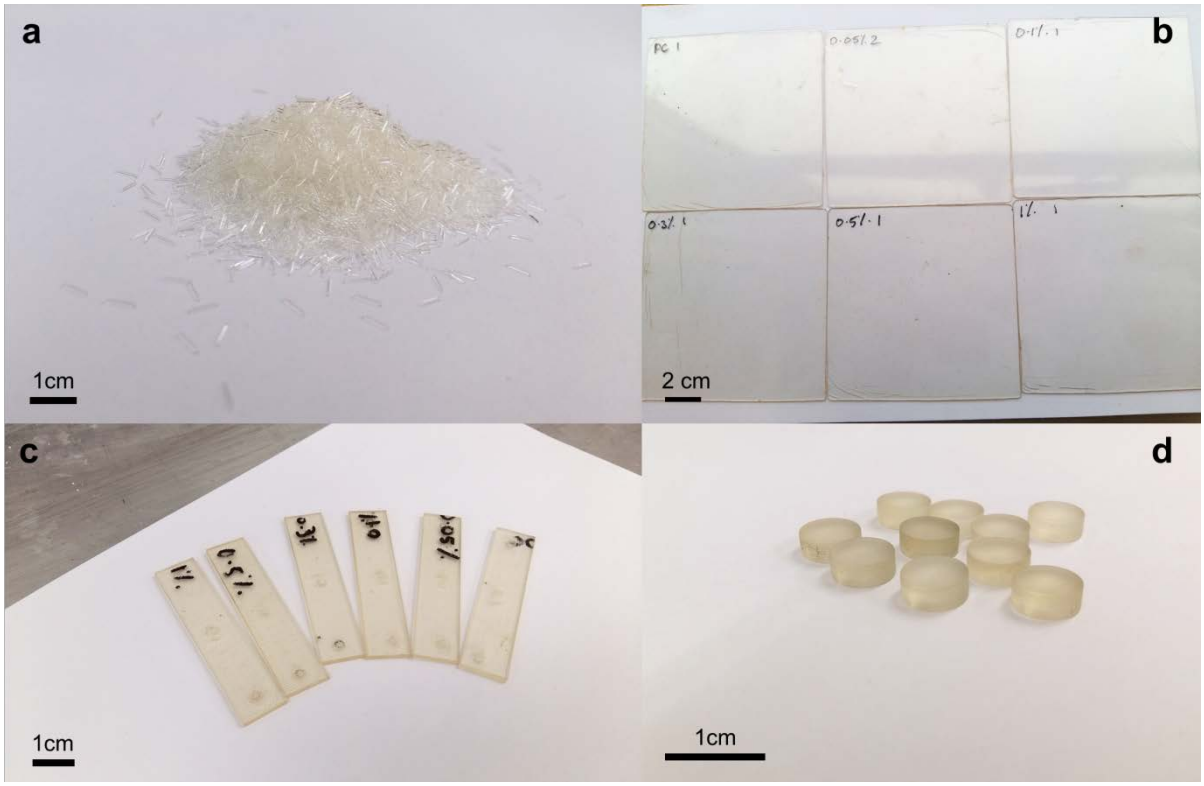

Figure 26 a) granulated material, b) compression moulded samples, c) DMA specimens and d) SHPB specimens

A maximum pressure of 200 bar was then applied to the material for a further three minutes, where it was then transferred rapidly to cooling plates to fully solidify before removal from the mould. Samples of 1 mm and 2 mm thickness were moulded using 1mm or 2mm thick moulding plates and, depending on test type, were subsequently cut using a band saw to the specific size/standard required.

Prior to compression moulding and all subsequent testing, samples were annealed in an oven at 110 °C for at least 24 hours to remove as much residual moisture as possible. Some polymers such as polycarbonate absorb moisture readily from the atmosphere. During compression moulding, the high temperatures result in hydrolysis of the moisture which lead to air bubbles from water vapour and CO_2. Air bubbles are detrimental to the mechanical properties. Moreover, hydrolysis also turns the material to a yellow or brown colour which is not ideal for optically transparent applications [76,190,191].

Figure 27 A Collin hydraulic press located in the Materials department, Loughborough University [192]

3.3. Characterisation Techniques

3.3.1. X-Ray Diffraction

The effect TSP-POSS has on the structure of polycarbonate was studied using X-ray diffraction. X-ray diffraction (XRD) is an analytical technique used to identify and characterise materials. XRD can provide information on the structure and unit cell dimensions of a crystalline material. It is a rapid and powerful tool that requires minimal sample preparation and, provided a reference database is available, data analysis is relatively simple to do.

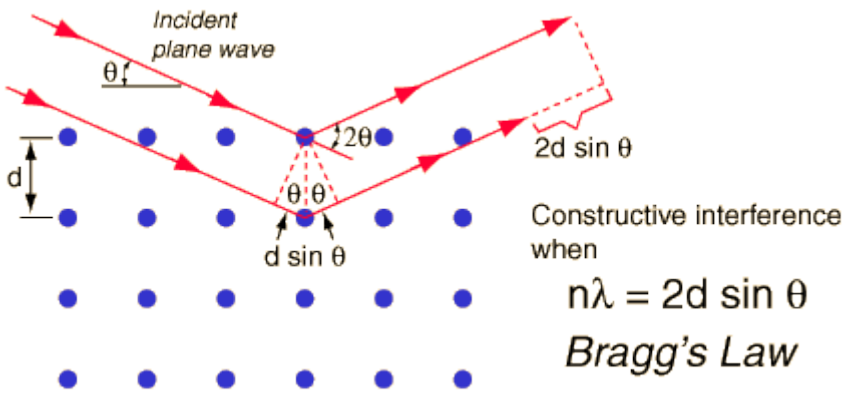

Figure 28 Bragg's Law [193]

Firstly, x-rays are directed onto the specimen where they interact at the atomic scale and scatter as a result. Scattered x-rays will then interfere; constructive interference or Bragg diffraction occurs when Bragg's law, $n\lambda = 2d\sin\theta$, is satisfied: λ is the wavelength of the x-rays, d is the lattice or *d*-spacing, θ is the scattering angle and n is an integral number. For constructive interference, Bragg's law states that the path difference between two scattered x-rays, $2d\sin\theta$, is equivalent to an integer multiple of the wavelength. It relates the electromagnetic radiation wavelength to the lattice spacing in a crystalline sample. On completion of the scan through a range of 2θ angles, a diffraction pattern consisting of a series of peaks is obtained. The angles at which Bragg's law is satisfied and constructive interference has occurred will give rise to very intense peaks in the spectra called Bragg peaks. The diffraction pattern will be unique to a material and can be used to identify a material by converting to d-spacing values using Bragg's law [194].

Figure 29 X-ray diffractometer located in the Physics department, Loughborough University [195]

A Bruker D2 Phaser bench-top X-ray diffractometer (fig. 29) using CuK_{α} radiation (λ = 1.5406 Å) was used at ambient temperature. Solid samples cut from 1 mm thick plaques were scanned from 1 to 40° in 0.02 increments. A receiving angle of 5.8° and 1 mm divergence slit were found to be ideal.

3.3.2. Electron Microscopy

Electron microscopes use a beam of high-speed electrons to form an image of a specimen. Higher magnification and better resolution can be achieved with electron microscopes compared to traditional light microscopes, where structures an order of magnitude smaller than the wavelength of light can be imaged. This is because electrons have a shorter wavelength than photons. As the resolving power of a microscope is inversely proportional to the wavelength of the radiation used, it follows that an electron microscope will have a better resolution than that of a light microscope. Furthermore, if the electrons are accelerated to higher velocity the wavelength of the particles will decrease and the resolution of the microscope will increase. This is the basis of electron microscopy.

Different lenses to those used in light microscopes are used to focus the electron beam. In light microscopes glass lenses are used however, these have no effect on an electron beam. Instead, electromagnetic lenses are used and consist of a solenoid. By passing current directly through the solenoid, the electron beam can be controlled by the electromagnetic field that is induced. As the electron beam passes through the lens, any stray electrons are focused by changing the current passing through the solenoid. The resolution of the microscope is controlled by the accelerating voltage of the electron beam and is usually quoted in kilovolts (kV) [196].

3.3.2.1. Field Emission Scanning Electron Microscopy

Scanning electron microscopy (SEM) can be used to examine the morphology of a sample as well as reveal information about its chemical composition.

A beam of accelerated electrons is focused on the specimen. The high kinetic energy of the incident electrons allows them to interact with the surface or near-surface atoms of the sample, causing the electrons to decelerate. The dissipation of energy results in the generation of a variety of signals. These can include secondary electrons (surface electrons emitted due to excitation by the primary electron beam), backscattered electrons, and diffracted backscattered electrons, photons (characteristic x-rays), visible light (cathodoluminescence), transmitted electrons and heat. Secondary electrons are used to generate high-resolution images of the sample morphology (micrographs) in the standard imaging mode, secondary electron imaging (SEI).

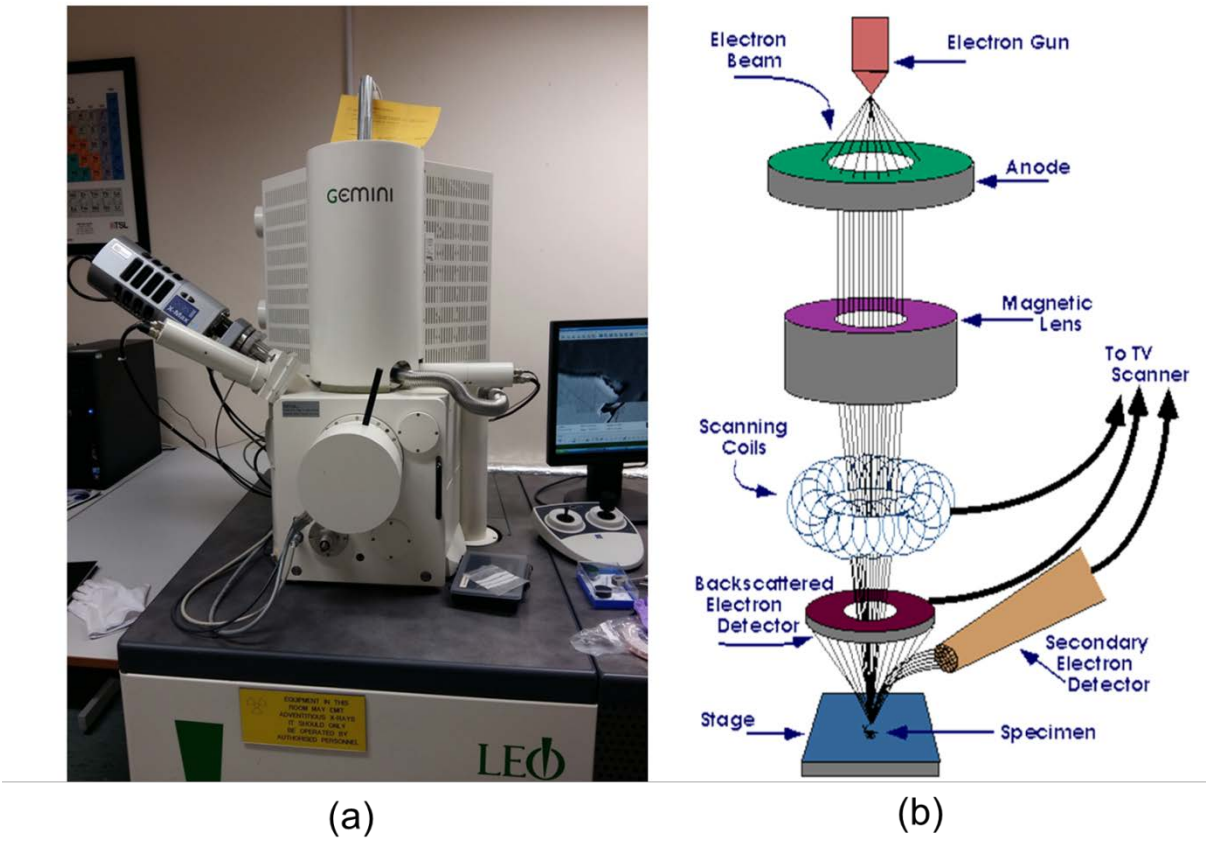

Figure 30 (a) FEGSEM located in the Materials department, Loughborough University and (b) a schematic of an SEM [197]

By using an energy-dispersive detector (EDS), the spectrum of the characteristic x-rays can be separated to give information on the specific elements present [198]. The SEM has a depth of field over a hundred times that of a light microscope and can provide images of the bulk of the specimen. Values beyond 100,000 X can be achieved.

An SEM consists of several components (figure 30(b)). An electron source (gun) generates the electron beam which is then focused to a smaller diameter by electromagnetic lenses. The beam targets a specimen, which has been mounted onto a stub and secured in place on the sample stage. Rather than forming a real image as in the case of a light microscope, the image is built up by scanning the electron beam in a raster pattern over the sample surface and then displayed on a cathode ray tube. Magnification of an SEM is calculated by the ratio of the image display size to the sample area scanned.

Several different types of detectors are required to distinguish the variety of signals generated and the specific capabilities of an SEM will depend on the detectors installed. An

SEM also requires infrastructure such as cooling systems and vacuum systems to prevent overheating and allow the electrons to travel in a straight line from the electron source to the sample.

The morphology and fracture surfaces of polycarbonate and its TSP-POSS based nanocomposites were characterised by a Carl Zeiss 1530 VP field emission gun scanning electron microscope (FEGSEM) (figure 30(a)). Samples of 1 mm thickness were freeze fractured: firstly, they were submerged in liquid nitrogen for 60 s and then snapped whilst holding both ends with pliers. Freeze fracturing can help to attain a smoother fracture surface. A smooth fracture surface makes is easier to view the structure of polycarbonate and the nanocomposites and assess the dispersion of TSP-POSS within the polymer matrix. The freeze fractured samples were mounted on stubs using electrically conductive carbon adhesive discs. Silver paint was applied to the sample where it was in contact with the metal stub in order to increase sample conductivity. Mounted samples were then sputter coated with Au/Pd for 60 s using a Quorum Q150T ES sputter coater to improve imaging resolution by preventing build-up of static charge and increasing the electrical conductivity of the insulating specimens. SE2 (secondary electron imaging) and In-Lens detectors were used with a 5 kV beam current to view the samples with minimal burning of the sample.

3.3.2.2 Transmission Electron Microscopy

Transmission electron microscopy involves partially transmitting an electron beam through an ultrathin specimen in order to gain information about its structure. A black and white image is built up on a phosphorescent screen, photographic plate or a light sensitive sensor such as a charge-coupled device (CCD) located below the sample. The spatial variations in the information carried by the beam forms the image. Some of the electrons are deflected or stopped by the material. These form dark spots on the image. The transmitted electrons will form bright spots and variations of grey depending on how much they have interacted with the sample. The image can then be displayed on a monitor in real-time.

TEM has a higher resolution than SEM, typically an order of magnitude higher, and can image structures less than 1 nm in size. It is ideal for determining the positions of atoms as well as visualising the local state of the dispersion of a nanofiller within a polymer matrix [196,199].

In order to gain the best imaging conditions, samples ideally need to be thin enough for electron transmission, possess high contrast, be able to withstand electron beam irradiation, be uncontaminated and non-volatile. However, it is unlikely that all criteria will be satisfied. A number of methods can be used to overcome these obstacles such as cleaning and drying the samples, staining low contrast samples, coating to avoid charging and damage of samples [200].

A Jeol 2000FX TEM was used to assess the dispersion of the POSS nanofiller within the polycarbonate matrix. Thin films of the control sample and nanocomposites were prepared by ultramicrotomy. The resultant thin films were then collected onto metal mesh "grids".

3.3.3. Gel Permeation Chromatography

Gel permeation chromatography (GPC), or size exclusion chromatography is a separation method used for chemical analysis.

A chromatography system employs a column, capillary or some other container containing a mobile and a stationary phase. The sample is dissolved in the mobile phase and is passed through the stationary phase. The time taken for different molecules to leave the container will vary and will result in the separation of the various constituents.

In GPC, the separation mechanism relies solely on the size of polymer molecules and is ideal for measuring the molecular weight distribution of polymeric materials. By separating out the different lengths of polymer chain present in a sample a relative length can be calculated. An organic solvent is used as the mobile phase and a column contains the stationary phase (usually polymer beads).

Firstly, the polymer sample is dissolved into an organic solvent where the polymer chains coil into a sphere, with the size of the sphere depending on the molecular weight of the polymer. The coiled spheres are then introduced into the mobile phase where they flow into the GPC column and are carried past the beads, which are porous. Those sphere coils that are larger than the largest bead pores will be carried straight past the beads. However, spheres that are smaller will be able to enter these and if they are small enough, they will be able to enter smaller pores and can potentially occupy all of the stationary phase.

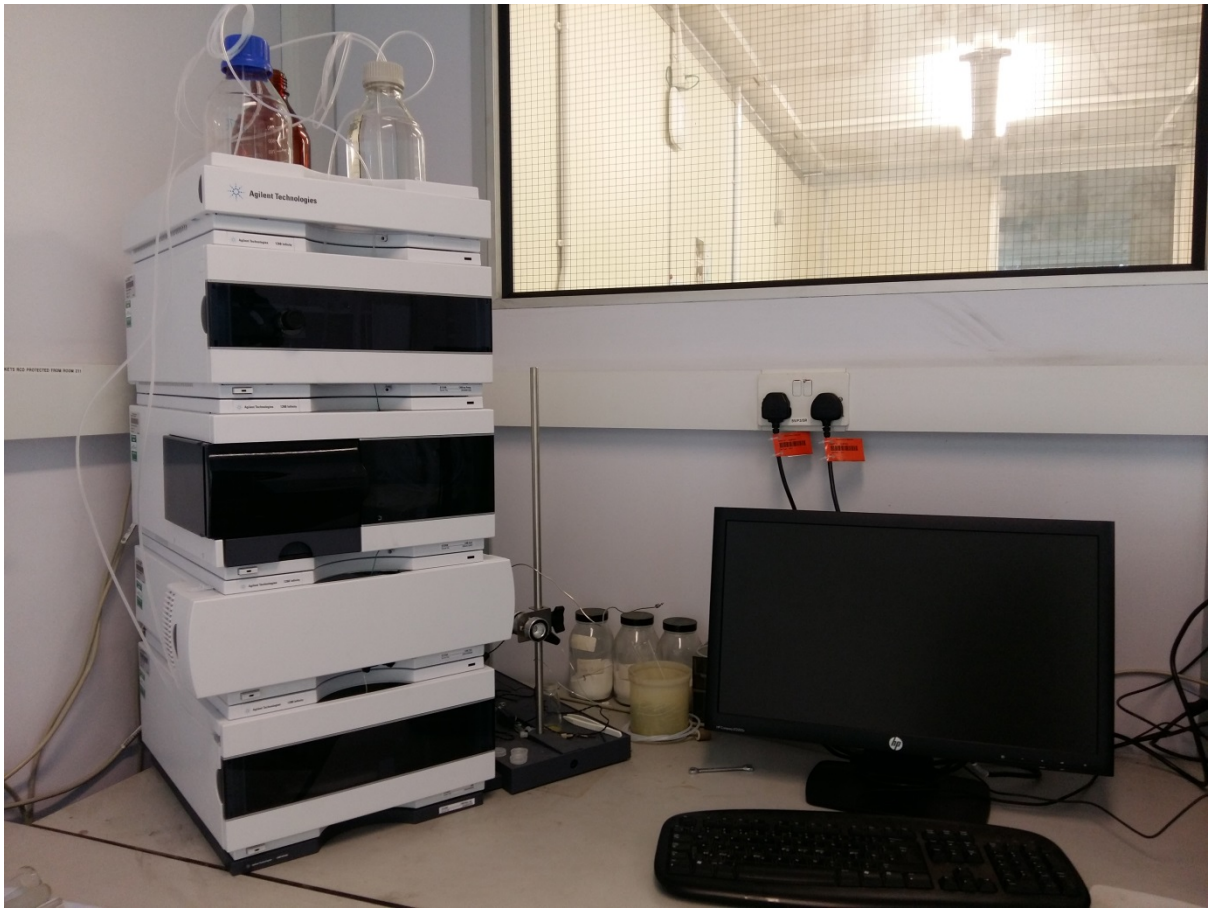

Figure 31 Agilent Technologies 1260 Infinity GPC located in the Materials department, Loughborough University

As the mobile phase containing the polymer sample flows through the column, this partitioning occurs repeatedly, with the molecules diffusing into and out of the pores. Therefore, the time it takes for the different sized molecules to transit the column will vary, with the larger spheres eluting in less time. As the components leave the column they are detected and a graph, or chromatogram, is produced to display the eluting behaviour. Higher molecular weight polymers will elute first followed by those of a lower molecular weight emerging from the column later.

The chromatogram is compared to a calibration graph containing the molecular weight of a series of polymers. From the calibration graph, the molecular weight distribution of the polymer sample can be determined [201].

An Agilent Technologies 1260 Infinity GPC (fig. 31) was used to confirm the molecular weight distribution of the three different grades of polycarbonate tested. 4mg of each polycarbonate resin was dissolved in tetrahydrofuran (THF) in a vial. The concentration was

2.2 mg/ml for each sample. Three chromatograms were produced and compared to a calibration graph in order to determine the molecular weight distribution of the samples.

3.3.4. Thermogravimetric Analysis

Thermogravimetric analysis (TGA) is a method of thermal analysis in which the mass of a sample is monitored as a function of temperature or time in response to heating or cooling. TGA can be used to characterise materials, provide information on any physical or chemical phenomena such as second-order phase transitions or oxidation and determine the presence of organic (or inorganic) content in a material.

A TGA consists of a furnace containing a sample pan supported by a precision balance. The pan is heated or cooled and the mass of the sample monitored throughout the temperature program. An inert purge gas is used to control the sample environment and prevent undesired reactions such as oxidation [202].

A TA Instruments Q5000 IR TGA (fig. 32) was used to characterise any differences between the three polycarbonate grades by measuring the weight percentage lost during thermal decomposition. Ten milligrams of each polycarbonate resin was placed in a platinum crucible and tested from 37 °C to 800 °C using a heating rate of 10 °C/minute. Air was used as the purge gas at 25 ml/min. Raw data of the weight (*%*) and derivative weight *(%/°C*) of sample degraded during heating was plotted into graphs of weight or derivative weight versus temperature and analysed.

Figure 32 TGA located in the LMCC, Materials department, Loughborough University [203]

3.3.5. Dynamic Mechanical Analysis

A TA Instruments Q800 DMA (fig. 33) was used to evaluate the glass transition and the viscoelastic properties of polycarbonate/TSP-POSS by measuring the dynamic mechanical response to temperature and frequency.

Viscoelasticity is studied using dynamic mechanical analysis (DMA), where a small sinusoidal stress is applied and the resulting strain is measured. The complex, or dynamic, modulus can subsequently be determined and is the ratio of stress to strain under vibratory conditions. The temperature or frequency of stress can be varied, which leads to variations in the complex modulus. Information on glass transitions, creep and stress relaxation, changes in crystallinity, occurrence of cross-linking, impact resistance, chain dynamics and features of polymer chains can be obtained via DMA.

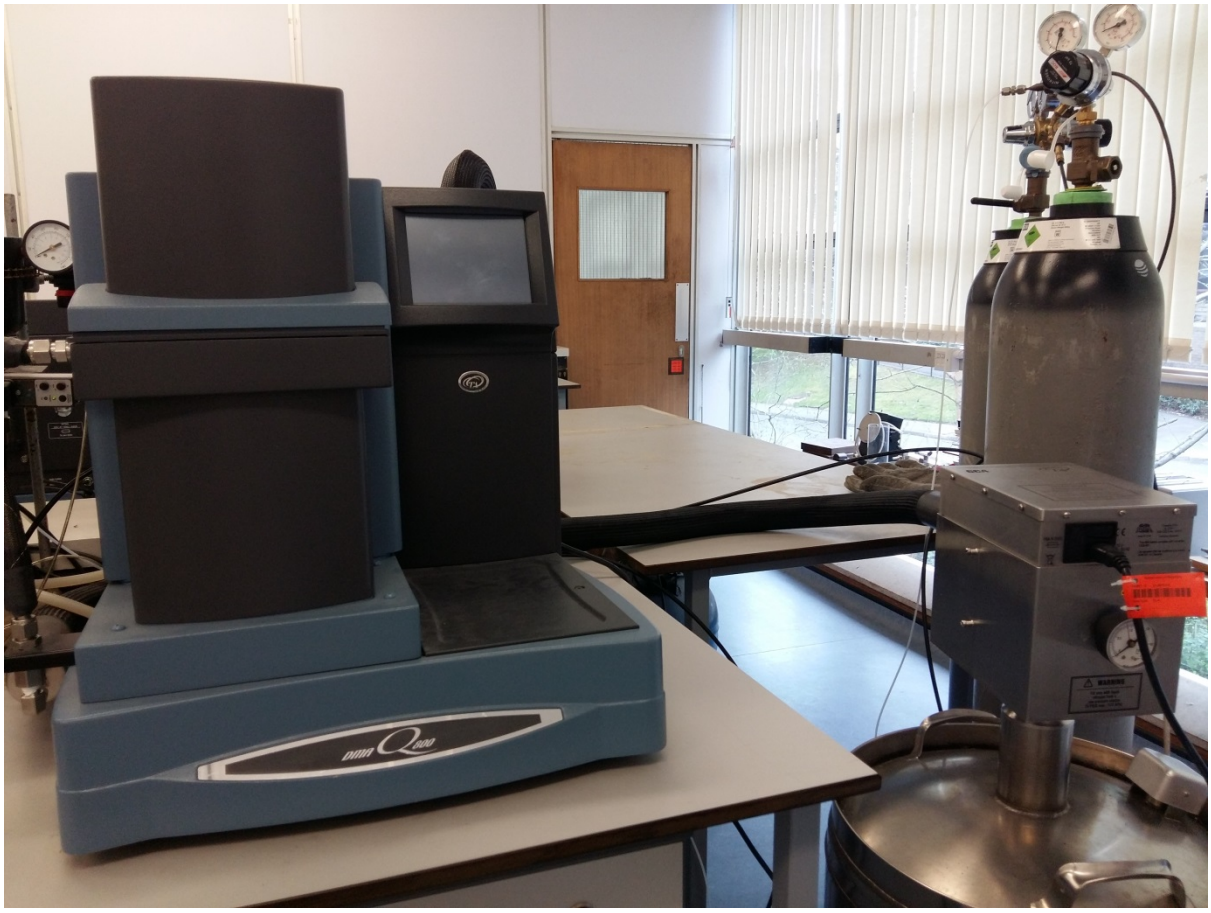

Figure 33 DMA located in the Materials department, Loughborough University

In a DMA instrument a bar-shaped sample with dimensions: 35 mm x 13 mm x 2 mm (length x width x thickness), is clamped at both ends and held in place in a thermal chamber. A sinusoidal oscillating deformation force is applied to the central point of the sample by a drive motor. The stress experienced by the sample is proportional to the current supplied to the drive motor and the strain is proportional to the resulting sample displacement and is measured by a transducer. Different clamping configurations and deformation modes (e.g. compression, shear, tension, and torsion) allow a range of tests to be carried out on a variety of materials using DMA. For example, hard samples or samples with a glossy surface are held in place by clamps with teeth; soft materials and films are held in place by flat clamps so as to avoid any damage to the sample.

The stress and strain of elastic materials are in phase as they are proportional to one another at small deformations, therefore the response of one caused by the other is immediate. Such a response is independent of strain rate. For viscous materials there is a

phase difference between stress and strain; the strain lags the stress by 90° (π/2). As viscoelastic materials exhibit behaviour between that of purely elastic and purely viscous materials there will be some phase lag between the applied stress and the strain within the material.

The applied sinusoidally varying stress, $\sigma(t)$, of frequency, ω is given by

$$\sigma(t) = \sigma_0 \sin(\omega t + \delta) \qquad (1)$$

It precedes strain by a phase angle, δ. The constant σ_0 is the amplitude of maximum stress. The induced sinusoidal strain within the material is

$$\varepsilon(t) = \varepsilon_0 \sin \omega t \qquad (2)$$

with the amplitude of maximum strain given by ε_0. A ratio between the above stress and strain can be used to determine the dynamic modulus and is as follows:

$$E^* = \frac{\sigma(t)}{\varepsilon(t)} \qquad (3)$$

The dynamic modulus has two components

$$E^*(\omega) = E'(\omega) + iE''(w) \qquad (4)$$

The storage modulus, $E'(\omega)$, measures the stored energy and represents the elastic portion of the material. It characterises the ability of a polymer to store energy i.e. it represents elastic behaviour. The second component of dynamic modulus, $E''(\omega)$, is the loss modulus and is defined as the tendency of a material to dissipate energy, in other words it characterises the viscous behaviour of a material. The equations of storage modulus and loss modulus are, respectively,

$$E'(\omega) = \frac{\sigma_0}{\varepsilon_0} \cos \delta \qquad (5)$$

and,

$$E''(w) = \frac{\sigma_0}{\varepsilon_0} \sin \delta \qquad (6)$$

The phase angle, δ, can then be calculated from

$$\tan\delta = \frac{E''(w)}{E'(\omega)} \qquad (7)$$

Equation 7 represents the damping factor of a viscoelastic system and is a measure of the energy dissipation of a material and tells us how effective a material is at absorbing energy.

The shear moduli, $G'(\omega)$ and $G''(w)$ can easily be found by replacing *G* with *E* in the above equations.

DMA can be used to determine the glass transition temperature (T_g) of a material. At T_g a simultaneous sharp drop in the storage modulus and a maximum peak in the loss modulus of the material can be observed. During a temperature-sweep test using DMA, which involves the use of a low frequency and varying the temperature, a characteristic curve is produced. A peak in the $tan\,\delta$ spectra appears at T_g and is a reliable method to determine the T_g of the material under observation. Multiple transitions can also be observed. For example, if two glass transitions are observed in a temperature-sweep DMA it is indicative that the polymer blend is immiscible. Separate transitions can also occur and can be attributed to different regions within the material e.g. semi-crystalline polymers will have separate transitions corresponding to the amorphous and crystalline portions within.

Combined sweeps utilising varying temperature and frequency in conjunction with one another can provide a more in-depth characterisation of the material and the nature of its molecular motions responsible for such transitions.

In this work, temperature ramps were performed using a temperature range between 80 °C and 180 °C at two frequencies (1 Hz and 10 Hz).

Isothermal frequency sweeps were carried out at two temperatures, 135 °C and 140 °C to assess how the behaviour changed as the samples approached a rubberier state. A frequency range between 0.1 Hz-100 Hz was used and the data was collected at 1 Hz intervals.

DMA was also used to assess the creep behaviour of polycarbonate and the nanocomposites at 140 °C. This temperature was used as it was found from the isothermal frequency sweeps that more information was gained when the samples were nearer to the rubbery state. The

samples were held under a strain of 0.2 MPa for 120 minutes. A pre-load stress of 0.2 N was applied to ensure the samples were taut before experimentation.

Universal Analysis software was employed to analyse the data. All samples were dried at 110 °C for 48 hours prior to testing to remove as much moisture absorbed by the samples as possible. Moisture can affect the final properties of the samples and obscure the results.

3.3.6. Modulated Differential Scanning Calorimetry

Differential scanning calorimetry (DSC) is a thermal analysis technique that measures how the heat capacity of a sample of known mass varies with a change in temperature. Heat flow, the movement of heat into and out of a sample, is monitored as a function of temperature against a reference pan. The difference in heat flow between the sample and the reference pan can provide information on glass transitions, phase changes, melting point, polymer degradation and whether the processes are exothermic or endothermic.

With a standard DSC, a single heat rate is used and so temperature is changed linearly and therefore a single heat flow rate signal is produced. In a modulated DSC (MDSC), two simultaneous heating rates are used; a linear heating rate which provides information similar to a standard DSC and a sinusoidal heating rate that allows the simultaneous measurement of the heat capacity of the sample. Modulation period and modulation temperature amplitude is selected to create the sinusoidal temperature change. This allows for increased sensitivity to small transitions and therefore better data interpretation [204].

A TA Instruments 2920 Modulated DSC (fig. 34) was used to measure the glass transition and study the physical aging of polycarbonate and its TSP-POSS based nanocomposites. Compression moulded plaques of 1mm thickness were annealed in an oven at 110 °C for at least 24 hours to remove any excess moisture. Annealed samples were then cut using a simple hole punch. The discs were weighed and then sealed in a DSC pan. Prior to all DSC experimentation, the pans containing the samples were annealed at 180 °C for 5 minutes to remove the thermal history. The DSC was used in the modulated mode for all tests. Universal Analysis software was used to analyse the data.

Figure 34 Modulated DSC located in the Materials department, Loughborough University [203]

To measure the glass transition temperature, samples were heated from 25 °C to 180 °C at a heating rate of 3 °C/minute. The time derivative of the complex heat capacity, C_p was calculated using Universal Analysis and the peak value of the resulting graph was taken as the glass transition temperature to minimise uncertainty in the value for T_g. A smoothing region width of 6 °C was used before measuring T_g to increase precision.

MDSC was also used to study the physical aging of polycarbonate and its TSP-POSS based nanocomposites. Physical aging involves changes in the physical properties of glassy polymers with time and is why such polymers tend to become brittle with age. Understanding the physical aging of polymers is an important aspect when considering their long-term performance.

Physical aging originates from the fact that a glassy polymer below its glass transition temperature is generally in a non-equilibrium state. A polymer melt, however, is considered thermodynamically stable. Changes in the physical properties are associated with physical aging whereas changes in thermal properties are associated with enthalpic relaxation. However, physical aging is in close correlation with enthalpic relaxation and has the effect of increasing relaxation times.

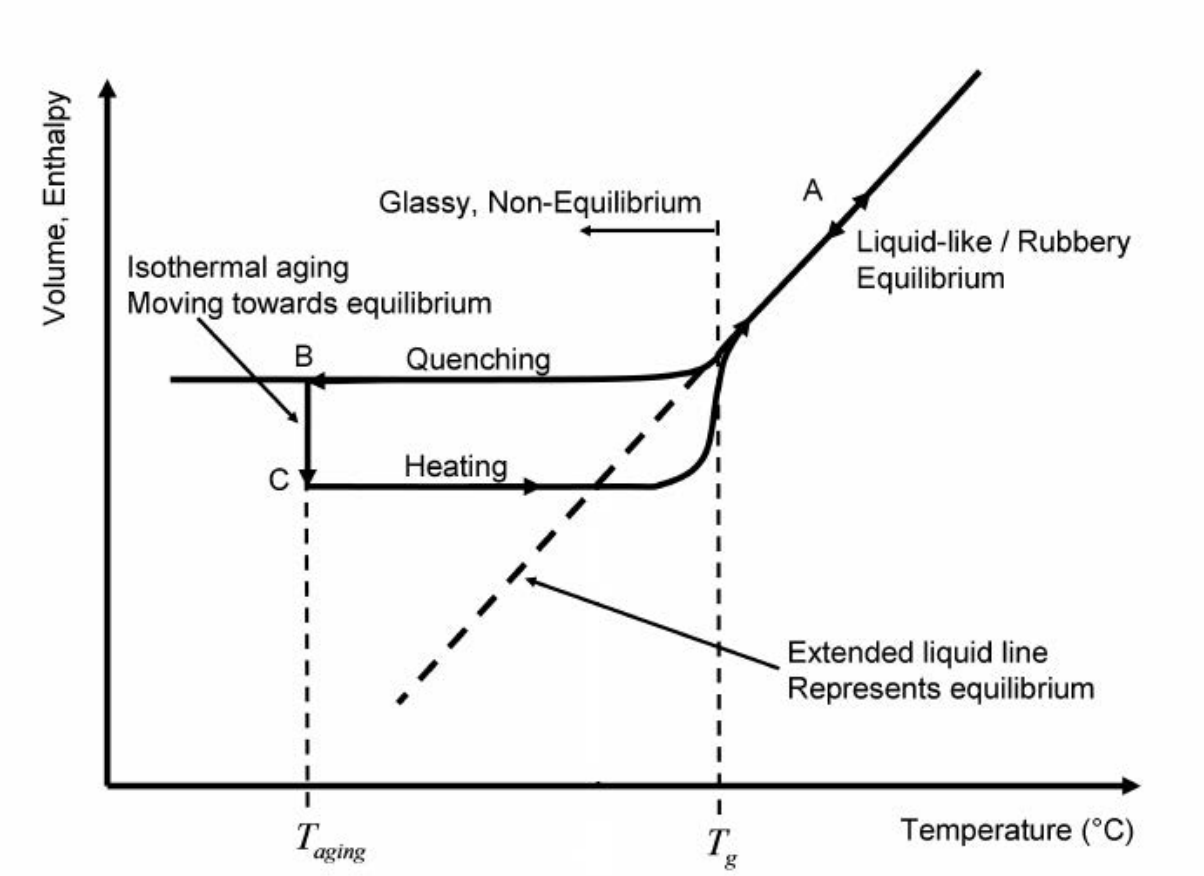

Figure 35 Graph representation of the enthalpy change as a function of temperature for a typical glassy polymer. T_{aging}, T_f' and T_g represent aging, and glass transition temperature, respectively. When the polymer is cooled (A to B) below the glass transition it is in a glassy, non-equilibrium state and tends to move towards equilibrium, a process known as physical aging (B to C) [205]

Enthalpic relaxation is the progressive change in the thermodynamic properties of the glass towards equilibrium; in the non-equilibrium state the thermodynamically stable state tends to be slowly recovered during physical aging. By monitoring the time-dependent evolution of thermodynamic variables such as enthalpy the relaxation process can be studied and therefore physical aging can also be studied. Firstly, the polymer sample is rapidly cooled from the equilibrium state to below the T_g, which marks the loss of thermodynamic equilibrium, at an aging temperature, T_a. Annealing a glassy polymer in a temperature range close to but below the T_g for an aging time, t_a results in a progressive decrease in the enthalpy of the polymer with ageing time as the polymer approaches equilibrium. The relaxation can be measured as the recovery of the lost enthalpy associated with the glass transition during the heating scan of an aged sample, where it is observed as an endotherm in the DSC spectra.

Consider the example of a liquid being cooled rapidly, or quenched, from a temperature above the melting point. When a liquid fails to crystallise during cooling, it enters the rubbery state and then undergoes the glass transition when the molecular motions are unable to keep up with the cooling rate. The excess enthalpy and entropy are frozen in at the glass transition. When a quenched sample is stored at a temperature, T_a close to T_g, it loses this excess enthalpy and moves towards the super-cooled liquid state (shown in figure 35). It is assumed then that the enthalpy regained upon heating through the glass transition is equal to that lost during aging below the T_g and can be used to study the physical aging and relaxation behaviour of a polymer [206].

Properties such as enthalpy and entropy decrease towards the equilibrium values at rates dependent upon the difference between the aging temperature and T_g and will decrease with an increase between T_a and T_g, ΔT. [86,206–208]. In this study, the aging temperatures will be varied to investigate the effect of ΔT on the physical aging behaviour of polycarbonate and its nanocomposites.

Enthalpic relaxation, $\Phi(t)$ can be characterised by the excess enthalpy lost on aging

$$\Delta H(t_a, T_a) = \int_{T_a}^{T_\beta} \Big(C_p(aged) - C_p(unaged) \Big) dT$$

$$= \Delta H_\infty(T_a)[1 - \Phi(t_a)] \qquad (8)$$

using the Williams-Watts stretched exponential function

$$\Phi(t) = e^{\left[-\left(\frac{t}{\tau_0}\right)^\beta\right]} \qquad (9)$$

where C_p is the specific heat capacity, $\Delta H_\infty(T_a)$ corresponds to the enthalpy difference between the values at the onset of ageing and the value if the sample was left to age for an infinitely long time to the super-cooled liquid, τ_0 is the characteristic relaxation time which is dependent on both the ageing temperature and the structure of the polymer and β is an inverse measure of the breadth of the relaxation spectrum.

% TSP-POSS	T_g (°C)	T_{a1} (°C)	T_{a2} (°C)	T_{a3} (°C)
PC	144.18	134	132	130
$\Delta T=T_g-T_{An}$ **(°C)**		**10.18**	**12.18**	**14.18**
0.1	144.57	134.59	132.39	129.39
0.5	143.83	133.65	131.65	128.65
1	143.63	133.45	131.45	128.45

(a)

t_{an}	**Annealing time (hours)**
ta_1	1
ta_2	3
ta_3	6
ta_4	10
ta_5	20
ta_6	35
ta_7	50
ta_8	120

(b)

Table 2 (a)Annealing temperatures T_{an} and (b) annealing times t_{an}

Enthalpic relaxation, $\Phi(t_a)$ can be calculated by rearranging equation (8) to

$$\Phi(t_a) = 1 - \left(\frac{\Delta H(t_a,T_a)}{k\Delta H_\infty(T_a)}\right) \qquad (10)$$

where *k* is a calibration factor given by equation (11):

$$k = \frac{C_p(PC)}{\frac{\delta C_p}{\delta T}} \qquad (11)$$

and

$$\Delta H_{\infty}(T_a) = \frac{\delta C_p}{\delta T}.\Delta T \qquad (12)$$

$C_p(PC)$ is the specific capacity of polycarbonate, $\frac{\delta C_p}{\delta T}$ is measured from the graph of $\frac{\delta C_p}{\delta T}$ against temperature, $\Delta H(t_a, T_a)$ is measured by integrating the area under the endotherm of the DSC graph of non-reversible heat flow, $\Delta H_{\infty}(T_a)$ and ΔT is the temperature differential. Endotherm limits were chosen by using the derivative of the non-reversible heat flow.

By plotting $\Phi(t_a)$ against $logt_a$, the characteristic relaxation time, t_c, can be found by fitting equation (13) to the graph:

$$\Phi(t_a) = A_o e^{-\frac{t_a}{t_c}} \qquad (13)$$

The effect of the annealing time and annealing temperature on the physical aging was studied by varying these parameters for polycarbonate and the nanocomposites. The annealing temperature T_{an}, where n is an integer, is selected always below the glass transition temperature. Annealing temperatures were chosen by first selecting three temperatures below the T_g of polycarbonate e.g. 130 °C, 132 °C and 134 °C. The difference, ΔT, between T_g and each annealing temperature was calculated and annealing temperatures for each nanocomposite loading were selected so that the ΔT values were the same as those for polycarbonate. The annealing temperatures and times can be found in table 2.

3.3.7. Ultraviolet-Visible Spectrophotometry

A Perkin-Elmer Lambda 35 UV-Vis Spectrophotometer (fig. 37) was used to assess the optical transparency and clarity of polycarbonate/TSP-POSS nanocomposites by measuring the diffuse transmission and reflectance for the wavelength range 300 nm - 1000 nm which uses adjacent UV and near-infra red (NIR) light. Three samples of 1 mm thickness were tested for each nanofiller loading. A slit width of 1 nm was used. The raw data of transmission values and wavelength values were plotted into graphs of transmission vs. wavelength.

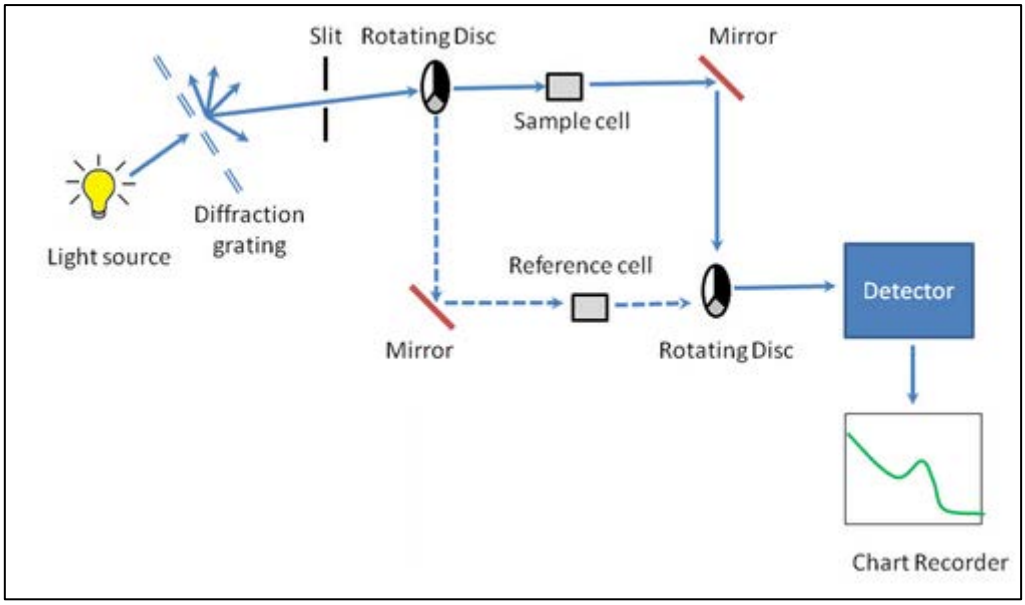

Figure 36 A schematic of a UV-Vis Spectrophotometer set up [209]

UV spectroscopy can be used to measure the amount of light transmitted through, absorbed by or reflected by a sample. In the adjacent regions of the UV and visible spectrum, photon absorption occurs and causes strong excitations of a specific group of electrons located in the chromophore of a system. The chromophore is responsible for the "colour" of the system [210].

The energy levels within a system depend on the molecular bonds present [211]. The atoms in a bond have their orbitals merged to form a molecular orbital (MO). Electrons can occupy bonding, antibonding or nonbonding MOs. Bonding electrons can be split into two types depending on how many bonds they form; π-electrons (single bonding) and σ-electrons (multi-bonding). Unshared or nonbonding electrons are known as n-electrons. When an electron absorbs energy from light radiation it transitions from the highest occupied molecular orbital to the lowest unoccupied molecular orbital, and results in an excited or antibonding state [210–212].

The σ-bond electrons have the lowest energy level and are the most stable electrons. A large amount of energy is required to displace these electrons to higher energy levels. As a result, these electrons generally absorb high energy photons in the lower wavelengths of the ultraviolet region and these transitions are rare. π-bond electrons have much higher energy levels for the ground state.

Figure 37 A Perkin Elmer Lambda 35 bench-top UV-Vis Spectrophotometer located in the Chemistry department, Loughborough University [213]

These electrons are therefore relatively unstable and can be excited more easily. They can be excited by absorption of lower energy photons with longer wavelengths, often in the visible region. The n-electrons or non-bonding electrons are electrons belonging to lone pairs of atoms. These are of higher energy levels than π-electrons and can be excited by ultraviolet and visible light [211,212].

A UV-Vis Spectrophotometer uses wavelengths of light in the range of 200 nm - 1000 nm, where 400 nm – 800 nm corresponds to the visible region. When a sample is exposed to light energy that matches the particular energy difference between possible electronic transitions within the molecule, a fraction of the light energy is absorbed by the molecule and an electron is excited from its ground state to an excited state at a higher energy level. A spectrophotometer measures the degree of absorption of a sample at different electromagnetic wavelengths and produces a spectrum [212].

Two electromagnetic radiation sources are required to cover the full wavelength range. EM radiation passes from source through to a monochromator, which can consist of a prism or a diffraction grating. This spreads out the spectral components, permitting a very narrow range to be sampled by a slit. The slit passes a finite bandwidth which must be less than 10% of the natural bandwidth of the spectral line to be measured to avoid error in peak intensity. Selected radiation passes into the sample [211]. The intensity of radiation passing through the specimen, I, is measured by the detector and then compared to the intensity of radiation prior to passing through the sample, I_0. The ratio I/I_0 is called the transmittance and is usually represented as a percentage. The detector is usually a photomultiplier, photodiode, photodiode array or a charge coupled device (CCD).

Solution samples are held in a cuvette, a standard cell with windows which must be made out of a material that is transparent in the UV-Vis region e.g. Pyrex cells or optics for the visible spectrum and quartz for the UV spectrum. With polymers, a thin parallel-sided solid sample can be mounted in place of a solution cell.

When direct transmittance is greater than 90% in the visible region, the film is considered transparent. The film is translucent when the light transmittance is less than 90% and more than 10% of the visible region is absorbed. An opaque material has a transmittance of 0% [214]. Differences in refractive indices (mismatch of refractive indices) of the medium and any dispersed particle or inhomogeneities will result in reflectance of the transmitted light and decrease the overall light transmittance of the material.

3.4. Mechanical Test Techniques

3.4.1. Tensile test

A Lloyd Instruments LR50K tensometer, shown in figure 38(b), was used to measure the tensile properties of polycarbonate and its TSP-POSS based nanocomposites. Four dumbbell-shaped specimens, adhering to the British Standard BS EN ISO 527-2:2012 type 5A, per TSP-POSS loading were tested at ambient temperature. Samples were held vertically at both ends by metal jaws, with the top jaw being attached to a 1 kN loading cell. Force was applied to the samples at a speed of 50 mm/min until total failure occurred. Raw data was produced in the form of load-extension curves. To ascertain tensile properties of the

specimens these were converted into stress-strain curves using equation 14 and 15 for stress, σ and strain ε, respectively:

$$\sigma = \frac{F}{A} \qquad (14)$$

where F is the force applied by the load cell and A is the area of the specimen (width and thickness of the ends).

$$\varepsilon = \frac{\Delta l}{l} \qquad (15)$$

where Δl is the change in length of the specimen (extension measured by tensometer) and l is the original gauge length of the sample.

Several important properties can be determined from the stress-strain curve. Figure 38(a) contains a typical stress-strain curve for polycarbonate. The region of the graph from the origin to the yield point (point A) follows Hooke's law, where the relationship between stress and strain is linear and corresponds to elastic behaviour of the specimen i.e. if the load is removed the sample will return to its original shape prior to deformation. By measuring the gradient of this slope the Young's modulus can be determined. Young's modulus gives information on the stiffness of a material. Beyond the yield point plastic deformation occurs and the specimen experiences some permanent change to its shape. The peak of the curve (point B) corresponds to the ultimate tensile strength and is generally taken as the maximum stress that the sample experiences before failure, although it does not take into account strain hardening and necking phenomena. The sample continues to stretch and eventually breaks (point C). The amount that the sample deforms is known as elongation at break and is a measure of the ductility of the sample. By integrating the area under the stress-strain curve the toughness of the sample can also be calculated.

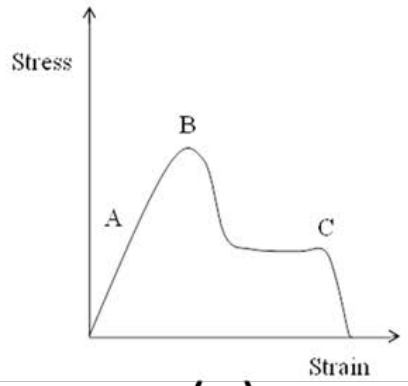

(a)

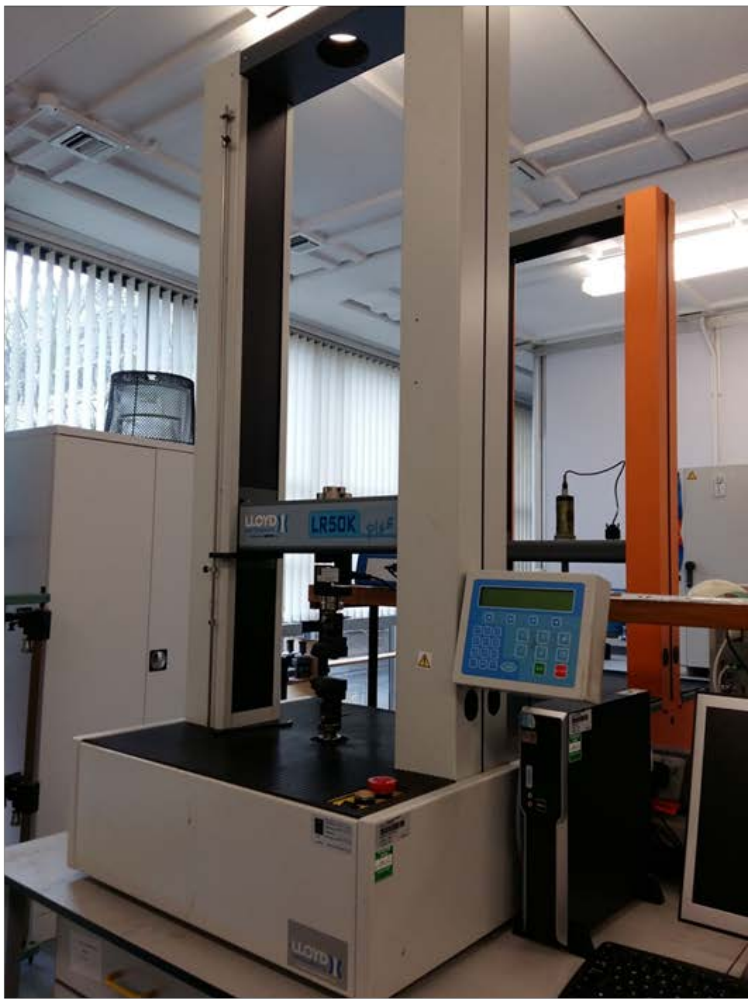

(b)

Figure 38 (a) Typical stress-strain curve for a polymer and (b) a Lloyds Instruments LR50K tensometer located in the Materials department, Loughborough University

3.4.2. Instrumented Falling Weight Impact Tester

The impact performance of polycarbonate/TSP-POSS at low velocities was assessed by implementing a Rosand type 4 falling weight impact tower. Six samples per TSP-POSS loading were tested and the data obtained averaged. The 1 mm thick samples were held in place by a clamp at the base of the tower. A dart striker with mass of 2kg was raised to heights between 0.5 m and 1.5 m corresponding to varying dart velocities and then dropped onto the sample. The effect of dart velocity on the impact behaviour of the nanocomposites could then be evaluated.

By equating the equations

$$K.E = \frac{1}{2}mv^2 \quad (16)$$

and,

$$P.E = mgh \quad (17)$$

and rearranging to,

$$v = \sqrt{2gh} \quad (18)$$

where *K.E*, *P.E*, *m*, *g*, *h* corresponds to the kinetic energy, potential energy, mass of dart, velocity of dart, gravitational constant and height of dart, the dart velocity, *v* can be calculated from equation (16). The dart velocities used were calculated to be 3.12 ms^{-1}, 3.96 ms^{-1}, 4.85 ms^{-1} and 5.45 ms^{-1}, corresponding to dart heights of 0.5 m, 0.8 m, 1.2 m and 1.5 m.

A typical force-displacement curve for polycarbonate can be found in figure 39. The curve is bisected into two halves; the area under the first portion of the graph represents the initiation energy, E_i, and is the amount of energy that can be absorbed by the specimen before a crack forms. The peak of the curve is simply the maximum load the material can withstand before a crack is initiated and is known as the maximum peak force. After this point plastic deformation occurs, which resists crack propagation, until the dart passes through fully and the specimen fails.

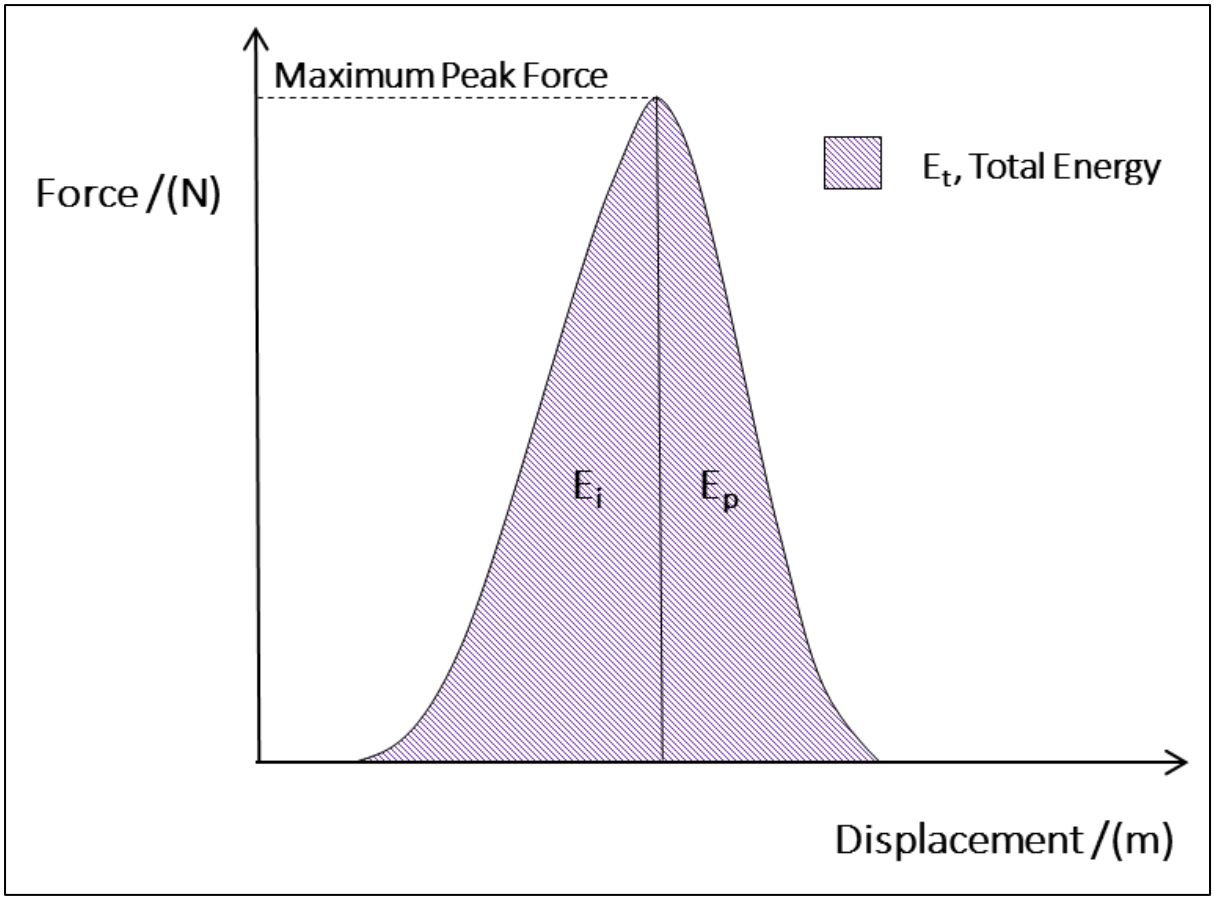

Figure 39 A typical force-displacement curve produced by an instrumented falling weight experiment

The propagation energy, E_p, is the energy used in plastic deformation. The total area, E_t, under the graph can therefore give an indication of the toughness of the specimen. The areas under the graph representing initiation, propagation and total energy are integrated to give values for these properties.

3.4.3. Drop-ball impact test

According to the American National Standard for Occupational and Educational Personal Eye and Face Protection and Devices, ANSI-ISEA Z87.1, protective eyewear must pass the drop ball impact test before use to ensure a minimum impact resistance. The procedure involves dropping a steel ball 1 inch in diameter of mass 68 g from a height 50 inches above the specimen, which is held horizontally face up. The projectile free falls through a loose fitting guide tube 4 inches above the specimen. Samples of 2 mm thickness are supported on a lens support acrylic tube measuring 1.25 " outside diameter x 1.0 " inside diameter x 1 " height. The sample will either pass or fail; to pass the sample must not crack, chip or break [215].

3.4.4. Split-Hopkinson Pressure Bars

Split-Hopkinson pressure bars (SHPB) are used to investigate the dynamic properties of materials at high-strain rates. Strain rates of up to $10^3\,s^{-1}$ can be achieved in both dynamic compression and dynamic tension tests. The stress-strain relationship of a material can be obtained from the experimental results.

In a compression test a cylindrically shaped sample is placed between two pressure bars which are typically made from a high strength elastic material such as maraging steel or aluminium. This is so that a wide range of materials can be tested and deform plastically whilst the pressure bars remain within their elastic limit.

In our traditional three-bar set-up (see fig. 40) a projectile is propelled along the gas chamber where it hits the striker bar. Firstly, the gas gun, shown in figure 41(a), is loaded with the projectile at the furthest point from the incident bar, and the gas gun is evacuated to a pressure between 8 bar to 10 bar. The projectile is then suddenly exposed to atmospheric pressure by releasing a lever which moves the end plate to uncover a hole in the aperture plate. The striker bar hits the incident pressure bar, creating an incident strain pulse which propagates through the incident bar and into the specimen. The pressure bar strain causes the incident bar to move which puts stress on the specimen and causes it to deform. Due to acoustic impedances between the material of the specimen and that of the incident pressure bar, a portion of the strain pulse is transmitted through to the transmitter pressure bar and reflected back through the incident pressure bar, inducing strain in both pressure bars. A momentum bar absorbs the energy which is attenuated by allowing the momentum bar to move freely into a plasticine filled box located at the free end of the momentum bar. This prevents the pulse from being reflected back into the transmitted bar. Strain gauges on the pressure bars measure the strain in the bars which is then amplified and recorded by a digital oscilloscope to produce a voltage-time graph.

Figure 40 The Split-Hopkinson Pressure Bar set-up at Loughborough University

The raw data of the reflected pulse and transmitted pulse is converted into stress-strain data values by a series of equations. Engineering stress, σ_S can then be calculated using the equation

$$\sigma_S = E\frac{A}{A_0}\varepsilon_T \qquad (19)$$

where *E* is Young's modulus, *A* is the cross-sectional area of the pressure bar, A_0 is the cross-sectional area of the specimen and ε_T is the strain in the transmitted bar. The engineering strain is directly proportional to the reflected pulse, ε_R. However, engineering stress and strain do not take into account the surface area of the specimen during deformation. True representations of stress and strain can be calculated from true stress and true strain values which are functions of the engineering stresses and strains. Stress-strain curves can then be produced and properties such as Young's modulus, yield stress and energy absorption can be calculated in a similar manner to that used when calculating tensile properties from the stress-strain curves of the tensile tests; Young's modulus is taken as the gradient of the

stress-strain curve up to the yield point which is where the curve begins to deviate from a linear shape. Energy absorption is taken as the integral of the area under the curve.

The projectile velocity and the subsequent force with which the sample is subjected to can be controlled by the removal of plugs located on the aperture plate, shown in figure 41(b). The apertures vary in diameter; basically, the larger the aperture, the larger the force due to increased amount of air entering the gas tube when the lever is released. In this test, two aperture settings were used; the removal of 12 mm and the removal of both 12 mm and 7.9 mm to give a strain gauge signal voltage of around 0.8 V and 1.2 V, respectively. As the ease with which the projectile moves through the chamber and therefore its velocity was affected by the ambient temperature and the number of times it had been previously been fired, the pressure in the gas cylinder was varied between 8 and 10 in order to keep the voltage at either 0.8 V and 1.2 V and thus the magnitude of the impact on the specimen similar.

It was found that aluminium bars were suitable to use with the polycarbonate-based specimens as the pulses were well defined and therefore ideal for analysis. The projectile and striker bars were made of the same material as the pressure bars to minimise any impedance mismatch.

A small amount of lubricant was placed on the sample-bar interfaces to reduce the effects of friction, such as barrelling of the specimen, which can cause non-uniform strain leading to poor results. The lubricant used in the testing was MolyKote molybdenum disulphide-based grease which was chosen for its low coefficient of friction. Vacuum grease was also applied on bar-bar interfaces to promote good transmission of the strain pulse.

Cylindrical shaped specimens with 4 mm thickness and an 8 mm diameter i.e. a Poisson's ratio of 0.5 were fabricated via compression moulding. A Poisson's ratio of 0.5 is said to minimise wave attenuation in specimens of low-impedance materials [2,216].

Due to the formation of a slight lip on one face, all samples to be tested were polished down therefore reducing their thickness slightly. The diameter and thickness of all samples were measured pre- and post-testing.

(a)

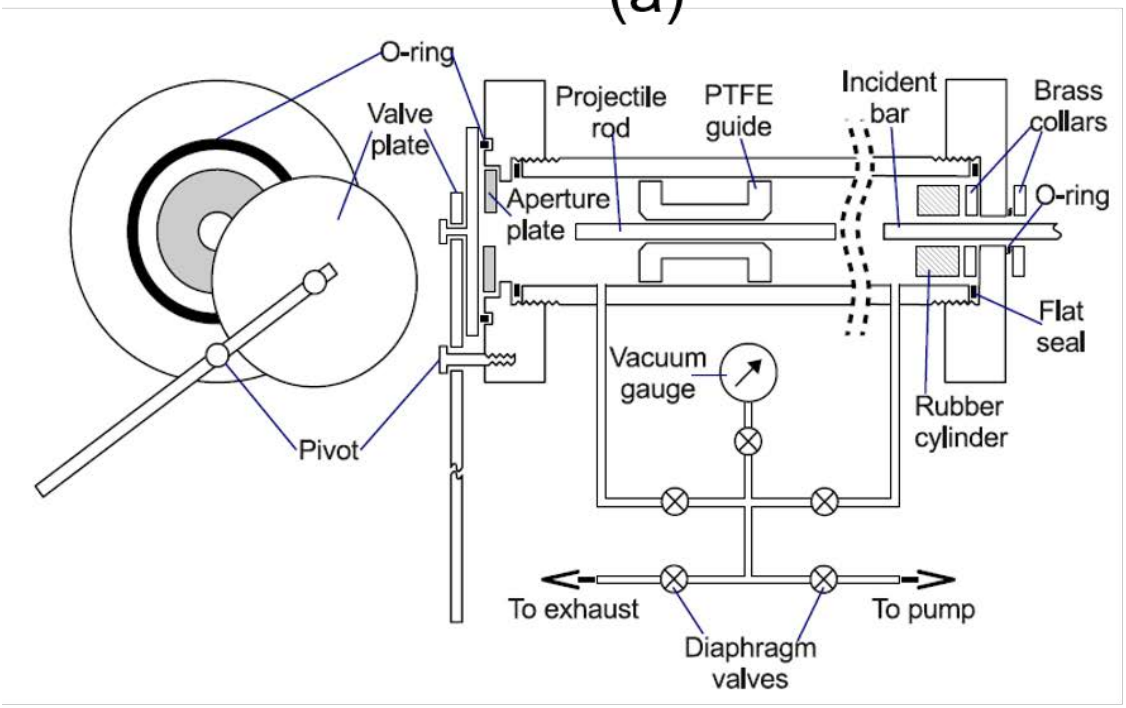

(b)

Figure 41 (a) the gas gun of the SHPB [217] **and (b) the aperture plate used to control the SHPB projectile velocity**

Chapter 4

Nanocomposite Characterisation

Chapter 4 Nanocomposite Characterisation

This chapter contains the results of various characterisation tests carried out on polycarbonate and its TSP-POSS based nanocomposites in order to assess the effect that TSP-POSS has on the structural, morphological, optical, thermal and viscoelastic properties if polycarbonate.

4.1. Structural and morphological properties

4.1.1. X-Ray Diffraction

X-ray diffraction was used to characterise the structure of the polycarbonate/TSP-POSS nanocomposites. By comparing the spectra of the nanocomposites to those of the control polymer and nanofiller samples, one can roughly determine how well dispersed the TSP-POSS is in the polymer matrix. XRD is a bulk analysis technique, as it averages over the whole of the sample. The quantity of TSP-POSS is very low, and as such if the sample were mixed adequately peaks would not be seen in the spectrum, even if nanometre sized aggregates had formed. If poor sample fabrication has occurred, and the TSP-POSS has not sufficiently blended in, the larger aggregate of TSP-POSS may be visible in the XRD spectrum. Polycarbonate and TSP-POSS samples were in raw powder form and the nanocomposites samples were made from the processed pellets. Figure 42 contains the spectra of the polycarbonate control, TSP-POSS and the nanocomposites.

From figure 42 it can be seen that the polycarbonate control sample possesses a typical diffraction pattern of an amorphous polymer; a single broad diffused peak, sometimes referred to as a halo, which results from the x-rays being scattered in many directions by the randomly oriented chain structure. TSP-POSS on the other hand produces a diffraction pattern comprised of sharp peaks, suggesting a highly crystalline structure. The largest of the peaks occurs at approximately $2\vartheta = 7°$ and corresponds to a d-spacing of 1.26 nm. This is the characteristic POSS peak as POSS molecules are typically 1-3 nm in size. Others have also documented this [130].

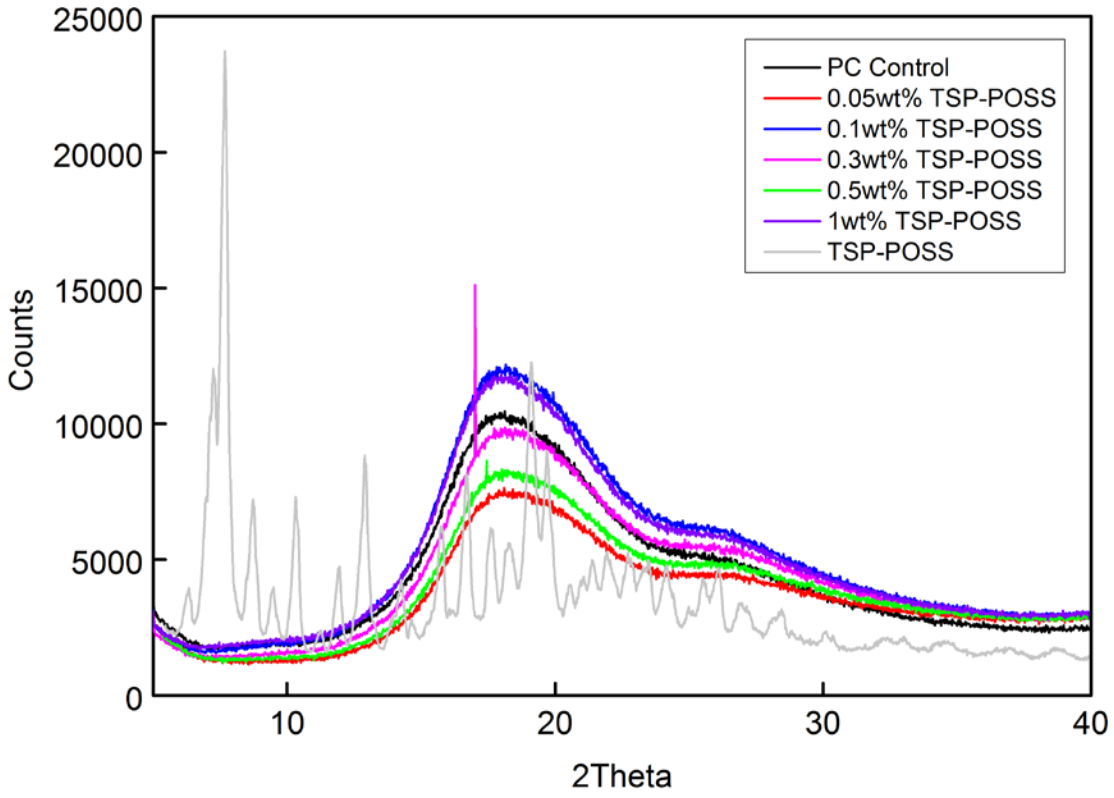

Figure 42 XRD spectra of TSP-POSS, polycarbonate and its TSP-POSS based nanocomposites

Since the spectra of the nanocomposites are virtually identical to that of the control sample, it can be implied that TSP-POSS has been sufficiently blended into the polycarbonate matrix. There is an anomalous data point in the PC/0.3wt% ($2\vartheta \approx 18°$) spectrum, which is caused by instrumental noise and can be discounted. As it is a single data point it is unlikely to correspond to a reflection from the TSP-POSS crystallites. The difference in height of the spectra is caused by slight differences in the thickness of the samples and is not important.

The absence of any intense peaks in the spectra of the TSP-POSS based polycarbonate nanocomposites implies that large aggregates of TSP-POSS do not exist in the polymer matrix as a secondary phase. It is impossible to determine from the XRD whether nanometre scale aggregates are formed, as XRD is a bulk analysis technique. An alternative method, such as Scanning Electron Microscopy, can provide more information and is far more suitable to determine how well dispersed the TSP-POSS is on a nanometre scale.

4.1.2. Scanning Electron Microscopy

Scanning electron microscopy was used to view the morphology of the nanocomposites and assess the dispersion of TSP-POSS in the polycarbonate matrix. Figures 43-50 contain micrographs of polycarbonate and PC/TSP-POSS nanocomposites.

Figure 43 shows the fracture surface of the polycarbonate matrix. It has a nodular type morphology and is relatively featureless. The micrographs of PC/0.05wt% TSP-POSS shown in fig. 44 are identical in appearance to those of the control sample, implying that TSP-POSS at this loading has not had an effect on the morphology and structure of the fracture surface of polycarbonate. From figures 45-47 it can be seen that there are no visible TSP-POSS aggregates in the polymer matrix up to a loading of 0.3wt%. This implies that the nanofiller is dispersed as molecules and is miscible in the polymer matrix. For this to occur requires high compatibility between the nanofiller and the polymer. Open-cage POSS structures are said to be more soluble in polymers than close/fully condensed structures. Moreover, it has been proposed that the phenyl groups of TSP-POSS make this type of POSS compatible with polycarbonate [90,92,97,107].

Stretched fibrils are seen in the samples containing 0.1wt% and 0.3wt% TSP-POSS and are more noticeable in PC/0.3wt% TSP-POSS. Stretched fibrils are a characteristic of ductile failure and increase the amount of energy required to break the sample. Figure 47 shows how the addition of 0.3wt% TSP-POSS has significantly changed the morphology of the polycarbonate matrix. However, for samples containing 0.5wt% and 1wt% TSP-POSS, the surface morphology is similar to that seen in the unmodified polymer. However, spherical aggregates between 100 nm and 200 nm are present throughout the matrix and are more numerous in the nanocomposite containing 1wt% TSP-POSS. However, the SEM images are not representative of the number of aggregates in the nanocomposite materials as the images are 2D. It is possible that the freeze fracture method used to prepare the SEM samples may influence the number of aggregates seen in the SEM i.e. some aggregates may fall off, some may be drawn out.

The presence of aggregates is to be expected as POSS-POSS interactions become stronger at increased POSS contents. Interestingly, figures 48-50 show that these aggregates reside in cavities in the matrix. This could be a result of void growth around the aggregates during

deformation. Such a process can increase the amount of energy required to break the sample and can therefore help to toughen the polymer matrix by increasing its energy absorbing capability. This toughening mechanism is seen in rubber-toughened polymer systems and involves cavitation of the rubber particles [218]. Milliman et al. studied a similar POSS/polymer system and proposed a toughening mechanism based on voided aggregates. Sanchez-Soto et al. [130] found holes and an absence of aggregates which suggests low particle-matrix adhesion, opposite to our research. From this, it can be said that there is good particle-matrix adhesion in our nanocomposite systems as a result of good compatibility between the nanofiller and the polymer which could promote surface interactions such as hydrogen bonding. Hydrogen bonding is known to occur in polymer-POSS nanocomposite systems and can increase successful dispersion in the polymer matrix [15,117,119,131,162,174,219,220].

The striations seen in the SEM images are features called craze remnants. Crazing is a typical fracture mechanism of polycarbonate and contributes to its high toughness [221,222].

It seems that TSP-POSS influences the fracture morphology of the polymer matrix at loadings below 0.3wt% and could potentially enhance the energy absorbing capability of the polymer via two different toughening mechanisms which depend on its loading in the matrix. The formation of stretched fibrils, observed for loadings between 0.1wt% and 0.3wt% (figures 45-47) could be explained by an increased in ductility, which may be caused by the presence of TSP-POSS in the polycarbonate matrix. A more nodular structure is observed for higher TSP-POSS loadings (figures 48-50), which is more consistent with the polycarbonate control, and due to increased POSS-POSS interactions, potential POSS aggregation. The presence of POSS aggregates would explain why the matrix morphology is nodular like the polycarbonate control and does not feature stretched fibrils like that seen in the nanocomposites containing 0.1-0.3wt% TSP-POSS; less TSP-POSS is dispersed as molecules in the matrix. Interestingly the aggregates seen appear to reside in a void, which is suggestive of the toughening mechanism involving cavitation and plastic void growth commonly seen in rubber-toughened polymer composite systems.

EDS was used to determine whether the white spherical objects were TSP-POSS aggregates by comparing the silicon distribution in the polymer matrix to that of the artefacts. This is

because POSS is silicon based whereas the polycarbonate matrix is not and so an increase in silicon content could infer the presence of TSP-POSS. Figure 51 contains an EDS result; there is a clear increase in the silicon peak height of spectrum 1, the artefact thought to be a TSP-POSS aggregate in comparison to spectrum 2 which is the polymer matrix, and is suggestive that the artefact is a TSP-POSS aggregate. EDS mapping of silicon was also carried out on an area containing one of the white spherical objects (figure 52). There appears to be a higher concentration of silicon in the area containing the artefact and again, this result indicates that the white spherical objects seen in the nanocomposites containing 0.5 and 1w% TSP-POSS are POSS aggregates. The intensity is relatively low due to the large interaction volume of the EDS detector (1µm) in comparison to the size of the artefacts but the resulting signal is not insignificant.

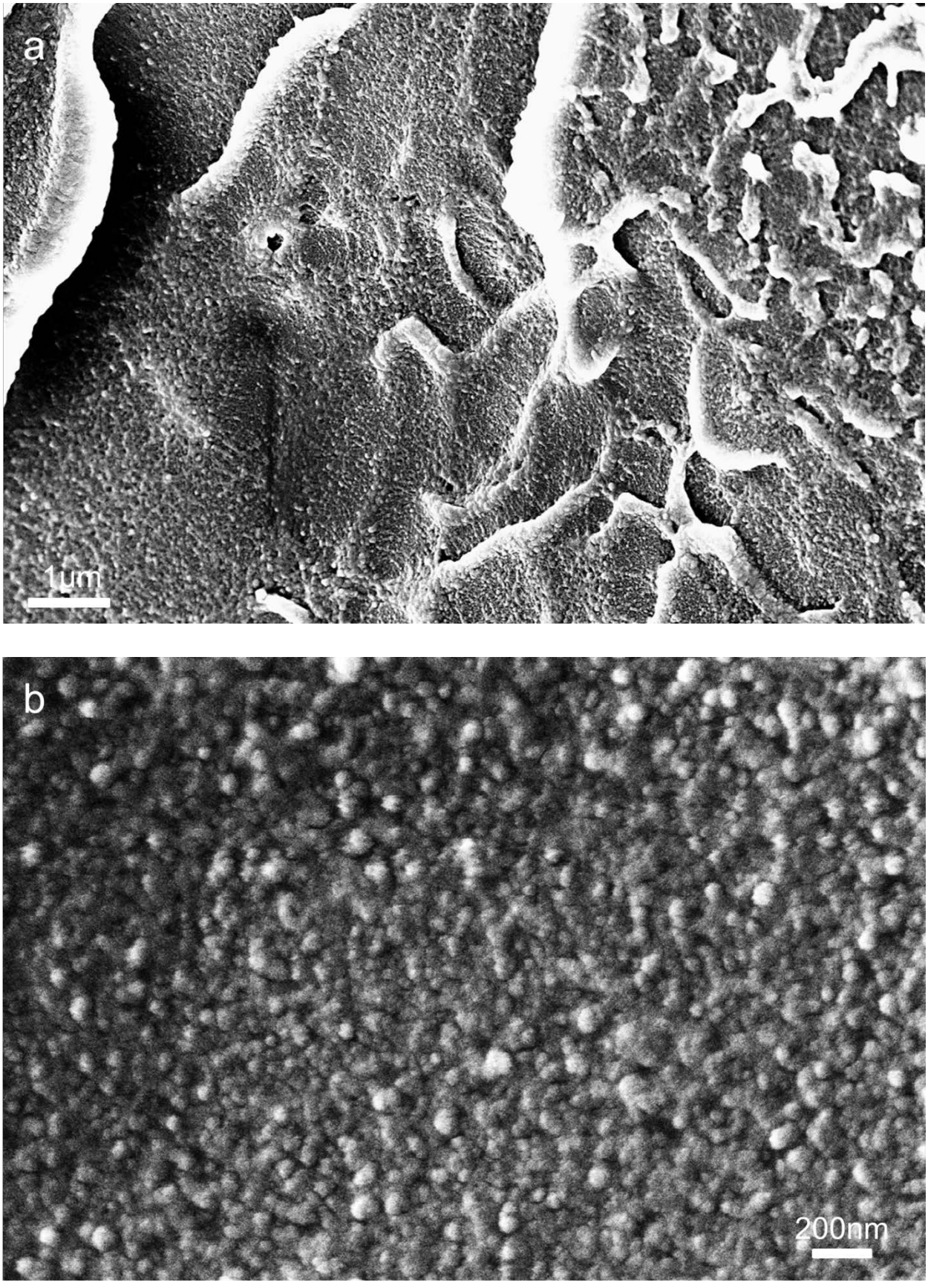

Figure 43 SEM micrographs of the polycarbonate control at a) low and b) high magnifications showing the morphology of the fracture surface

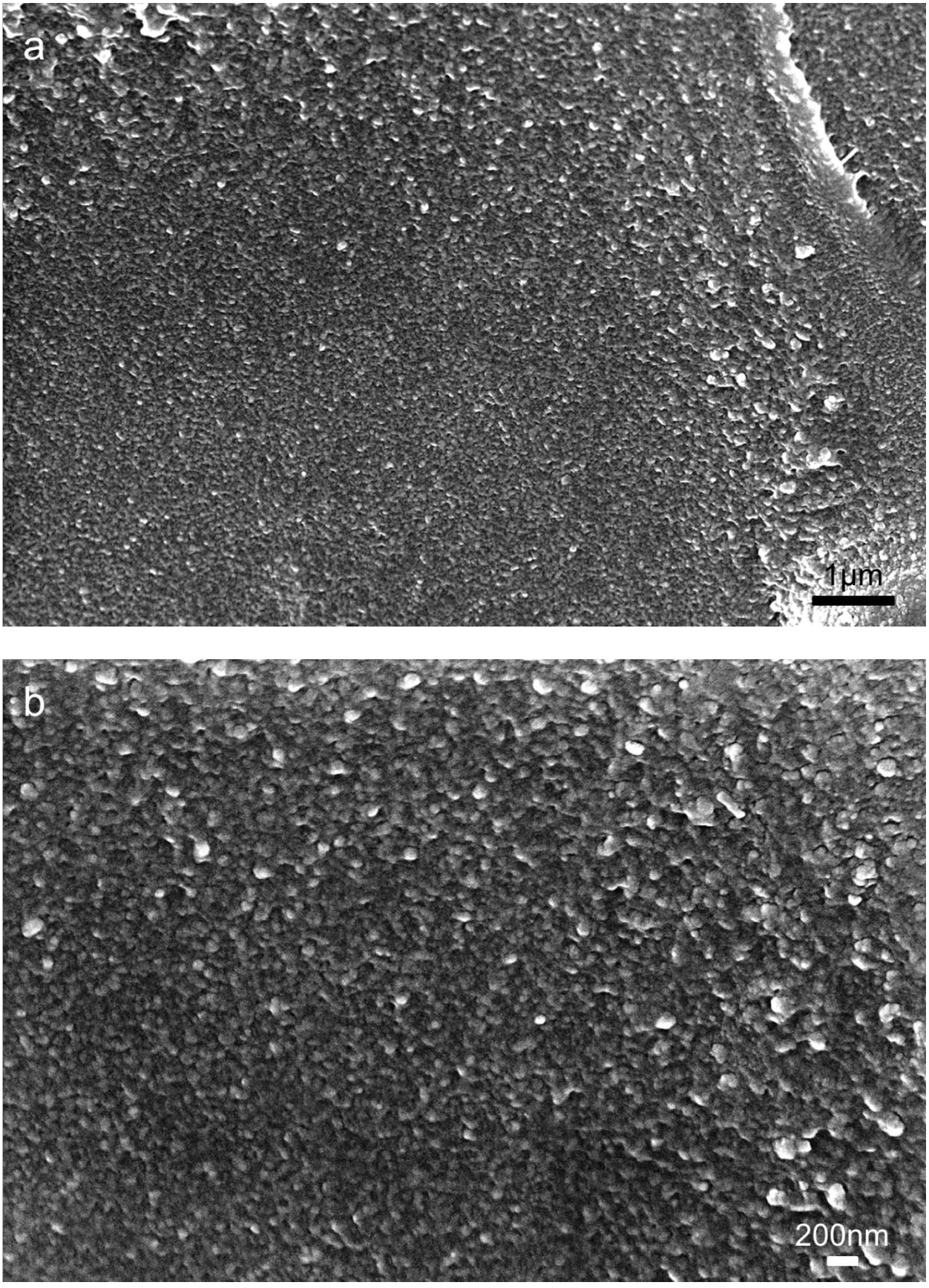

Figure 44 SEM micrographs of the fracture surface of PC/0.05wt% TSP-POSS at a) low and b) high magnifications. It is similar in appearance to fig. 43

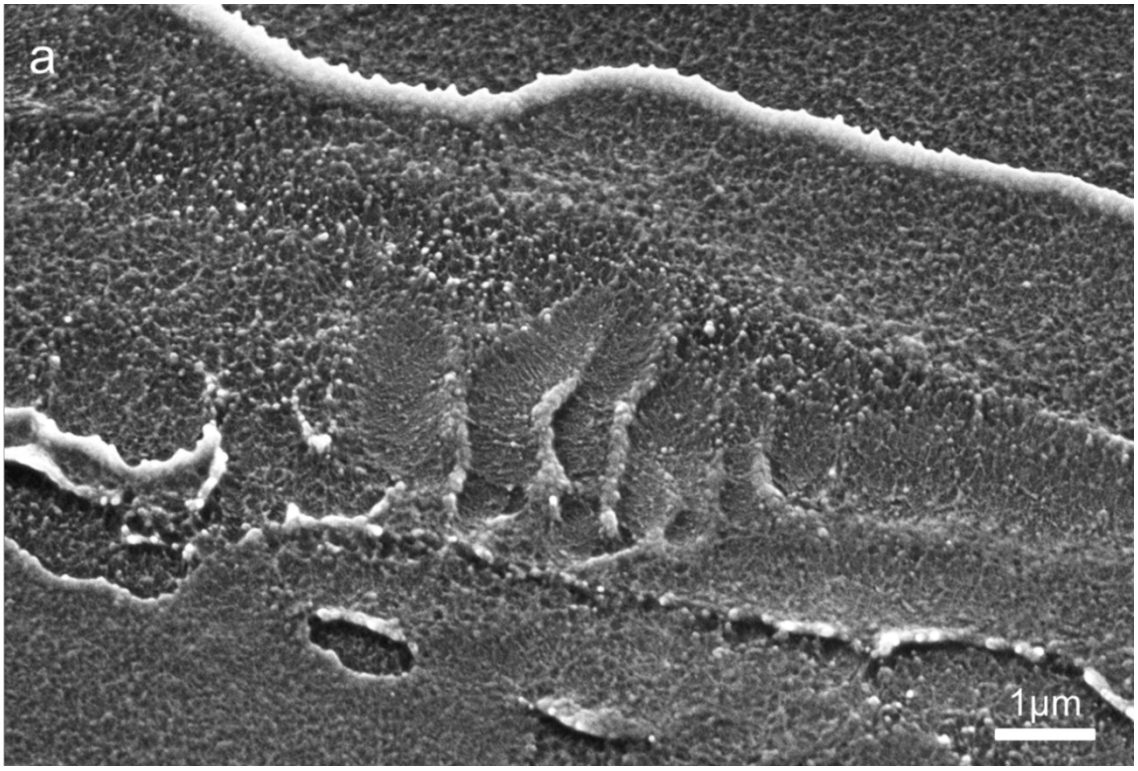

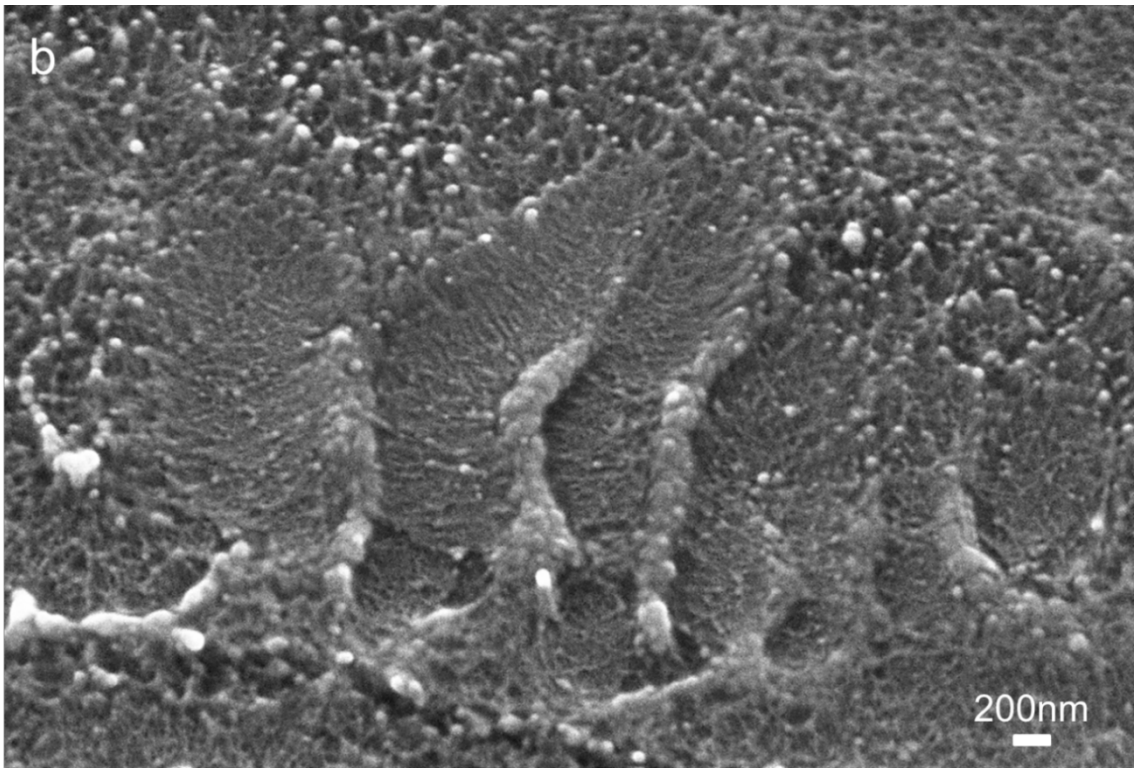

Figure 45 SEM micrographs of the fracture surface of PC/0.1wt% TSP-POSS at a) low and b) high magnifications. Ductile features known as stretched fibrils are beginning to appear on the craze remnants. Crazing is a typical fracture mechanism of polycarbonate and is an important source of fracture toughness [221,222]

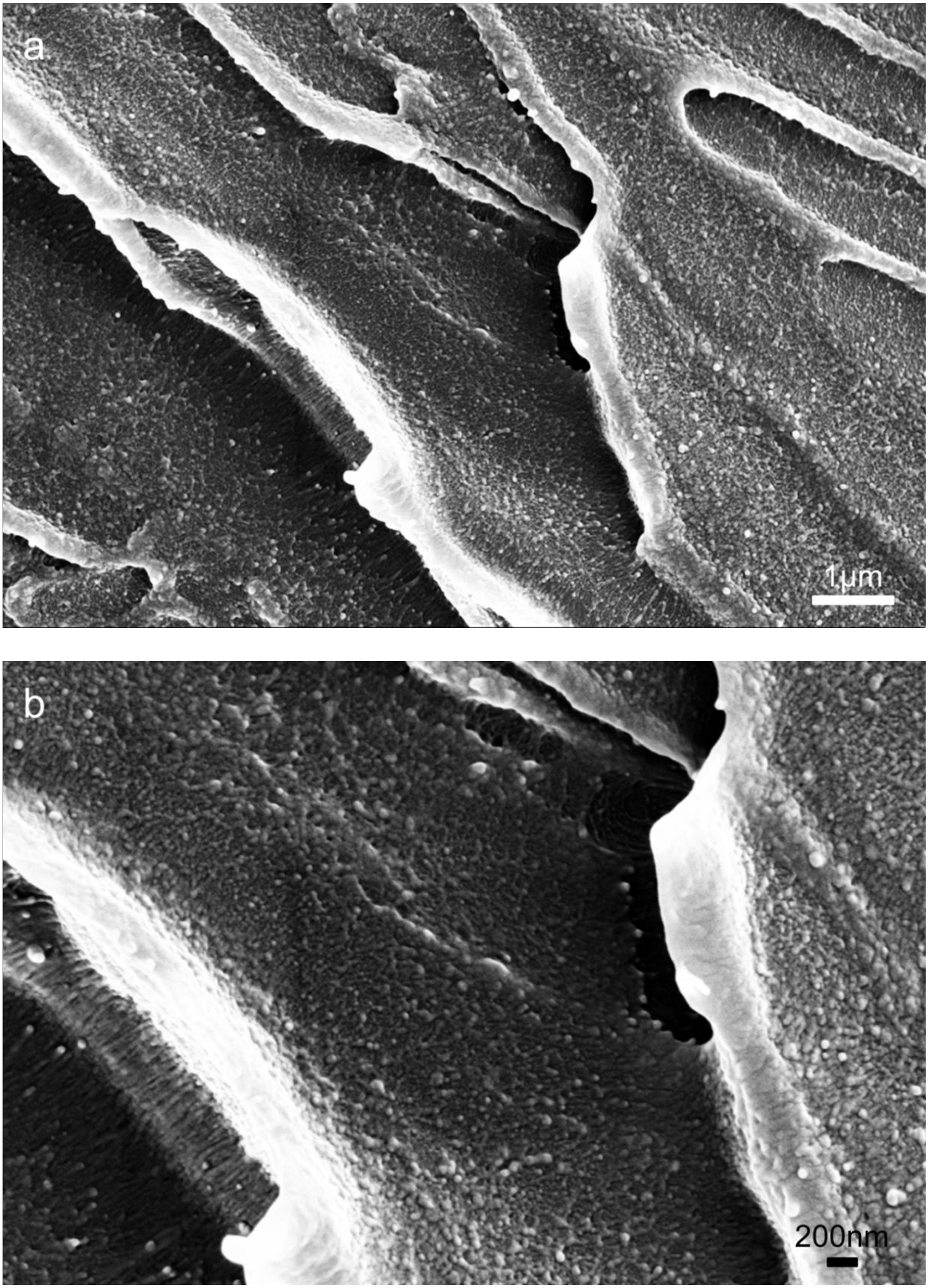

Figure 46 SEM micrographs of fracture surface of PC/0.3wt% TSP-POSS at a) low and b) high magnifications. Stretched fibrils are becoming more numerous with increased TSP-POSS content

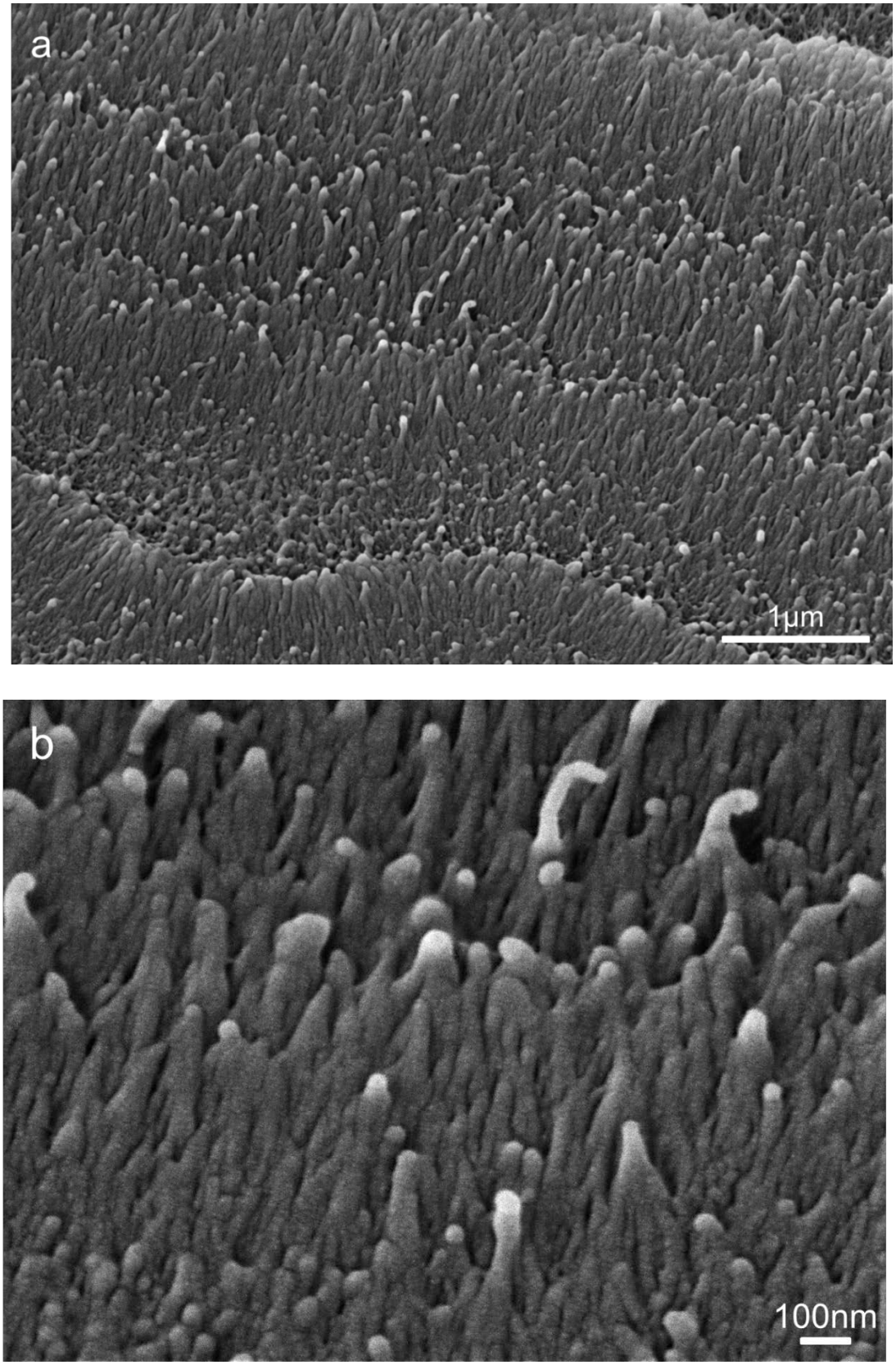

Figure 47 SEM micrographs of the fracture surface of PC/0.3wt% TSP-POSS at a) low and b) high magnifications. Stretched fibrils are clearly evident and again have increased in number with increasing TSP-POSS content

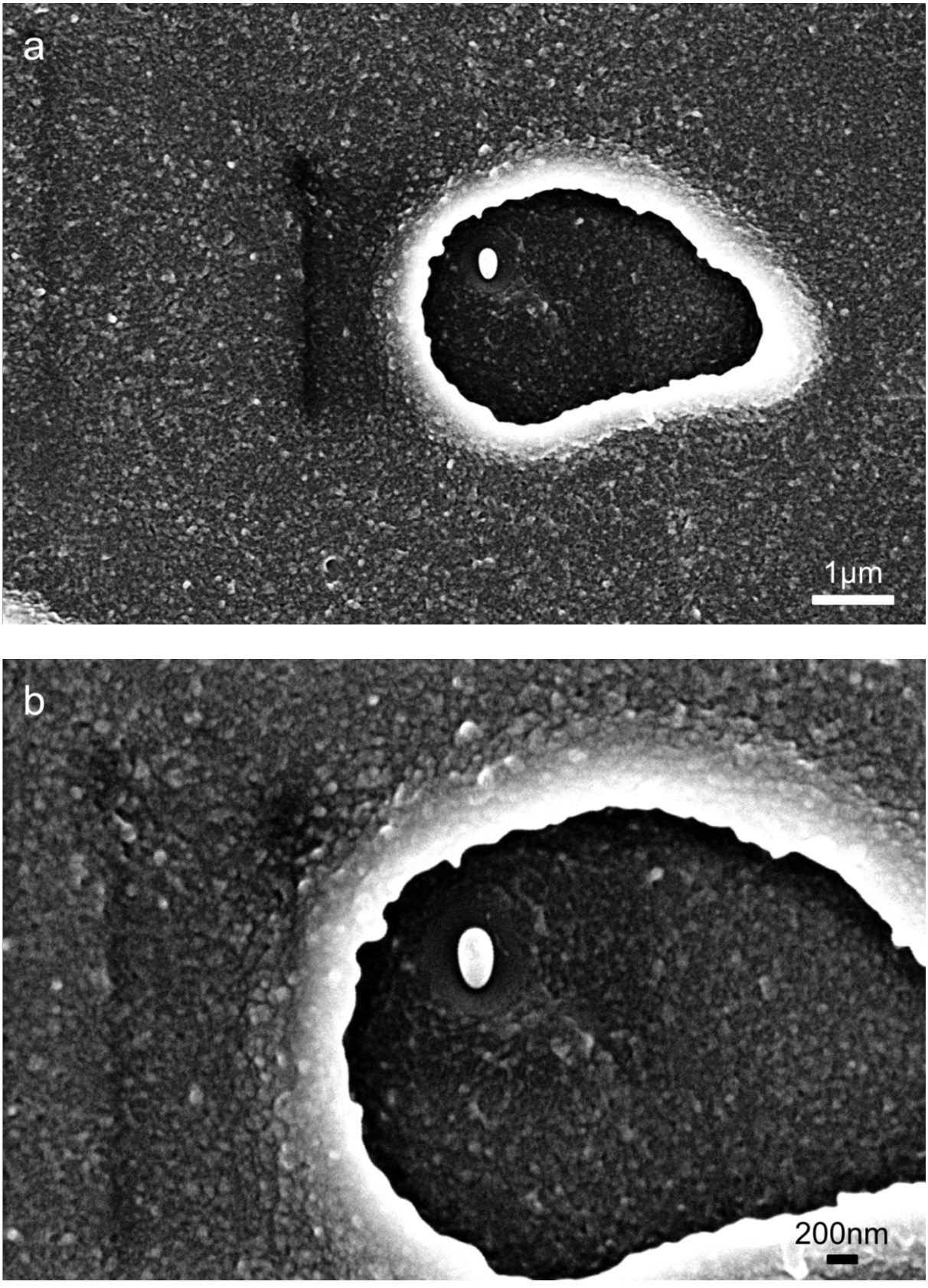

Figure 48 SEM micrographs of the fracture surface of PC/0.5wt% TSP-POSS at a) low and b) high magnifications. Spherical features are now present in the polymer matrix and are thought to be TSP-POSS aggregates

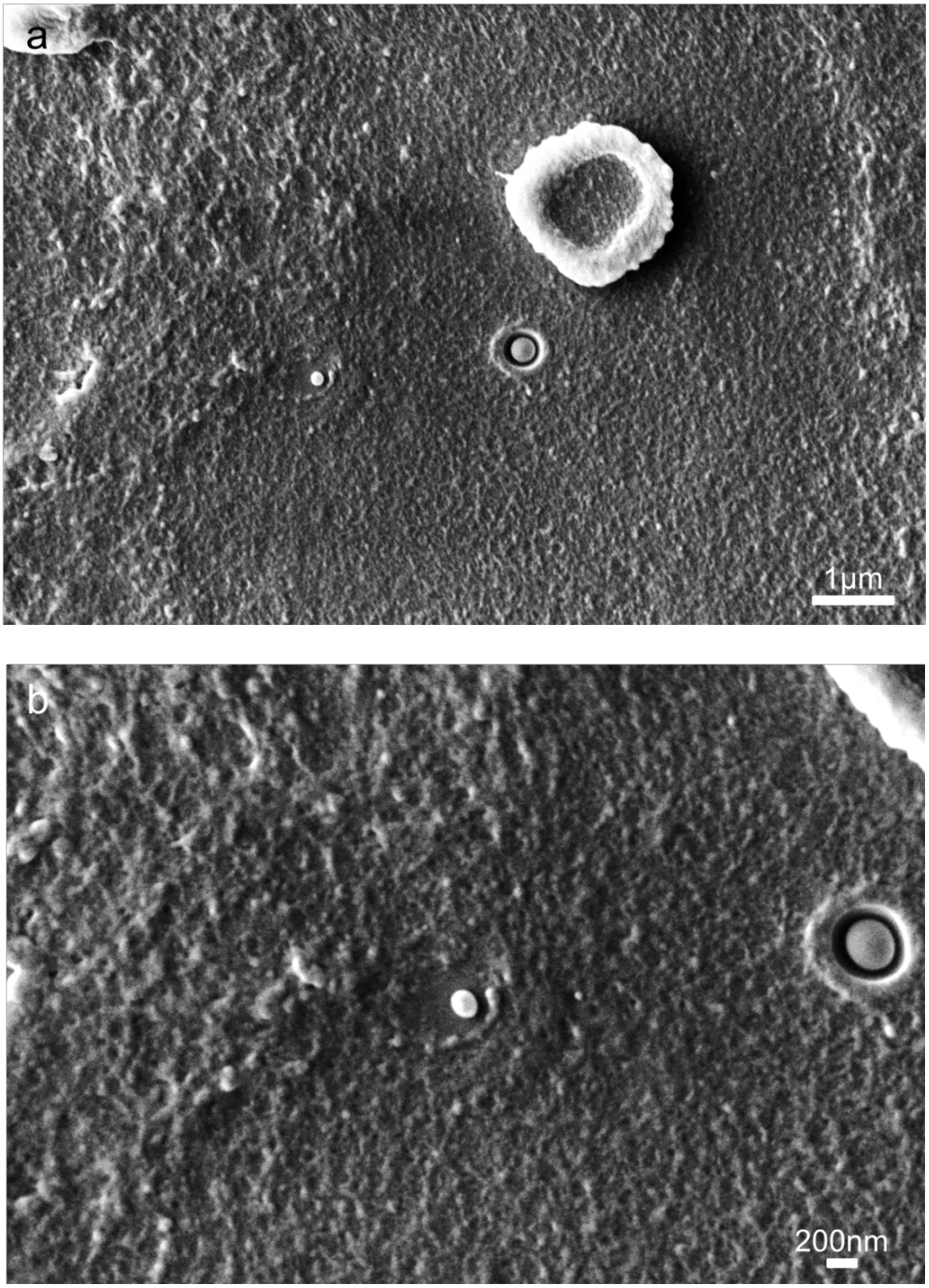

Figure 49 SEM micrographs of the fracture surface of PC/1wt% TSP-POSS at a) low and b) high magnifications. Spherical objects are becoming more numerous at increased TSP0POSS content. The objects are thought to be TSP-POSS aggregates and they appear to reside in a void which could be a feature of a toughening mechanism found in rubber toughened systems.

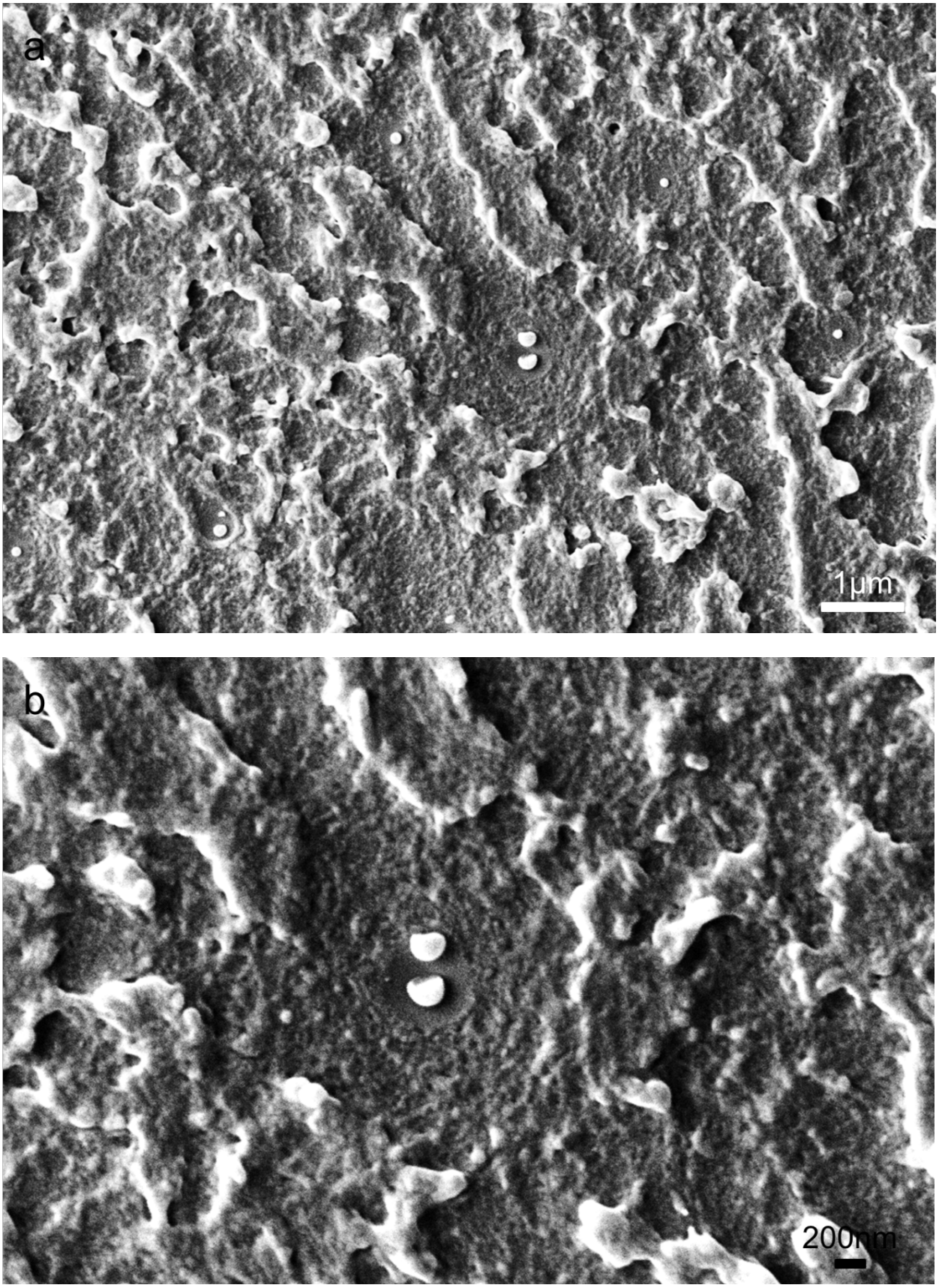

Figure 50 SEM micrographs of the fracture surface of PC/1wt% TSP-POSS at a) low and b) high magnifications. The white spherical objects could be potential TSP-POSS aggregates.

a

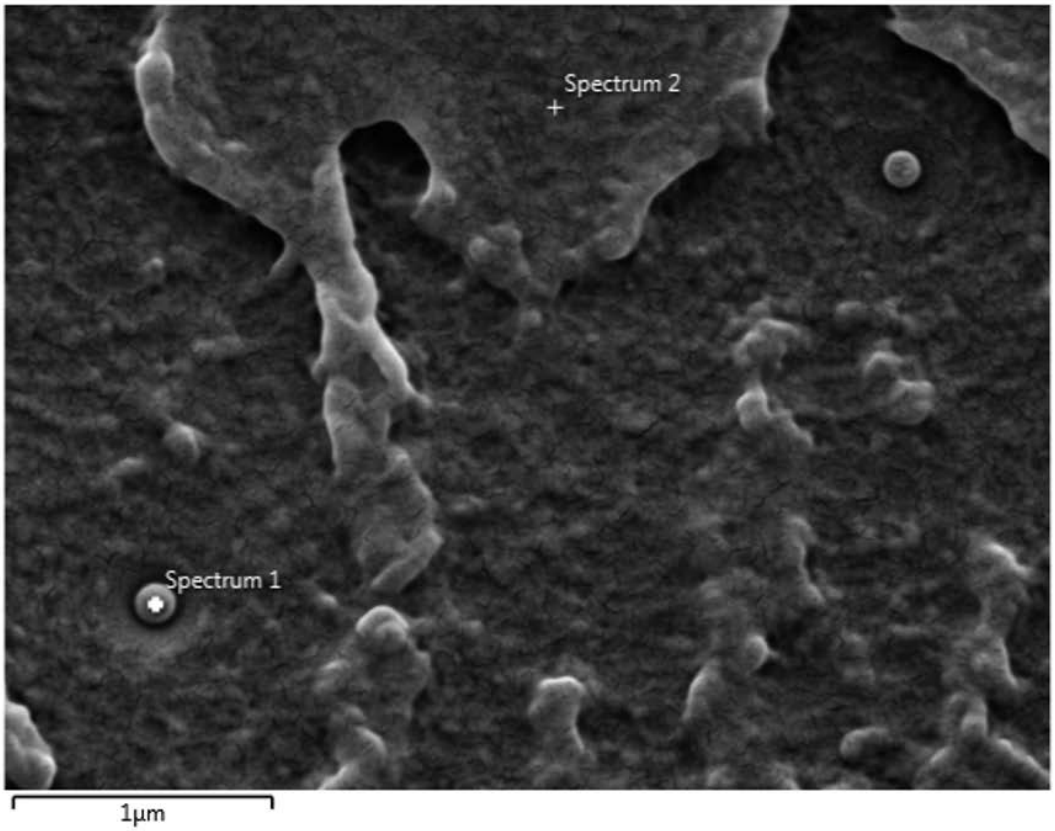

b

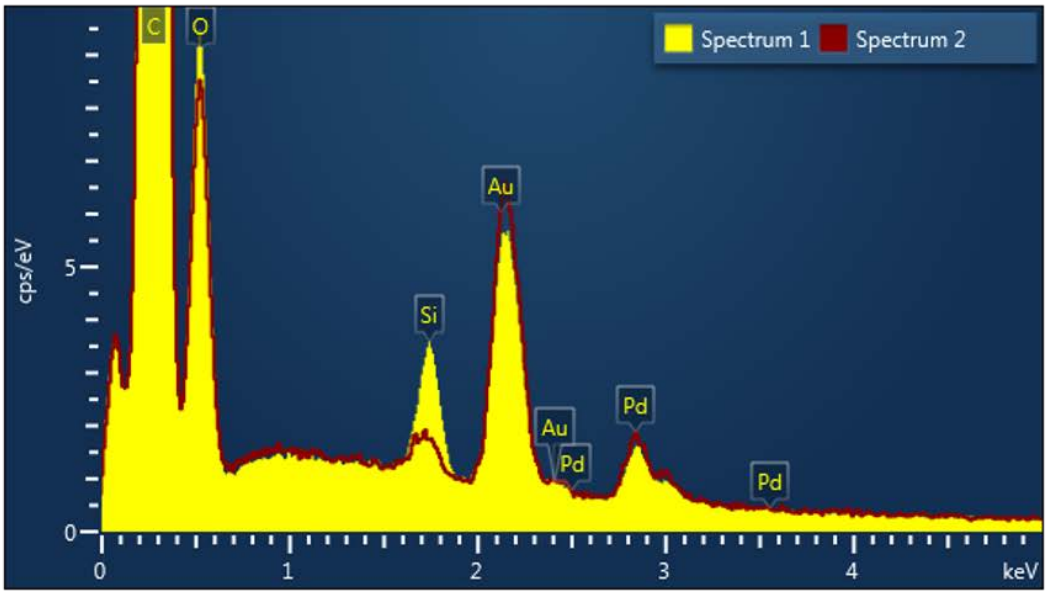

Figure 51 (a) Electron image of the artefacts thought to be TSP-POSS aggregates (spectrum 1) and the polymer matrix (spectrum 2) (b) EDS spectrum of spectrum 1 and spectrum 2 showing the increase in silicon content between the two areas. The increase in silicon content is an indicator that the artefacts are indeed TSP-POSS aggregates

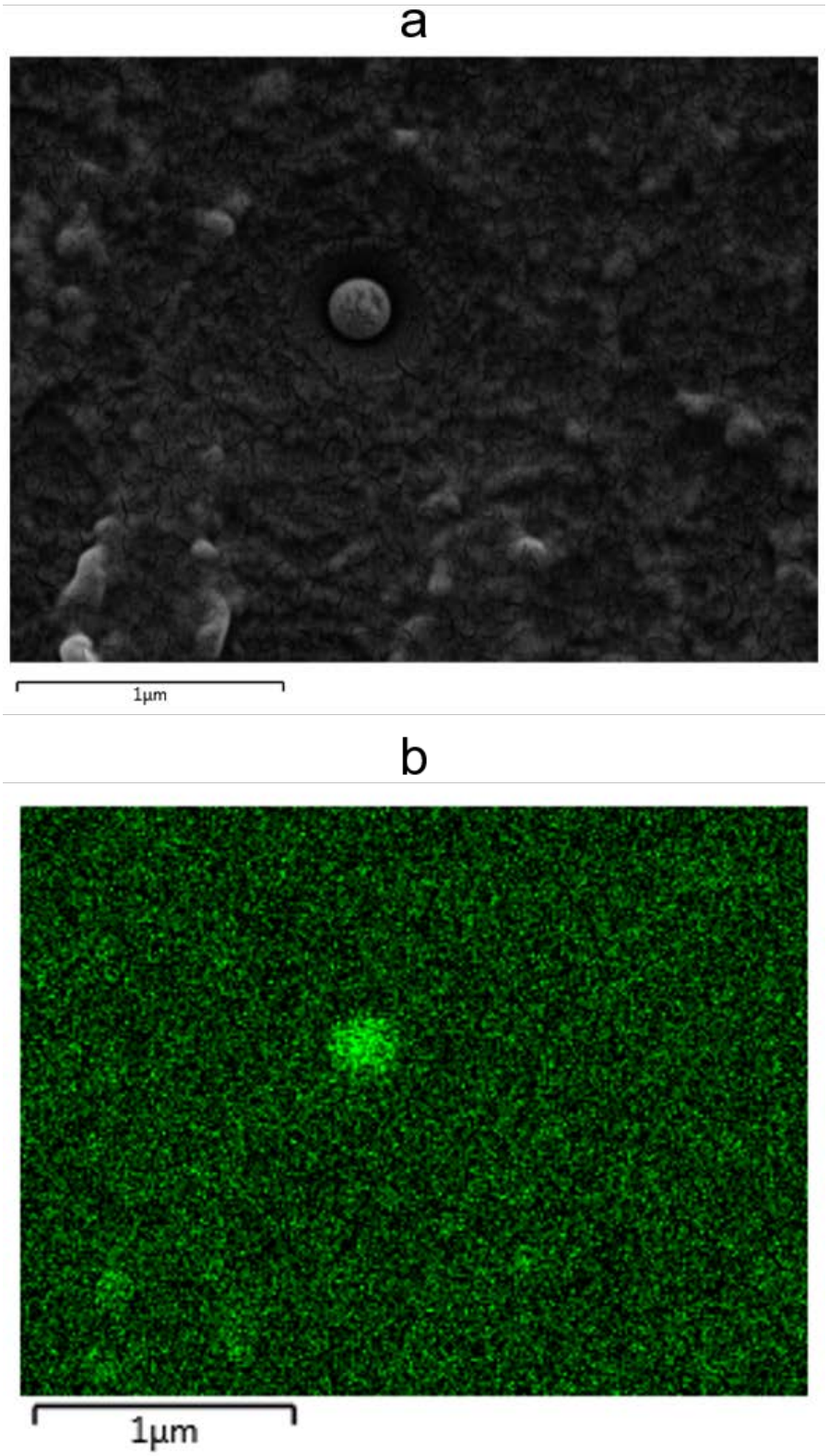

Figure 52 (a) Electron image of an artefact which is thought to be a TSP-POSS aggregate and (b) EDS mapping of silicon of the area containing the artefact. There is a clearly an increase in silicon content concentrated around the area of the artefact. This is an indicator that the artefact is a TSP-POSS aggregate

4.1.3. Transmission Electron Microscopy

Transmission electron microscopy (TEM) was also used to assess the dispersion state of TSP-POSS in the polycarbonate matrix. As TEM typically has a higher resolution than SEM it was hoped that a more detailed picture of the dispersion state and of TSP-POSS itself could be gained.

Microtomed specimens of the unmodified polycarbonate and the nanocomposites containing 0.05wt% to 1wt% TSP-POSS were viewed at magnifications of 20,000 and 50,000.

Nanocomposites containing up to 0.5wt% TSP-POSS appeared visually identical to the control sample and completely featureless (see figure 53(a)). From the manufacturer's POSS user guide, it is stated that good compatibility between POSS and polymer will allow the POSS to "dissolve" in the polymer matrix and will result in a clear TEM image. These results indicate that TSP-POSS is miscible in the polymer matrix as molecules.

Figure 53(b) contains a TEM image of PC/1wt% TSP-POSS. Ellipsoidal objects of no more than 100nm are observed. Elemental analysis was carried out on the sample containing 1wt% TSP-POSS to determine whether the artefacts were TSP-POSS aggregates. As TSP-POSS contains silicon, any increase in the concentration of this element was used to indicate the presence of TSP-POSS. However, no change in silicon concentration was detected, suggesting that: (i) The observed objects seen in figure 53(b) are not TSP-POSS aggregates and are probably just debris/chippings introduced during the sample preparation and (ii) TSP-POSS is miscible in the polycarbonate matrix and has dispersed at the nanoscale. Any TSP-POSS aggregates present could have been removed during the sample preparation process.

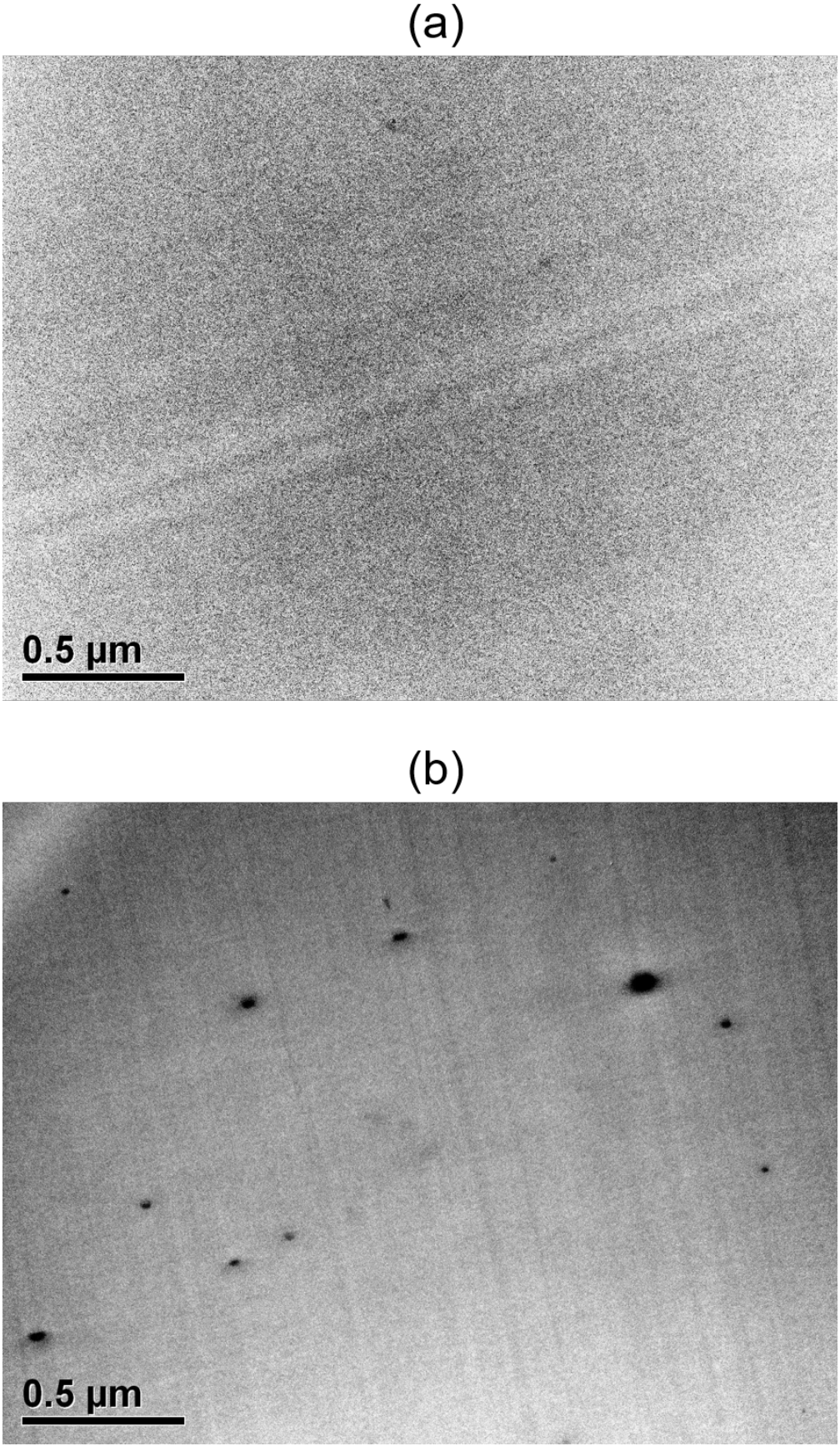

Figure 53 TEM images of (a) PC/0.5wt% TSP-POSS and (b) PC/1wt% TSP-POSS at 20k magnification.

4.2. Optical Properties

4.2.1. Ultraviolet-Visible Spectroscopy

The effect of TSP-POSS on the optical transparency of polycarbonate was assessed using UV-Vis spectroscopy. The diffuse transmittance of polycarbonate and nanocomposites containing between 0.05wt% and 1wt% TSP-POSS is shown in figure 55 for the wavelength range, 300 nm-1000 nm.

It is clear from figure 55 that the addition of TSP-POSS does not have a detrimental effect on the transparency of the polymer matrix. Miscibility of POSS in the polymer matrix will result in maintenance of optical transparency. Immiscibility will result in haze in the samples [88]. Similar results were attained by Iyer and Schiraldi for a PC/TSP-POSS nanocomposites system and again, it was proposed that such a result suggests that POSS is dispersed at the nanoscale or is soluble in the polymer matrix [107]. This is confirmed by SEM as visible aggregates were less than 200 nm in size. In fact, all nanocomposite samples exhibit higher levels of transparency than the control sample, with the transmission increasing with increasing TSP-POSS content. PC/1wt% TSP-POSS transmits approximately 5% more light from λ = 400 to 1000nm than the unmodified polymer. The trend is not insignificant, however the experimental error and variation in thickness between samples cannot be ruled out and as such the trend could be a coincidence.

Yari and Mohseni [131] also observed an enhancement in optical transparency of a POSS modified acrylic melamine clearcoat but did not specify why. It has also been stated in the literature that transparency of polymers can be increased by the addition of nanofillers but the exact reasons are not given [223].

In our research, it could be that TSP-POSS can reduce the diffuse reflectance of the polycarbonate and decrease its absorption coefficient. This may be because the TSP-POSS has modified the structure of polycarbonate somewhat or decreased the surface roughness. Further testing and analysis would be required to fully understand this effect but due to time limitation this was not able to be conducted in the course of the project.

Ultimately, the addition of TSP-POSS to the polycarbonate does not have a harmful effect on the optical transparency of the polymer and is a good result for transparent armour applications.

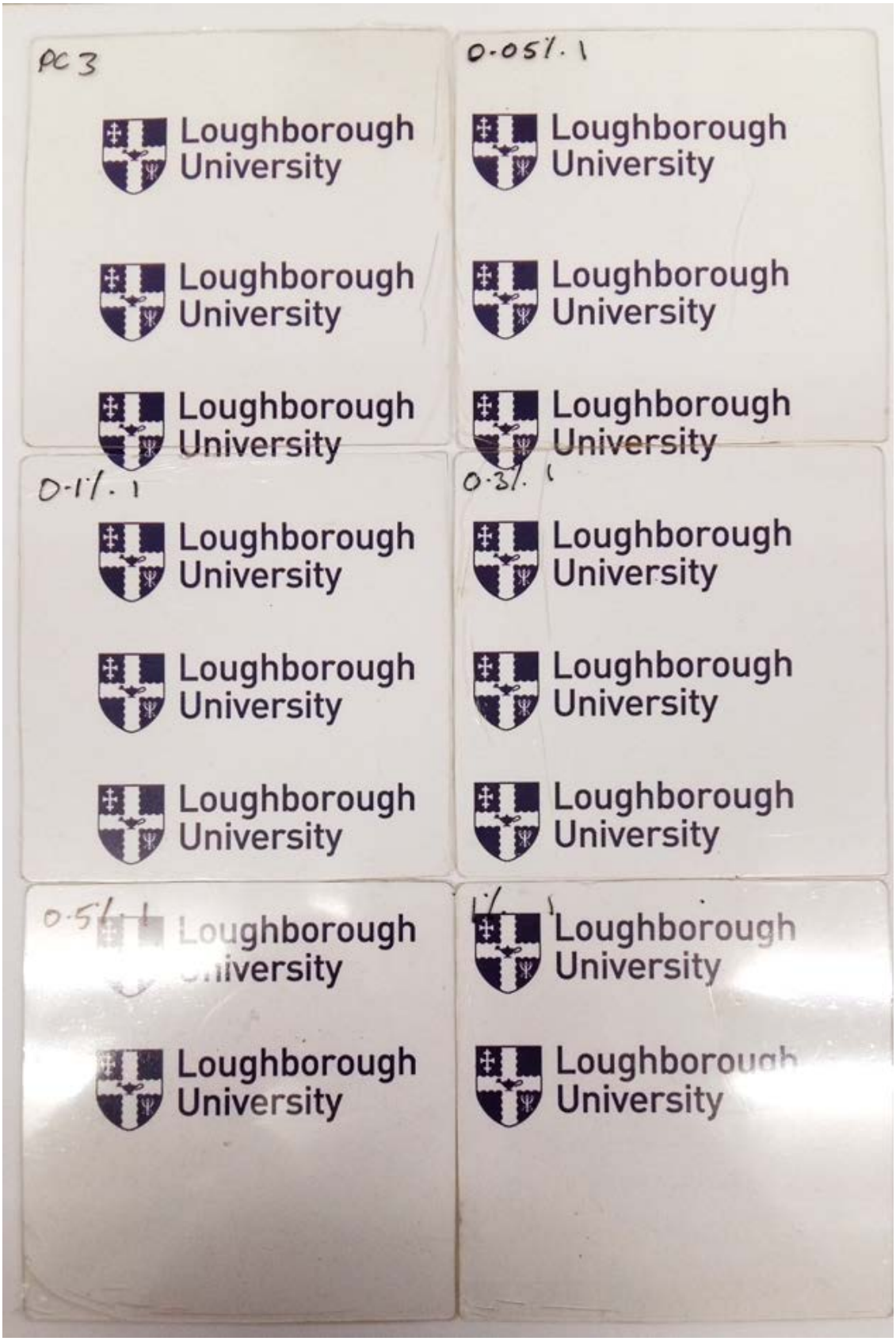

Figure 54 Visual assessment of the transparency of the samples used in UV-Vis spectroscopy

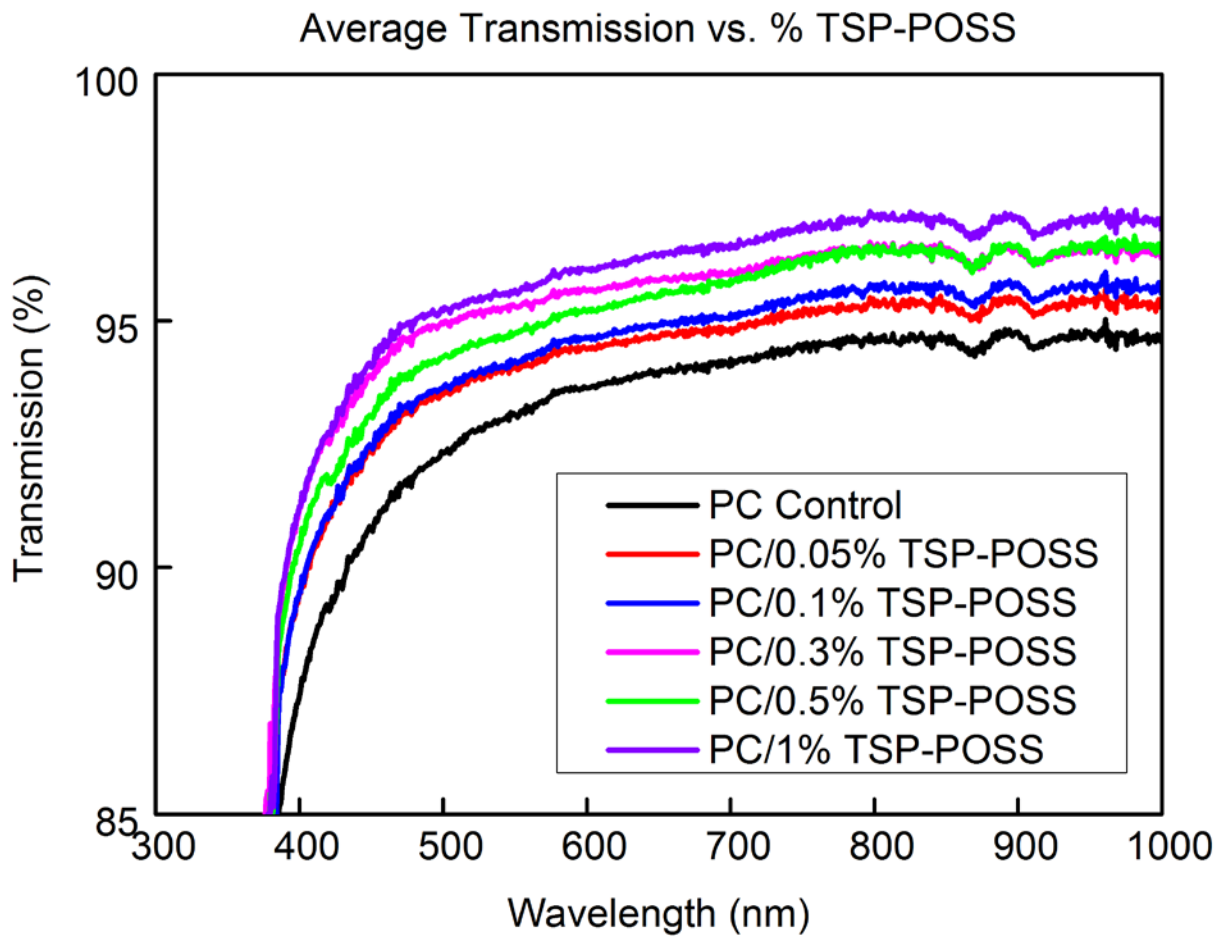

Figure 55 Transmission spectra of polycarbonate and its TSP-POSS modified nanocomposites measured using UV-vis spectroscopy. TSP-POSS does not have a detrimental effect on the transparency of polycarbonate and appears to increase it somewhat

4.3. Thermal Properties

4.3.1. Differential Scanning Calorimetry

To determine the annealing temperatures for the physical aging study, the glass transition temperatures, T_g, of polycarbonate and three nanocomposites (containing 0.1wt%, 0.5wt% and 1wt% TSP-POSS loading) were first measured using modulated differential scanning calorimetry. T_g values were taken as the peak values of $\frac{dC_p}{dT}$.

Table 3 contains the T_g values for the polycarbonate control sample and the three nanocomposites obtained from the MDSC heating scans. The effect of TSP-POSS on T_g of polycarbonate is marginal.

wt% TSP-POSS	T_g (°C)	T_{a1} (°C)	T_{a2} (°C)	T_{a3} (°C)
PC Control	144.2	134	132	130
ΔT		10.2	12.2	14.2
0.1	144.6	134.4	132.4	129.4
0.5	143.8	133.6	131.6	128.6
1	143.6	133.4	131.4	128.4

Table 3 The glass transition and aging temperatures of polycarbonate and its nanocomposites containing 0.1wt%, 0.5wt% and 1wt% TSP-POSS

At the lowest loading of 0.1wt%, TSP-POSS increases T_g of polycarbonate from 144.18 °C to 144.57 °C, a difference of 0.39 °C. At higher loadings (0.5-1wt%), TSP-POSS decreases T_g of polycarbonate to 143.83 °C and 143.63 °C, respectively. As these differences are small they fall within the margin of error and can be lost in the noise of the experiments. Therefore, it should be concluded that TSP-POSS addition of up to 1wt% has a negligible effect on the T_g of polycarbonate.

The variation in heat flow and complex heat capacity for polycarbonate and the nanocomposites is shown in figure 56. Figure 56(a) shows that the heat flow is negative for all samples, signifying an endothermic reaction i.e. a transition which takes in energy. It is clear from figure 56(a) that the nanocomposites require the absorption of more heat to undergo the glass transition than the polycarbonate control sample. This implies reduced mobility of the polymer chains with the addition of TSP-POSS. Moreover, the dip in the heat flow spectra of the nanocomposites (ca. 140°C), which represents the glass transition, is larger than that of the polycarbonate control. Again, this symbolises an increased amount of heat absorption in the nanocomposite samples. This idea is reflected in the heat capacity curves displayed in figure 56(b). Specific heat capacity is a measure of the capability of a substance to absorb energy and is therefore related to molecular mobility [224,225]. Figure 56(b) shows the peaks in the heat capacity (ca. 145°) which represent the glass transition

temperature. It occurs at virtually the same temperature for the control sample and the nanocomposite sample (Table 3 contains the T_g values estimated from figure 56(b)). However, the magnitude of the peaks is much larger in the spectra of the nanocomposite than that of the control sample suggesting that TSP-POSS has increased the amount of energy absorbed by the sample and that more energy is required to raise the temperature of the sample and through the glass transition. This could be because POSS has impeded the chain motion. This could either be due to the rigid structure of TSP-POSS or the formation of bonds, such as hydrogen bonds, between the active Si-OH groups on the TSP-POSS and the polar carbonyl groups of polycarbonate. The presence of such interactions would link the nanofiller and the polymer chains together to form a network of sorts, which would require more energy to go through the glass transition.

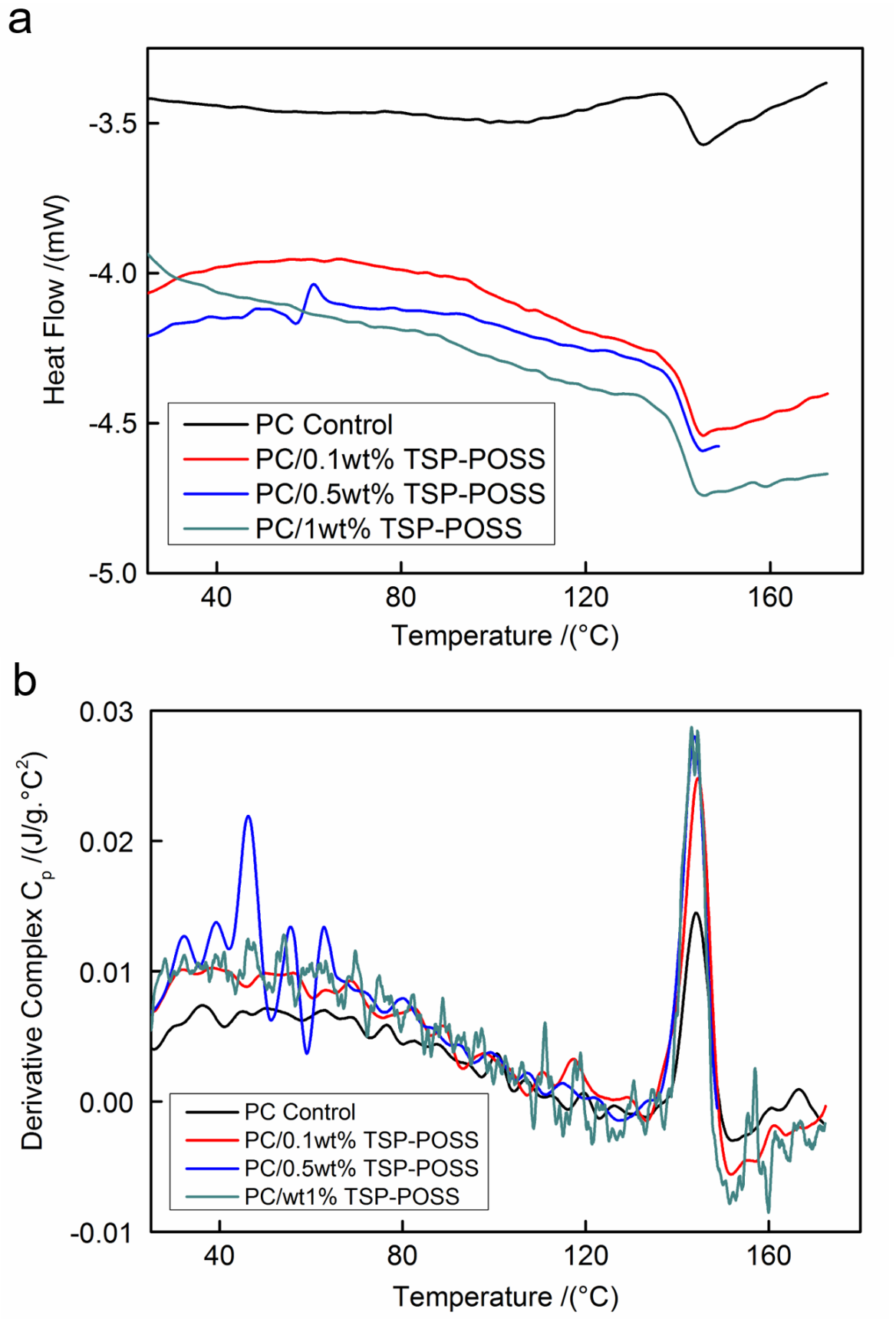

Figure 56 (a) DSC heat flow and (b) derivative complex heat capacity of polycarbonate and its TSP-POSS based nanocomposites

4.4. Viscoelastic Properties

4.4.1. Dynamic Mechanical Analysis

Dynamic mechanical analysis was used to assess the effect of TSP-POSS on the viscoelastic properties and glass transition of polycarbonate. The results can give information on the dispersion of TSP-POSS in the polymer matrix and its effect on the chain dynamics. Temperature ramps and frequency sweeps were performed on polycarbonate and nanocomposite samples containing 0.05wt% - 1wt% TSP-POSS. The creep behaviour of the nanocomposites was also studied using DMA.

4.4.1.1. Effect of Temperature

The temperature was varied from 80 °C – 180 °C during the temperature ramp at a heating rate of 3 °C/min and using driving frequencies of 1 Hz and 10 Hz. Spectra of these results can be seen in figures 57-59. The values of glass transition temperature, T_g taken from the peak value of the *tanδ* spectra can be found in figure 60 for the control samples and the TSP-POSS based nanocomposites.

Focusing on figure 57(a), there are two observations that can be made in regards to how TSP-POSS affects the storage modulus of polycarbonate at 1 Hz. Firstly, below 130 °C, all nanocomposites except PC/0.05wt% TSP-POSS have a lower storage modulus than the control sample. Perhaps a loading of 0.05wt% TSP-POSS is not high enough to have a noticeable effect on the storage modulus of polycarbonate. SEM images show that the fracture surface morphology of PC/0.05wt% TSP-POSS is similar in appearance to the control sample and could explain the result in figure 57. Above 130 °C, the glass transition temperature however, all nanocomposites (except PC/0.1wt% TSP-POSS) exhibit a larger storage modulus than the control sample.

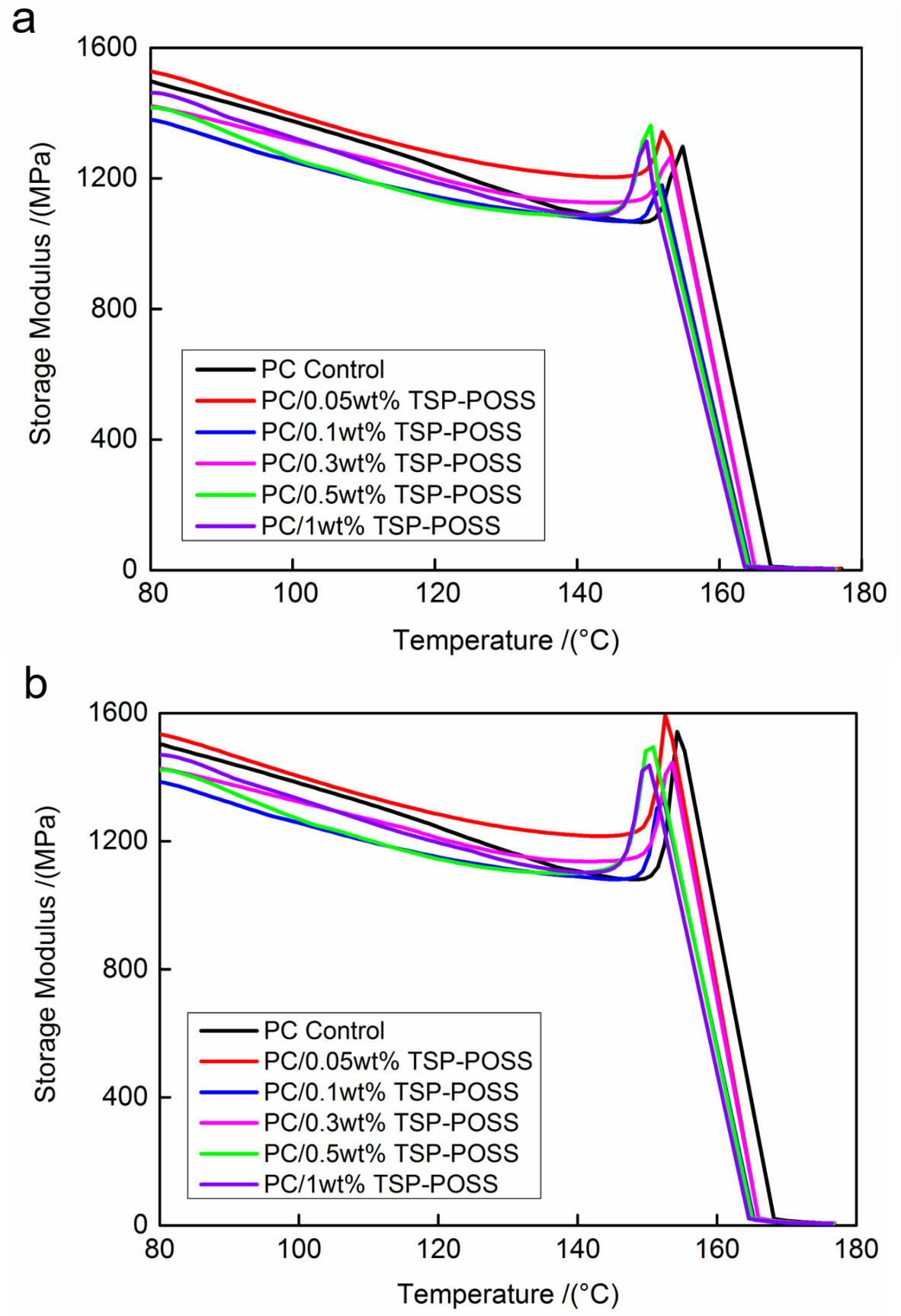

Figure 57 Storage modulus of polycarbonate and its TSP-POSS based nanocomposites at a) 1Hz and b) 10Hz showing the glass transition

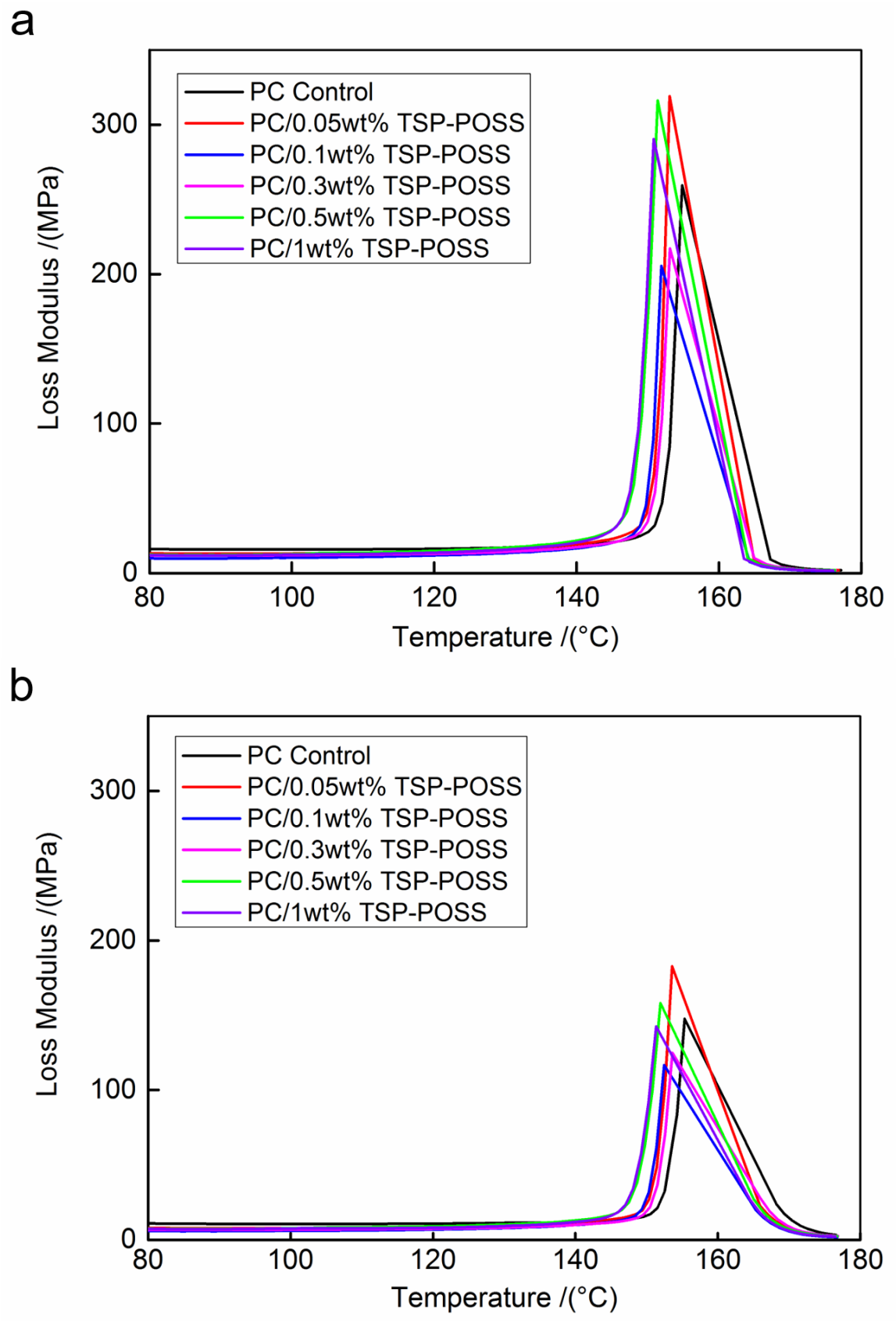

Figure 58 Loss modulus of polycarbonate and its TSP-POSS based nanocomposites at a) 1Hz and b) 10Hz over the glass transition

A similar result was found by Martins et al. in a PVDF/Methacryl POSS system [123]. The onset of the glass transition occurs earlier in the nanocomposites than it does in the unmodified polycarbonate. When a frequency of 10 Hz is used, similar behaviour can be seen. Overall, the results shown in figure 57 suggest TSP-POSS has a slight plasticising effect on the polycarbonate matrix. Plasticisers work by increasing the free volume of the polymer i.e. the amount of space a molecule has for internal movement. At the glass transition temperature, the polymer chains gain enough kinetic energy to move around and relieve stresses placed on them. This is exhibited as a decrease in the storage modulus and an increase in the loss modulus of a polymer. Therefore, if the free volume of a polymer is increased, the resulting increased chain mobility will mean less energy is required for the chains to relieve the stresses placed on them, resulting in a reduction in T_g. It is possible that TSP-POSS is able to increase the free volume of polycarbonate.

At both frequencies, there is a peak in the storage modulus spectra that precedes the glass transition. According to literature, this corresponds to a rearrangement in the molecules to relieve stresses that were “frozen in” below the glass transition temperature caused by the polymer processing method. For this reason, it is common to anneal the sample prior to DMA testing in order to eliminate processing effects [226]. However, this was not feasible in our work as annealing the samples would cause them to soften and lose the required dimensions for the DMA tests. Remoulding them would require processing again and would nullify the effects of annealing.

Figure 58 shows the effect POSS has on the loss modulus of polycarbonate. Again, the effect of TSP-POSS is two-fold; below 120 °C, loss modulus is lower for all nanocomposites in comparison to that of the polycarbonate control, indicating a lower dissipation of energy and more elastic behaviour. The peak of the loss modulus for the nanocomposites shifts to the left, representing a glass transition that occurs earlier than that of the control sample. The magnitude of the loss modulus is much lower when frequency is increased to 10 Hz. This is because at higher frequencies polymer chains “freeze” slightly and exhibit reduced mobility. As a result, less energy is dissipated and the result is a decrease in loss modulus.

The spectra in figure 59 show that upon addition of TSP-POSS there is a clear shift to the left of the *tanδ* peak for both driving frequencies used. In this study the peak is taken as an

estimation of the T_g and the values are plotted in figure 60 showing that TSP-POSS reduces the T_g of polycarbonate at all loadings.

Dintcheva et al. [90] investigated the effect of structural and chemical differences on polystyrene nanocomposites by using five different types of POSS, either with open or closed cages and different organic groups. They found that cage structure affects the rheological properties of the polymer and POSS dispersability; open cage structures have a more pronounced plasticising effect than closed cage structured POSS types as they are more flexible. TSP-POSS has an open cage structure, which would explain why it appears to have a plasticising effect on the polycarbonate. It is proposed that the plasticiser effect is due to 1) an increase in free volume, 2) a reduction in entanglement density and/or 3) a reduction in frictional effects between matrix macromolecules. A lower T_g suggests that the free volume of the polymer matrix has increased. As POSS is comparable in size to the polymer chain segments it has the potential to be able to integrate itself between chains, spacing them out so they can move past one another more easily at lower temperatures. This would imply that TSP-POSS is dispersed at the molecular scale. Moreover, TSP-POSS has an open-cage structure.

For a driving frequency of 10 Hz, the height of the *tanδ* peaks of the nanocomposites containing 0.3wt% - 1wt% TSP-POSS is larger than that of the polycarbonate control. As *tanδ* represents the damping factor this result suggests that TSP-POSS increases the efficiency of energy dissipation at these loadings [226]. Similar results were found by Zeng et al. who studied a PVDF/FP-POSS system. In their work *tanδ* of the polymer increased with increasing POSS content, reflecting greater viscous flow and corresponding to more efficient energy dissipation [165]. The increased energy dissipation could be due to the potential toughening mechanisms observation using SEM analysis (see figures 43-50). The height of the 10 Hz *tanδ* peak is much larger in magnitude than that of the 1 Hz *tanδ* peak. This is because the loss modulus for samples is lower at the higher testing frequency whilst the magnitude of the storage modulus is virtually unaffected by an increase in frequency.

Overall, the results shown in figures 57-59 suggest TSP-POSS is able to form a single uniform phase with the polymer implying good dispersion of the nanofiller. TSP-POSS is able to interact with the polymer where it has a slight plasticising effect. This is shown by an earlier

onset of the glass transition and lower T_g values. Similar behaviour in other POSS/polymer systems has also been found [124,125]. It is known that the type of polymer can determine the effect that POSS has on its thermo-mechanical properties; bulky POSS cages can increase the free volume of polymers and is generally the dominant effect when incorporated into stiff, glassy polymers. In the case of rubbery polymers, the rigidity of POSS helps to reinforce the polymer by restricting chain movement and reducing chain flexibility [106]. Our work agrees with this statement; polycarbonate is a glassy polymer and our research shows that TSP-POSS has a plasticising effect. As plasticisers work by embedding themselves between polymer chains it follows that TSP-POSS is dispersed at the nanoscale, either as single molecules or nanosized domains. The increase in free volume may contribute to increased energy dissipation capability of polycarbonate, due to increased chain motion and introduction of new toughening mechanisms, as suggested by increases in the *tanδ* peak height of nanocomposites containing 0.3wt% - 1wt% TSP-POSS and the observations made from the SEM micrographs of these nanocomposites.

The observation that TSP-POSS acts as a plasticiser contrasts with the conclusions drawn from the DSC results, which is that TSP-POSS impedes chain motion perhaps due to the formation of hydrogen bonds with the polymer. DSC is purely related to heating a sample and breaking bonds whereas DMA involves applying heat and subjecting the sample to a stress simultaneously. Perhaps, the proposed plasticising effects outweigh the potential restricting effects of TSP-POSS seen in DSC when a stress is applied to the system.

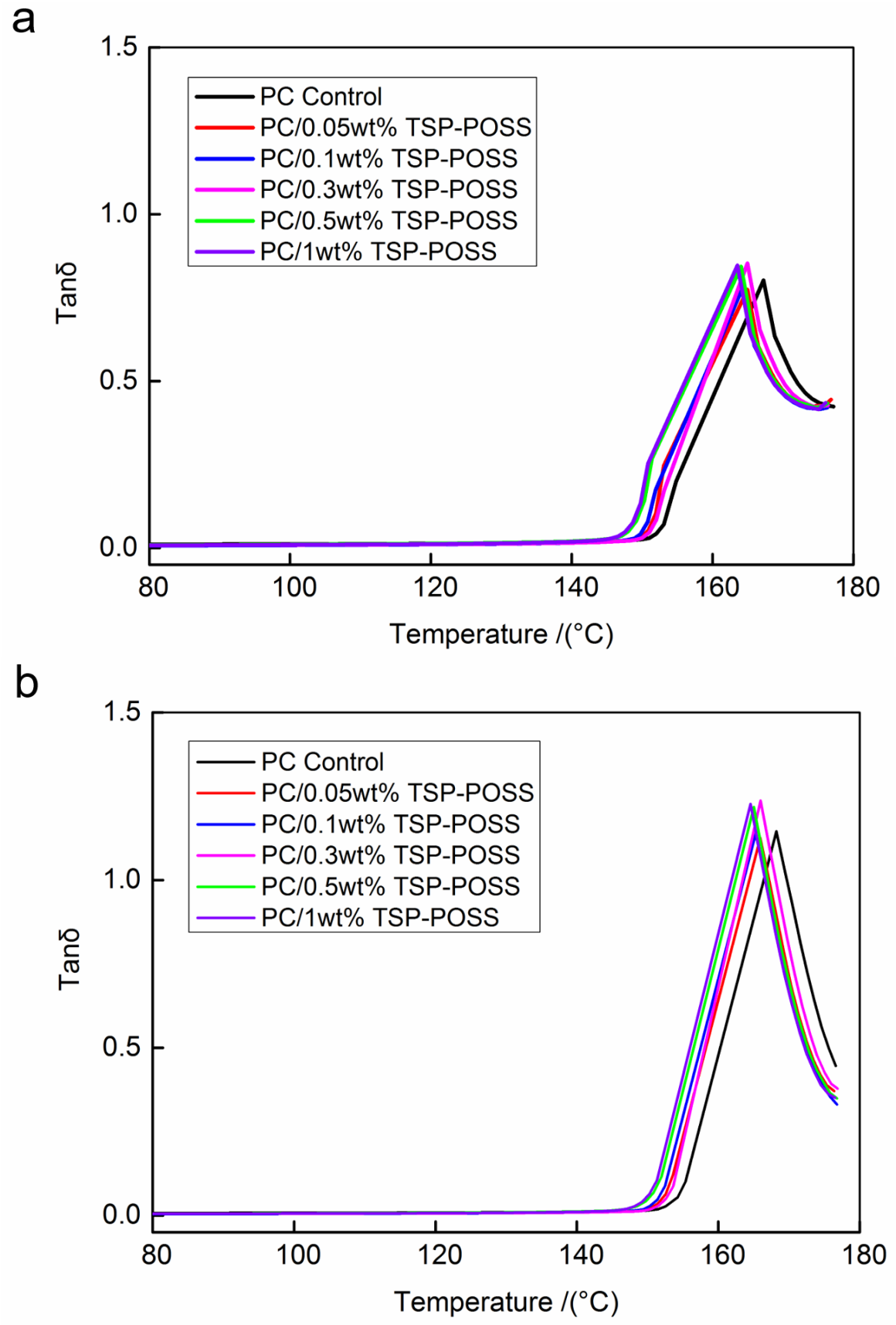

Figure 59 *Tanδ* of polycarbonate and its TSP-POSS based nanocomposites at a) 1Hz and b) 10Hz over the glass transition

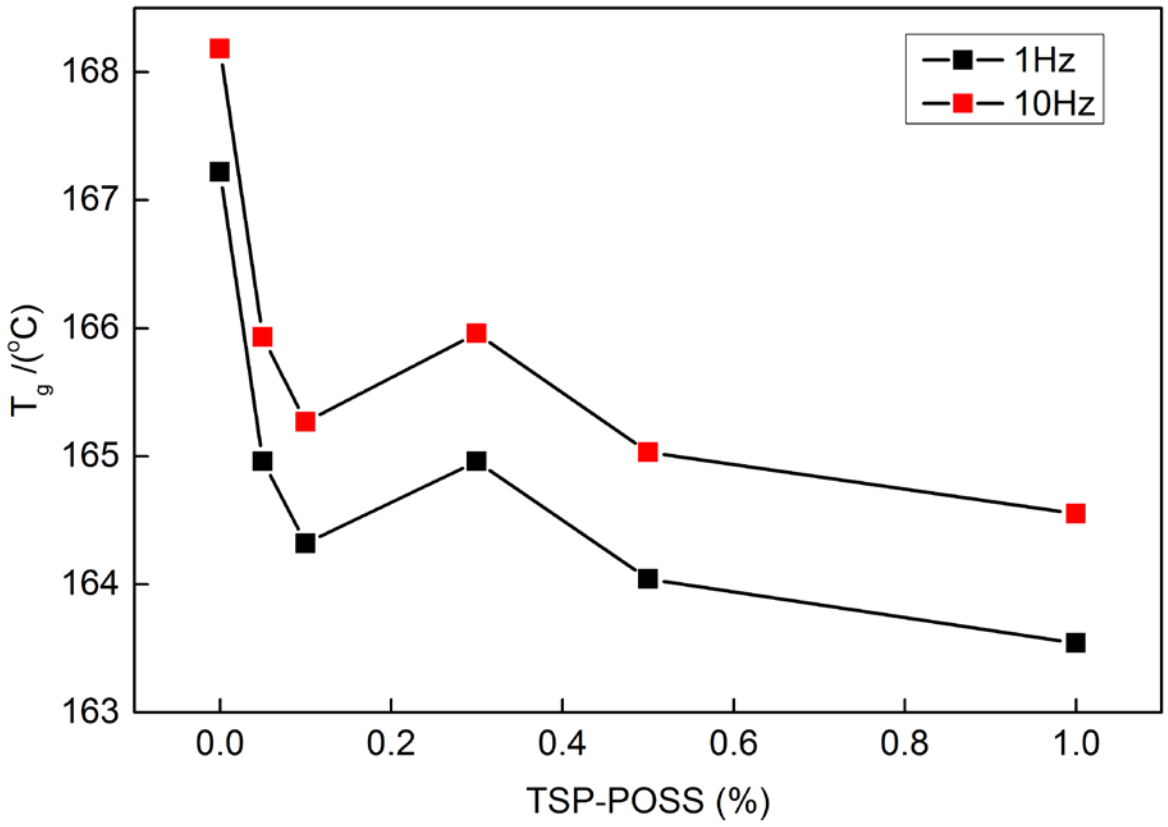

Figure 60 T_g values estimated from the peak of the *tanδ* curves

4.4.1.2. Effect of Frequency

The effect of frequency on the viscoelastic properties of polycarbonate and its TSP-POSS based nanocomposites can be seen in figure 61.

In figure 61(a), the storage modulus increases as frequency increases for both modified and unmodified PC. This is because higher frequencies induce more elastic-like behaviour. At lower frequencies, viscous behaviour dominates as the material has more time to relax and respond [226]. There is not a clear trend with respect to POSS concentration; an increase in polycarbonate storage modulus is seen with the addition of 0.05wt%, 0.3wt% and 0.5wt% TSP-POSS, however the storage modulus of the nanocomposites containing 0.1wt% and 1wt% TSP-POSS is lower than that of the polycarbonate control sample. However, at around 80 Hz, the storage modulus of PC/1wt% TSP-POSS begins to surpass that of the control sample. It would be interesting to perform frequency sweeps above 100 Hz to determine the potential of TSP-POSS to reinforce the polycarbonate matrix at higher frequencies. Frequency corresponds to strain rate as both are reciprocals of time and so subjecting the polymer

nanocomposites to higher frequencies would give information on their response to higher strain rates [227]. Unfortunately, we did not have the facilities to do such tests.

The peaks present in the curves represent the harmonics: natural resonant frequencies of the samples. Unfortunately, these can obscure desired information. Changing the sample dimensions can reduce resonance [226].

Figure 61(b) shows that for TSP-POSS loadings of 0.5wt% and 1wt%, the loss modulus is larger in magnitude than that of the polycarbonate control. This implies that at higher loadings of TSP-POSS the polycarbonate matrix becomes more viscous and is able to dissipate more energy.

At lower loadings however, the loss modulus is similar or marginally lower. A higher *tanδ* implies that the chains are less restricted. This follows on from the temperature ramp results; nanocomposites containing 0.5wt% and 1wt% TSP-POSS have the lowest T_g values out of all samples tested (see figure 60).

The *tanδ* spectra shown in figure 61(c) display the same trend as that of the loss modulus spectra; higher loadings cause an increase in *tanδ* whereas lower loadings do not have much of an effect. It would appear that at higher loadings (<0.3wt%) POSS could slightly increase the amount of energy the matrix can absorb and dissipate i.e. it increases the damping factor of polycarbonate and could be due to the possible toughening mechanisms observed in the SEM micrographs of these nanocomposites. At lower loadings POSS has a negligible effect on the energy absorption and dissipation capabilities of polycarbonate. This could be because at lower loadings TSP-POSS is miscible in the polymer matrix and has formed a single uniform phase and cannot drastically affect the chain dynamics of the polymer.

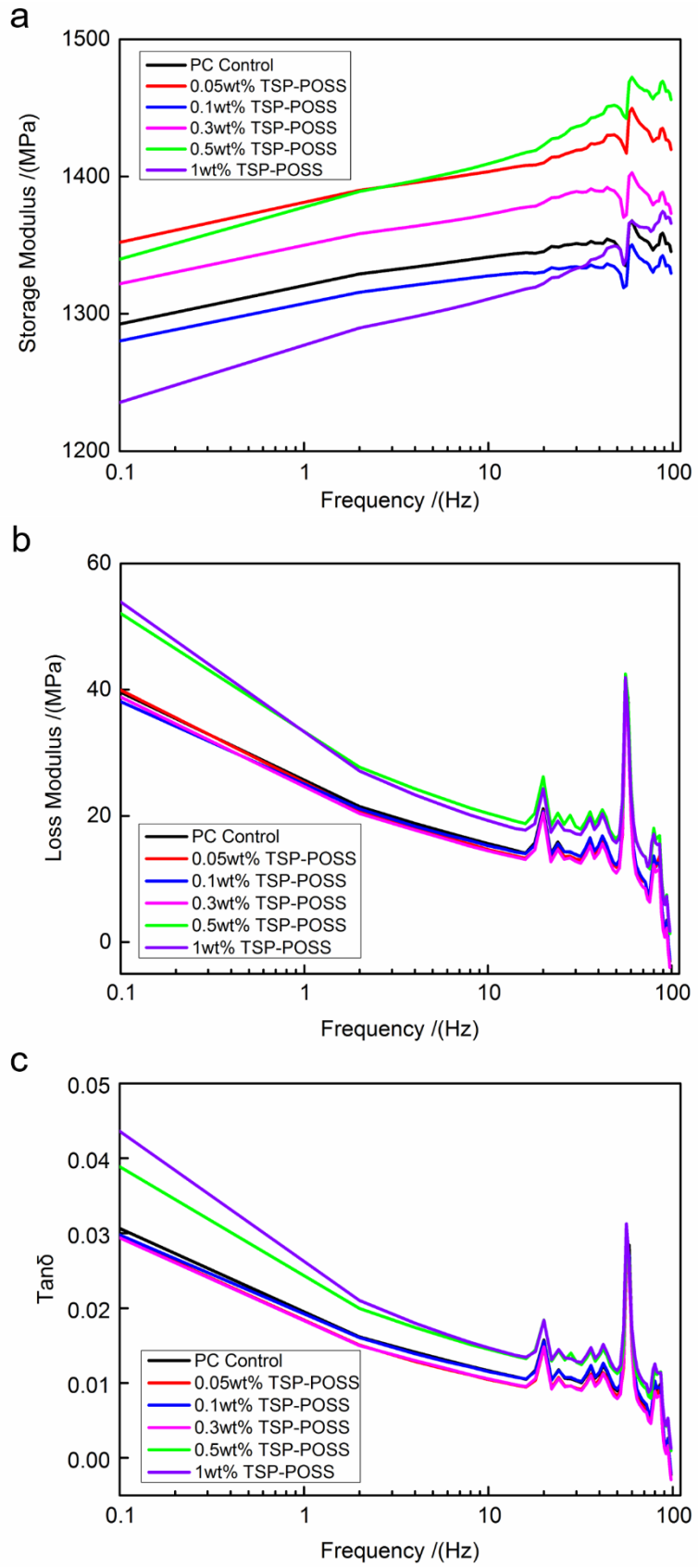

Figure 61 Frequency sweeps of polycarbonate and its TSP-POSS based nanocomposites a) storage and b) loss modulus and c) *tanδ* at 140ºC

4.4.1.3. Creep Behaviour

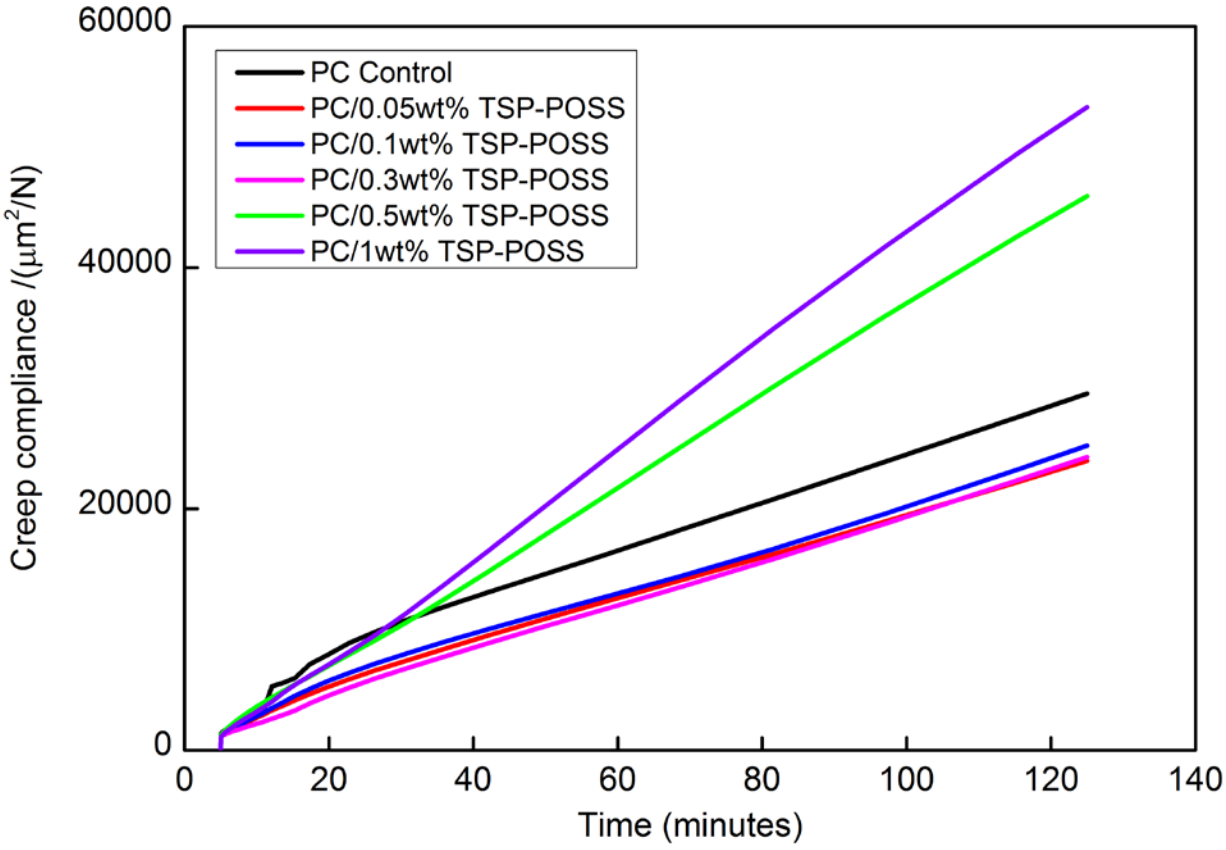

Figure 62 Creep spectra of polycarbonate and its TSP-POSS based nanocomposites at 140ºC

The creep behaviour of polycarbonate and the TSP-POSS based nanocomposites was characterised using DMA. The temperature was held at a constant 140 °C throughout the test. Figure 62 contains the results from the creep experiments.

The polycarbonate control creeps at an increasing rate at the beginning of the experiment (t<30minutes). The polycarbonate sample then creeps at a constant rate until the end of the experiment where it reaches a creep compliance of 29550 $\mu m^2/N$. The nanocomposites creep at a slower rate at the beginning of the test in comparison to the control sample and reach a more constant creep rate much faster (t<20minutes). Overall, the nanocomposites containing up to 0.3wt% TSP-POSS creep less than the polycarbonate control, with PC/0.3wt% performing the best. However, when TSP-POSS loading is increased to 0.5wt% and 1wt%, the resulting nanocomposites creep at a much faster rate than the other samples throughout the whole test, as shown by a steeper gradient, and overall deform more, with

PC/0.5wt% and PC/1wt% reaching a creep compliance of 45936 $\mu m^2/N$ and 53302 $\mu m^2/N$, respectively.

These results suggest that TSP-POSS can have one of two effects on the creep behaviour of polycarbonate. At lower loadings (below 0.5wt%) TSP-POSS reduces the amount that the matrix deforms under a constant load. As the size of TSP-POSS molecules are comparable in size to the polymer chains perhaps the more rigid TSP-POSS molecules are able to control the movement of the polymer chains by restricting their motion and thus reducing the amount the polymer creeps. TSP-POSS may have formed hydrogen bonds with the polymer chains which increases the energy needed to compress the material. This would imply there is a good dispersion of the nanofiller. Conversely, at higher loadings (above 0.3wt%) the polycarbonate matrix deforms more. This could be due to the potential POSS aggregates observed using SEM. It was proposed that these were involved in plastic void growth. Therefore, it follows then that the nanocomposites may creep more due to this toughening mechanism. This would also follow on from the decreases in T_g measured from the *tanδ* peak and nano-sized aggregates seen in the SEM images.

Chapter 5

Mechanical Properties

Chapter 5 Mechanical Properties of Polycarbonate and its TSP-POSS based nanocomposites

5.1. Tensile Test

Tensile tests were carried out at ambient temperature on polycarbonate and its TSP-POSS based nanocomposites. The average values of Young's modulus, tensile strength, elongation at break and toughness of the nanocomposites were calculated and plotted into graphs. The results can be found in figure 63 and table 4.

Figure 63(a) shows the Young's modulus of polycarbonate and its TSP-POSS based nanocomposites. The average Young's modulus of the polycarbonate control was (1.98 ± 0.04 GPa). This figure agrees with previously documented values of ca. 2 GPa [228]. With the addition of 0.05wt% TSP-POSS, the Young's modulus measures as (1.97 ± 0.07 GPa), similar to that of polycarbonate. Increasing the concentration of TSP-POSS to 0.1wt%, the Young's modulus increases to (2.08 ± 0.06 GPa) yet decreases to (2.03 ± 0.05 GPa) for 0.3wt% nanofiller loading. The Young's modulus reaches a maximum for PC/0.5wt% TSP-POSS (2.13 ± 0.06 GPa), which is an 8% increase over the Young's modulus of the control sample. This can be explained by the higher amount of rigid nanoparticles/aggregates present which can have a reinforcing effect on the polymer matrix which could either impede chain motion or the propagation of cracks. However, for samples containing 1wt% TSP-POSS Young's modulus decreases to a value similar to the control sample (1.97 ± 0.03 GPa). At this loading, the high concentration of POSS results in numerous aggregates (see section 4.1.2) which could cause premature failure and brittleness as they act as potential stress concentrators in the matrix. Overall TSP-POSS slightly increases the stiffness of the polycarbonate matrix below concentrations of 1wt%. Looking at the graph as a whole and taking into account the error bars, it would be expected that PC/0.3wt% TSP-POSS would have a Young's modulus value somewhere between the values of samples containing 0.1wt% and 0.5wt%.

Figure 63(b) shows that TSP-POSS only slightly increases the average tensile strength of polycarbonate at all loadings. A maximum of (113 ± 2 MPa) is achieved with 0.5wt% TSP-POSS loading, which is an 8% increase over the tensile strength of the unmodified polycarbonate (104 ± 4MPa). However, the sample containing 0.3wt% does not follow the trend of increasing tensile strength with increasing POSS content and again is expected to have a tensile strength between that of 0.1wt% and 0.5wt% TSP-POSS loading.

wt% TSP-POSS	Young's Modulus (GPa)	Tensile Strength (MPa)	Elongation at Break (%)	Toughness (Jm^{-3})
Control	1.98 ± 0.04	104 ± 4	8.44 ± 0.58	5.26 ± 0.66
0.05	1.98 ± 0.07	108 ± 2	9.06 ± 0.07	5.83 ± 0.15
0.1	2.08 ± 0.06	112 ± 3	9.69 ± 0.54	6.56 ± 0.34
0.3	2.03 ± 0.05	109 ± 1	9.81 ± 0.43	6.41 ± 0.36
0.5	2.13 ± 0.04	113 ± 2	8.74 ± 0.20	5.75 ± 0.15
1	1.97 ± 0.03	111 ± 1	9.60 ± 0.86	6.1 ± 0.68

Table 4 Tensile properties of polycarbonate and its TSP-POSS modified nanocomposites

At 1wt% TSP-POSS loading, the tensile strength starts to decrease once more but is still higher than that of the unmodified polycarbonate. From figure 63(b), tensile strength is largely independent of TSP-POSS concentration from 0.1wt% to 1wt% TSP-POSS.

The influence of TSP-POSS on the elongation at break of polycarbonate can be seen in figure 63(c). There is a clear increase in the elongation at break with the addition of TSP-POSS, with the ductility of the polycarbonate matrix increasing at all nanofiller loadings and a maximum reached with 0.3wt% TSP-POSS loading (a 16% increase over that of the polymer control). PC/0.5wt% TSP-POSS is the least ductile of all the nanocomposites with only a 4% increase in comparison to the polycarbonate control. One would expect it to perform somewhere between loadings of 0.3wt% and 1wt% TSP-POSS following the trend. The increases in ductility could be related to the presence of stretched fibrils (see figures 45-47) which increase the amount that the polymer chains can stretch/deform before breaking.

There appears to be a turning point in the data between 0.3wt% and 0.5wt% where a sacrifice between strength and ductility occurs. The nanocomposite containing 0.3wt% TSP-POSS is on average, the most ductile yet at this loading this comes with a decrease in tensile strength and stiffness. Conversely, the opposite is seen in the nanocomposite containing 0.5wt% TSP-POSS; at this loading, a maximum is seen in the tensile strength and Young's modulus but this occurs alongside a reduction in ductility. SEM analysis suggests that POSS forms aggregates at loadings higher than 0.3wt%.

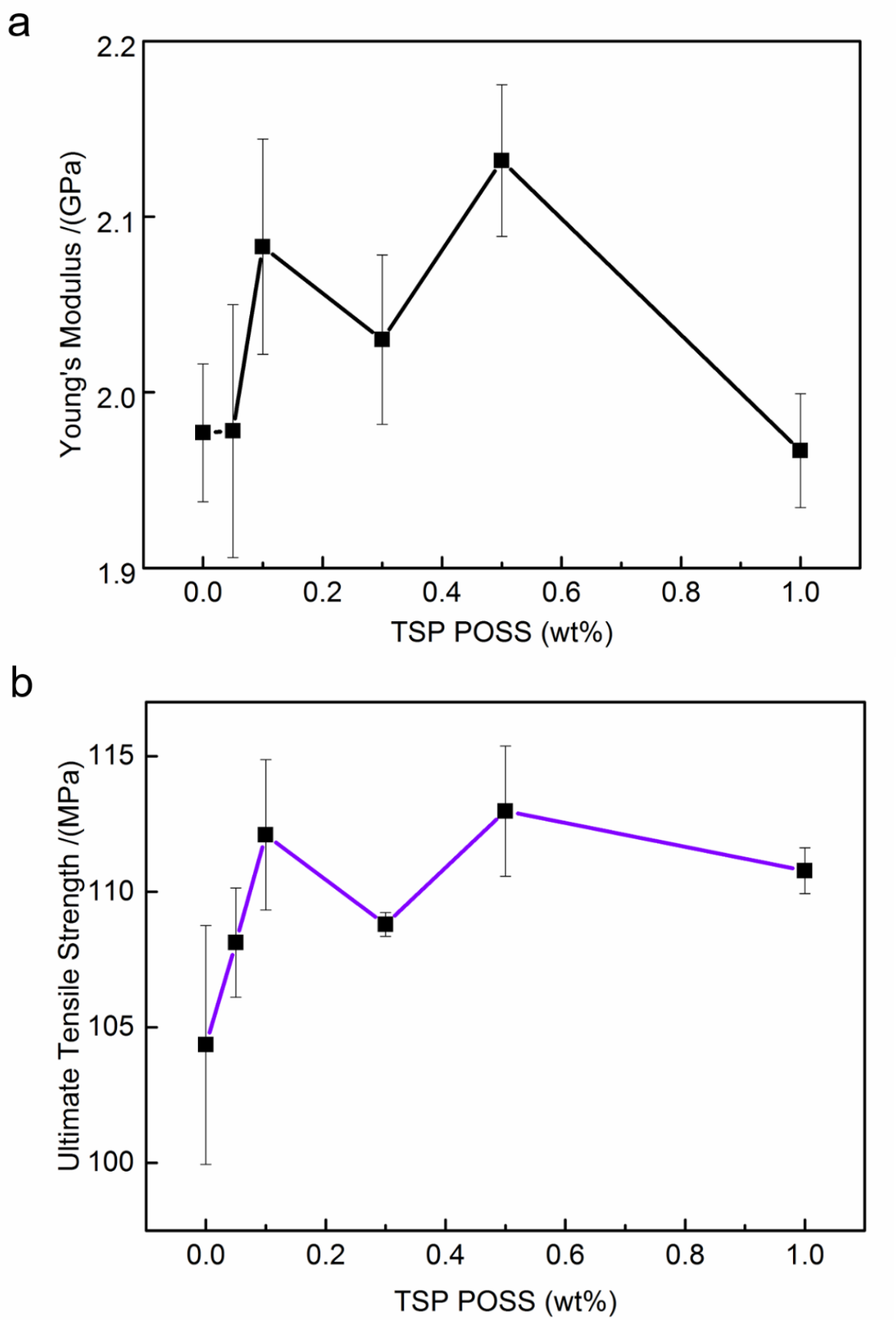
a
Young's Modulus /(GPa)
2.2
2.1
2.0
1.9
0.0
0.2
0.4
0.6
0.8
1.0
TSP POSS (wt%)
b
Ultimate Tensile Strength /(MPa)
115
110
105
100
0.0
0.2
0.4
0.6
0.8
1.0
TSP POSS (wt%)

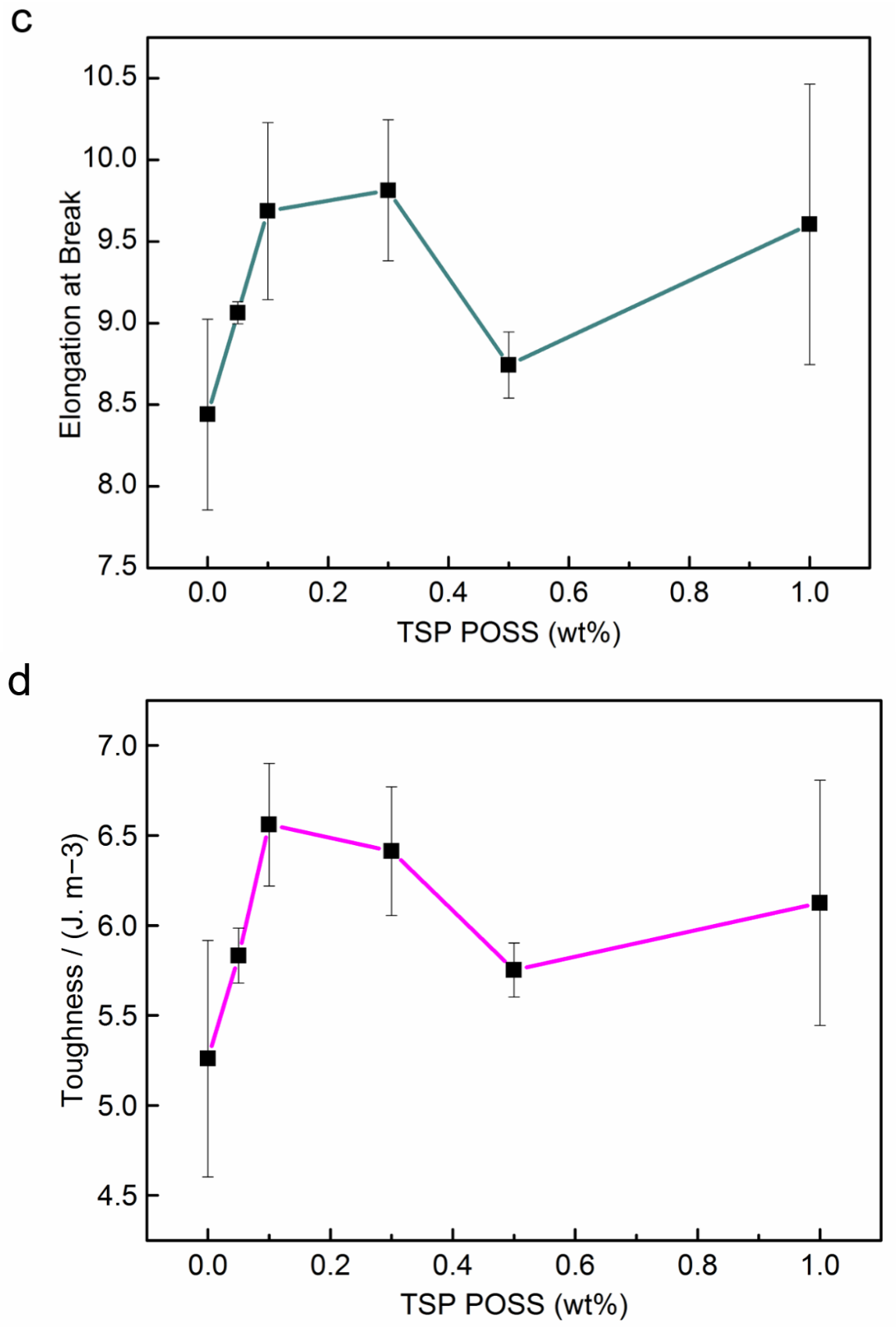

Figure 63 Average values of (a) Young's modulus, b) ultimate tensile strength, c) elongation at break and d) toughness of polycarbonate and its TSP-POSS modified nanocomposites

From the SEM micrographs, below this loading POSS appears to be finely dispersed within the polymer matrix and exist at the molecular scale or as domains of a few nanometres. Such dispersion would mean that POSS is able to locate itself between polymer chains where it can interact more with the polymer chains and potentially form hydrogen bonds which "link" together the polymer chains to form a stretchy network that allows the chains to deform more before failure, thus increasing the energy absorption capability of the polymer. This could explain why stretched fibrils are formed in these nanocomposites. Energy will also be required to break the hydrogen bonds between the filler and polymer. The tensile tests show that below 0.3wt% loading, POSS increases the ductility and strength of the polycarbonate but at 0.3wt% loading the POSS molecules simply plasticise the matrix. This could be due to the increased number of stretched fibrils seen in this nanocomposite which may increase the ductility at the sacrifice of strength. At 0.5wt%, the presence of POSS aggregates appear to increase the strength and stiffness but at the sacrifice of ductility. From the SEM micrographs, the amount of visible aggregates increased in number as POSS loading increased to 1wt%. At this loading, the Young's modulus decreased sharply so that it was similar to the control sample. Perhaps the amount of aggregates surpassed a critical value, above which they collectively increase stress concentration in the matrix and cause premature failure, resulting in decreased stiffness of the polymer.

The results so far can be better understood by measuring the toughness of the nanocomposites. This was done by calculating the area under the stress-strain graphs. Figure 63(d) shows that on average, all nanocomposites were tougher than the unmodified polycarbonate. Toughness increases from ($5.26 \pm 0.66\ Jm^{-3}$) for the polycarbonate control to ($6.56 \pm 0.34\ Jm^{-3}$) for 0.1wt% TSP-POSS loading, where it reaches a maximum (a 24% increase over the original polymer). Toughness then begins to decrease after 0.1wt% TSP-POSS loading but is still improved by 21% (0.3wt%), 9%(0.5wt%) and 16% (1wt%) on average. This agrees with the observation of a turning point in the data; smaller enhancement of the toughness of polycarbonate at loadings above 0.3wt% TSP-POSS, which could be due to the TSP-POSS aggregates observed during SEM acting as stress concentrators and/or reducing chain mobility (see figures 43-50 section4.1.2).

Results show that the optimum loading of TSP-POSS is between 0.1wt% and 0.5wt% TSP-POSS loading. Ductility reaches a maximum at 0.3wt% loading, perhaps due to increased

plasticisation. We can see from the SEM analysis that the morphology of PC/0.3wt% is the most ductile from the increased number of stretched fibrils present. Tensile strength and Young's modulus is optimised at a higher loading of 0.5wt% perhaps due to a restriction in chain motion by the TSP-POSS aggregate. Or, the TSP-POSS aggregates act as obstacles to the crack path. In figures 51 and 52, small cracks can be seen on the TSP-POSS aggregates. This suggests that the crack has passes through the aggregates during fracture. As the aggregates are stiffer than the polycarbonate matrix due to the rigid nature of TSP-POSS, the strength of the polycarbonate would increase. The toughness reaches a maximum with a TSP-POSS loading between 0.1wt%-0.3wt% TSP-POSS. This could be due to an increase in ductility, as suggested by the formation of stretched fibrils (figures 45-47). Perhaps in these nanocomposites the apparent molecular dispersion of TSP-POSS allows the formation of a hydrogen bonded stretchy network, which holds together the polymer chains and allows them to deform more until failure which results in the formation stretched fibrils. DSC suggests that there is an increase in the energy needed to go through the glass transition for the nanocomposite which could be a result of a possible hydrogen bonded network within the nanocomposites.

5.2. Drop test

A simple drop test was performed on polycarbonate and the TSP-POSS modified nanocomposites in order to determine if the materials satisfied the minimum impact resistance required for eye protection applications following the US ANSI Z87.1 standard. In order to pass a sample must not break or exhibit any cracks or chips.

Table 5 contains the drop test results. All nanocomposites passed the test except PC/0.5wt% TSP-POSS loading and one of the polycarbonate samples. Figure 64 contains images of the failed samples and it shows how cracks formed at the site of impact. The second sample containing 0.5wt% TSP-POSS completely broke into two pieces as a result of the cracking. The surface of the samples was not completely smooth. This was because it was difficult to get a completely even surface during compression moulding. The Kapton film had a tendency to wrinkle and cause slight bumps and ridges on the sample surface. When the ball impacts the uneven surface, the impact energy is not spread evenly and will result in more concentrated areas, resulting in premature failure. This could explain why the samples containing 0.5wt% TSP-POSS failed. Overall, the results obtained from the test prove that

the samples have the minimum impact resistance for protective eyewear and that the addition of TSP-POSS does not have a detrimental effect on the suitability of polycarbonate for such applications.

wt% TSP-POSS	Sample no.	Outcome
Polycarbonate control	1	Pass
	2	Fail
	3	Pass
0.05	1	Pass
	2	Pass
	3	Pass
0.1	1	Pass
	2	Pass
	3	Pass
0.3	1	Pass
	2	Pass
	3	Pass
0.5	1	Fail
	2	Fail
1	1	Pass
	2	Pass
	3	Pass

Table 5 The results from the drop test following the US ANSI Z87.1 standard for protective eyewear

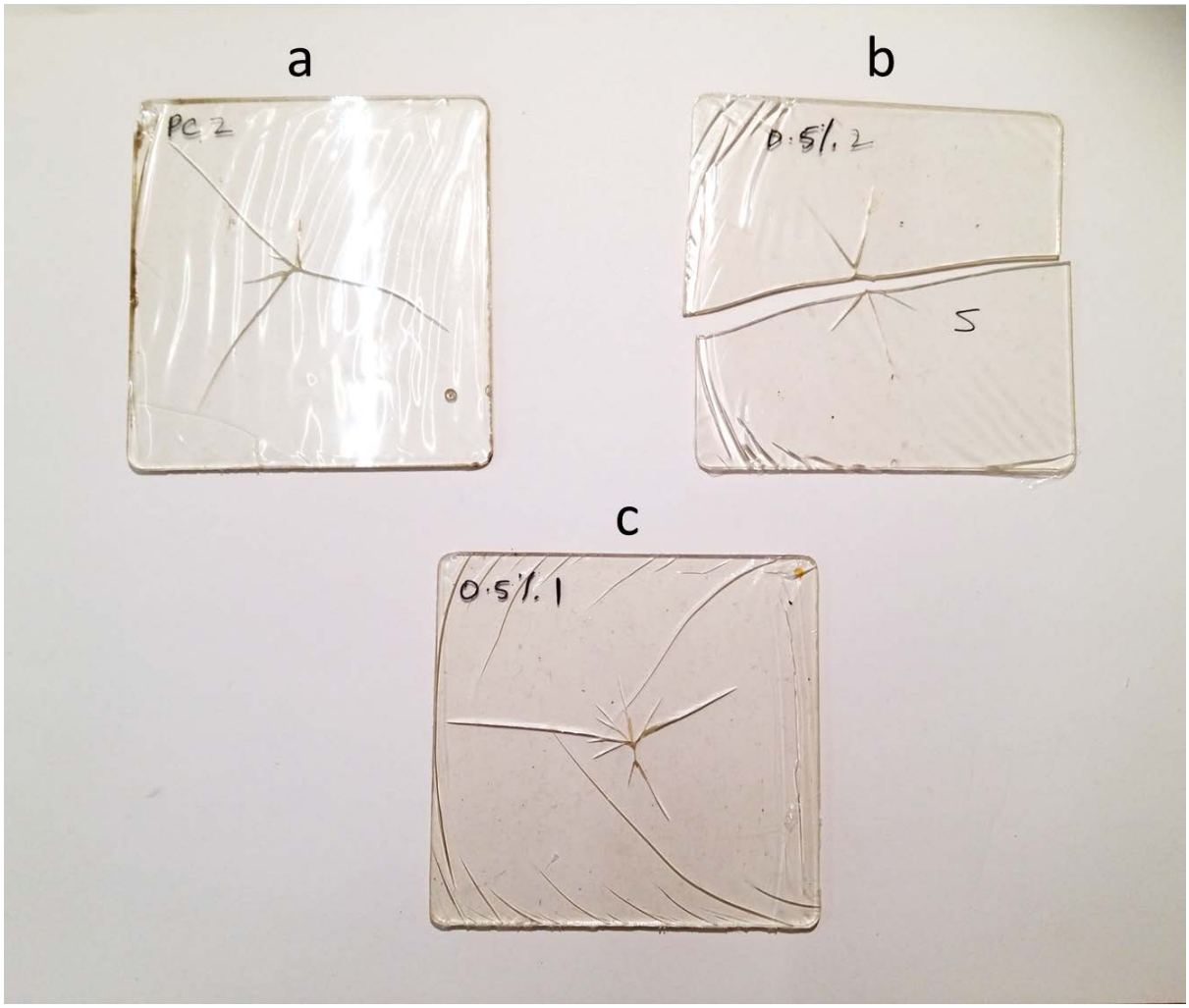

Figure 64 Failed drop-ball test samples: (a) Polycarbonate control, (b-c) PC/0.5wt% TSP-POSS

5.3. Instrumented Falling Weight Impact Test (IFWIT)

Instrumented falling weight impact testing was carried out on polycarbonate and its TSP-POSS based nanocomposites to assess the effect that TSP-POSS has on the impact properties of polycarbonate at low velocities. A 2 kg mass was attached to the dart so that the total mass striking the specimen was 2.2 kg. Average values for maximum peak force and initiation, propagation and total energy were calculated from the force-distance curves obtained from the tests.

5.3.1. Effect of dart velocity

5.3.1.1. Dart Velocity: 3.12 ms^{-1}

Overall, all nanocomposites exhibited better impact resistance than the polycarbonate control. Average values for maximum peak force and initiation, propagation and total energy of the nanocomposites were higher than those of the unmodified polymer. This shows that the addition of TSP-POSS into the polycarbonate matrix improves the performance of polycarbonate and simultaneously enhances its strength and energy absorption capabilities. The results can be found in figure 65 and table 6.

The maximum peak force increases with increasing TSP-POSS content up to 0.5wt% TSP-POSS, where the maximum reaches an average of (746 ± 14 N), an increase of 12% over that of the polycarbonate control. Thereafter, the average value decreases to (735 ± 32 N) for PC/1wt% TSP-POSS (11% increase), although taking into account the large statistical error, the value is still higher than that of the polycarbonate control and potentially the PC/0.5wt% TSP-POSS. Perhaps in some samples, there are more POSS aggregates or defects which act as stress concentrators, causing premature failure. The results show that TSP-POSS increases the maximum amount of force polycarbonate can withstand before failure. The presence of POSS particles at the molecular scale may increase energy dissipation by inducing the formation of stretched fibrils perhaps due to the formation of a hydrogen bonded network and again, TSP-POSS aggregates may increase the energy required to break the samples and thus the strength of the polymer matrix by obstructing the path of cracks.

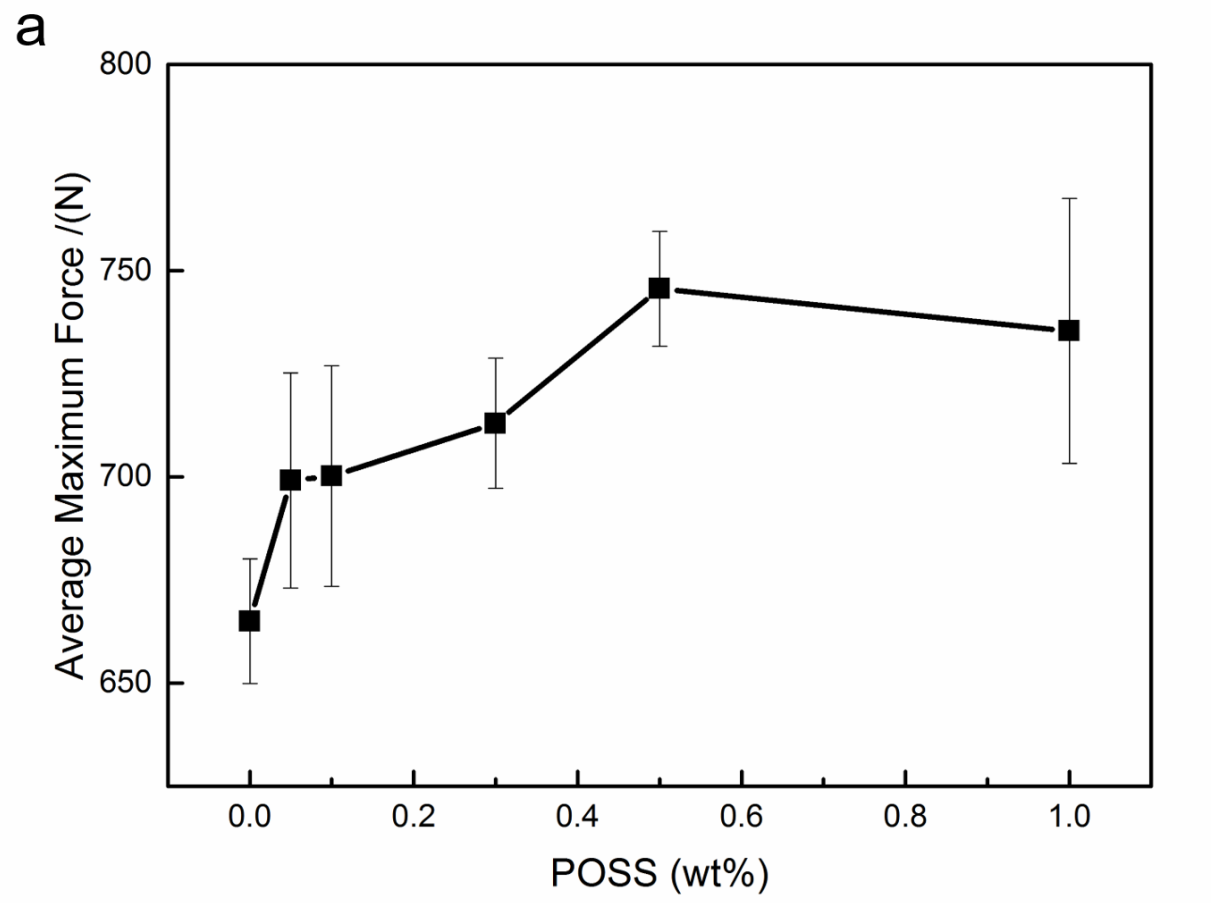
a
800
750
700
650
Average Maximum Force /(N)
0.0
0.2
0.4
0.6
0.8
1.0
POSS (wt%)

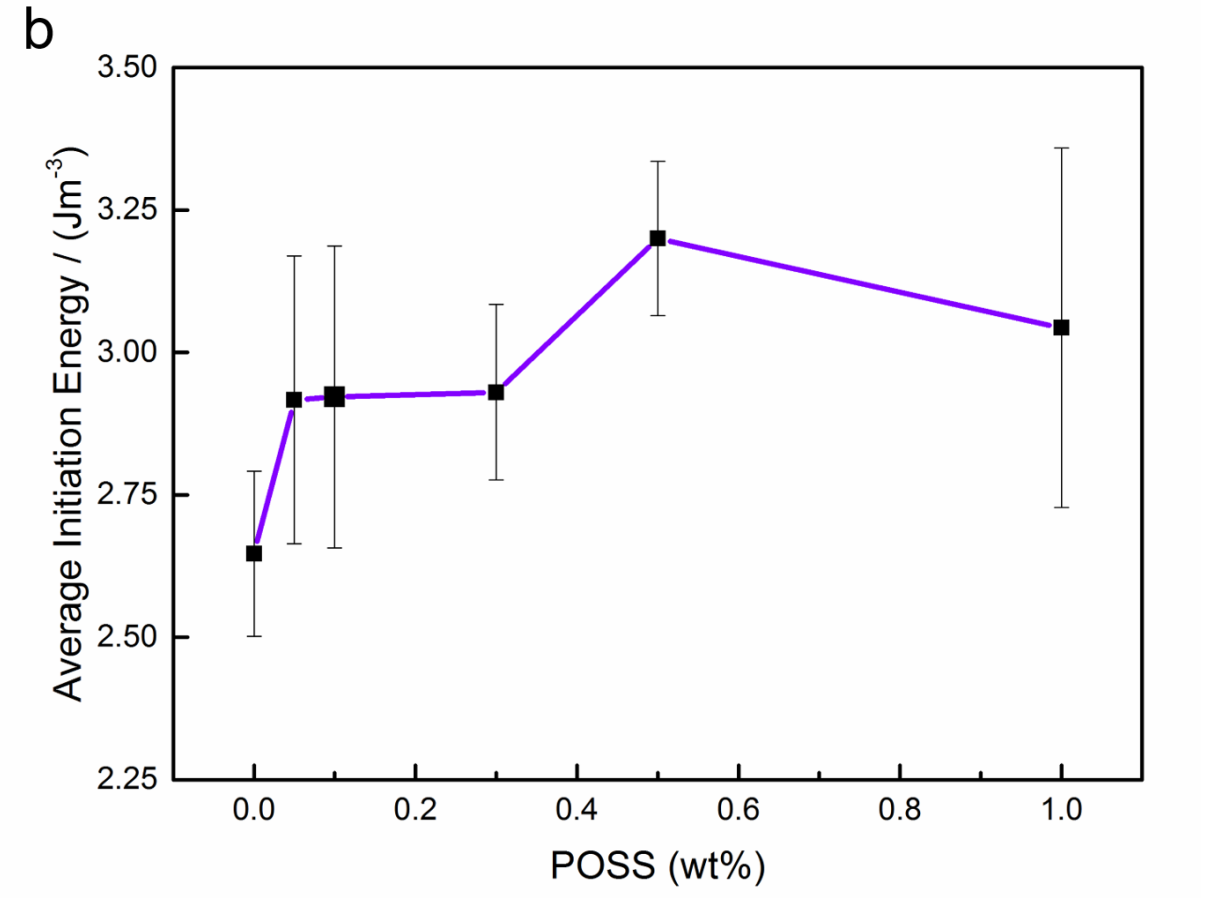
b
3.50
3.25
3.00
2.75
2.50
2.25
Average Initiation Energy / (Jm-3)
0.0
0.2
0.4
0.6
0.8
1.0
POSS (wt%)

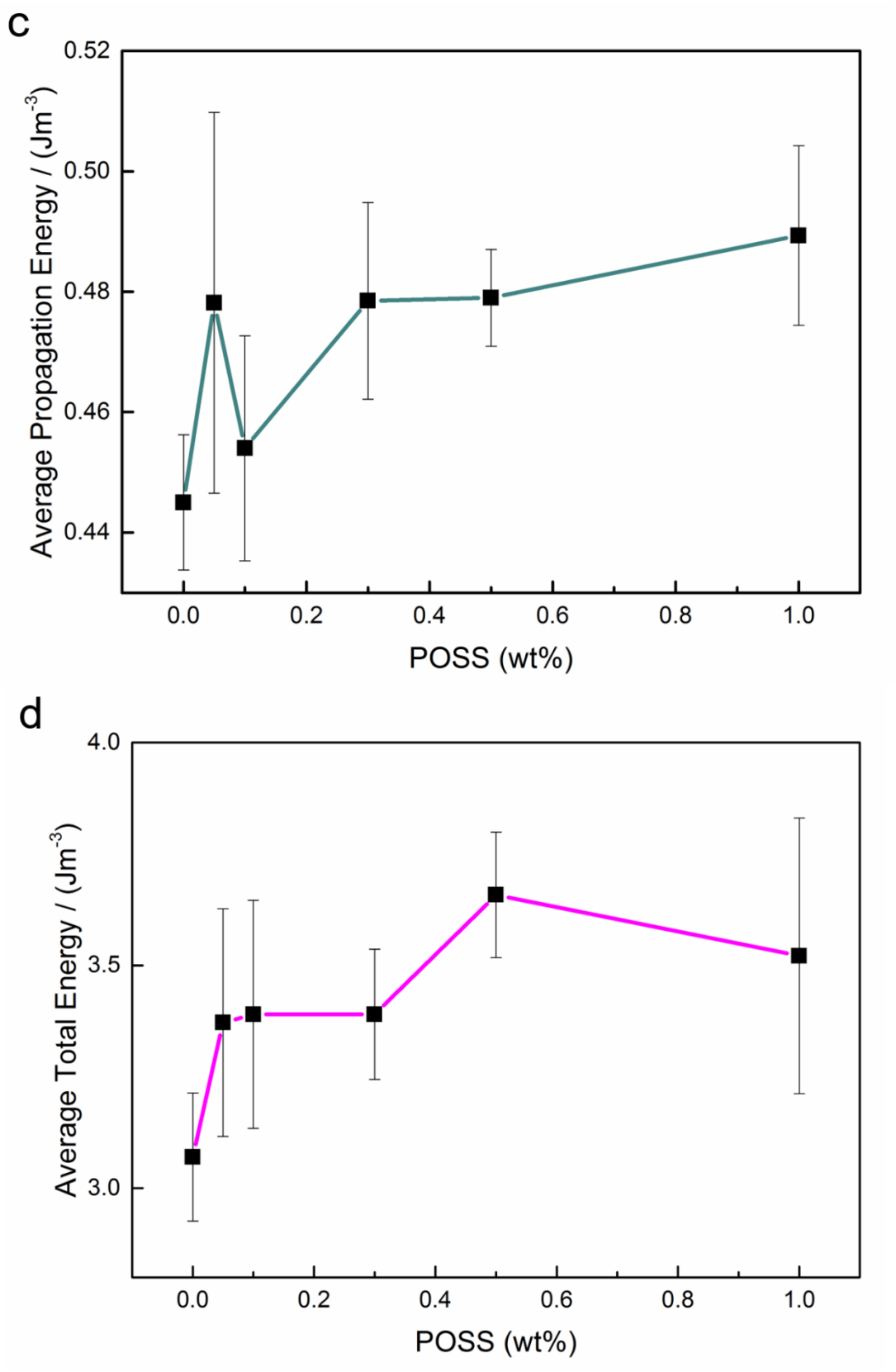

Figure 65 Graphs of average (a) maximum peak force, (b) initiation energy, (c) propagation energy and (d) total energy of absorbed by polycarbonate and its TSP-POSS based nanocomposites using dart velocity, 3.12 ms^{-1}

wt% TSP-POSS	Maximum Force (N)	Initiation Energy (Jm^{-3})	Propagation Energy (Jm^{-3})	Total Energy (Jm^{-3})
Control Sample	665 ± 15	2.65 ± 0.14	0.445 ± 0.011	3.07± 0.14
0.05	699 ± 26	2.92 ± 0.25	0.478 ± 0.032	3.37 ± 0.26
0.1	700 ± 27	2.92 ± 0.27	0.454 ± 0.019	3.39 ± 0.26
0.3	713 ± 16	2.93 ± 0.15	0.479 ± 0.016	3.39 ± 0.15
0.5	746 ± 14	3.2 ± 0.14	0.479 ± 0.008	3.66 ± 0.14
1	735 ± 32	3.04 ± 0.32	0.489 ± 0.015	3.52 ± 0.31

Table 6 Average values of maximum peak force, initiation energy, propagation energy and total energy of absorbed by polycarbonate and its TSP-POSS based nanocomposites using dart velocity, 3.12 ms^{-1}

Initiation energy, the amount of energy required to create a crack in the sample, follows the same trend as the maximum peak force result; a maximum of (3.2 ± 0.14 Jm^{-3}) is obtained upon addition of 0.5wt%, an increase of 21% over the original polycarbonate. This result agrees with the previous idea that the addition of TSP-POSS increases the energy absorption and dissipation capabilities of polycarbonate. Again, the addition of 1wt% TSP-POSS results in a smaller enhancement of the average initiation energy which causes a slight downward trend from 0.5wt% loading but the initiation energy of polycarbonate is still increased by 14% with 1wt% TSP-POSS. However, there is a large statistical error for this loading and could be a result of increased aggregates in some or parts of the samples which act as stress concentrators to cause premature failure and decreased energy absorption/dissipation capabilities.

Again, the propagation energy of the nanocomposites was higher than that of the control sample, albeit following a slightly different pattern than the trend displayed in the maximum peak force and initiation energy graphs. The average propagation energy of polycarbonate measured (0.445 ± 0.011 Jm^{-3}), which increased by 7% to (0.478 ± 0.031 Jm^{-3}) upon addition of 0.05wt% TSP-POSS into the matrix. However, increasing the loading to 0.1wt% caused the propagation energy to decrease to (0.454 ± 0.019 Jm^{-3}) which is only a 2% increase over the value of the original polymer. It then began to increase again until it reached a maximum average of (0.489 ± 0.015 Jm^{-3}) for PC/1wt% TSP-POSS, an increase of

10%. PC/0.05wt% TSP-POSS has a large standard deviation shown as a large error bar. This could be due to defects in the sample from processing, which decrease the propagation energy and result in premature failure of some of the samples. Fitting a cubic curve to the graph of the average results shows a positive trend i.e. the addition of TSP-POSS increases the propagation energy of polycarbonate.

The average values for the total energy absorbed by the nanocomposites were larger than that of the unmodified polycarbonate. The average total energy absorbed by the polycarbonate control sample was (3.07 ± 0.14 Jm^{-3}). A maximum of (3.66 ± 0.14 Jm^{-3}) was reached by the sample containing 0.5wt% TSP-POSS, an increase of over 19% of the unmodified polymer. The average value then decreased once more upon further TSP-POSS loading to (3.52 ± 0.31 Jm^{-3}). Again, the data value of PC/1wt% TSP-POSS has a large statistical error which could be due to stress concentration from increased number of POSS aggregates causing some samples to fail early.

These results show that the addition of TSP-POSS increases the toughness of polycarbonate up to 0.5wt% TSP-POSS by increases in initiation energy and total energy. Beyond this loading, the total energy begins to decrease once more although samples containing 1wt% TSP-POSS still possess a higher amount of energy absorption than the control sample. This could be due to aggregates or defects in the samples. It is interesting to note that PC/1wt% possessed the highest average propagation energy value, which could be a result of aggregates involved in crack pinning. The formation of a void around the potential POSS aggregates and cracks on the surface of the aggregates seen by SEM (figures 43-52) could be an indicator of this mechanism whereby the POSS aggregates slow down the crack propagation by increasing the amount of energy needed to pass through the aggregates.

Considering the data presented in figure 65 and table 6, the optimum nanofiller loading at low velocities is 0.5wt%. Generally, the error bars are the largest when 1wt% TSP-POSS loading is used and is probably due to the increased number of aggregates in the samples which can act as stress concentrators causing premature failure of the samples. Overall, the addition of TSP-POSS increases the total amount of impact energy the polycarbonate can withstand before failure and could be due to (i) increased ductility by the formation of stretched fibrils which could be a result of the formation of a hydrogen bonded network at

loadings below 0.5wt%, whereby the TSP-POSS is miscible in the matrix and dispersed at the molecular scale. At loadings of 0.5wt% and 1wt% TSP-POSS aggregates may slow down crack movement and thus increase the energy required for the crack to form in the sample, this increasing the toughness of the material via this mechanism.

5.3.1.2. Dart Velocity: 3.96 ms^{-1}

The dart velocity was increased to 3.96 ms^{-1} by increasing the height of the dart from 0.5 m to 0.8 m above the specimen. The results can be found in figure 66 and table 7.

Figure 66 shows that overall the optimum TSP-POSS loading has shifted to a lower value of 0.1wt% and that at higher loadings the degree of enhancement is reduced or even that the properties are reduced in comparison to the control samples. However, the results of the sample with 0.3wt% appear to be anomalous as they do not fit in with the trend displayed in the graphs. This could be due to the amount of POSS having a larger plasticising effect or presence of defects in the sample introduced during processing.

The maximum peak force reaches a maximum of (757 ± 25 N), an increase of 6% over the unmodified polycarbonate, upon addition of 0.1wt% TSP-POSS. It then decreases with further loading, where samples containing 0.3wt% and 1wt% have average maximum peak force values lower than that of the control. As previously discussed, PC/1wt% TSP-POSS seems to contain an increased amount of aggregates which could act as stress concentrators in the polymer matrix.

The graphs containing the average values of initiation and total energy of polycarbonate and its TSP-POSS based nanocomposites also show the same trend as the maximum peak force results with maximum values being reached with 0.1wt% loading and minimum average values with 0.3wt% TSP-POSS loading. The initiation energy and total energy of polycarbonate increases by over 22% and 18%, respectively, with the addition of 0.1wt% TSP-POSS. Both the initiation energy and total energy of polycarbonate is reduced by just over 5% with the addition of 0.3wt% TSP-POSS.

However, the propagation energy reaches on average a minimum value with the addition of 0.1wt% TSP-POSS (~4% decrease) and a maximum value with the addition of 0.3wt% TSP-POSS (2%). These differences are insignificant when taking error into account and therefore

it can be taken that the propagation energy of polycarbonate at this dart velocity is largely unaffected by TSP-POSS.

Overall, at this dart velocity the total energy of polycarbonate i.e. the total energy absorbed is increased with the addition of 0.1wt% TSP-POSS, which appears to be the optimum loading. The results in figure 66 and table 7 suggest that this is achieved by increasing the initiation energy (the amount of energy required to initiate a crack in the sample). Further loading leads to a more ductile material as indicated by increased number of fibrils (PC/0.3wt% TSP-POSS) which decrease impact resistance or aggregation which act as stress concentrators (PC/0.5wt% TSP-POSS and PC/1wt% TSP-POSS) to create a more brittle material.

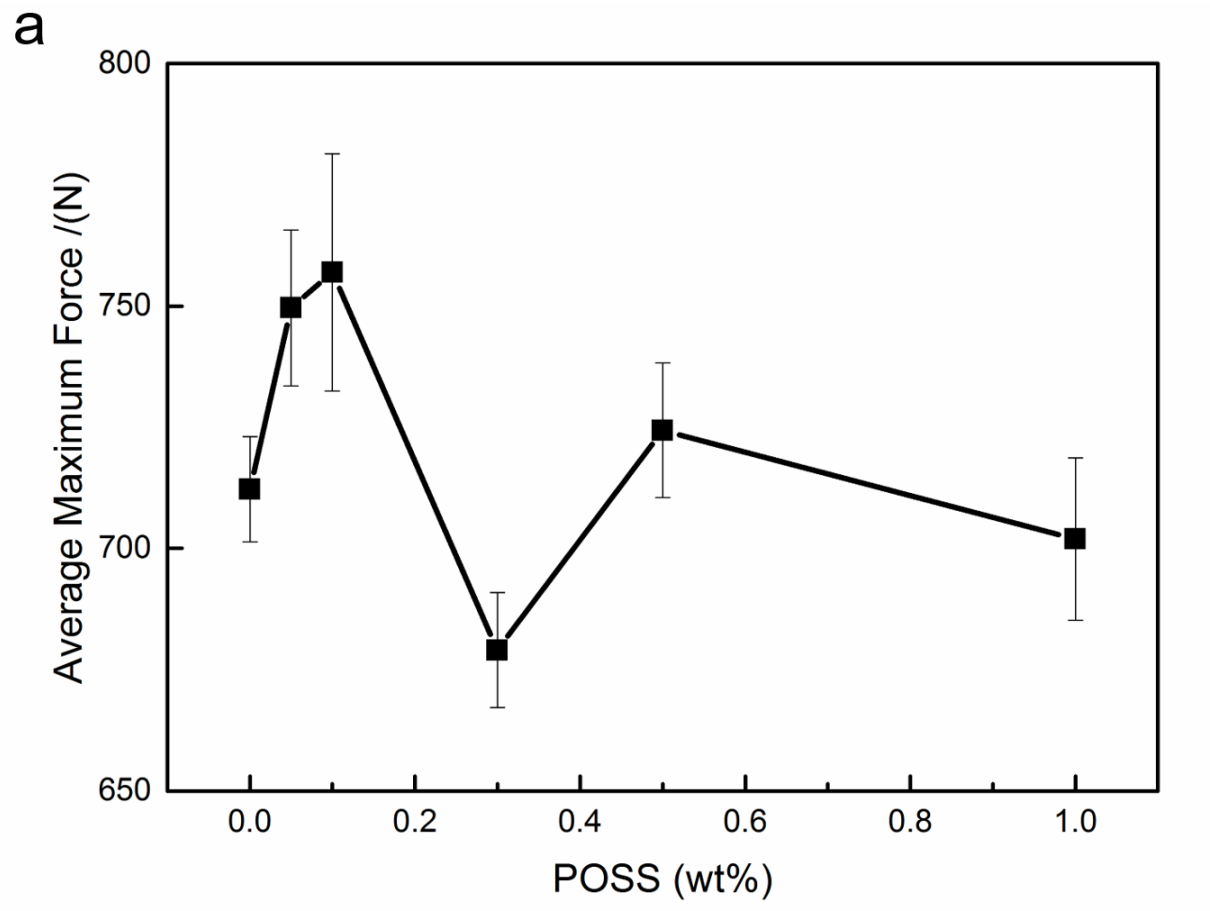
a
800
750
700
650
Average Maximum Force /(N)
0.0
0.2
0.4
0.6
0.8
1.0
POSS (wt%)

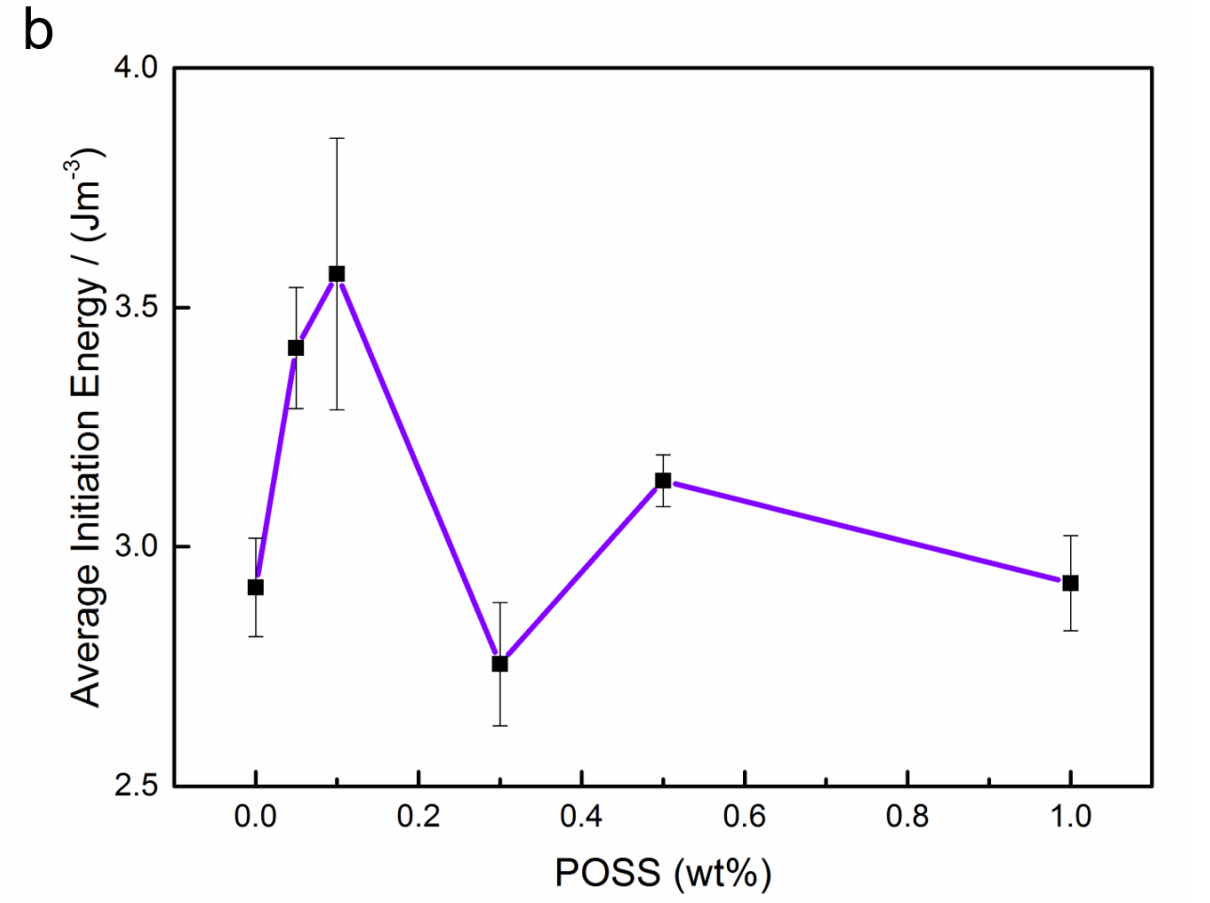
b
4.0
3.5
3.0
2.5
Average Initiation Energy / (Jm-3)
0.0
0.2
0.4
0.6
0.8
1.0
POSS (wt%)

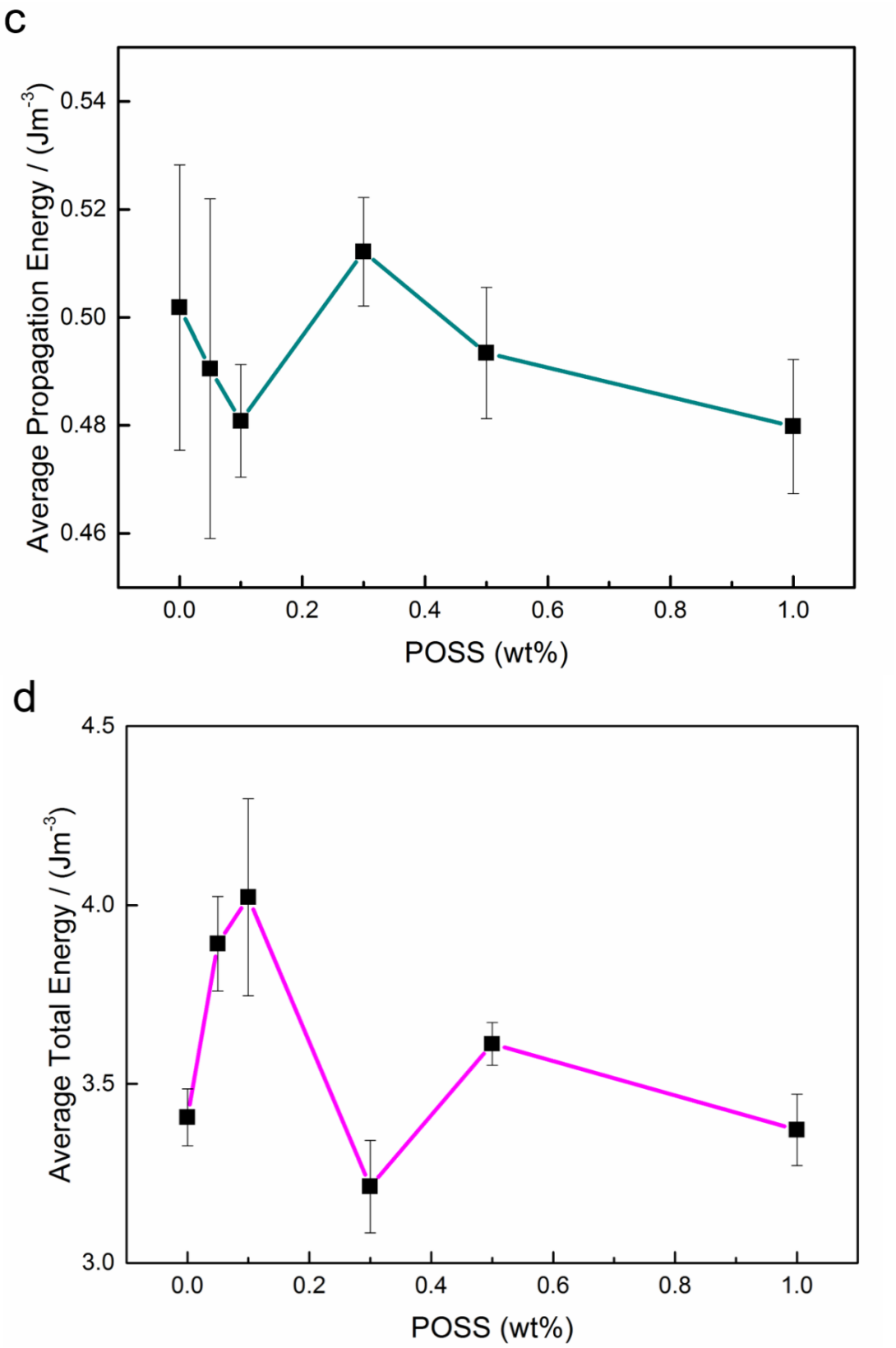

Figure 66 Average (a) maximum peak force, (b) initiation energy, (c) propagation energy and (d) total energy of absorbed by polycarbonate and its TSP-POSS based nanocomposites using dart velocity, 3.96 ms^{-1}

wt% TSP-POSS	Maximum Force (N)	Initiation Energy (Jm^{-3})	Propagation Energy (Jm^{-3})	Total Energy (Jm^{-3})
Control	712 ± 11	2.92 ± 0.10	0.502 ± 0.065	3.41 ± 0.08
0.05	750 ± 16	3.42 ± 0.13	0.491 ± 0.077	3.89 ± 0.13
0.1	757 ± 24	3.57 ± 0.28	0.481 ± 0.026	4.02 ± 0.28
0.3	679 ± 12	2.76 ± 0.13	0.512 ± 0.025	3.21 ± 0.13
0.5	724 ± 14	3.13 ± 0.05	0.493 ± 0.027	3.61 ± 0.06
1	702 ± 17	2.92 ± 0.10	0.48 ± 0.028	3.37 ± 0.10

Table 7 Average values of maximum peak force, initiation energy, propagation energy and total energy of absorbed by polycarbonate and its TSP-POSS based nanocomposites using dart velocity, 3.96 ms^{-1}

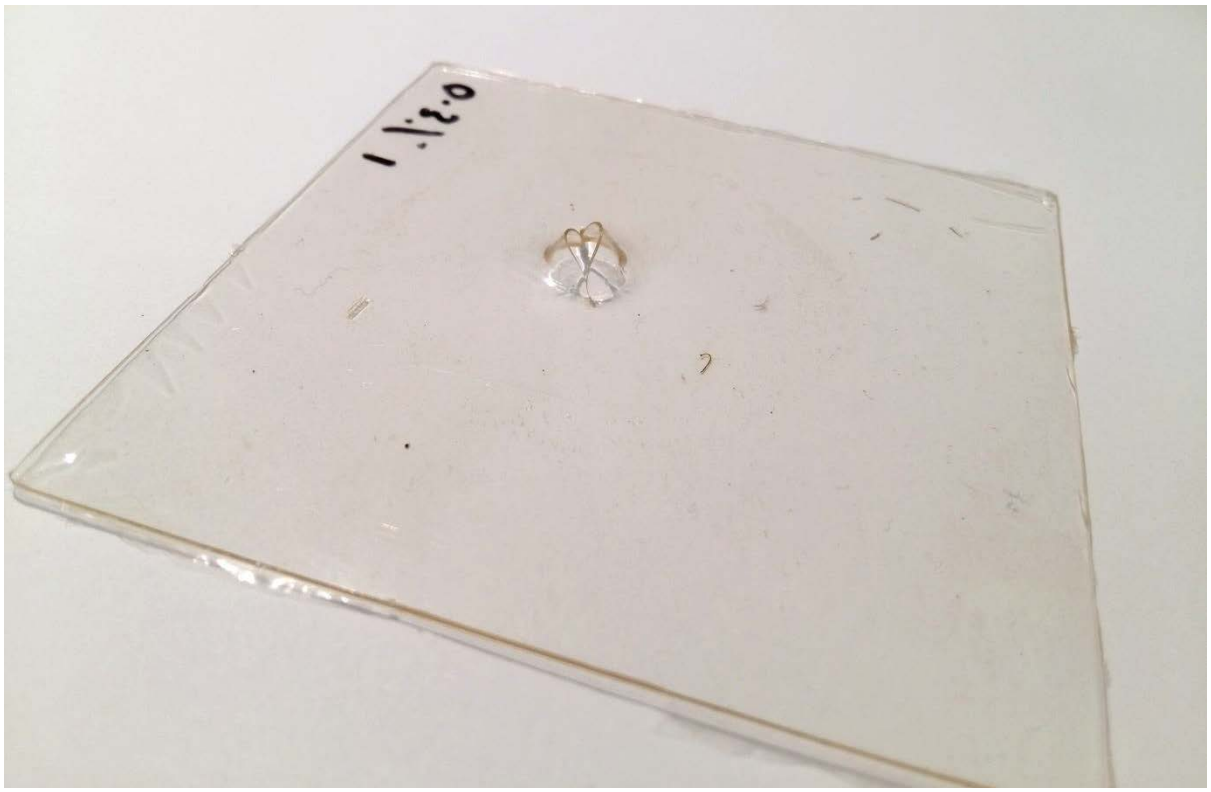

Figure 67 Evidence of petalling in post-FWIT sample

5.3.1.3. Dart Velocity: 4.85 ms^{-1}

The dart velocity was increased further by raising the height of the dart to 1.2 m. The results can be found in figure 68 and table 8.

The maximum peak force of all nanocomposites was on average higher in value than polycarbonate however, there does seem to be some irregularities. Initially the maximum peak force increases with the addition of TSP-POSS up to a loading of 0.1wt%, where it reaches a maximum value of (847 ± 11 N), a 23% increase over the control sample. For samples containing 0.3wt%, 0.5wt% and 1wt% the maximum peak force increases by 16%, 6% and 17%, respectively over that of the polycarbonate control.

Initiation energy and total energy follow the same trend as shown in the maximum peak force results. Initiation energy reaches a maximum value of (3.86 ± 0.14 Jm^{-3}) upon addition of 0.1wt% TSP-POSS, a 55% increase in comparison to the control polymer. This results in a maximum in total energy in PC/0.1wt% TSP-POSS: (4.56 ± 0.14 Jm^{-3}), a 22% increase over that of the unmodified polycarbonate.

The shape of the propagation energy is a mirror image of the shape of the graphs of maximum peak force, initiation energy and total energy, with all nanocomposites having lower propagation energy on average; the propagation energy decreases and reaches a minimum value for the sample containing 0.1wt% TSP-POSS. It then begins to increase again for nanocomposites containing between 0.3wt% and 0.5wt% TSP-POSS but decreases once more upon the addition of 1wt% TSP-POSS. These results imply that if the initiation energy increases, the propagation energy must decrease and vice versa. In other words, the sample becomes resistant to cracking as it is able to absorb more energy but once a crack has been formed it is easier for it to propagate through the sample to complete failure. If the propagation energy increases, the sample must plastically deform more.

a

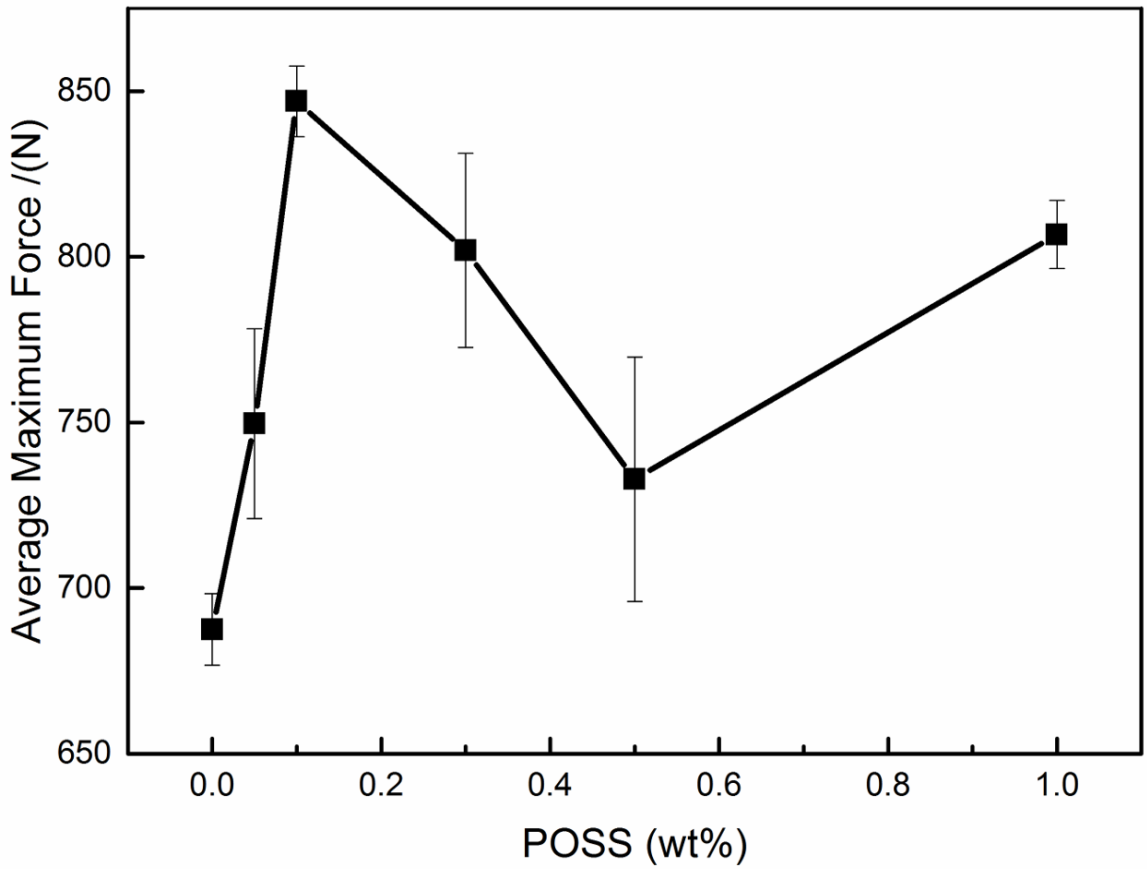
Average Maximum Force /(N)
850
800
750
700
650
0.0
0.2
0.4
0.6
0.8
1.0
POSS (wt%)

b

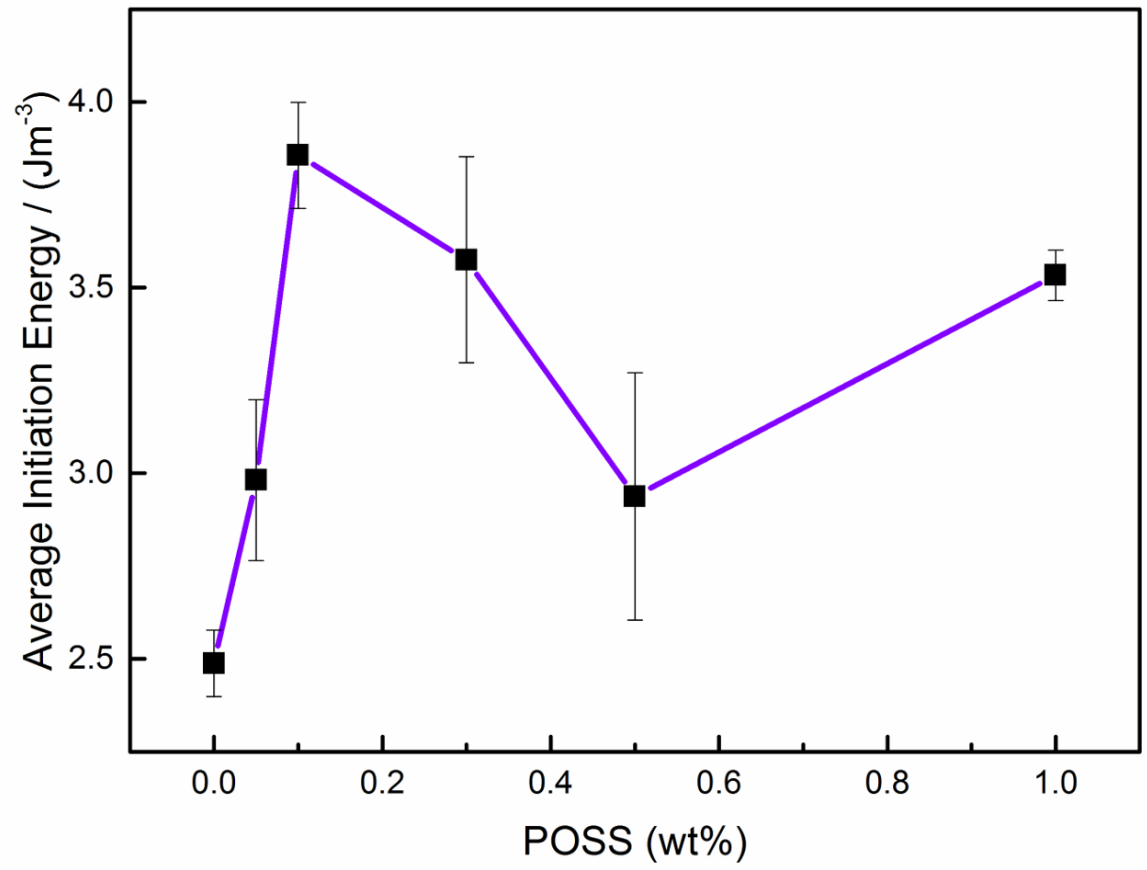
Average Initiation Energy / (Jm-3)
4.0
3.5
3.0
2.5
0.0
0.2
0.4
0.6
0.8
1.0
POSS (wt%)

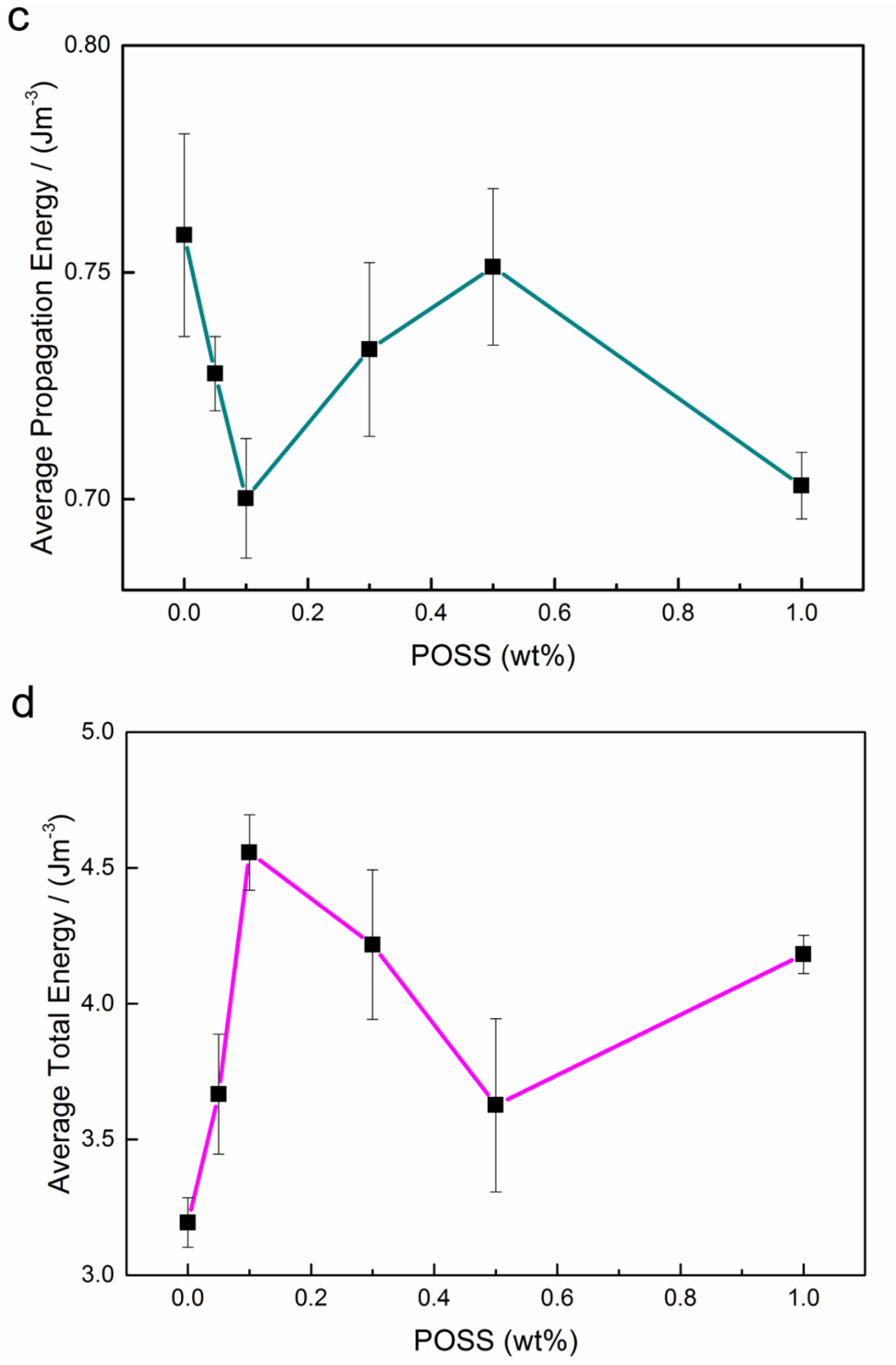

Figure 68 Average (a) maximum peak force, (b) initiation energy, (c) propagation energy and (d) total energy of absorbed by polycarbonate and its TSP-POSS based nanocomposites using dart velocity, 4.85 ms^{-1}

wt% TSP-POSS	Maximum Force (N)	Initiation Energy (Jm^{-3})	Propagation Energy (Jm^{-3})	Total Energy (Jm^{-3})
Control	687 ± 11	2.49 ± 0.09	0.758 ± 0.022	3.19 ± 0.09
0.05	750 ± 29	2.98 ± 0.22	0.728 ± 0.008	3.67 ± 0.22
0.1	847 ± 11	3.86 ± 0.14	0.700 ± 0.013	4.56 ± 0.14
0.3	802 ± 29	3.58 ± 0.28	0.733 ± 0.019	4.22 ± 0.28
0.5	733 ± 37	2.94 ± 0.33	0.751 ± 0.017	3.63 ± 0.32
1	807 ± 10	3.53 ± 0.07	0.703 ± 0.007	4.18 ± 0.07

Table 8 Average values of maximum peak force, initiation energy, propagation energy and total energy of absorbed by polycarbonate and its TSP-POSS based nanocomposites using dart velocity, 4.85 ms^{-1}

5.3.1.1. Dart Velocity: 5.42 ms^{-1}

The dart velocity was once again increased by increasing the height of the dart to 1.5 m, the maximum height used in this experiment. Figure 69 and table 9 contains the results. Overall, on average the optimum TSP-POSS loading when using this dart velocity is 0.5wt% although the improvements are lower in magnitude. Further loading to 1wt% again decreases the impact properties of polycarbonate potentially due to increased stress concentration caused by the presence of more TSP-POSS aggregates, as mentioned previously.

The maximum peak force of polycarbonate is generally increased slightly with the addition of TSP-POSS. It reaches a maximum of (775 ± 21 N) with the addition of 0.5wt% TSP-POSS, which is only a 5% increase over the value for the polycarbonate. However, with 1wt% TSP-POSS loading, on average the maximum peak force of the resultant nanocomposite is similar to that of the control sample. This follows on from the observations on PC/1wt% TSP-POSS so far.

The results shown in figure 69(c) show that with the addition of the higher loadings of TSP-POSS (<0.1wt%), the propagation energy increases in comparison to the control sample. It reaches a maximum of (0.801 ± 0.023 Jm^{-3}) with the addition of 0.5wt% TSP-POSS, although this is only a 3% increase over the value of the unmodified polycarbonate and falls within the error margins.

The total energy absorbed by polycarbonate is generally increased slightly with the addition of TSP-POSS (see figure 69(d)). It reaches a maximum of (4.22 ± 0.24 Jm^{-3}), an increase of 12% over that of the polycarbonate control sample.

Figure 70 contains graphs of the ratios between initiation energy and total energy and also between propagation energy and total energy. The graphs can show if TSP-POSS affects the initiation energy of polycarbonate more or the propagation energy. Essentially, the impact resistance of polycarbonate is increased with the addition of TSP-POSS and that most of the energy absorption occurs in the initiation event; total energy during the event is roughly estimated as a ratio of 4:1 between initiation energy and propagation energy.

Figure 70(a) shows that despite some variation in the data, the overall trend is that at all velocities the addition of TSP-POSS does not have a detrimental effect on the initiation energy and generally increases it when loadings of up to 0.1wt% are used.

Conversely, figure 70(b) shows that a reduction in propagation energy of polycarbonate occurs on adding up to 0.1wt% TSP-POSS, and upon further loading the propagation energy is generally unaffected. Generally, the minimum values of propagation energy and maximum of initiation energy values occur when 0.1wt% TSP-POSS loading is used. This implies that at this loading more energy is required to form a crack but once a crack has formed, it is easier for it to propagate through the sample until complete failure occurs.

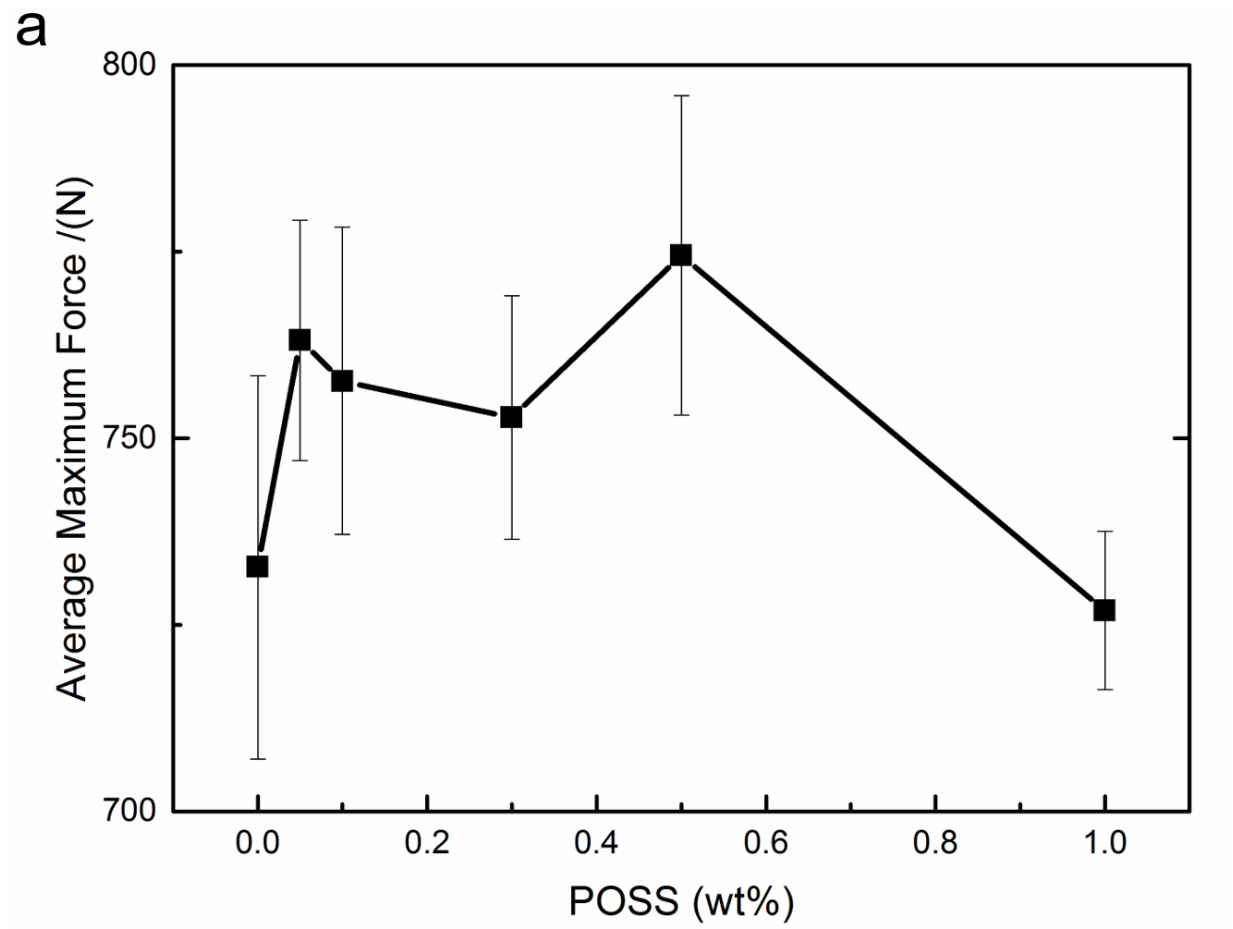
a
800
750
700
Average Maximum Force /(N)
0.0
0.2
0.4
0.6
0.8
1.0
POSS (wt%)

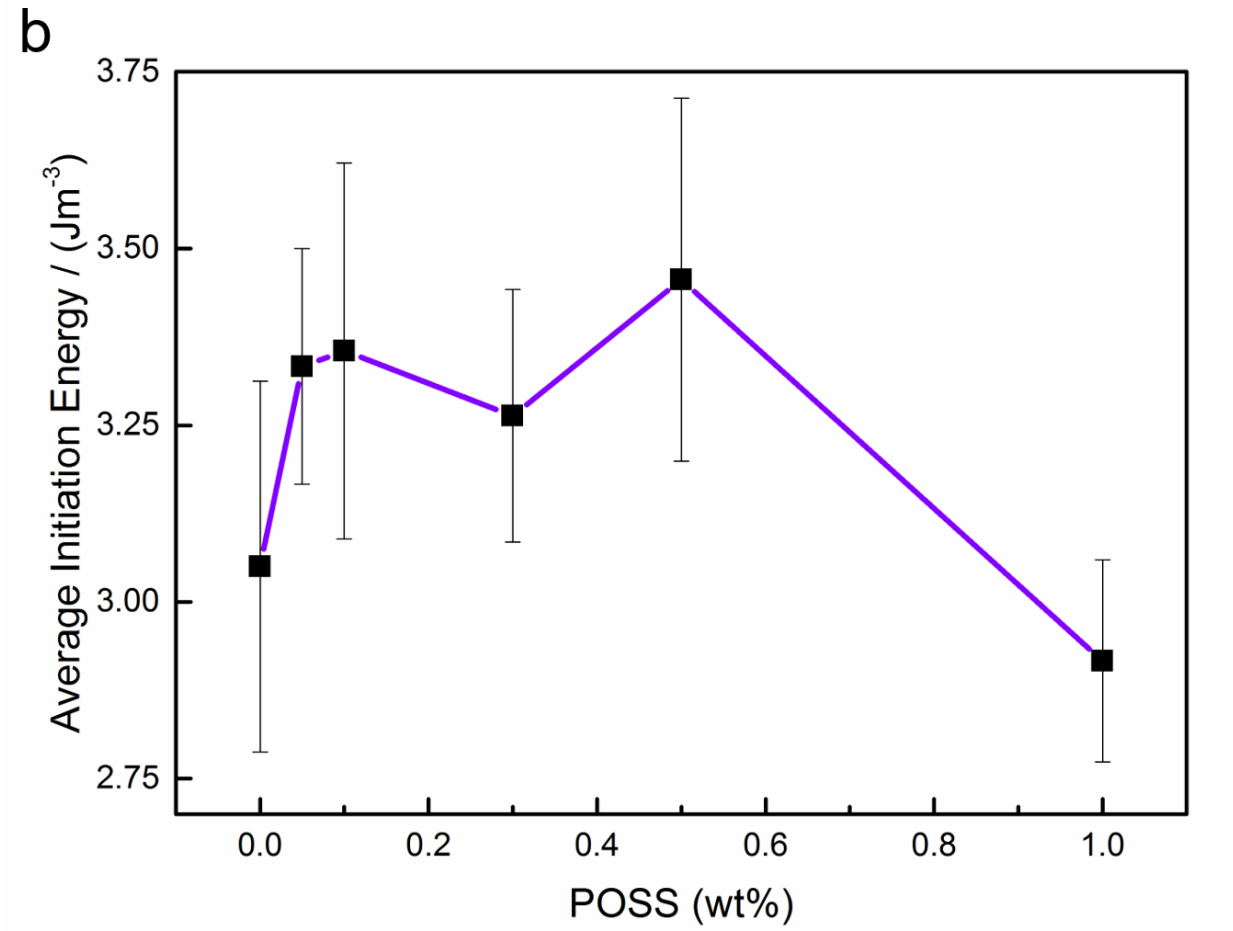
b
3.75
3.50
3.25
3.00
2.75
Average Initiation Energy / (Jm-3)
0.0
0.2
0.4
0.6
0.8
1.0
POSS (wt%)

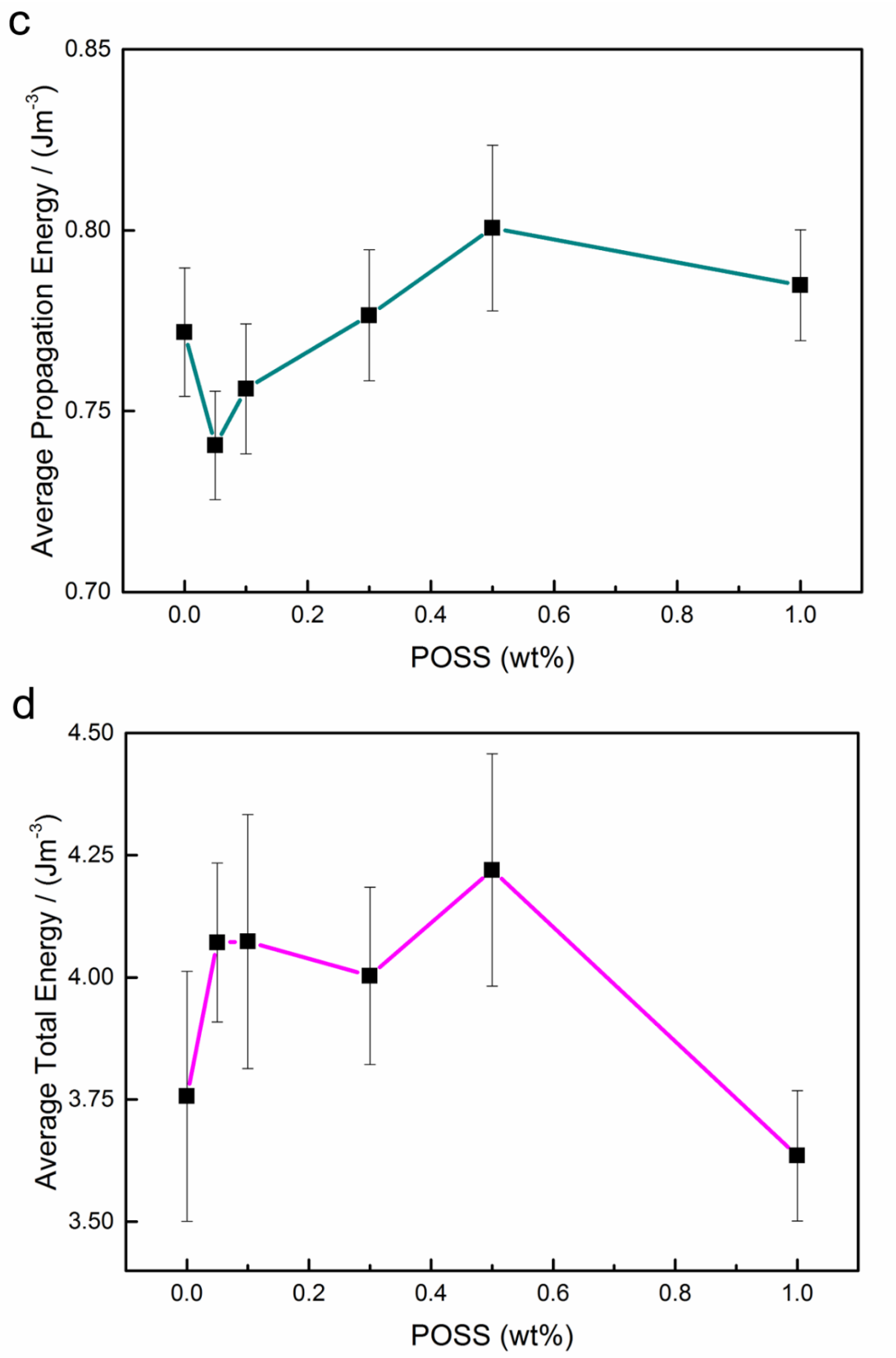

Figure 69 Average (a) maximum peak force, (b) initiation energy, (c) propagation energy and (d) total energy of absorbed by polycarbonate and its TSP-POSS based nanocomposites using dart velocity, 5.42 ms^{-1}

wt% TSP-POSS	Maximum Force (N)	Initiation Energy (Jm^{-3})	Propagation Energy (Jm^{-3})	Total Energy (Jm^{-3})
Control	733 ± 26	3.05 ± 0.26	0.772 ± 0.018	3.76 ± 0.26
0.05	763 ± 16	3.33 ± 0.17	0.741± 0.015	4.07 ± 0.16
0.1	758 ± 21	3.36 ± 0.27	0.756 ± 0.018	4.07 ± 0.26
0.3	753 ± 16	3.26 ± 0.18	0.777 ± 0.018	4.00 ± 0.18
0.5	775 ± 21	3.46 ± 0.26	0.801 ± 0.023	4.22 ± 0.24
1	727 ± 11	2.92 ± 0.14	0.785 ± 0.015	3.64 ± 0.13

Table 9 Average values of maximum peak force, initiation energy, propagation energy and total energy of absorbed by polycarbonate and its TSP-POSS based nanocomposites using dart velocity, 5.42 ms^{-1}

Figure 71 shows how the maximum peak force and total energy is affected by TSP-POSS content at all dart velocities. Mostly, the maximum peak force (figure 71a)) and the total energy (figure 71b)) of the nanocomposites does not fall lower than the values of the polycarbonate control and in fact, in the vast majority of cases the addition of TSP-POSS results in improvements in these properties.

To summarise the general improvement in the impact resistance of polycarbonate by the addition of TSP-POSS depends on the dart velocity, the loading of TSP-POSS in the polycarbonate matrix which in turn, from the SEM micrographs (figures 43-52) affects the morphology and nanostructure of the nanocomposites and potentially their fracture mechanisms.

At dart velocities of 3.12 m/s and 5.42m/s, the optimum TSP-POSS loading is 0.5wt% and could be a result of the TSP-POSS aggregates (see figures 48-52) which impede the crack formation by potential void formation and evidence of cracks on the surface of the TSP-POSS aggregates.

At the other two dart velocities used, the optimum TSP-POSS loading decreases to 0.1wt%. At the lower loading of 0.1wt%, TSP-POSS appears to be miscible in the polymer matrix and contribute to increased stretched fibril formation, perhaps as a result of hydrogen bonding within the polymer matrix. However, this cannot be proven.

Dart velocity (ms^{-1})	Optimum TSP-POSS loading (wt%)	Initiation energy (Jm^{-3})	Propagation energy (Jm^{-3})	Total energy (Jm^{-3})	Maximum peak force (N)
3.12	0.5	21% Increase	8% Increase	19% Increase	12% Increase
3.96	0.1	22% Increase	4% Decrease	18% Increase	6% Increase
4.85	0.1	55% Increase	8% Decrease	22% Increase	23% Increase
5.42	0.5	2% Increase	3% Increase	12% Increase	5% Increase

Table 10 The optimum TSP-POSS loadings for each dart velocity and the effect that these had on the impact properties measured from the results of the falling weight impact tests

This appears to increase the ductility of the matrix and its energy absorbing capabilities (seen as increases in total energy, E_T) by increasing the energy needed to initiate a crack (evidenced by increases in initiation energy, E_i). It could be that the aggregates acted as stress concentrators at these dart velocities causing premature failure.

Overall, the addition of TSP-POSS mainly improves the impact resistance of polycarbonate by increasing the energy required to form a crack which increases the energy absorbing capabilities of the polycarbonate matrix. Most of the energy absorption occurs in the initiation event; total energy during the event is roughly estimated as a ratio of 4:1 between initiation energy and propagation energy. Table 10 highlights the optimum values for each dart velocity and the effect these loadings had on the average impact properties measured during the FWIT.

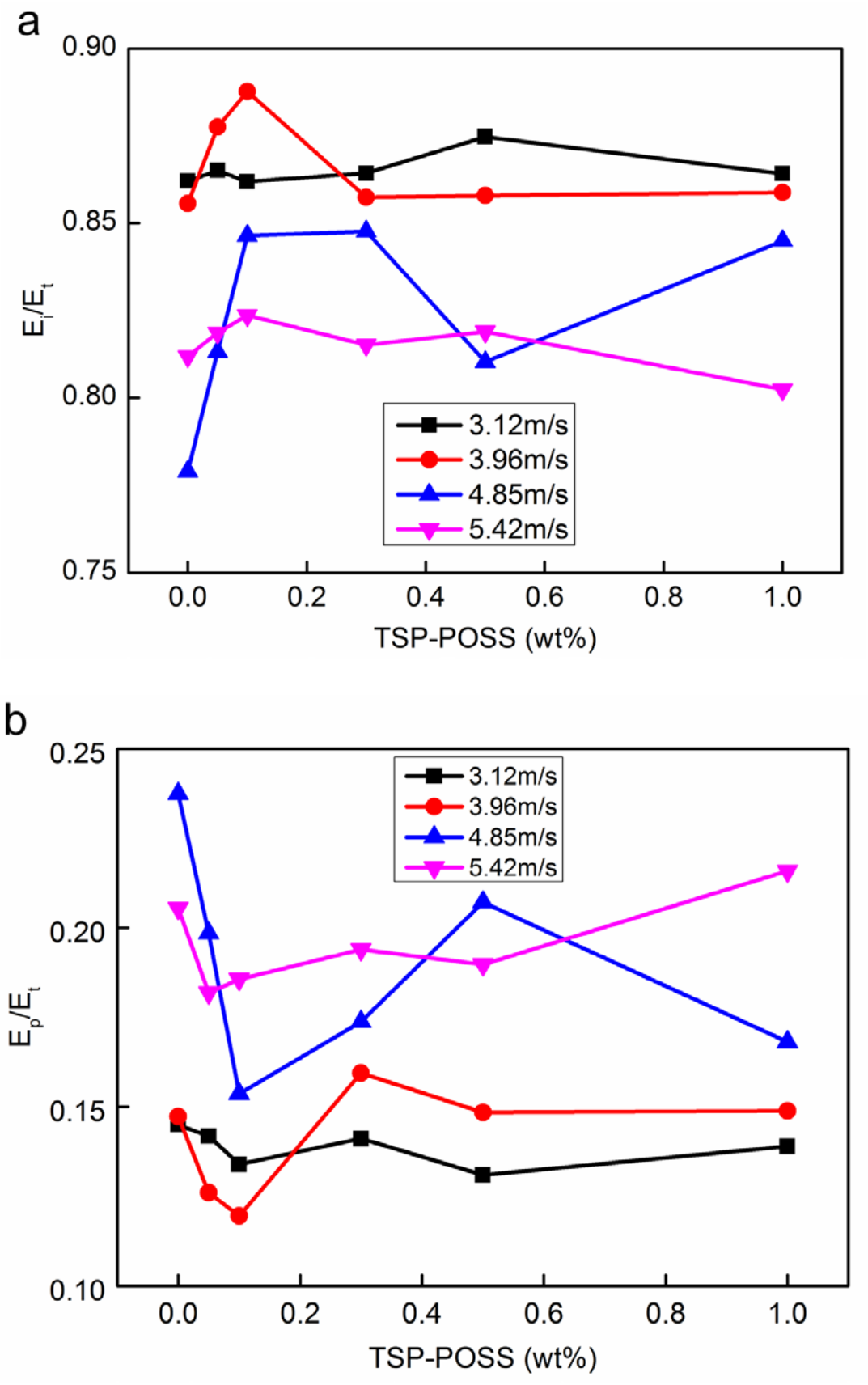

Figure 70 (a) E_i/E_t and (b) E_p/E_t for polycarbonate and its TSP-POSS based nanocomposites at all dart velocities

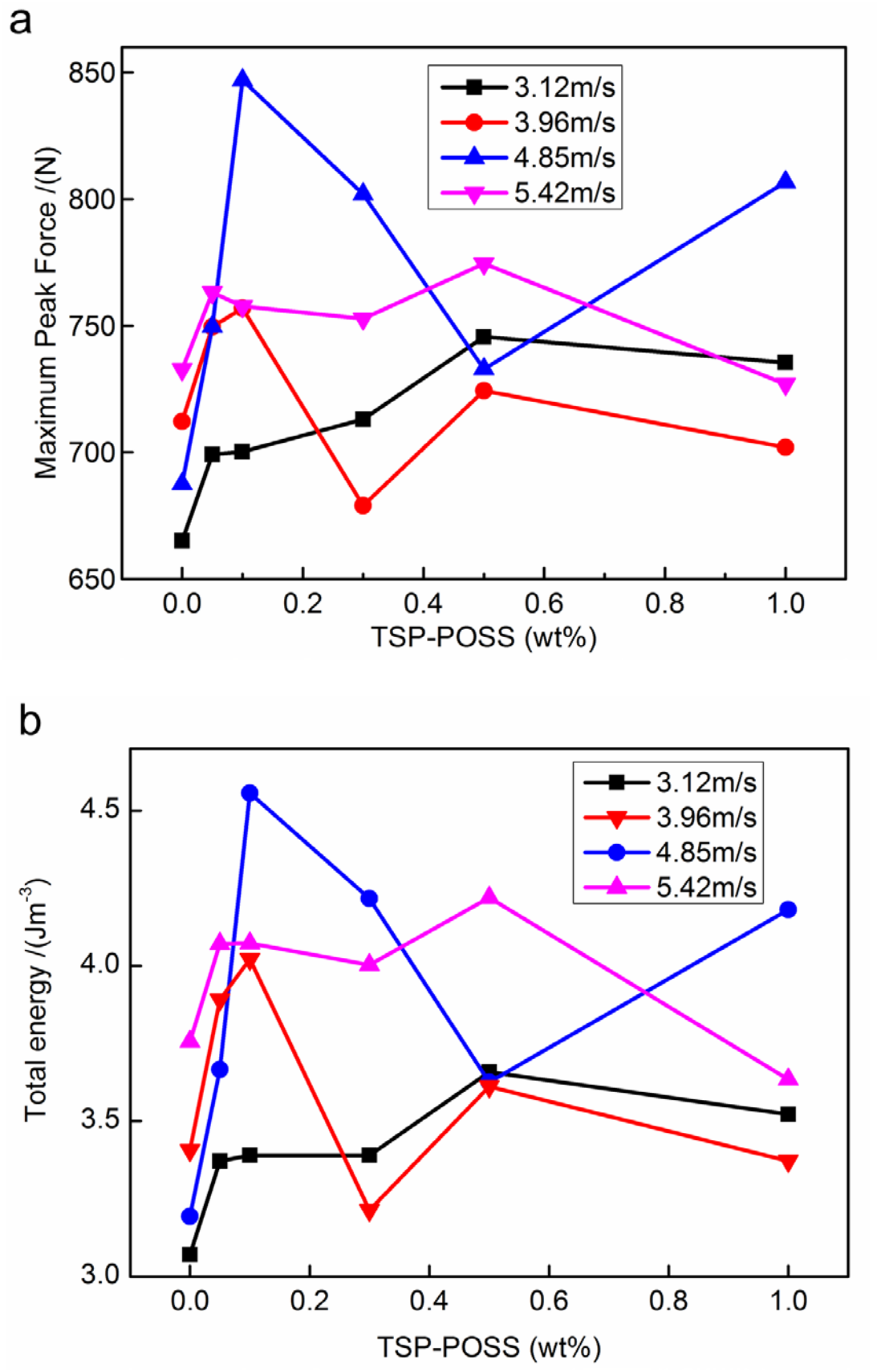

Figure 71 (a) Maximum peak force and (b) total energy for polycarbonate and its TSP-POSS based nanocomposites at all dart velocities

5.4. Split-Hopkinson Pressure Bars (SHPB)

Split-Hopkinson pressure bars were used to test the performance of the polymer nanocomposites at higher strain rates (magnitude ~10^3 s^{-1}). Two aperture settings were used, 7.9 mm and 7.9 mm + 12 mm, to vary the speed at which the projectile moves through the chamber in order to investigate the effect of impact velocity on the specimen. The voltage-time curves that were produced were converted into stress-strain graphs so that properties such as Young's modulus, yield stress and energy absorption of the nanocomposites could be determined. As there was little variation in the data, three samples per TSP-POSS concentration were tested to give average values of the above properties.

5.4.1. Aperture: 12 mm

The aperture of diameter 12 mm corresponding to an area of 1.13E^{-4} m^2 was used. The strain rate in the samples ranged from 2490.8 s^{-1} to 8359.3 s^{-1} and depended on TSP-POSS concentration

Samples did not exhibit any cracking or visible marks post-testing but rather absorbed energy through deformation so that thickness decreased and diameter increased.

From figure 72 it can be seen that the stress-strain curves of the control sample and the polymer nanocomposites are similar in shape; the sample obeys Hooke's law until it reaches the elastic limit, thereafter the sample yields and deforms plastically and exhibits some limited strain hardening until the sample fails. The maximum strain increases with the addition of TSP-POSS at all nanofiller concentrations.

Figures 73-77, contain the average values of Young's modulus, yield stress, energy absorption evolution, ultimate strength and strain rate. Overall, the addition of TSP-POSS does not have a clear effect on the Young's modulus of polycarbonate (figure 73). The average Young's modulus of polycarbonate measured as (29.2 ± 1.8 GPa). Initially, the addition of 0.05% TSP-POSS decreases the average Young's modulus by 4% to (28 ± 2.2 GPa), however, taking error into account it can be seen that this effect is negligible. Increasing the TSP-POSS loading to 0.1wt% does not affect the average value of Young's modulus of polycarbonate. Increasing the TSP-POSS content further increases the Young's modulus to (31.8 ±2.2 GPa), a 7% increase over that of the unmodified polymer.

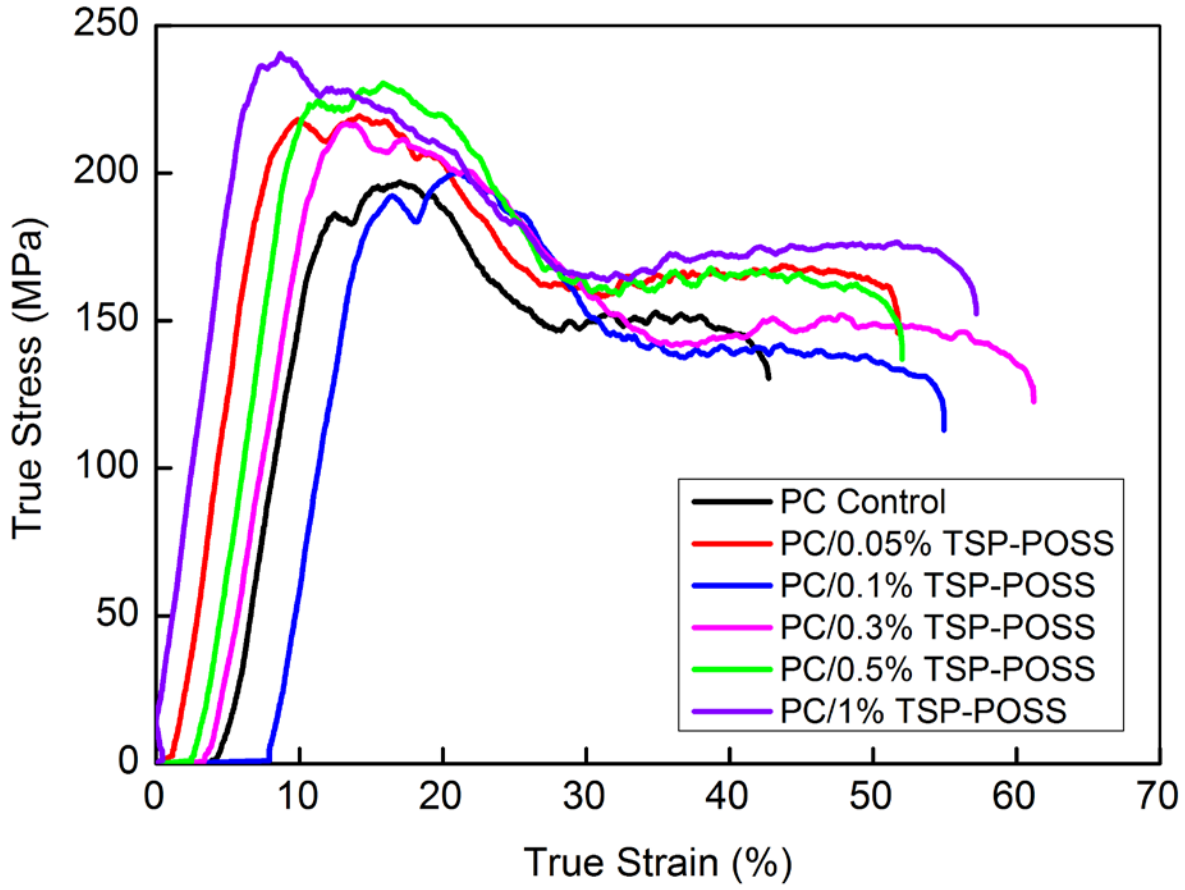

Figure 72 Stress-strain curves from SHPB testing of polycarbonate and its TSP-POSS based nanocomposites using a 12 mm aperture

It then decreases again for PC/0.5wt% TSP-POSS to (25.8 ± 2.9 GPa) but increases to (34.1 ± 1.5 GPa) when 1wt% TSP-POSS is incorporated into the polycarbonate matrix, a 17% increase in comparison to the polycarbonate control and the highest value obtained in the test. Perhaps when the deformation is of a compressive nature, the higher amount of rigid POSS aggregates present in the matrix (from SEM analysis) of PC/1wt% TSP-POSS increase the stiffness of the polymer by restricting the chain motion.

Figure 74 shows that overall, the addition of TSP-POSS to the polycarbonate matrix has a positive effect on the yield stress of the polymer. The average yield stress of polycarbonate was measured to be (173 ± 7 MPa). All nanocomposites exhibited a higher average yield stress in comparison to that of the control sample, however, the average value for PC/0.5wt% TSP-POSS appears to be an outlier as it only increases by 4% which falls within experimental error.

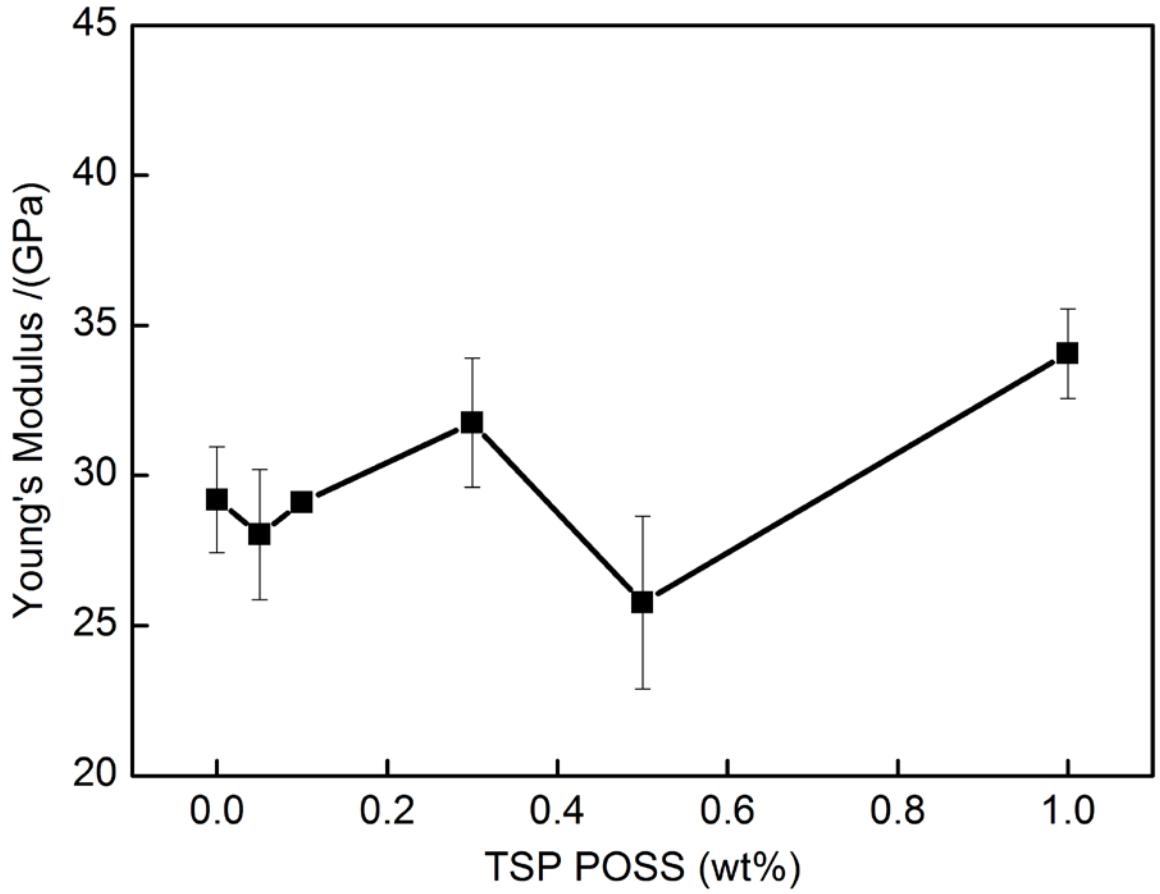

Figure 73 Average Young's modulus of polycarbonate and its TSP-POSS based nanocomposites using a 12 mm aperture

Initially the yield stress increases for 0.05wt% and 0.1wt% where it reaches (212 ± 14 MPa), however it then decreases to (206 ± 4 MPa) and (180 ± 12 MPa) for PC/0.3wt% TSP-POSS and PC/0.5wt% TSP-POSS, respectively. However, upon further addition of TSP-POSS, the sample containing 1wt% TSP-POSS reaches a maximum of (227 ± 6 MPa), a 31% increase over that of the unmodified polycarbonate control. This suggests that the polymer chains in PC/1wt% TSP-POSS are restricted somehow so that they do not plastically deform as early on in the test. Again, this could be due to the presence of numerous rigid POSS aggregates which impede the chain movement during compressive deformation and/or form hydrogen bonds with the polymer chains, further increasing their rigidity and yield strength. Notably, the maximum yield stress is achieved with the maximum loading of 1wt% TSP-POSS, which is also the sample that exhibited the largest amount of aggregates. It could be that the aggregates are able to restrict the chain motion more therefore increasing the yield strength of polycarbonate.

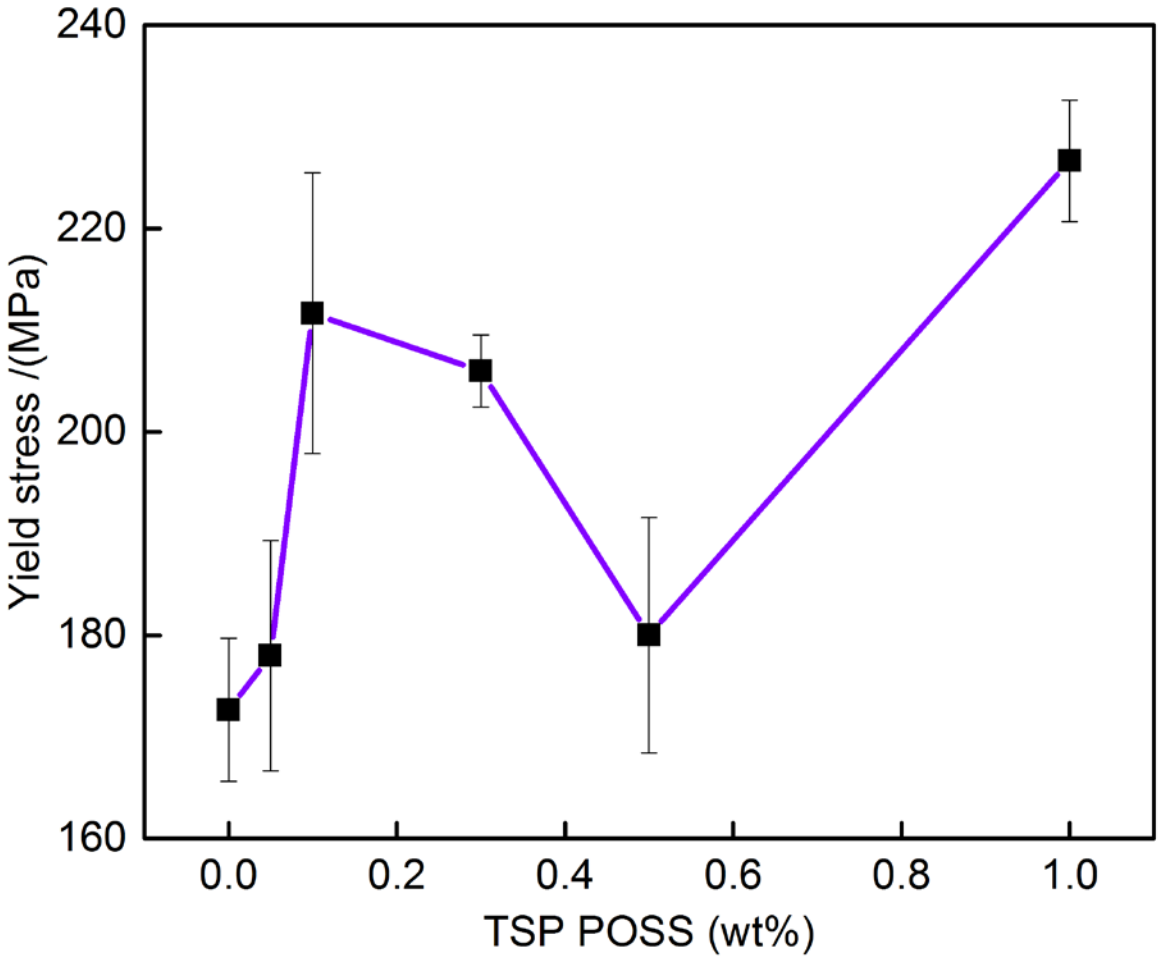

Figure 74 Average yield stress of polycarbonate and its TSP-POSS based nanocomposites using a 12 mm aperture

The energy absorption was measured at strain values of 5%, 10%, 20%, 30% 40% and 50% to produce energy evolution graphs (see figure 75). Overall, it can be seen that the energy absorption capability of polycarbonate is improved with the addition of TSP-POSS and could be due to the formation of a stretchy hydrogen bonded network between the TSP-POSS molecules and the polymer chains at loadings below 0.5wt% and the presence of TSP-POSS aggregates at loadings of 0.5wt% and 1wt%, as proposed previously. All nanocomposites failed at a strain value above 40% whereas polycarbonate did not. The nanocomposite containing 1wt% TSP-POSS performed the best over the entire strain range, absorbing the largest amount of energy out of all samples tested. At 50% strain, PC/1wt% TSP-POSS absorbed 8.99 $MJ.m^{-3}$. At 40% strain, polycarbonate absorbed 5.87 $MJ.m^{-3}$ whereas PC/1wt% TSP-POSS absorbed 7.28 $MJ.m^{-3}$, a 24% increase in energy absorption.

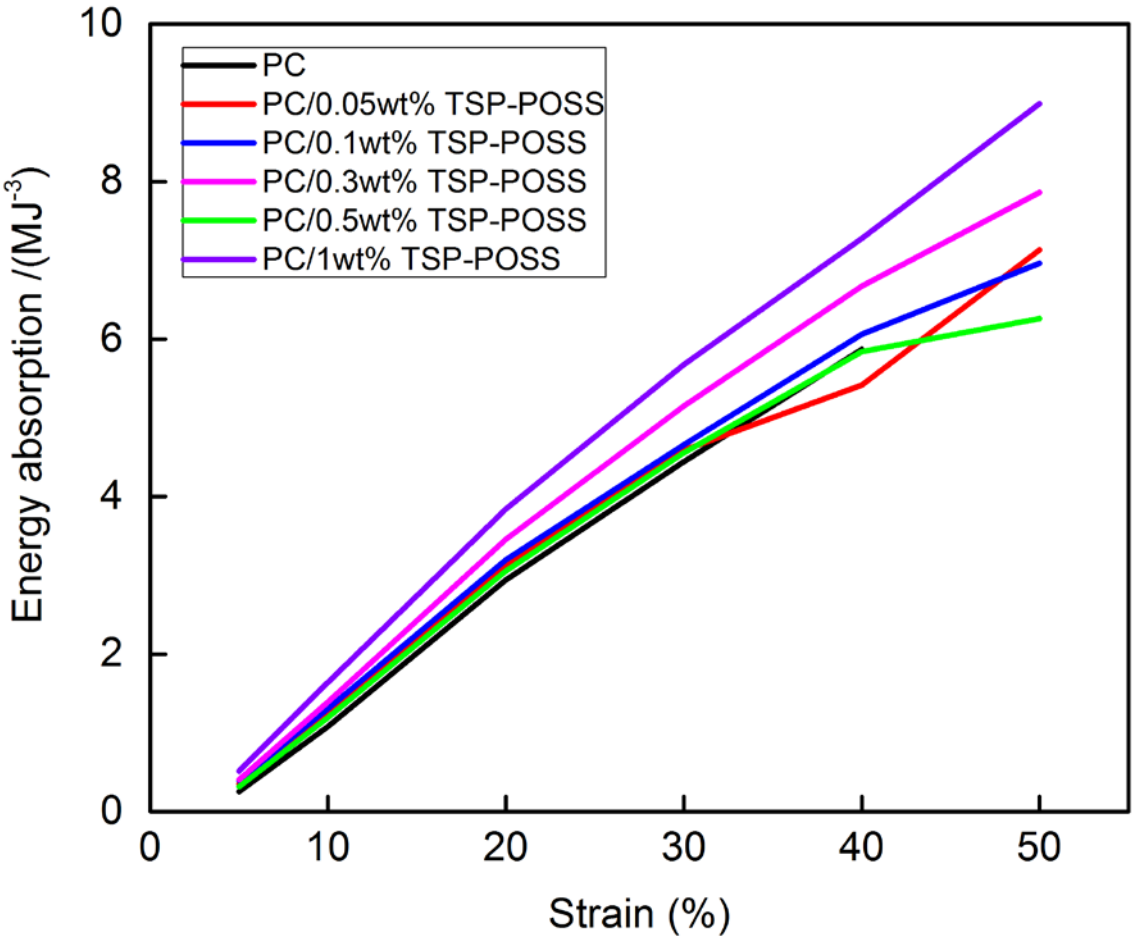

Figure 75 Average energy absorption evolution graphs for polycarbonate and its TSP-POSS based nanocomposites using a 12 mm aperture

This enhancement in energy absorption could again be due to the presence of aggregates (≈100 nm – 200 nm in diameter) which may be involved in void formation which acts as a toughening mechanism (see section 4.1.2 and figures 48-52).

Figure 76 shows the ultimate stress reached in the specimens, i.e. their ultimate compressive strength. The average ultimate stress of the polycarbonate was (195 ± 1 MPa). Samples containing 0.1wt%, 0.3wt% and 1wt% TSP-POSS were stronger than the polycarbonate control sample, with a maximum of (235 ± 5 MPa) being reached in the sample containing 1wt% TSP-POSS, a 21% increase over the unmodified polymer. Nanocomposites containing 0.05wt% and 0.5wt% TSP-POSS performed similarly to the polycarbonate control samples but had large statistical errors.

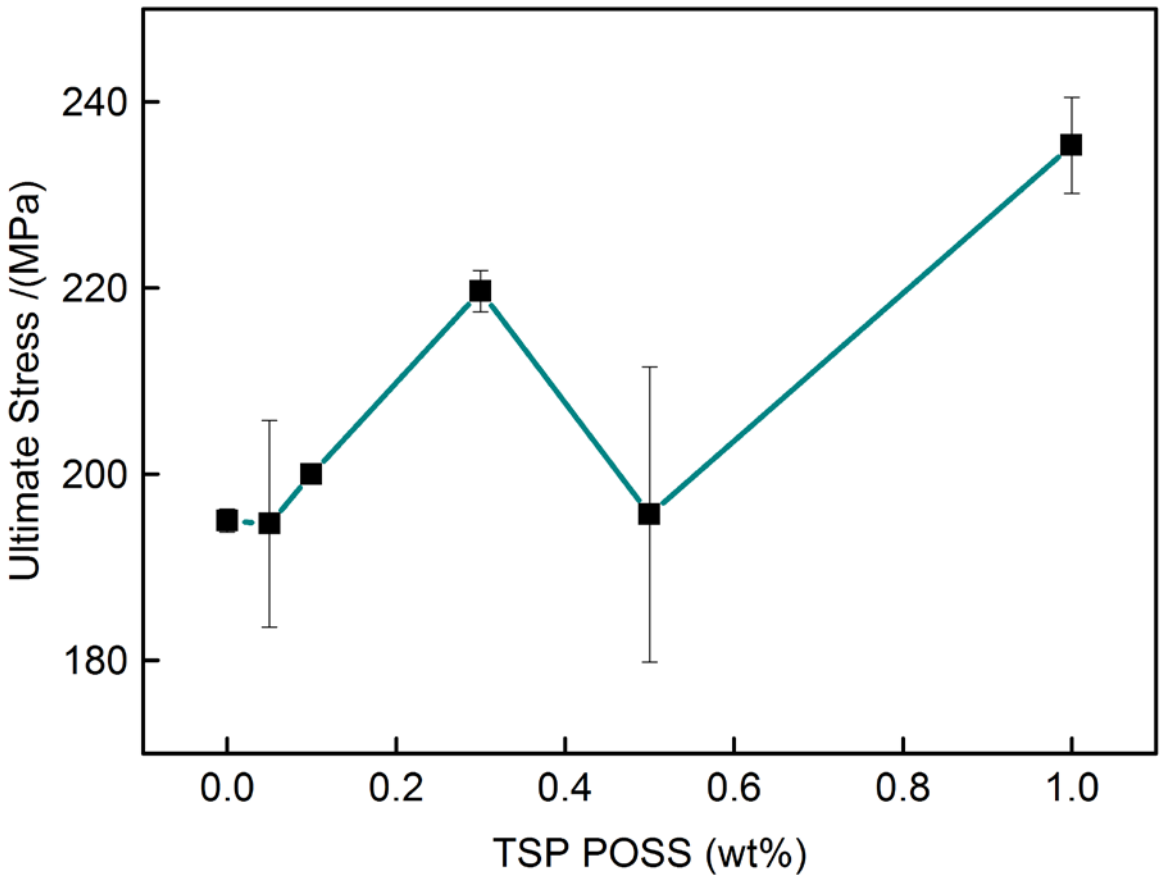

Figure 76 Average ultimate stress of polycarbonate and its TSP-POSS based nanocomposites using a 12 mm aperture

The strain rate was calculated for each sample. The average values can be found in figure 77, showing that strain rate is larger in the nanocomposites than it is in the unmodified polymer i.e. the change in strain with respect to time is increased. The average strain rate in polycarbonate is 3165 s^{-1}. The average strain rate reaches a maximum of (6826 ± 735 s^{-1}) in the sample containing 0.5wt% TSP-POSS.

Higher strain rates induce stiffer behaviour and result in increases in stiffness and modulus; from these results it would seem that the addition of TSP-POSS to the polycarbonate matrix could result in a stronger and stiffer material with increased elastic behaviour and load-bearing capabilities before failure.

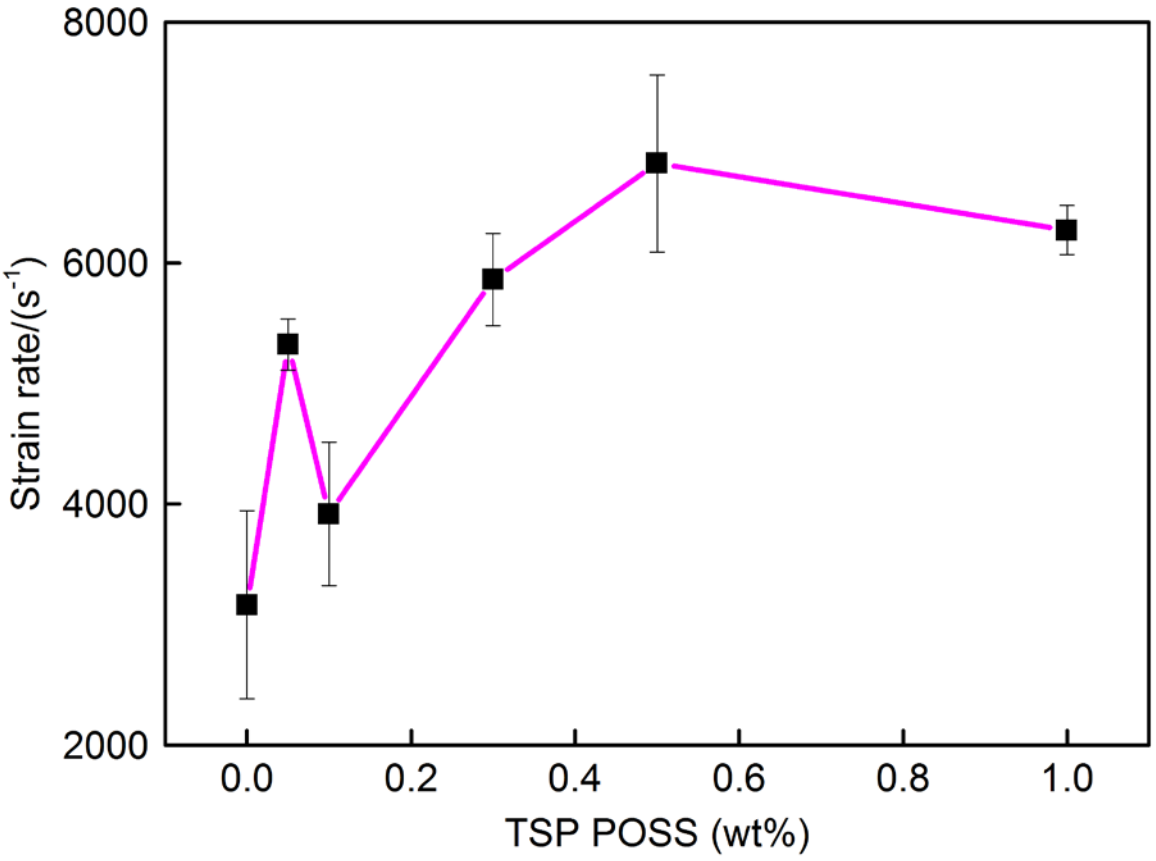

Figure 77 Average strain rate in the SHPB testing of polycarbonate and its TSP-POSS based nanocomposites using a 12 mm aperture

Overall, the addition of TSP-POSS has a positive effect on the impact properties of polycarbonate at high strain rates by enhancing both yield stress and energy absorption capability of polycarbonate and having a modest effect on the stiffness and strength of the polymer. The optimum loading was 1wt% TSP-POSS, which displayed the maximum values in all properties measured. This could be due to the increased presence of TSP-POSS aggregates in PC/1wt% TSP-POSS which may help to further reinforce the polymer matrix via restriction of chain mobility. As energy absorption increases along with yield stress, it would appear that the mechanism by which TSP-POSS enhances the matrix during impact of a compressive nature simultaneously reinforces the polymer chain matrix and allows it to absorb more energy. This could be because two mechanisms are involved; the restriction of polymer chains in the vicinity of TSP-POSS aggregates and the toughening of the matrix by the formation of a hydrogen bonded network of polymer chains and the TSP-POSS molecules situated between them and/or the potential void formation around the TSP-POSS aggregates seen in figures 48-52.

5.4.2. Aperture: 7.9 mm + 12 mm

The apertures of diameter 7.99 mm and 12 mm which corresponded to an area of $5.03E^{-5}$ m^2 and $1.13E^{-4}$ m^2, respectively, was removed during the test to increase the speed at which the projectile is fired. Again, the samples did not exhibit any cracking or visible marks post-testing but absorbed energy through deformation so that thickness decreased and diameter increased.

Figure 78 shows that again, the stress-strain curves of the control sample and the polymer nanocomposites are similar in shape. Strain hardening is more noticeable in the curves and follows on from the fact that the projectile velocity has been increased.

Figures 79-81, contain the average values of Young's modulus, yield stress, energy absorption evolution, ultimate strength and strain rate.

From figure 79(a), it can be seen that the addition of TSP-POSS to the polycarbonate matrix can increase the Young's modulus of the polymer. The sample containing 0.05wt% TSP-POSS has a lower average Young's modulus than polycarbonate (29.7 ± 3.31 GPa) in comparison to (31.5 ± 1.4 GPa) but with error taken into account the nanocomposite performs similarly to the control sample.

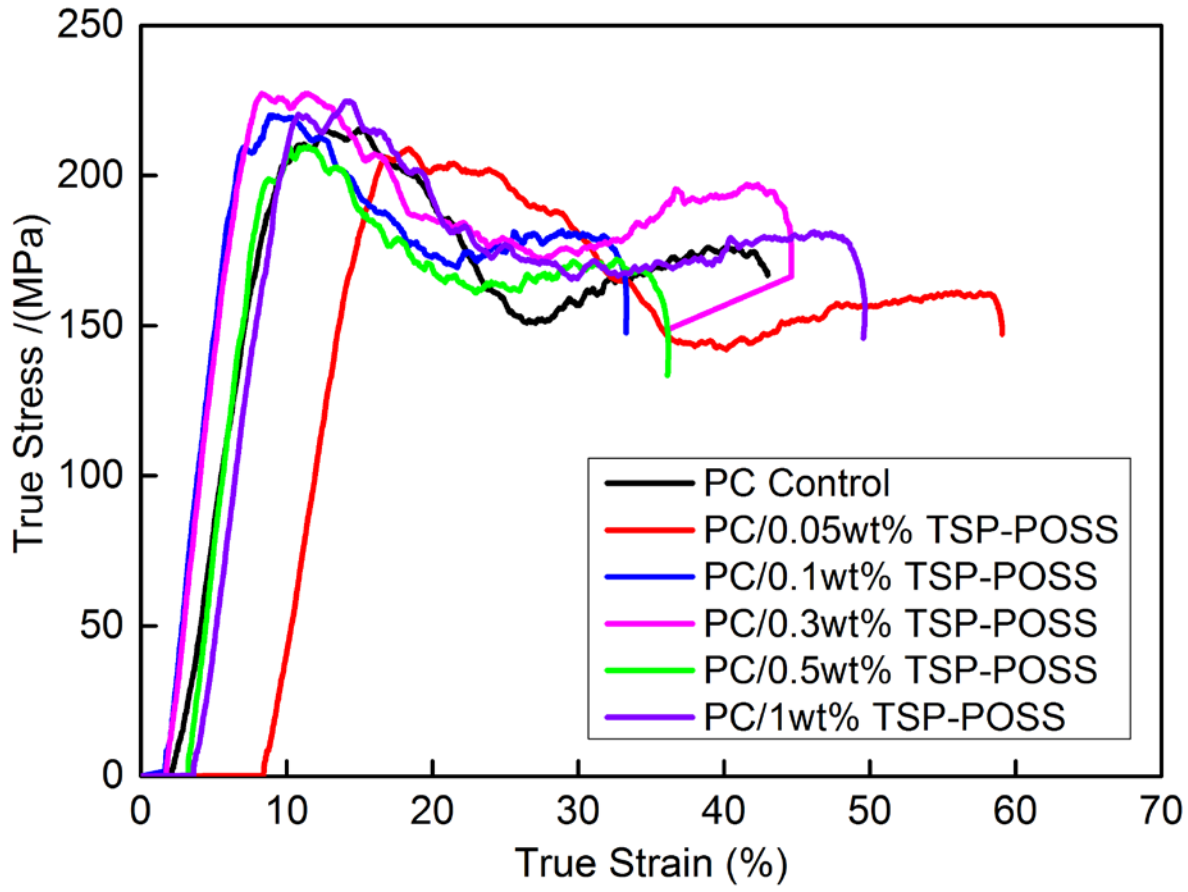

Figure 78 Stress-strain curves from SHPB testing of polycarbonate and its TSP-POSS based nanocomposites using apertures of 7.99 mm and 12 mm diameter

The Young's modulus reaches a maximum of (42.1 ± 1.17 GPa), a 42% increase in stiffness over the original polymer. This is higher in value than the maximum Young's modulus value achieved when a smaller aperture combination was used. This is because the higher impact velocity will induce stiffer, more elastic-like behaviour in the viscoelastic polymer due to its time-dependent strain properties. Upon further TSP-POSS loading, the Young's modulus is still higher in the nanocomposites than that of the control sample but displays a declining trend from the value for PC/0.1wt% TSP-POSS. Perhaps at this higher impact velocity the enhancements of TSP-POSS seen in section 5.4.1 and the proposed mechanisms responsible are not strong enough to resist the increased impact energy.

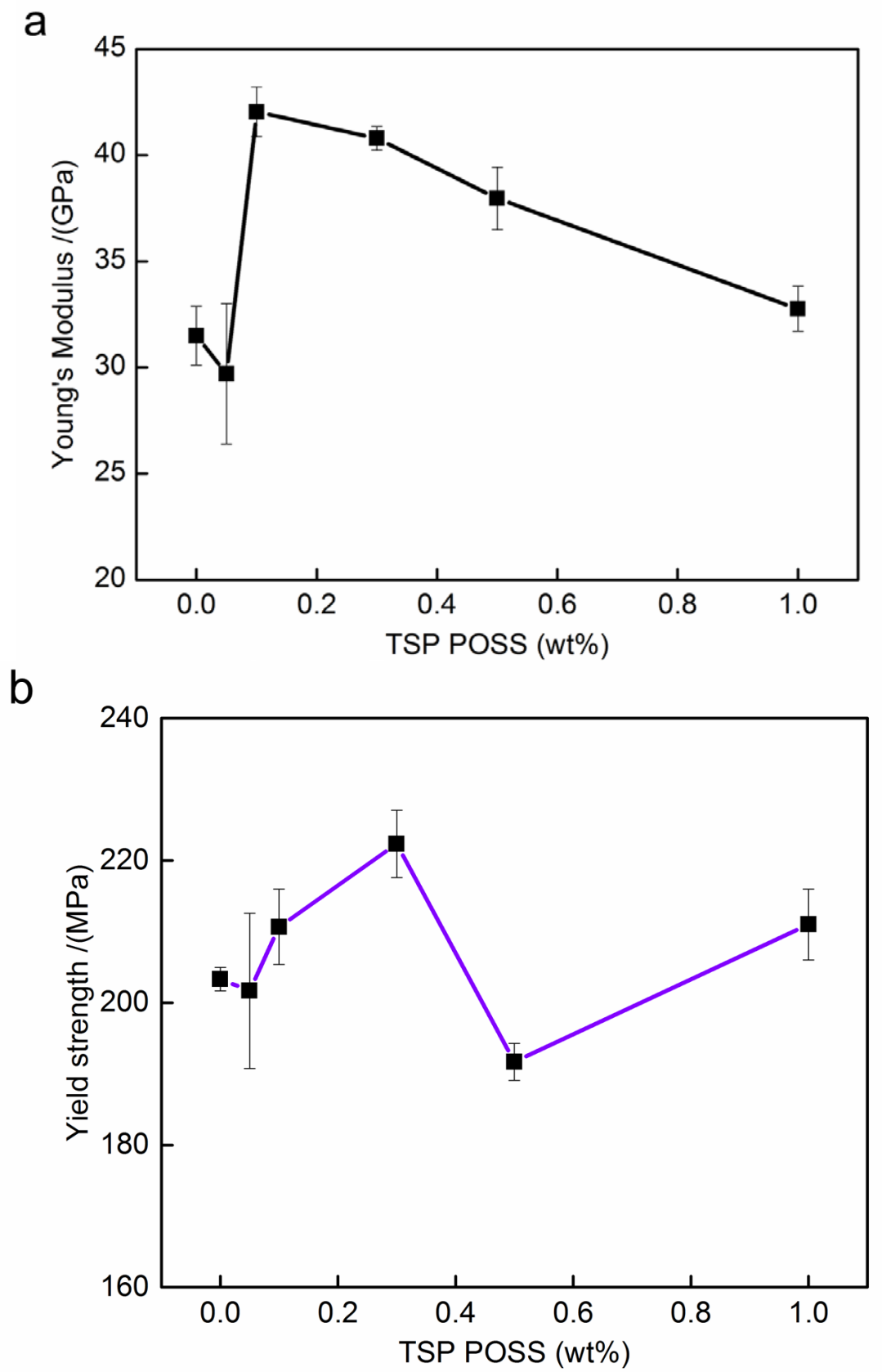

Figure 79 (a) Young's modulus and (b) yield stress of polycarbonate and its TSP-POSS based nanocomposite using apertures of 7.99 mm and 12 mm diameter

Figure 79(b) shows that at the higher impact velocity, the yield stress was not influenced as much by the addition of TSP-POSS, with the maximum enhancement of 9% achieved with the addition of 0.3wt%. The average yield stress of PC/0.05wt% TSP-POSS and PC/0.5wt% were similar or slightly lower in value than the control sample (0.5%-5% decrease). This could be because the influence of TSP-POSS on the chain mobility and energy absorption capability is not strong enough to overcome the higher impact velocity.

The energy evolution curves can be found in figure 80(a). The energy absorption capabilities of the nanocomposites are poorer compared to figure 75 in section 5.4.1 when a lower projectile velocity was used. The nanocomposites perform either similar or worse than the control sample. The nanocomposite containing 0.05wt% TSP-POSS on average did fail at a higher strain that the polycarbonate control.

Figure 80(b) shows the ultimate stress reached in the polycarbonate and nanocomposite samples. Overall, TSP-POSS did not have much of an effect on the strength of the material. The average ultimate stress of polycarbonate was (219 ± 2 MPa). The maximum ultimate stress reached in the test was (227 ± 0.35 MPa) with the addition of 0.3wt% TSP-POSS; only a 4% increase over that of the control sample. Minimum values in ultimate stress were found for the nanocomposite systems containing 0.05wt% and 0.5wt% TSP-POSS and the same trend is found in fig. 79(b) for the yield strength, where these nanocomposites display decreased strength. Regarding PC/0.05wt%, the addition of 0.05wt% may not be enough to increase the performance of polycarbonate at the higher projectile impact speed. Young's modulus was also unaffected using this loading. As for PC/0.5wt% it is not clear why the strength of this sample was lower than the other nanocomposites and did not perform similarly to nanocomposite containing the highest TSP-POSS loading (1wt%). Perhaps a decrease in quality occurred in these samples from processing.

Strain rate did not vary much with TSP-POSS concentration (figure 81), although the average strain rate in 0.05wt% was (5454 ± 580 s^{-1}), larger in value than polycarbonate (4138 ± 122 s^{-1}). This explains why the properties of the nanocomposites were not that much different to the polycarbonate control; TSP-POSS was not able to affect the strain-rate behaviour of polycarbonate when the impact velocity increased.

Overall, at a higher impact velocity the nanocomposites exhibit more elastic-like behaviour as shown by increases in Young's modulus in comparison to the polycarbonate control value, perhaps due to strain hardening induced by the POSS molecules/aggregate which restrict polymer chain motion. The enhancement in energy absorption capabilities seen at lower impact velocity disappears when the velocity is increased. It would seem that the positive effect TSP-POSS has on the polycarbonate matrix at the lower velocity is not strong enough to withstand the higher impact velocity and the nanofiller effect disappears.

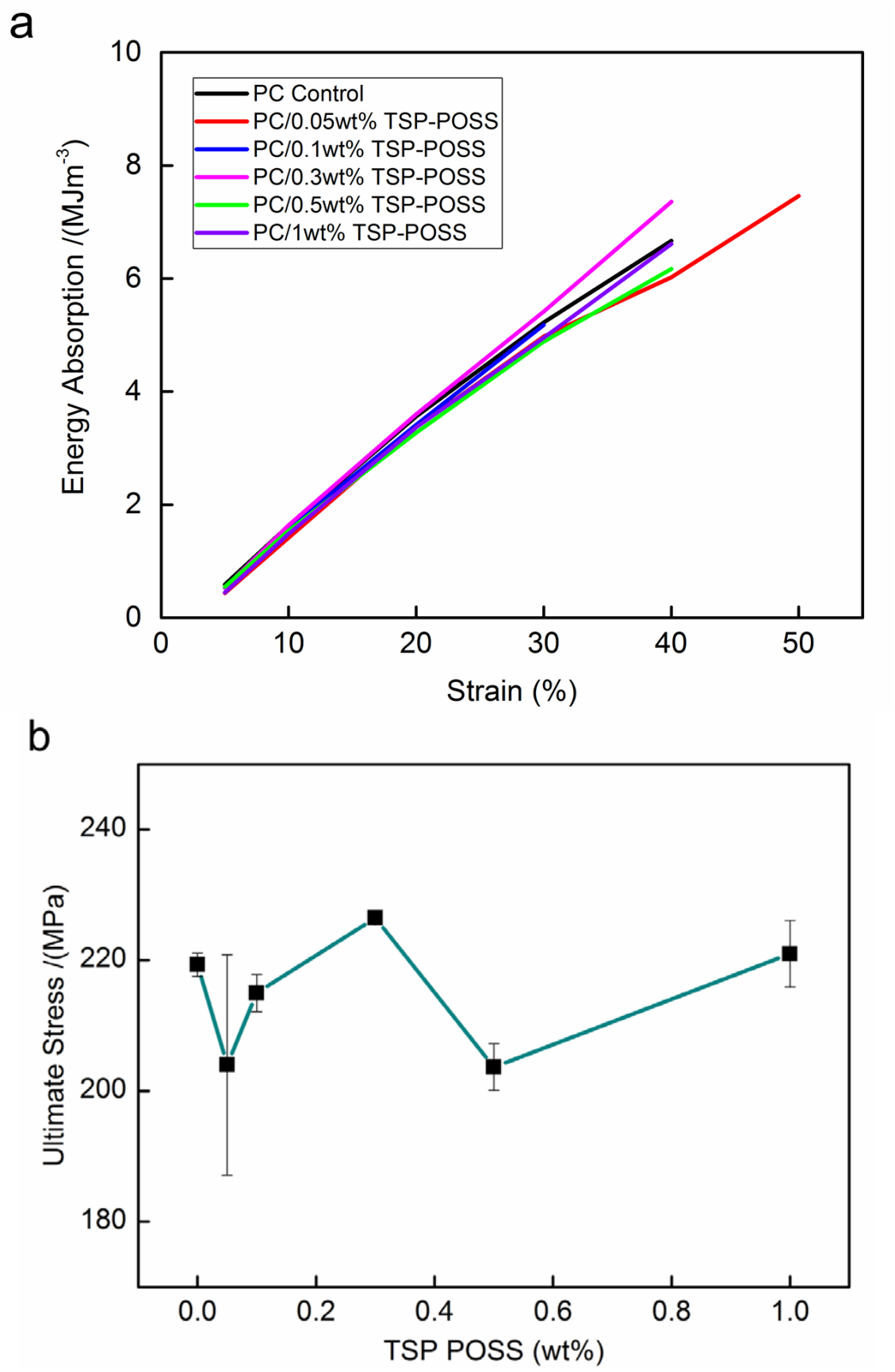

Figure 80 (a) Energy absorption evolution and (b) ultimate stress of polycarbonate and its TSP-POSS based nanocomposites using apertures of 7.99 mm and 12 mm diameter

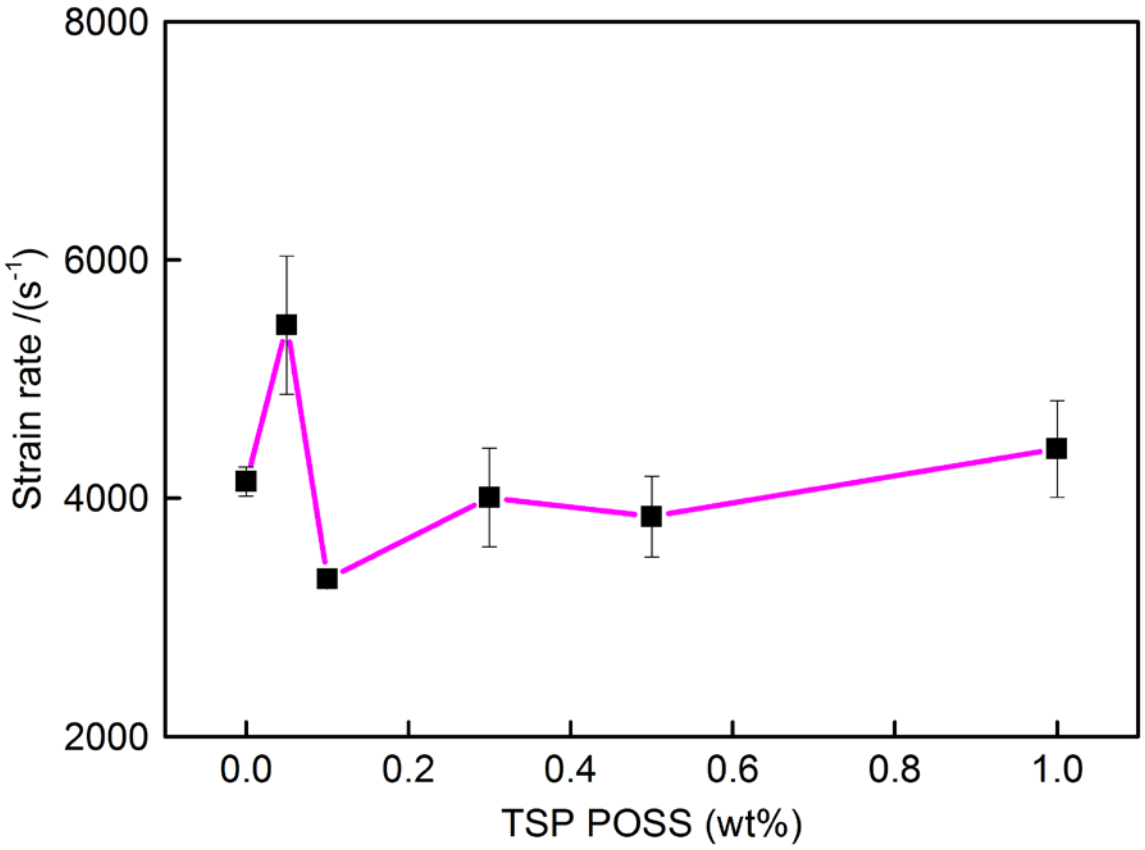

Figure 81 Average strain rate in the SHPB testing of polycarbonate and its TSP-POSS based nanocomposites using apertures of 7.99 mm and 12 mm diameter

Chapter 6

Preliminary Study: Nanocomposite Physical Aging

Chapter 6 Preliminary investigation into the physical aging of polycarbonate and its TSP-POSS based nanocomposites

The effect of TSP-POSS on the physical aging of polycarbonate was investigated by MDSC. Samples were isothermally held at temperatures specific to the sample glass transition temperature, T_g, for certain lengths of time in order to assess the effect of annealing time, t_a, and annealing temperature, T_a, on physical aging. Table 11 contains the annealing parameters. After annealing, heat scans from 120 °C to 180 °C were performed on the aged samples to measure the enthalpy differential, ΔH, over the glass transition. Change in enthalpy was plotted against annealing time and annealing temperatures for polycarbonate and the nanocomposites containing 0.1wt%, 0.5wt% and 1wt% TSP-POSS.

6.1. Effect of Annealing Time

The effect of annealing time on the enthalpy differential, $\Delta H\ (t_a,\ T_a)$ of the polycarbonate control sample and the POSS-based nanocomposites can be found in fig. 82 for each annealing temperature used. The enthalpy differential is a measure of the excess enthalpy lost and is an indicator of the extent of physical aging of the sample. Therefore, by plotting $\Delta H\ (t_a,\ T_a)$ against annealing time, the effect of t_a on the amount of physical aging that occurs in the samples can be assessed.

Overall, figure 82 shows that $\Delta H\ (t_a,\ T_a)$ increases in value as annealing time is increased. This is to be expected as the longer the samples are annealed, the more the enthalpy of the system decreases. Therefore, upon heating through the glass transition, a greater amount of enthalpy is recovered at longer annealing times.

At T_{a1}, $\Delta H\ (t_a,\ T_a)$ of the nanocomposites was lower in value than that of the unmodified polymer. The addition of TSP-POSS at all loadings did not increase the aging of polycarbonate but instead slightly decreased it and had a positive effect. $\Delta H\ (t_a,\ T_a)$ decreased with increasing TSP-POSS loadings with PC/1wt% TSP-POSS aging the least out of all samples at all annealing times. From figure 82(a), it appears that the nanocomposites age less than the polycarbonate control sample and that the rate of enthalpy recovery decreases with the addition of TSP-POSS.

TSP-POSS	T_g (°C)	T_{A1} (°C)	T_{A2} (°C)	T_{A3} (°C)
PC	144.18	134	132	130
ΔT		**10.18**	**12.18**	**14.18**
0.1	144.57	134.59	132.39	129.39
0.5	143.83	133.65	131.65	128.65
1	143.63	133.45	131.45	128.45

t_{an}	Annealing time (hours)
ta_1	1
ta_2	3
ta_3	6
ta_4	10
ta_5	20
ta_6	35
ta_7	50
ta_8	120

Table 11 Annealing parameters used in the aging of polycarbonate and its TSP-POSS based nanocomposites

The results in figure 82(a) imply that POSS has a restricting effect on the polymer chains by (i) the formation of bulky POSS aggregates which either restrict or slow down chain movement by impeding their movement and/or (i) the formation of a hydrogen bonded network which holds together the chains and hinders their movement.

At T_{a2}, ΔH (t_a, T_a) of PC/0.1wt% and PC/1wt% TSP-POSS is larger than that of the polycarbonate control at all annealing times (figure 82(b)). This suggests that with an increase in ΔT, these nanocomposites age more.

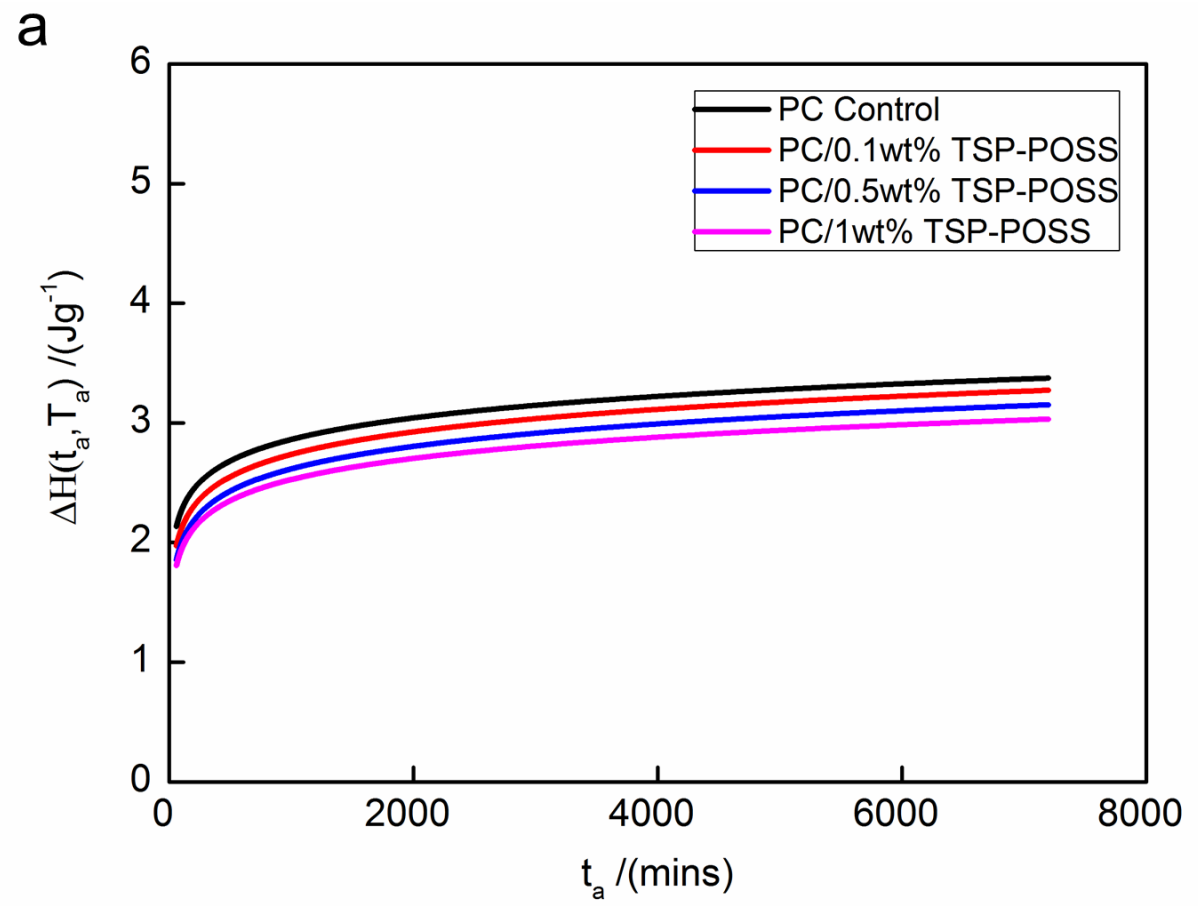
a
PC Control
PC/0.1wt% TSP-POSS
PC/0.5wt% TSP-POSS
PC/1wt% TSP-POSS
ΔH(t_a,T_a) /(Jg^-1)
t_a /(mins)
0
1
2
3
4
5
6
0
2000
4000
6000
8000

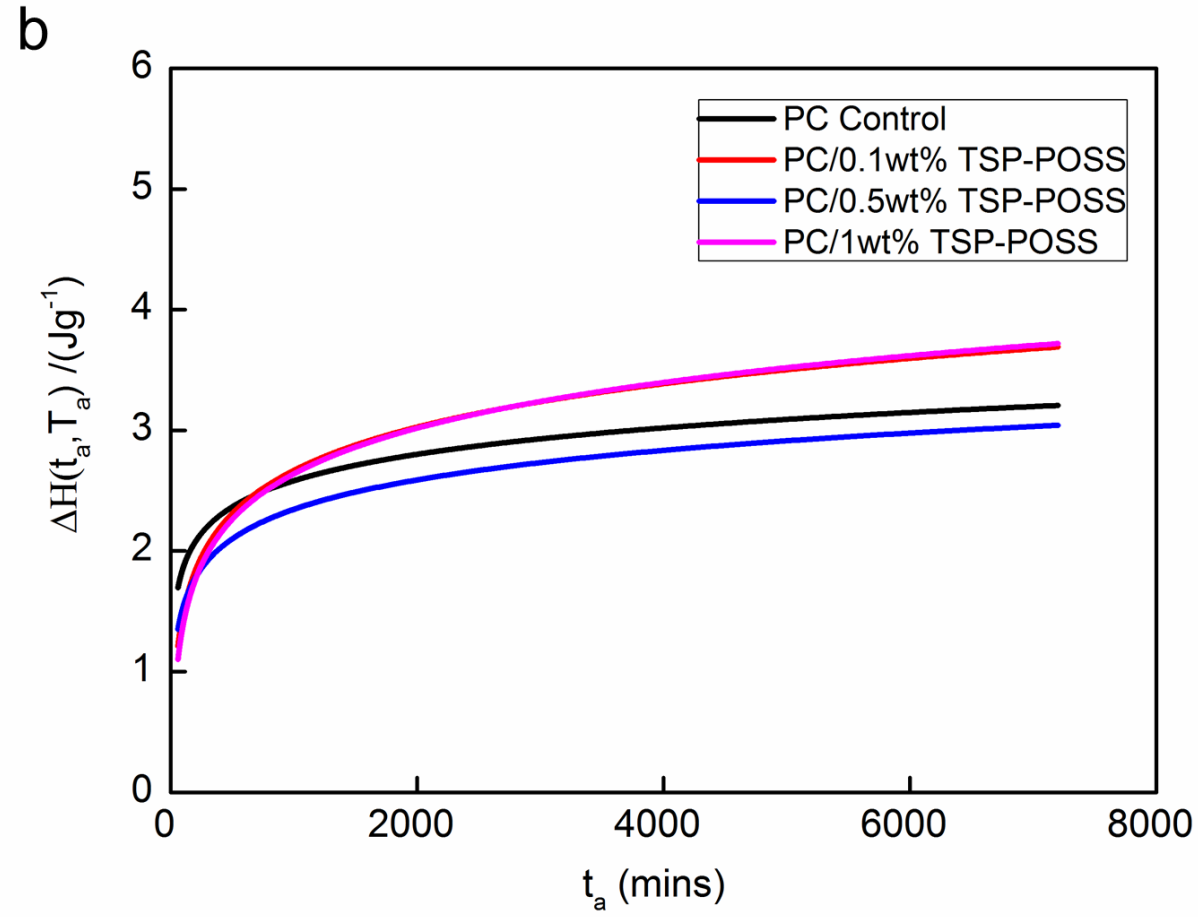
b
PC Control
PC/0.1wt% TSP-POSS
PC/0.5wt% TSP-POSS
PC/1wt% TSP-POSS
ΔH(t_a,T_a) /(Jg^-1)
t_a (mins)
0
1
2
3
4
5
6
0
2000
4000
6000
8000

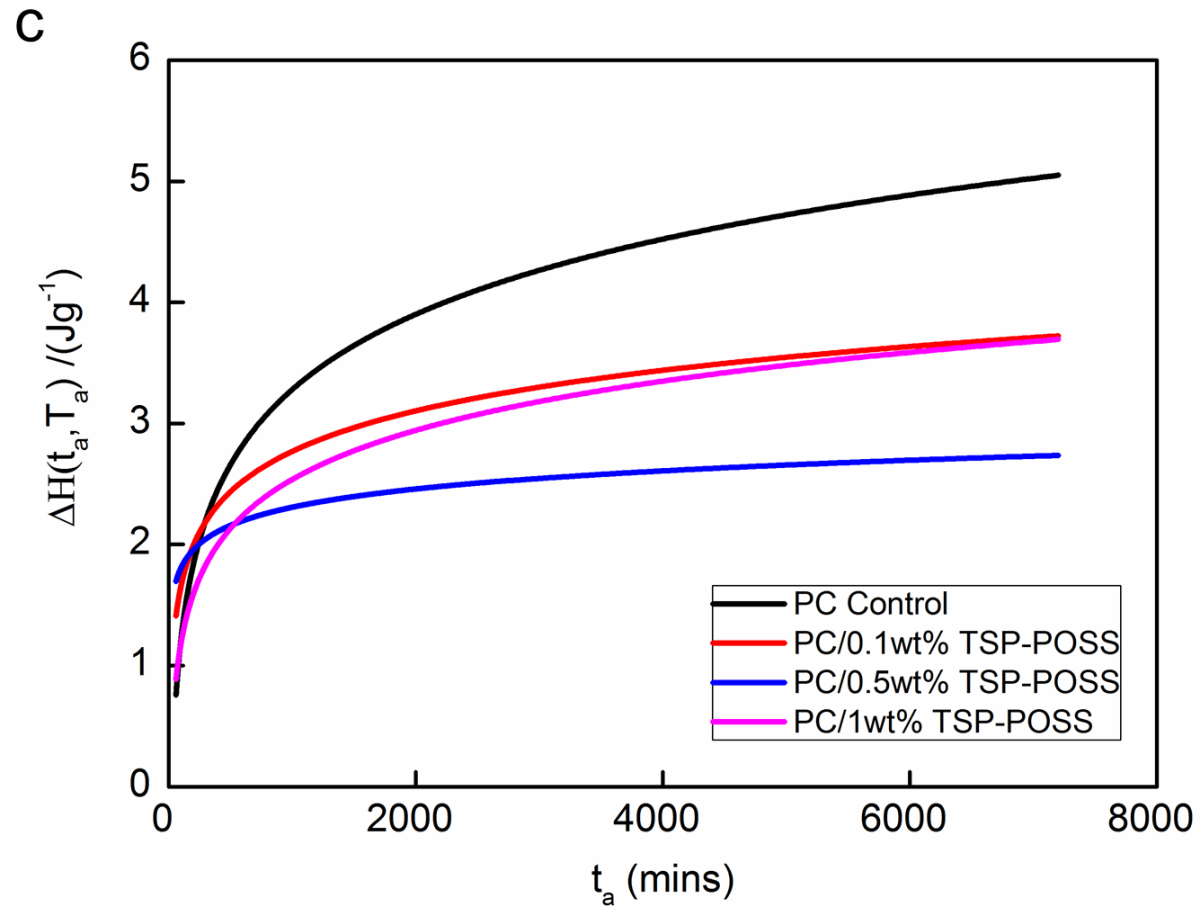

Figure 82 The effect of annealing time on the enthalpy change of polycarbonate and its TSP-POSS based nanocomposites at a) T_{a1}, b) T_{a2} and c) T_{a3}

This could be due to an increase in free volume relaxation as a result of TSP-POSS increasing the free volume of the polymer by situating itself between the polycarbonate chains. Conversely, the nanocomposite containing 0.5wt% TSP-POSS ages less than the control polymer at all annealing times.

Increasing ΔT further to T_{a3}, causes an increase in the range of $\Delta H\ (t_a, T_a)$ values. At the lowest t_a used, initially, the $\Delta H\ (t_a, T_a)$ values of the nanocomposites is higher than that of the control sample and again could be due to the increased free volume present in these samples which results in a larger free volume relaxation contribution. There is a turning point in the data presented in fig. 82(c) where the nanocomposites age less than the polycarbonate control. The results in fig. 82(c) suggest that there could be two mechanisms involved in the physical aging process of the nanocomposites; the increase in free volume relaxation and the impedance of chain relaxation by TSP-POSS and which one dominates the physical aging process depends on factors such as annealing temperature/ΔT.

Considering the results presented in figure 82(a), one would expect an increase in aging of the samples as the samples are aged at a temperature nearer to the glass transition and should therefore have more kinetic energy. Perhaps the potential reinforcing effect of TSP-POSS is enhanced at this temperature due to the increased chain motion. More data is required to better understand the results presented in figure 82.

6.2. Effect of Annealing Temperature

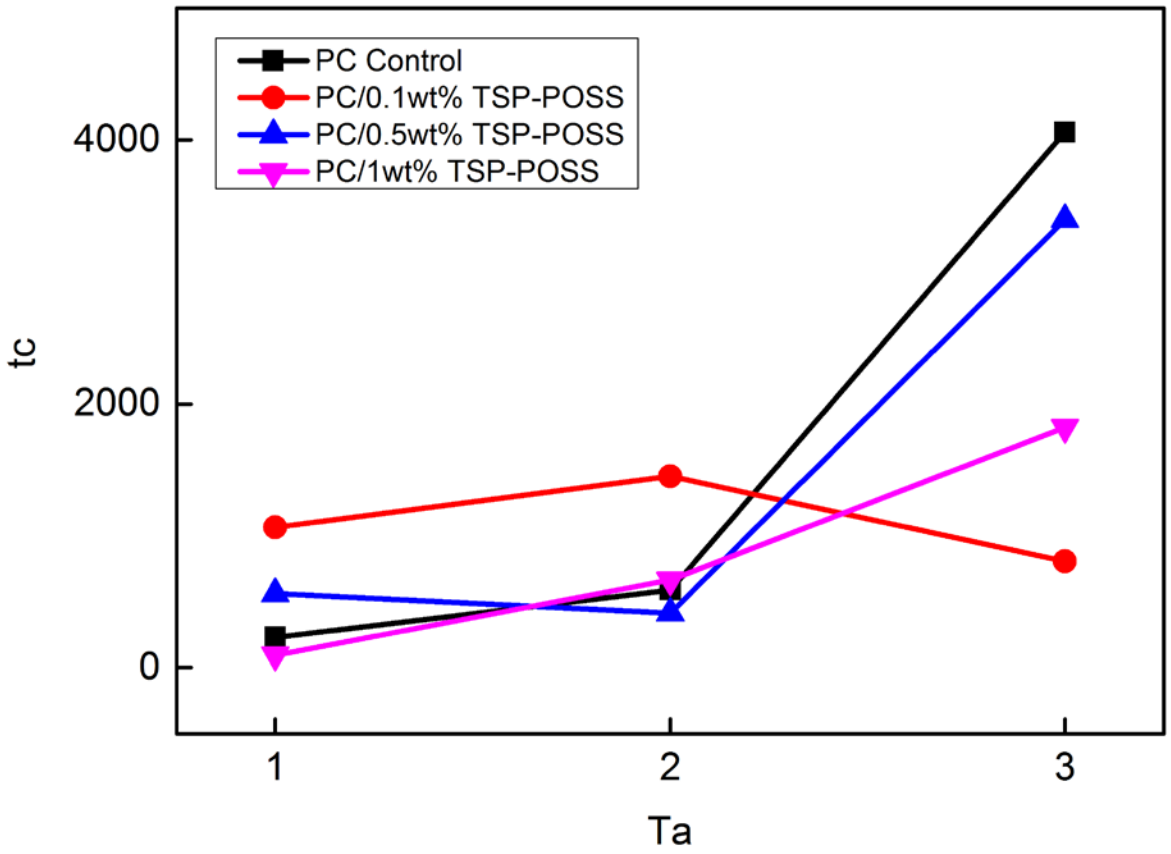

Figure 83 The effect of annealing temperature on the characterisation time of polycarbonate and the TSP-POSS based nanocomposites

The relaxation time, t_c is the time constant which characterises the relaxation process that occurs in the glassy state of an amorphous polymer to a state of equilibrium. It is both time and temperature dependant.

Figure 83 shows the effect of annealing temperature on the characteristic relaxation times of the polycarbonate control sample and the three nanocomposites. Generally, as ΔT increases t_c of the polymer also increases. The nanocomposites generally follow the same trend. This is because more time is required for the sample to reach equilibrium as it is further away.

The effect of TSP-POSS changes with annealing temperature. At T_{a1}, t_c of the nanocomposites containing between 0.1 and 0.5wt% TSP-POSS is higher than that of the control whereas t_c of PC/1wt% TSP-POSS is slightly lower. Overall, at T_{a1}, it would appear that the nanocomposites age at a similar or slower rate than the polycarbonate control sample.

As ΔT is increased to T_{a2}, the relaxation time of all nanocomposites, except PC/0.1wt%, is similar or higher in value than that of the unmodified polymer.

However, at T_{a3}, t_c of all the nanocomposites is less than that of the polycarbonate control sample i.e. the nanocomposites age faster than the control sample.

The results for T_{a3} suggest that TSP-POSS increases the relaxation rate and causes the polycarbonate to age at a faster rate. However, smaller t_c values of the nanocomposites are more likely to be linked to the results in figure 82; generally, less enthalpy was recovered in the nanocomposites than in the polycarbonate i.e. the nanocomposites generally aged less. Therefore, less time is needed for the samples to relax as TSP-POSS has reduced the amount of recoverable enthalpy.

It has been reported that when phase separation occurs in rubber toughened epoxy blends the enthalpy in the epoxy blend will recover similarly to the pure epoxy whereas when little phase separation occurs the enthalpy recovers in a different manner relative to the pure resin [229]. Fine nanofiller dispersion at the nano- or molecular-scale would increase the degree of interaction between TSP-POSS and polycarbonate. Hydrogen bonding between filler molecules and polymer chains is also a possibility and would reinforce the system. The SEM micrographs suggest that in our nanocomposite system, POSS is dispersed at this level throughout the matrix. Moreover, the potential POSS aggregates evidenced by SEM would be more rigid and therefore hinder chain segmental motion, essentially slowing down the chain dynamics of the nanocomposite system.

In conclusion, TSP-POSS does appear to have an effect on the physical aging behaviour of polycarbonate. From the results the amount of enthalpy recovered, $\Delta H\ (t_a,\ T_a)$, is generally reduced with the addition of POSS (figure 82), however from fig. 83 at larger temperature differentials, ΔT, TSP-POSS has the potential to decrease the characteristic relaxation time of

polycarbonate and accelerate the physical aging process. Increases in free volume induced by POSS would enhance chain mobility giving rise to accelerated physical aging, yet it would follow that more enthalpy would be recovered in the nanocomposites in comparison to the control sample. In this work, this is not the case. This is thought to be because the POSS has reduced physical aging, thus reducing the amount of enthalpy recovered in the nanocomposites in comparison to the unmodified polymer; less recoverable enthalpy means less time is required to recover it, resulting in lowered relaxation times. As this is only a preliminary investigation, more data is required to further understand the effect that TSP-POSS has on the physical aging of polycarbonate.

Chapter 7

Conclusions & Further Work

Chapter 7 Conclusions and Further Work

7.1. Conclusions

In this research, polycarbonate-based nanocomposites were studied for the potential use in transparent armour applications. The project involved 1) the synthesis and preparation of the nanocomposites, 2) the characterisation of the structural, morphological, viscoelastic and optical properties of the various properties of the nanocomposites and 3), the mechanical testing of the nanocomposites at various strain rates and types of strain. A preliminary study into the physical aging behaviour of the polymer nanocomposites was also carried out.

The nanocomposites were synthesised via a multi-step process involving pre-dispersion, melt mixing and compression moulding. The structure and morphology of the resultant polymer nanocomposites was studied using spectroscopy and microscopy techniques. All suggested good dispersion of TSP-POSS either at the molecular scale or as nanosized aggregates depending on TSP-POSS loading and as a result of high compatibility between TSP-POSS and polycarbonate. SEM showed that the effect of TSP-POSS on the polycarbonate matrix depended on the nanofiller concentration in the nanocomposite; at lower loadings (between 0.1wt% and 0.3wt%), TSP-POSS increased the ductility of the matrix and induced the formation of stretched fibrils in the matrix. At higher loadings (≤0.5wt%), TSP-POSS aggregates were visible and were observed to reside in cavities in the polymer matrix: an indication of plastic void growth and something previously seen in rubber toughened polymeric systems. Small cracks were present on the surface of the TSP-POSS aggregates and are thought to increase energy absorption capabilities by impeding crack growth.

The optical transparency of the nanocomposites was assessed using ultraviolet visible spectroscopy (UV-Vis). The results confirmed that the high optical transparency of polycarbonate was maintained with the addition of TSP-POSS at all loadings over the entire wavelength range tested. This result again implies good nanofiller dispersion and is a positive result for the application of the TSP-POSS based polycarbonate nanocomposites in transparent armour applications.

Dynamic mechanical analysis (DMA) was used to study the effect of TSP-POSS on the viscoelastic properties and chain dynamics of polycarbonate. This result suggests that TSP-

POSS has a slight plasticising effect on the polycarbonate matrix. With good filler-polymer compatibility TSP-POSS is miscible in the polycarbonate matrix as 1 nm-3 nm sized molecules and thus they have the potential to situate themselves between polymer chains, where they can then increase the free volume, thus increasing the chain mobility. The effect of TSP-POSS on the dynamical response of polycarbonate to frequency again is not that substantial. At some loadings it has the potential to increase the storage modulus, implying a reinforcing effect. At higher loadings, the damping factor of polycarbonate increases suggesting increased viscous behaviour and energy absorbing capabilities.

Tensile tests showed that TSP-POSS enhanced the toughness of polycarbonate via simultaneous improvements in tensile strength and elongation at break at loadings below 1wt%. Young's modulus was relatively unaffected. This suggests that TSP-POSS does not behave as a typical plasticiser. Kopesky et al. also stated that TSP-POSS did not act as a typical plasticiser in their TSP-POSS/PMMA nanocomposite system due to the active Si-OH sites on the nanofiller which allowed TSP-POSS to retain the modulus and yield stress of the PMMA and they stated that this was likely due to hydrogen bonding and molecular dispersion. It could be that in our research TSP-POSS is also able to interact with the polymer chains when it is miscible in the matrix at loadings below 0.5wt%. SEM micrographs (figures 45-47) show that TSP-POSS could induce the formation of stretched fibrils which increase the ductility of the polycarbonate matrix. This could be via hydrogen bonding which may result in the formation of a stretchy network of polymer chains and TSP-POSS molecules that increases the energy absorption capability of the polycarbonate. Hydrogen bonding could occur at the active Si-OH sites of TSP-POSS and the carbonyl groups of the polycarbonate. At higher loadings of 0.5wt%, TSP-POSS aggregates begin to appear in the matrix and these could help to increase the tensile strength and Young's modulus by impeding chain motion. Higher loadings of TSP-POSS cause reductions in tensile properties. The increased amount of TSP-POSS aggregates as seen in the results of the SEM analysis (figure 50) may contribute to increased stress concentration in the polycarbonate matrix which results in premature failure.

Impact tests were carried out on polycarbonate and its TSP-POSS based nanocomposites using an instrumented falling weight tower. Overall, TSP-POSS generally had a positive effect on the impact resistance by increasing the energy absorption in the initiation event;

total energy during the event is estimated as a ratio of 4:1 between initiation and propagation energy, respectively. Maximum peak force was generally higher in the nanocomposites than that of the control sample however propagation energy generally decreased with the addition of TSP-POSS. In conclusion, TSP-POSS generally enhanced the impact resistance of polycarbonate by increasing the energy required to form a crack.

Creep tests were performed on polycarbonate and its TSP-POSS based nanocomposites using DMA. At lower loadings (below 0.5wt%) TSP-POSS reduces the amount that the matrix deforms under a constant load. This could be due to the fact that TSP-POSS appears to be miscible in the polymer matrix and can therefore interact more and potentially form hydrogen bonds with the polymer which reducing the amount the polymer creeps. Conversely, at higher loadings (above 0.3wt%) the polycarbonate matrix deforms more. This could be due to the potential POSS aggregates observed using SEM. It was proposed that these were involved in plastic void growth. It follows then that the nanocomposites may creep more due to this toughening mechanism.

The results from SHPB tests suggest that at higher strain rates, TSP-POSS can have a reinforcing effect on the performance of the polycarbonate even in aggregate form (assuming the artefacts observed during SEM are POSS aggregates). The Young's modulus and yield stress both reached a maximum when the highest TSP-POSS loading was used (1wt%). Moreover, the energy absorption capability was also highest at this concentration suggesting simultaneous enhancement in both strength and toughness. However, at a higher projectile impact velocity, the stiffness of the nanocomposites increases and the energy absorption capability decreases. This is not surprising; as strain rate increases, polymers exhibit more elastic-like behaviour as the material has less time to relax and respond in order to dissipate the energy. It seems that any toughening effect that TSP-POSS had on the polycarbonate chains has been overcome at the higher projectile velocity and could be due to an increase in temperature in the sample from more rapid and larger energy transfer.

A brief study into the effect of TSP-POSS on the physical aging behaviour of polycarbonate was carried out using MDSC. The enthalpy recovered, $\Delta H\ (t_a,\ T_a)$, during the heat scans of the nanocomposites is lower when compared with the unmodified polymer. At larger

temperature differentials, ΔT, the characteristic relaxation time, t_c, of the nanocomposites is less than t_c of polycarbonate which suggests that TSP-POSS accelerates the physical aging process in the polymer. However, it would be expected that more enthalpy would be recovered in the nanocomposites in comparison to the control sample yet this is not the case. This is thought to be because TSP-POSS has impeded physical aging; less recoverable enthalpy means less time is required to recover it, resulting in lowered relaxation times.

The effect of TSP-POSS depends on its concentration in the polycarbonate matrix and the type and rate of strain the sample is subjected to i.e. compressive or tensile. At loadings below 0.5wt%, TSP appears to be miscible in the matrix. At loadings above 0.3wt% TSP-POSS appears to form nanosized aggregates. During experiments involving compressive strains (creep tests and SHPB testing), TSP-POSS may: (i) toughen polycarbonate by increasing its energy absorption capabilities through plastic void growth around TSP-POSS aggregates and/or the formation of a hydrogen bonded polymer-POSS network and (ii) strengthen polycarbonate through restriction of polymer chains by rigid TSP-POSS aggregates which could also impede crack formation, in a synergetic effect. However, the positive effect of TSP-POSS is not strong enough when a higher projectile velocity is used during the SHPB testing. Tests involving tensile strains (tensile tests and falling weight impact tests) see TSP-POSS toughen the polymer matrix again, however loadings ≤0.3wt% enhance the properties by a smaller amount and in some cases have a detrimental effect on the properties. This could be due to the TSP-POSS aggregates acting as stress concentrators which cause premature failure in the specimen or in the case of PC/0.3wt% this amount of TSP-POSS has resulted in a plasticising effect. Crucially, the optical transparency of polycarbonate was maintained in the nanocomposites at all concentration of TSP-POSS and is due to the good compatibility between polymer and nanofiller which results in molecular and nanoscale dispersion of the nanofiller in the polymer matrix.

The use of the nanofiller TSP-POSS has potential in transparent, lightweight protective applications due to its toughening effect on polycarbonate whilst maintaining the superior optical transparency of the polymer. The nanocomposites would be more suitable for transparent armour applications involving low velocity projectiles or as lightweight, energy damping backing materials.

7.2. Further Work

- Further study into the physical aging behaviour of the nanocomposites, particularly for longer aging times;
- Carry out structure and morphology analysis on samples post-testing (fractographic analysis) to determine more information on the failure mechanisms involved in the various mechanical tests;
- Carry out free volume measurements of the samples to assess the effect of TSP-POSS;
- Scale up of the samples and subsequent measurement of their properties to determine any change in performance due to larger size;
- Quantitative measurements of toughness e.g. K_{IC} tests;
- Investigate the possibility of a hydrogen bonded network between TSP-POSS and the polycarbonate chains;
- Further testing at higher strain rates and even ballistic tests to test limits of the nanocomposites. This could also involve the use of thermal imaging cameras which are sensitive enough to measure the heat variation in the samples during testing in order to further understand the decreased performance of the nanocomposites at higher strain rates.

Chapter 8

References

Chapter 8 References

8.1. References

[1] Kulkarni SG, Gao X-L, Horner SE, Zheng JQ, David NV. Ballistic helmets – Their design, materials, and performance against traumatic brain injury. Compos Struct 2013;101:313–31.

[2] Hughes F. The high strain-rate behaviour of polymers and nanocomposites for lightweight armour applications n.d.

[3] Shah QH. Impact resistance of a rectangular polycarbonate armor plate subjected to single and multiple impacts. Int J Impact Eng 2009;36:1128–35.

[4] Kevlar n.d. http://www.explainthatstuff.com/kevlar.html (accessed November 28, 2016).

[5] Curved Bullet Resistant Vehicle Glass FAQ | Bulldog Direct Protective Systems n.d. http://www.bulldogdirect.com/curved-bullet-resistant-glass-faq/ (accessed November 28, 2016).

[6] Police riot shield n.d. http://www.telegraph.co.uk/news/picturegalleries/royalty/5487689/Prince-Charles-observes-riot-police-in-action.html?image=3 (accessed November 28, 2016).

[7] Body armour n.d. https://us.vocuspr.com/Newsroom/MultiQuery.aspx?SiteName=DupontEMEA&Entity=PRAsset&SF_PRAsset_PRAssetID_EQ=123637&XSL=NewsRelease&IncludeChildren=True&Lang=English (accessed November 28, 2016).

[8] Polycarbonate visor n.d. http://www.globalindustrial.com/p/safety/head-face-protection/faceshields-visors/clear-aluminum-bound-pc-face-shield (accessed November 28, 2016).

[9] VAB Mk3 6x6 medium armoured vehicle n.d. http://www.army-technology.com/projects/vab-mk3-6x6-medium-armoured-vehicle/vab-mk3-6x6-medium-armoured-vehicle2.html (accessed November 28, 2016).

[10] Kurahatti R V, Surendranathan AO, Kori SA, Singh N. Defence Applications of Polymer Nanocomposites 2010;60:551–63.

[11] Bhatnagar A. Lightweight Ballistic Composites: Military and Law-Enforcement Applications. Elsevier Science; 2006.

[12] Mohagheghian I, McShane GJ, Strongea WJ. Impact response of polyethylene nanocomposites. Procedia Eng 2011;10:704–9. doi:10.1016/j.proeng.2011.04.117.

[13] Haro EE, Odeshi AG, Szpunar JA. The energy absorption behavior of hybrid composite laminates containing nano-fillers under ballistic impact. Int J Impact Eng 2016;96:11–22. doi:10.1016/j.ijimpeng.2016.05.012.

[14] Raman N, Sudharsan S, Pothiraj K. Synthesis and structural reactivity of inorganic-

organic hybrid nanocomposites - A review. J Saudi Chem Soc 2012;16:339–52. doi:10.1016/j.jscs.2011.01.012.

[15] Ayandele E, Sarkar B, Alexandridis P. Polyhedral Oligomeric Silsesquioxane (POSS)-Containing Polymer Nanocomposites. Nanomaterials 2012;2:445–75. doi:10.3390/nano2040445.

[16] Peponi L, Puglia D, Torre L, Valentini L, Kenny JM. Processing of nanostructured polymers and advanced polymeric based nanocomposites. Mater Sci Eng R Reports 2014;85:1–46. doi:10.1016/j.mser.2014.08.002.

[17] Tjong SC. Structural and mechanical properties of polymer nanocomposites. Mater Sci Eng R Reports 2006;53:73–197.

[18] Sun L, Gibson RF, Gordaninejad F, Suhr J. Energy absorption capability of nanocomposites: A review. Compos Sci Technol 2009;69:2392–409.

[19] Wichmann MHG, Schulte K, Wagner HD. On nanocomposite toughness. Compos Sci Technol 2008;68:329–31. doi:10.1016/j.compscitech.2007.06.027.

[20] Vahabi H, Eterradossi O, Ferry L, Longuet C, Sonnier R, Lopez-Cuesta J-M. Polycarbonate nanocomposite with improved fire behavior, physical and psychophysical transparency. Eur Polym J 2013;49:319–27. doi:10.1016/j.eurpolymj.2012.10.031.

[21] Luan J, Wang S, Hu Z, Zhang L. Synthesis Techniques , Properties and Applications of Polymer Nanocomposites 2012;86:114–36.

[22] Mittal V. Synthesis of Polymer Nanocomposites. Polymer (Guildf) 2015:1–26. doi:10.1002/9783527670307.

[23] Beyou E, Akbar S, Chaumont P, Cassagnau P. Polymer Nanocomposites Containing Functionalised Multiwalled Carbon NanoTubes: a Particular Attention to Polyolefin Based Materials. Synth. Appl. Carbon Nanotub. Their Compos., InTech; 2013. doi:10.5772/50710.

[24] Pavlidou S, Papaspyrides CD. A review on polymer–layered silicate nanocomposites. Prog Polym Sci 2008;33:1119–98.

[25] Hussain F. Polymer-matrix Nanocomposites, Processing, Manufacturing, and Application: An Overview. J Compos Mater 2006;40:1511–75. doi:10.1177/0021998306067321.

[26] Isfahani AP, Mehrabzadeh M, Morshedian J. The effects of processing and using different types of clay on the mechanical, thermal and rheological properties of high-impact polystyrene nanocomposites. Polym J 2012;45:346–53. doi:10.1038/pj.2012.138.

[27] Uysal Unalan I, Cerri G, Marcuzzo E, Cozzolino C a., Farris S. Nanocomposite films and coatings using inorganic nanobuilding blocks (NBB): current applications and future opportunities in the food packaging sector. RSC Adv 2014;4:29393–428.

doi:10.1039/C4RA01778A.

[28] Song P, Cao Z, Cai Y, Zhao L, Fang Z, Fu S. Fabrication of exfoliated graphene-based polypropylene nanocomposites with enhanced mechanical and thermal properties. Polymer (Guildf) 2011;52:4001–10. doi:10.1016/j.polymer.2011.06.045.

[29] Li Z, Young RJ, Wang R, Yang F, Hao L, Jiao W, et al. The role of functional groups on graphene oxide in epoxy nanocomposites. Polymer (Guildf) 2013;54:5821–9. doi:10.1016/j.polymer.2013.08.026.

[30] Ryu SH, Shanmugharaj a. M. Influence of long-chain alkylamine-modified graphene oxide on the crystallization, mechanical and electrical properties of isotactic polypropylene nanocomposites. Chem Eng J 2014;244:552–60. doi:10.1016/j.cej.2014.01.101.

[31] Layek RK, Samanta S, Chatterjee DP, Nandi AK. Physical and mechanical properties of poly(methyl methacrylate) -functionalized graphene/poly(vinylidine fluoride) nanocomposites: Piezoelectric β polymorph formation. Polymer (Guildf) 2010;51:5846–56. doi:10.1016/j.polymer.2010.09.067.

[32] Sayyar S, Murray E, Thompson BC, Gambhir S, Officer DL, Wallace GG. Covalently linked biocompatible graphene/polycaprolactone composites for tissue engineering. Carbon N Y 2013;52:296–304. doi:10.1016/j.carbon.2012.09.031.

[33] Yang S-Y, Lin W-N, Huang Y-L, Tien H-W, Wang J-Y, Ma C-CM, et al. Synergetic effects of graphene platelets and carbon nanotubes on the mechanical and thermal properties of epoxy composites. Carbon N Y 2011;49:793–803. doi:10.1016/j.carbon.2010.10.014.

[34] Cheng HKF, Sahoo NG, Tan YP, Pan Y, Bao H, Li L, et al. Poly(vinyl alcohol) nanocomposites filled with poly(vinyl alcohol)-grafted graphene oxide. ACS Appl Mater Interfaces 2012;4:2387–94. doi:10.1021/am300550n.

[35] Dong J, Yin C, Zhao X, Li Y, Zhang Q. High strength polyimide fibers with functionalized graphene. Polymer (Guildf) 2013;54:6415–24. doi:10.1016/j.polymer.2013.09.035.

[36] Liu F, Guo K. Reinforcing epoxy resin through covalent integration of functionalized graphene nanosheets. Polym Adv Technol 2014:n/a-n/a. doi:10.1002/pat.3256.

[37] Cao Y, Zhang J, Feng J, Wu P. Compatibilization of immiscible polymer blends using graphene oxide sheets. ACS Nano 2011;5:5920–7. doi:10.1021/nn201717a.

[38] Luong ND, Hippi U, Korhonen JT, Soininen AJ, Ruokolainen J, Johansson L-S, et al. Enhanced mechanical and electrical properties of polyimide film by graphene sheets via in situ polymerization. Polymer (Guildf) 2011;52:5237–42. doi:10.1016/j.polymer.2011.09.033.

[39] Rafiq R, Cai D, Jin J, Song M. Increasing the toughness of nylon 12 by the incorporation of functionalized graphene. Carbon N Y 2010;48:4309–14. doi:10.1016/j.carbon.2010.07.043.

[40] Soitong T, Pumchusak J. The relationship of crystallization behavior, mechanical properties, and morphology of polypropylene nanocomposite fibers. J Mater Sci 2010;46:1697–704. doi:10.1007/s10853-010-4987-1.

[41] Rama Sreekanth PS, Kanagaraj S. Assessment of bulk and surface properties of medical grade UHMWPE based nanocomposites using Nanoindentation and microtensile testing. J Mech Behav Biomed Mater 2013;18:140–51. doi:10.1016/j.jmbbm.2012.11.011.

[42] Augustine JM, Maiti SN, Gupta AK. Mechanical properties and crystallization behavior of toughened polyamide-6/carbon nanotube composites. J Appl Polym Sci 2012;125:E478–85. doi:10.1002/app.33975.

[43] Royan RN, Sulong AB, Sahari J. Effect of Loading Concentration on the Electrical and Hardness Properties of MWCNT/Epoxy Nanocomposites. Key Eng Mater 2011;471–472:157–61. doi:10.4028/www.scientific.net/KEM.471-472.157.

[44] Kokil A, Saito T, Depolo W, Elkins CL, Wilkes GL, Long TE. Introduction of Multiple Hydrogen Bonding for Enhanced Mechanical Performance of Polymer-Carbon Nanotube Composites. J Macromol Sci Part A 2011;48:1016–21. doi:10.1080/10601325.2011.620428.

[45] Liao H-T, Wu C-S. Poly(3-hydroxybutyrate)/multi-walled carbon nanotubes nanocomposites: preparation and characterizations. Des Monomers Polym 2013;16:99–107. doi:10.1080/15685551.2012.705495.

[46] Fan J, Wang J, Shi Z, Yu S, Yin J. Kevlar nanofiber-functionalized multiwalled carbon nanotubes for polymer reinforcement. Mater Chem Phys 2013;141:861–8. doi:10.1016/j.matchemphys.2013.06.015.

[47] Montazeri A, Montazeri N, Pourshamsian K, Tcharkhtchi A. The Effect of Sonication Time and Dispersing Medium on the Mechanical Properties of Multiwalled Carbon Nanotube (MWCNT)/Epoxy Composite. Int J Polym Anal Charact 2011;16:465–76. doi:10.1080/1023666X.2011.600517.

[48] Inam F, Vo T, Jones JP, Lee X. Effect of carbon nanotube lengths on the mechanical properties of epoxy resin: An experimental study. J Compos Mater 2012;47:2321–30. doi:10.1177/0021998312457198.

[49] Miquelard-Garnier G, Guinault A, Fromonteil D, Delalande S, Sollogoub C. Dispersion of carbon nanotubes in polypropylene via multilayer coextrusion: Influence on the mechanical properties. Polymer (Guildf) 2013;54:4290–7. doi:10.1016/j.polymer.2013.06.007.

[50] Chen C, Bortner M, Quigley JP, Baird DG. Using supercritical carbon dioxide in preparing carbon nanotube nanocomposite: Improved dispersion and mechanical properties. Polym Compos 2012;33:1033–43. doi:10.1002/pc.22222.

[51] Matin Ghahfarokhi Z, Golestanian H. Effects of nanotube helical angle on mechanical properties of carbon nanotube reinforced polymer composites. Comput Mater Sci 2011;50:3171–7. doi:10.1016/j.commatsci.2011.05.046.

[52] Jia X, Zhang Q, Zhao M-Q, Xu G-H, Huang J-Q, Qian W, et al. Dramatic enhancements in toughness of polyimide nanocomposite via long-CNT-induced long-range creep. J Mater Chem 2012;22:7050. doi:10.1039/c2jm15359a.

[53] Ivakina K, Skadins E, Kiyanitsa A, Gaidukov S, Tupureina V, Cābulis U, et al. Influence of Nanoclay Additive on Mechanical Properties of Bio-Based Polyurethane Nanocomposites. Key Eng Mater 2013;559:37–42. doi:10.4028/www.scientific.net/KEM.559.37.

[54] Jollands M, Gupta RK. Effect of mixing conditions on mechanical properties of polylactide/montmorillonite clay nanocomposites. J Appl Polym Sci 2010;118:n/a-n/a. doi:10.1002/app.32475.

[55] Adinoyi MJ, Merah N, Gasem ZM, Al-Aqeeli N. Variation of Mechanical Properties of Epoxy-Clay Nanocomposite with Sonication Time and Clay Loading. Key Eng Mater 2011;471–472:496–501. doi:10.4028/www.scientific.net/KEM.471-472.496.

[56] Rangasamy L, Shim E, Pourdeyhimi B. Structure and tensile properties of Nanoclay-Polypropylene fibers produced by melt spinning. J Appl Polym Sci 2011;121:410–9. doi:10.1002/app.33619.

[57] Zaidi L, Bruzaud S, Bourmaud A, MÃ©dÃ©ric P, Kaci M, Grohens Y. Relationship between structure and rheological, mechanical and thermal properties of polylactide/Cloisite 30B nanocomposites. J Appl Polym Sci 2009;116:NA-NA. doi:10.1002/app.31655.

[58] Chen J-H, Chen C-C, Yang M-C. Characterization of Nanocomposites of Poly(butylene adipate-co-terephthalate) blending with Organoclay. J Polym Res 2011;18:2151–9. doi:10.1007/s10965-011-9625-3.

[59] Khonakdar HA, Ehsani M, Asadinezhad A, Jafari S-H, Wagenknecht U. Nanofilled Polypropylene/Poly(trimethylene terephthalate) Blends: A Morphological and Mechanical Properties Study. J Macromol Sci Part B 2013;52:897–909. doi:10.1080/00222348.2012.742816.

[60] Pistek D, Mertnska D, Dujkova Z, Tupy M. The mechanical and optical properties of the PVB nanocomposites with modified nanofiller. Adv. Sensors, Signals Mater. - 3rd WSEAS Int. Conf. Sensors Signals, SENSIG'10, 3rd WSEAS Int. Conf. Mater. Sci. Mater., 2010, p. 26–9.

[61] Yusoh K, Jin J, Song M. Subsurface mechanical properties of polyurethane/organoclay nanocomposite thin films studied by nanoindentation. Prog Org Coatings 2010;67:220–4. doi:10.1016/j.porgcoat.2009.10.003.

[62] Wang C-A, Chen K, Huang Y, Le H. Electrochemical synthesis and properties of layer-structured polypyrrole/montmorillonite nanocomposite films. J Mater Res 2011;25:658–64. doi:10.1557/JMR.2010.0093.

[63] Nalini R, Nagarajan S, Reddy BSR. Polypropylene-blended organoclay nanocomposites – preparation, characterisation and properties. J Exp Nanosci 2013;8:480–92. doi:10.1080/17458080.2011.597436.

[64] Joulazadeh M, Navarchian AH. Effect of process variables on mechanical properties of polyurethane/clay nanocomposites. Polym Adv Technol 2009;21:263–71. doi:10.1002/pat.1424.

[65] Wang C-A, Chen K, Huang Y, Le H. Electrochemical synthesis and properties of layer-structured polypyrrole/montmorillonite nanocomposite films. J Mater Res 2011;25:658–64. doi:10.1557/JMR.2010.0093.

[66] Hanif WYW, Risby MS, Noor MM. Influence of Carbon Nanotube Inclusion on the Fracture Toughness and Ballistic Resistance of Twaron/Epoxy Composite Panels. Procedia Eng 2015;114:118–23. doi:10.1016/j.proeng.2015.08.049.

[67] Rahman M, Hosur M, Zainuddin S, Vaidya U, Tauhid A, Kumar A, et al. Effects of amino-functionalized MWCNTs on ballistic impact performance of E-glass/epoxy composites using a spherical projectile. Int J Impact Eng 2013;57:108–18. doi:10.1016/j.ijimpeng.2013.01.011.

[68] Jindal P, Pande S, Sharma P, Mangla V, Chaudhury A, Patel D, et al. High strain rate behavior of multi-walled carbon nanotubes–polycarbonate composites. Compos Part B Eng 2013;45:417–22. doi:10.1016/j.compositesb.2012.06.018.

[69] Brühwiler PA, Barbezat M, Necola A, Kohls DJ, Bunk O, Schaefer DW, et al. Comparison of quasistatic to impact mechanical properties of multiwall carbon nanotube/polycarbonate composites. J Mater Res 2010;25:1118–30. doi:10.1557/JMR.2010.0139.

[70] Hosur M V., Rahman T, Brundidge-Young S, Jeelani S. Mechanical and Thermal Properties of Amine Functionalized Multi-walled Carbon Nanotubes Epoxy-Based Nanocomposite. Compos Interfaces 2010;17:197–215. doi:10.1163/092764410X490608.

[71] Matadi Boumbimba R, Wang K, Bahlouli N, Ahzi S, Rémond Y, Addiego F. Experimental investigation and micromechanical modeling of high strain rate compressive yield stress of a melt mixing polypropylene organoclay nanocomposites. Mech Mater 2012;52:58–68. doi:10.1016/j.mechmat.2012.04.006.

[72] Balaganesan G, Velmurugan R, Srinivasan M, Gupta NK, Kanny K. Energy absorption and ballistic limit of nanocomposite laminates subjected to impact loading. Int J Impact Eng 2014;74:57–66. doi:10.1016/j.ijimpeng.2014.02.017.

[73] Zhou R, Burkhart T. Optical Properties of Particle-Filled Polycarbonate , Polystyrene , and Poly (methyl methacrylate) Composites 2009. doi:10.1002/app.

[74] Larijani MM, Khamse EJ, Davoodi J, Ziaie F, Safa S, Arbabi K, et al. The effect of carbon nanotube concentration on the physical properties of CNT-polycarbonate composites. Optoelectron Adv Mater 2011;5:252–7.

[75] Suin S, Maiti S, Shrivastava NK, Khatua BB. Mechanically improved and optically transparent polycarbonate/clay nanocomposites using phosphonium modified organoclay. vol. 54. 2014.

[76] Patel T, Suin S, Bhattacharya D, Khatua BB. Transparent and Thermally Conductive Polycarbonate (PC)/Alumina (Al 2 O 3) Nanocomposites: Preparation and Characterizations. Polym Plast Technol Eng 2013;52:1557–65. doi:10.1080/03602559.2013.824464.

[77] Zhou R-J, Burkhart T. Mechanical and Optical Properties of Nanosilica-filled Polycarbonate Composites. J Thermoplast Compos Mater 2009;23:487–500. doi:10.1177/0892705709353720.

[78] Chandra A, Turng L-S, Li K, Huang H-X. Fracture behavior and optical properties of melt compounded semi-transparent polycarbonate (PC)/alumina nanocomposites. Compos Part A Appl Sci Manuf 2011;42:1903–9. doi:10.1016/j.compositesa.2011.08.015.

[79] Struik LCE. Physical Aging in Plastics and Other Glassy Materials. Polym Eng Sci 1977;17:165–73. doi:10.1002/pen.760170305.

[80] Cangialosi D, Boucher VM, Alegría A, Colmenero J. Enhanced physical aging of polymer nanocomposites: The key role of the area to volume ratio. Polymer (Guildf) 2012;53:1–30. doi:10.1016/j.polymer.2012.01.033.

[81] Ramakrishnan V, Harsiny S, Goossens JGP, Hoeks TL, Peters GWM. Physical aging in polycarbonate nanocomposites containing grafted nanosilica particles: A comparison between enthalpy and yield stress evolution. J Polym Sci Part B Polym Phys 2016;54:2069–81. doi:10.1002/polb.24125.

[82] Boucher VM, Cangialosi D, Alegrìa A, Colmenero J, González-Irun J, Liz-Marzan LM. Physical aging in PMMA/silica nanocomposites: Enthalpy and dielectric relaxation. J Non Cryst Solids 2011;357:605–9. doi:10.1016/j.jnoncrysol.2010.05.091.

[83] Pluta M, Paul MA, Alexandre M, Dubois P. Plasticized polylactide/clay nanocomposites. I. The role of filler content and its surface organo-modification on the physico-chemical properties. J Polym Sci Part B Polym Phys 2006;44:299–311. doi:10.1002/polb.20694.

[84] Flory AL, Ramanathan T, Brinson LC. Physical aging of single wall carbon nanotube polymer nanocomposites: Effect of functionalization of the nanotube on the enthalpy relaxation. Macromolecules 2010;43:4247–52. doi:10.1021/ma901670m.

[85] Rittigstein P, Torkelson JM. Polymer–nanoparticle interfacial interactions in polymer nanocomposites: Confinement effects on glass transition temperature and suppression of physical aging. J Polym Sci Part B Polym Phys 2006;44:2935–43. doi:10.1002/polb.20925.

[86] Cangialosi D, Boucher VM, Alegría A, Colmenero J. Physical aging in polymers and polymer nanocomposites: recent results and open questions. Soft Matter 2013;9:8619. doi:10.1039/c3sm51077h.

[87] Fina A, Monticelli O, Camino G. POSS-based hybrids by melt/reactive blending. J Mater Chem 2010;20:9297. doi:10.1039/c0jm00480d.

[88] Hybrid Plastics. POSS User Guide n.d.:0–34. http://www.hybridplastics.com/docs/user-v2.06.pdf (accessed December 8, 2016).

[89] Phillips SH, Haddad TS, Tomczak SJ. Developments in nanoscience: polyhedral oligomeric silsesquioxane (POSS)-polymers. Curr Opin Solid State Mater Sci 2004;8:21–9.

[90] Dintcheva NT. Structure-properties relationships of polyhedral oligomeric silsesquioxane (POSS) filled PS nanocomposites. Express Polym Lett 2012;6:561–71. doi:10.3144/expresspolymlett.2012.59.

[91] Ghermezcheshme H, Mohseni M, Yahyaei H. Use of nanoindentaion and nanoscratch experiments to reveal the mechanical behavior of POSS containing polyurethane nanocomposite coatings: The role of functionality. Tribol Int 2015;88:66–75. doi:10.1016/j.triboint.2015.02.023.

[92] Zhao Y, Schiraldi DA. Thermal and mechanical properties of polyhedral oligomeric silsesquioxane (POSS)/polycarbonate composites. Polymer (Guildf) 2005;46:11640–7.

[93] Yilmaz S, Kodal M, Yilmaz T, Ozkoc G. Fracture toughness analysis of O-POSS/PLA composites assessed by essential work of fracture method. Compos Part B Eng 2014;56:527–35.

[94] Hybrid Plastics®: What is POSS® Technology? n.d. http://www.hybridplastics.com/about/tech.htm.

[95] Li G, Charles UP. Polyhedral Oligomeric Silsesquioxane (POSS) Polymers, Copolymers, and Resin Nanocomposites. Macromol. Contain. Met. Met. Elem. Gr. IVA Polym., vol. 4, 2005, p. 79–131. doi:10.1002/0471712566.ch5.

[96] General POSS 2007. https://www.google.com/patents/EP1918294B1?cl=en (accessed December 7, 2016).

[97] Mulliken AD, Boyce MC. Polycarbonate and a Polycarbonate-POSS Nanocomposite at High Rates of Deformation. J Eng Mater Technol 2006;128:543. doi:10.1115/1.2345446.

[98] Crompton TR. Polymer Reference Book. iSmithers Rapra Publishing; 2006.

[99] Ayandele E, Sarkar B, Alexandridis P. Polyhedral Oligomeric Silsesquioxane (POSS)-Containing Polymer Nanocomposites. Nanomaterials 2012;2:445–75. doi:10.3390/nano2040445.

[100] Kuo S-W, Chang F-C. POSS related polymer nanocomposites. Prog Polym Sci 2011;36:1649–96. doi:10.1016/j.progpolymsci.2011.05.002.

[101] Zhang D, Shi Y, Liu Y, Huang G. Influences of polyhedral oligomeric silsesquioxanes (POSSs) containing different functional groups on crystallization and melting behaviors of POSS/polydimethylsiloxane rubber composites. RSC Adv 2014;4:41364–70. doi:10.1039/C4RA07242A.

[102] Boček J, Matějka L, Mentlík V, Trnka P, Šlouf M. Electrical and thermomechanical

properties of epoxy-POSS nanocomposites. Eur Polym J 2011;47:861–72. doi:10.1016/j.eurpolymj.2011.02.023.

[103] Sirin H, Turan D, Ozkoc G, Gurdag S. POSS reinforced PET based composite fibers: "Effect of POSS type and loading level." Compos Part B Eng 2013;53:395–403. doi:10.1016/j.compositesb.2013.05.033.

[104] Matějka L, Amici Kroutilová I, Lichtenhan JD, Haddad TS. Structure ordering and reinforcement in POSS containing hybrids. Eur Polym J 2014;52:117–26. doi:10.1016/j.eurpolymj.2014.01.005.

[105] Zheng L, Waddon AJ, Farris RJ, Coughlin EB. X-ray characterizations of polyethylene polyhedral oligomeric silsesquioxane copolymers. Macromolecules 2002;35:2375–9. doi:10.1021/ma011855e.

[106] Matějka L, Murias P, Pleštil J. Effect of POSS on thermomechanical properties of epoxy–POSS nanocomposites. Eur Polym J 2012;48:260–74. doi:10.1016/j.eurpolymj.2011.11.009.

[107] Iyer S, Schiraldi D. Role of specific interactions and solubility in the reinforcement of bisphenol A polymers with polyhedral oligomeric silsesquioxanes. Macromolecules 2007:4942–52.

[108] Starostenko O, Bershtein V, Fainleib A, Egorova L, Grigoryeva O, Sinani A, et al. Thermostable Polycyanurate-Polyhedral Oligomeric Silsesquioxane Hybrid Networks: Synthesis, Dynamics and Thermal Behavior. Macromol Symp 2012;316:90–6. doi:10.1002/masy.201250612.

[109] Pan R, Shanks R, Kong I, Wang L. Trisilanolisobutyl POSS/polyurethane hybrid composites: preparation, WAXS and thermal properties. Polym Bull 2014;71:2453–64. doi:10.1007/s00289-014-1201-7.

[110] Pan H, Qiu Z. Biodegradable Poly(l -lactide)/Polyhedral Oligomeric Silsesquioxanes Nanocomposites: Enhanced Crystallization, Mechanical Properties, and Hydrolytic Degradation. Macromolecules 2010;43:1499–506. doi:10.1021/ma9023685.

[111] Montero B, Bellas R, Ramírez C, Rico M, Bouza R. Flame retardancy and thermal stability of organic–inorganic hybrid resins based on polyhedral oligomeric silsesquioxanes and montmorillonite clay. Compos Part B Eng 2014;63:67–76. doi:10.1016/j.compositesb.2014.03.023.

[112] Spoljaric S. Novel elastomer dye-functionalised POSS nanocomposites: Enhanced colourimetric, thermomechanical and thermal properties. Express Polym Lett 2012;6:354–72. doi:10.3144/expresspolymlett.2012.39.

[113] Florea NM, Lungu a., Badica P, Craciun L, Enculescu M, Ghita DG, et al. Novel nanocomposites based on epoxy resin/epoxy-functionalized polydimethylsiloxane reinforced with POSS. Compos Part B Eng 2015;75:226–34. doi:10.1016/j.compositesb.2015.01.043.

[114] Bershtein V, Fainleib A, Egorova L, Grigoryeva O, Kirilenko D, Konnikov S, et al. The

impact of ultra-low amounts of introduced reactive POSS nanoparticles on structure, dynamics and properties of densely cross-linked cyanate ester resins. Eur Polym J 2015;67:128–42. doi:10.1016/j.eurpolymj.2015.03.022.

[115] Zhang Q, He H, Xi K, Huang X, Yu X, Jia X. Synthesis of N -Phenylaminomethyl POSS and Its Utilization in Polyurethane. Macromolecules 2011;44:550–7. doi:10.1021/ma101825j.

[116] Gu S-Y, Jin S-P, Liu L-L. Polyurethane/polyhedral oligomeric silsesquioxane shape memory nanocomposites with low trigger temperature and quick response. J Polym Res 2015;22:142. doi:10.1007/s10965-015-0779-2.

[117] Milliman HW, Ishida H, Schiraldi DA. Structure Property Relationships and the Role of Processing in the Reinforcement of Nylon 6-POSS Blends. Macromolecules 2012;45:4650–7. doi:10.1021/ma3002214.

[118] Wang X, Xuan S, Song L, Yang H, Lu H, Hu Y. Synergistic Effect of POSS on Mechanical Properties, Flammability, and Thermal Degradation of Intumescent Flame Retardant Polylactide Composites. J Macromol Sci Part B 2012;51:255–68. doi:10.1080/00222348.2011.585334.

[119] Lee KS, Chang Y-W. Thermal and mechanical properties of poly(ε-caprolactone)/polyhedral oligomeric silsesquioxane nanocomposites. Polym Int 2013;62:64–70. doi:10.1002/pi.4309.

[120] Spoljaric S. Novel elastomer-dumbbell functionalized POSS composites: Thermomechanical and Morphological Properties. J Appl … 2012;123. doi:10.1002/app.

[121] Huang J chao, He C bin, Xiao Y, Mya KY, Dai J, Siow YP. Polyimide/POSS nanocomposites: Interfacial interaction, thermal properties and mechanical properties. Polymer (Guildf) 2003;44:4491–9. doi:10.1016/S0032-3861(03)00434-8.

[122] Efrat T, Dodiuk H, Kenig S, McCarthy S. Nanotailoring of polyurethane adhesive by polyhedral oligomeric silsesquioxane (POSS). J Adhes Sci Technol 2006;20:1413–30. doi:10.1163/156856106778456645.

[123] Martins JN, Bassani TS, Oliveira RVB. Morphological, viscoelastic and thermal properties of poly(vinylidene Fluoride)/POSS nanocomposites. Mater Sci Eng C 2012;32:146–51. doi:10.1016/j.msec.2011.10.009.

[124] Sterzyński T, Tomaszewska J, Andrzejewski J, Skórczewska K. Evaluation of glass transition temperature of PVC/POSS nanocomposites. Compos Sci Technol 2015;117:398–403. doi:10.1016/j.compscitech.2015.07.009.

[125] Barczewski M, Sterzyński T, Dutkiewicz M. Thermo-rheological properties and miscibility of linear low-density polyethylene-silsesquioxane nanocomposites. J Appl Polym Sci 2015;132:n/a-n/a. doi:10.1002/app.42825.

[126] Yari H, Mohseni M. Curing and thermo-mechanical studies of a modified thermosetting clearcoat containing OH-functional POSS nanocages. Prog Org Coatings

2015;87:129–37. doi:10.1016/j.porgcoat.2015.05.024.

[127] Raftopoulos KN, Koutsoumpis S, Jancia M, Lewicki JP, Kyriakos K, Mason HE, et al. Reduced Phase Separation and Slowing of Dynamics in Polyurethanes with Three-Dimensional POSS-Based Cross-Linking Moieties. Macromolecules 2015;48:1429–41. doi:10.1021/ma5023132.

[128] Silva R, Salles C, Mauler R, Oliveira R. Investigation of the thermal, mechanical and morphological properties of poly(vinyl chloride)/polyhedral oligomeric silsesquioxane nanocomposites. Polym Int 2010;59:1221–5. doi:10.1002/pi.2851.

[129] Gao JG, Du YG, Li X. Rheological Behavior and Mechanical Properties of PVC/V-POSS Nanocomposites. Adv Mater Res 2011;217–218:555–8. doi:10.4028/www.scientific.net/AMR.217-218.555.

[130] Sánchez-Soto M, Schiraldi DA, Illescas S. Study of the morphology and properties of melt-mixed polycarbonate–POSS nanocomposites. Eur Polym J 2009;45:341–52. doi:10.1016/j.eurpolymj.2008.10.026.

[131] Yari H, Mohseni M, Messori M, Ranjbar Z. Tribological properties and scratch healing of a typical automotive nano clearcoat modified by a polyhedral oligomeric silsesquioxane compound. Eur Polym J 2014;60:79–91. doi:10.1016/j.eurpolymj.2014.08.023.

[132] Yari H, Mohseni M, Messori M. Toughened acrylic/melamine thermosetting clear coats using POSS molecules: Mechanical and morphological studies. Polymer (Guildf) 2015;63:19–29. doi:10.1016/j.polymer.2015.02.040.

[133] Turan D, Sirin H, Ozkoc G. Effects of POSS particles on the mechanical, thermal, and morphological properties of PLA and Plasticised PLA. J Appl Polym Sci 2011;121:1067–75. doi:10.1002/app.33802.

[134] Jeziorska R, Swierz-Motysia B. Effect of POSS on morphology, thermal and mechanical properties of polyamide 6. Polimery 2011.

[135] Dodiuk H, Kenig S, Blinsky I, Dotan A, Buchman A. Nanotailoring of epoxy adhesives by polyhedral-oligomeric-sil-sesquioxanes (POSS). Int J Adhes Adhes 2005;25:211–8. doi:10.1016/j.ijadhadh.2004.07.003.

[136] Xu H, Yang B, Wang J, Guang S, Li C. Preparation , Thermal Properties , and T g Increase Mechanism of Poly (acetoxystyrene-co-octavinyl-polyhedral oligomeric silsesquioxane) Hybrid Nanocomposites. Ratio 2005:10455–60.

[137] Zhang D, Huang G, Shi Y, Zhang G, Liu Y. Polyhedral oligomeric silsesquioxane/silica/polydimethylsiloxane rubber composites with enhanced mechanical and thermal properties. J Appl Polym Sci 2015;132:n/a-n/a. doi:10.1002/app.42173.

[138] Li GZ, Wang L, Toghiani H, Daulton TL, Pittman CU. Viscoelastic and mechanical properties of vinyl ester (VE)/multifunctional polyhedral oligomeric silsesquioxane (POSS) nanocomposites and multifunctional POSS-styrene copolymers. Polymer

(Guildf) 2002;43:4167–76. doi:10.1016/S0032-3861(02)00232-X.

[139] Wang L, Hu S, Yang L, Sun Z, Zhu J, Lai H, et al. Development of experimental methods for impact testing by combining Hopkinson pressure bar with other techniques. Acta Mech Solida Sin 2014;27:331–44. doi:10.1016/S0894-9166(14)60041-0.

[140] Ni Y, Zheng S, Nie K. Morphology and thermal properties of inorganic-organic hybrids involving epoxy resin and polyhedral oligomeric silsesquioxanes. Polymer (Guildf) 2004;45:5557–68. doi:10.1016/j.polymer.2004.06.008.

[141] Liu Y, Shi Z, Xu H, Fang J, Ma X, Yin J. Preparation, Characterization, and Properties of Novel Polyhedral Oligomeric Silsesquioxane−Polybenzimidazole Nanocomposites by Friedel−Crafts Reaction. Macromolecules 2010;43:6731–8. doi:10.1021/ma1011792.

[142] Zhou Z, Cui L, Zhang Y, Zhang Y, Yin N. Preparation and properties of POSS grafted polypropylene by reactive blending. Eur Polym J 2008;44:3057–66. doi:10.1016/j.eurpolymj.2008.05.036.

[143] Schiraldi, David A., Iyer S. What does it take to make a stable POSS/polymer composite? Prepr Polym 2006;47:1219–20.

[144] Hu K, Cui ZK, Yuan Y, Zhuang Q, Wang T, Liu X, et al. Synthesis, structure, and properties of high-impact polystyrene/octavinyl polyhedral oligomeric silsesquioxane nanocomposites. Polym Compos 2014;37:1049–55. doi:10.1002/pc.23265.

[145] Verker R, Grossman E, Gouzman I, Eliaz N. TriSilanolPhenyl POSS–polyimide nanocomposites: Structure–properties relationship. Compos Sci Technol 2009;69:2178–84. doi:10.1016/j.compscitech.2009.06.001.

[146] Bach QV, Choi J, Joung YK, Park BJ, Han DK. Improvement of mechanical properties and blood compatibility of PLLA nanocomposites by incorporation of polyhedral oligomeric silsesquioxane. Macromol Res 2012;20:996–1001. doi:10.1007/s13233-012-0196-x.

[147] Kamal T, Park S-Y, Choi M-C, Chang Y-W, Chuang W-T, Jeng U-S. An in-situ simultaneous SAXS and WAXS survey of PEBAX® nanocomposites reinforced with organoclay and POSS during uniaxial deformation. Polymer (Guildf) 2012;53:3360–7. doi:10.1016/j.polymer.2012.05.037.

[148] Cozza ES, Monticelli O, Cavalleri O, Marsano E. Preparation, characterization, and properties of nanofibers based on poly(vinylidene fluoride) and polyhedral oligomeric silsesquioxane. Polym Adv Technol 2012;23:1252–7. doi:10.1002/pat.2037.

[149] Lim S-K, Hong E-P, Song Y-H, Choi HJ, Chin I-J. Thermodynamic interaction and mechanical characteristics of Nylon 6 and polyhedral oligomeric silsesquioxane nanohybrids. J Mater Sci 2011;47:308–14. doi:10.1007/s10853-011-5799-7.

[150] Panaitescu DM, Frone AN, Radovici C, Nicolae C, Perrin FX. Influence of octyl substituted octakis(dimethylsiloxy)octasilsesquioxane on the morphology and thermal and mechanical properties of low density polyethylene. Polym Int 2014;63:228–36. doi:10.1002/pi.4488.

[151] Butola BS, Joshi M, Kumar S. Hybrid organic-inorganic POSS (polyhedral oligomeric silsesquioxane)/polypropylene nanocomposite filaments. Fibers Polym 2010;11:1137–45. doi:10.1007/s12221-010-1137-y.

[152] Geng Z, Huo M, Mu J, Zhang S, Lu Y, Luan J, et al. Ultra low dielectric constant soluble polyhedral oligomeric silsesquioxane (POSS)-poly(aryl ether ketone) nanocomposites with excellent thermal and mechanical properties. J Mater Chem C 2014;2:1094–103. doi:10.1039/c3tc31557f.

[153] Lee E-S, Lei D, Devarayan K, Kim B-S. High strength poly(vinyl alcohol)/poly(acrylic acid) cross-linked nanofibrous hybrid composites incorporating nanohybrid POSS. Compos Sci Technol 2015;110:111–7. doi:10.1016/j.compscitech.2015.02.001.

[154] Yang G, Xue Z, Zhuang Q, Liu X, Zhang K, Han Z. Hybrid organic–inorganic nanocomposite: Fluorinated poly-(2,5-thienylbenzobisoxazole)/POSS and its properties. Synth Met 2013;175:112–9. doi:10.1016/j.synthmet.2013.05.006.

[155] Li Z, Yang R. Flame retardancy, thermal and mechanical properties of sulfonate-containing polyhedral oligomeric silsesquioxane (S-POSS)/polycarbonate composites. Polym Degrad Stab 2015;116:81–7. doi:10.1016/j.polymdegradstab.2015.03.023.

[156] Ding Y, Chen G, Song J, Gou Y, Shi J, Jin R, et al. Properties and morphology of supertoughened polyamide 6 hybrid composites. J Appl Polym Sci 2012;126:194–204. doi:10.1002/app.36624.

[157] Milliman HW, Sánchez-Soto M, Arostegui A, Schiraldi DA. Structure-property evaluation of trisilanolphenyl POSS®/polysulfone composites as a guide to POSS melt blending. J Appl Polym Sci 2012;125:2914–9. doi:10.1002/app.36229.

[158] Svetlichnyi VM, Romashkova KA, Subbotina LI, Yudin VE, Popova E V., Gofman I V., et al. Nanocomposites based on polyamidoimide and octahedral silsesquioxanes. Russ J Appl Chem 2013;86:415–22. doi:10.1134/S107042721303021X.

[159] Sirin H, Turan D, Ozkoc G, Gurdag S. POSS reinforced PET based composite fibers: "Effect of POSS type and loading level." Compos Part B Eng 2013;53:395–403. doi:10.1016/j.compositesb.2013.05.033.

[160] Lim S-K, Hong E-P, Choi HJ, Chin I-J. Polyhedral oligomeric silsesquioxane and polyethylene nanocomposites and their physical characteristics. J Ind Eng Chem 2010;16:189–92. doi:10.1016/j.jiec.2010.01.049.

[161] Fina A, Tabuani D, Camino G. Polypropylene–polysilsesquioxane blends. Eur Polym J 2010;46:14–23. doi:10.1016/j.eurpolymj.2009.07.019.

[162] Kopesky ET, McKinley GH, Cohen RE. Toughened poly(methyl methacrylate) nanocomposites by incorporating polyhedral oligomeric silsesquioxanes. Polymer (Guildf) 2006;47:299–309. doi:10.1016/j.polymer.2005.10.143.

[163] Fu J, Shi L, Chen Y, Yuan S, Wu J, Liang X, et al. Epoxy nanocomposites containing mercaptopropyl polyhedral oligomeric silsesquioxane: Morphology, thermal properties, and toughening mechanism. J Appl Polym Sci 2008;109:340–9.

doi:10.1002/app.27917.

[164] Zeng J. Reinforcement of Poly(ethylene terephthalate) Fibers with Polyhedral Oligomeric Silsesquioxanes (POSS). High Perform Polym 2005;17:403–24. doi:10.1177/0954008305055562.

[165] Zeng F, Liu Y, Sun Y, Hu E, Zhou Y. Nanoindentation, nanoscratch, and nanotensile testing of poly(vinylidene fluoride)-polyhedral oligomeric silsesquioxane nanocomposites. J Polym Sci Part B Polym Phys 2012;50:1597–611. doi:10.1002/polb.23159.

[166] Fina A, Tabuani D, Peijs T, Camino G. POSS grafting on PPgMA by one-step reactive blending. Polymer (Guildf) 2009;50:218–26. doi:10.1016/j.polymer.2008.11.002.

[167] Dorigato A, Pegoretti A, Migliaresi C. Physical properties of polyhedral oligomeric silsesquioxanes-cycloolefin copolymer nanocomposites. J Appl Polym Sci 2009;114:2270–9. doi:10.1002/app.30593.

[168] Wang X, Xuan S, Song L, Yang H, Lu H, Hu Y. Synergistic Effect of POSS on Mechanical Properties, Flammability, and Thermal Degradation of Intumescent Flame Retardant Polylactide Composites. J Macromol Sci Part B 2012;51:255–68. doi:10.1080/00222348.2011.585334.

[169] Jeon HG, Mather PT, Haddad TS. Shape memory and nanostructure in poly (norbornyl-POSS) copolymers. Polym Int 2000;457:453–7. doi:10.1002/(SICI)1097-0126(200005)49:5<453::AID-PI332>3.0.CO;2-H.

[170] Lee KS, Chang Y-W. Thermal and mechanical properties of poly(ε-caprolactone)/polyhedral oligomeric silsesquioxane nanocomposites. Polym Int 2013;62:64–70. doi:10.1002/pi.4309.

[171] Frone AN, Perrin FX, Radovici C, Panaitescu DM. Influence of branched or un-branched alkyl substitutes of POSS on morphology, thermal and mechanical properties of polyethylene. Compos Part B Eng 2013;50:98–106. doi:10.1016/j.compositesb.2013.01.028.

[172] Irshidat M, Al-Ostaz A, Cheng AH. Correlating Micromorphology and Nanomorphology to High Strain Rate Performance of Nanoparticle Reinforced Polymeric Materials. J Nanomechanics Micromechanics 2012;2:55–64. doi:10.1061/(ASCE)NM.2153-5477.0000045.

[173] Thitsartarn W, Fan X, Sun Y, Yeo JCC, Yuan D, He C. Simultaneous enhancement of strength and toughness of epoxy using POSS-Rubber core–shell nanoparticles. Compos Sci Technol 2015;118:63–71. doi:10.1016/j.compscitech.2015.06.011.

[174] Soong SY, Cohen RE, Boyce MC, Mulliken AD. Rate-dependent deformation behavior of POSS-filled and plasticized poly(vinyl chloride). Macromolecules 2006;39:2900–8. doi:10.1021/ma052736s.

[175] Deschanel S, Boyce MC, Cohen RE. Rate Dependent Mechanical Performance of Ethylene Methacrylic Acid (EMAA) Copolymers and POSS-enhanced EMAA

Nanocomposites. Polym Prepr 2007:842.

[176] Mya KY, Wang Y, Shen L, Xu J, Wu Y, Lu X, et al. Star-like polyurethane hybrids with functional cubic silsesquioxanes: Preparation, morphology, and thermomechanical properties. J Polym Sci Part A Polym Chem 2009;47:4602–16. doi:10.1002/pola.23512.

[177] Misra R, Alidedeoglu AH, Jarrett WL, Morgan SE. Molecular miscibility and chain dynamics in POSS/polystyrene blends: Control of POSS preferential dispersion states. Polymer (Guildf) 2009;50:2906–18. doi:10.1016/j.polymer.2009.03.057.

[178] Fan H, Yang R, Li X. Organic/inorganic hybrid epoxy nanocomposites based on octa(aminophenyl)silsesquioxane. Chinese J Polym Sci 2012;31:148–58. doi:10.1007/s10118-013-1196-9.

[179] Araki H, Naka K. Syntheses of dumbbell-shaped trifluoropropyl-substituted POSS derivatives linked by simple aliphatic chains and their optical transparent thermoplastic films. Macromolecules 2011;44:6039–45. doi:10.1021/ma2008095.

[180] Ganesh VA, Nair a. S, Raut HK, Yuan Tan TT, He C, Ramakrishna S, et al. Superhydrophobic fluorinated POSS–PVDF-HFP nanocomposite coating on glass by electrospinning. J Mater Chem 2012;22:18479. doi:10.1039/c2jm33088a.

[181] Iwamura T, Adachi K, Sakaguchi M, Chujo Y. Synthesis of organic-inorganic polymer hybrids from poly(vinyl chloride) and polyhedral oligomeric silsesquioxane via CH/?? interaction. Prog Org Coatings 2009;64:124–7. doi:10.1016/j.porgcoat.2008.08.035.

[182] Zubrowska A, Piorkowska E, Kowalewska A, Cichorek M. Novel blends of polylactide with ethylene glycol derivatives of POSS. Colloid Polym Sci 2014;293:23–33. doi:10.1007/s00396-014-3344-3.

[183] Iacono ST, Budy SM, Mabry JM, Smith Jr DW. Synthesis, characterization, and surface morphology of pendant polyhedral oligomeric silsesquioxane perfluorocyclobutyl aryl ether copolymers. Macromolecules 2007;40:9517–22. doi:10.1021/ma071732f.

[184] Amerio E, Sangermano M, Colucci G, Malucelli G, Messori M, Taurino R, et al. UV Curing of Organic-Inorganic Hybrid Coatings Containing Polyhedral Oligomeric Silsesquioxane Blocks. Macromol Mater Eng 2008;293:700–7. doi:10.1002/mame.200800080.

[185] Cheng C-C, Liao H-W, Chen J-K, Lee D-J, Xin Z. New transparent poly(L-lactide acid) films as high-performance bio-based nanocomposites. RSC Adv 2016;6:23949–55. doi:10.1039/C6RA03937E.

[186] Misra RDK, Yuan Q, Venkatsurya PKC. Mechanics of nanoscale surface deformation in polypropylene-clay nanocomposite. Mech Mater 2012;45:103–16. doi:10.1016/j.mechmat.2011.10.006.

[187] Lee a, Lichtenhan J. Viscoelastic Responses of Polyhedral Oligosilsesquioxane Reinforced Epoxy Systems. Macromolecules 1998;31:4970–4. doi:10.1021/ma9800764.

[188] Yong WF, Kwek KHA, Liao KS, Chung TS. Suppression of aging and plasticization in highly permeable polymers. Polym (United Kingdom) 2015;77:377–86. doi:10.1016/j.polymer.2015.09.075.

[189] Hybrid Plastics®: Nanostructured® POSS® Chemicals n.d. http://www.hybridplastics.com/products/catalog.htm (accessed November 23, 2016).

[190] Guo Z, Kim H, Park Y, Hahn HT, Saotome T. TRANSPARENT STRUCTURAL COMPOSITES FOR SPACE APPLICATIONS n.d.:1–5.

[191] Aldousiri B, Dhakal HN, Onuh S, Zhang ZY, Bennett N, Richardson MOW. Effect of layered silicate reinforcement on the structure and mechanical properties of spent polyamide-12 nanocomposites. Compos Part B Eng 2012;43:1363–7. doi:10.1016/j.compositesb.2011.08.005.

[192] collinslabpress n.d. https://equipment.lboro.ac.uk/search/item/189/hydraulic-press.html?q=collins+press (accessed April 6, 2016).

[193] Bragg's Law n.d. http://hyperphysics.phy-astr.gsu.edu/hbase/quantum/bragg.html (accessed November 29, 2013).

[194] X-ray Powder Diffraction (XRD) n.d. http://serc.carleton.edu/research_education/geochemsheets/techniques/XRD.html.

[195] web-ready n.d. https://equipment.lboro.ac.uk/search/item/2083/x-ray-diffraction-system.html?q=bruker+d2 (accessed April 6, 2016).

[196] What is Electron Microscopy? n.d. http://www.jic.ac.uk/microscopy/intro_em.html.

[197] Scanning Electron Microscope n.d. http://www.purdue.edu/rem/rs/sem.htm (accessed November 29, 2013).

[198] Scanning Electron Microscopy (SEM) n.d. http://serc.carleton.edu/research_education/geochemsheets/techniques/SEM.html.

[199] Background information - What is transmission electron microscopy? | MyScope n.d. http://www.ammrf.org.au/myscope/tem/background/.

[200] Schrand a. Polymer sample preparation for electron microscopy. Microsc Microanal 2005;11 Suppl 2:702–3. doi:10.1017/S143192760551064X.

[201] Agilent Technologies. An Introduction to Gel Permeation Chromatography and Size Exclusion Chromatography 2014.

[202] Thermogravimetric T, Family I. Thermogravimetric Analysis (TGA) A Beginner ' s Guide. Analysis n.d.:1–19.

[203] tainstruments2820 n.d. https://equipment.lboro.ac.uk/search/item/210/ta-instruments-2920-modulated-dsc.html?q=mdsc (accessed April 7, 2016).

[204] Thomas LC. Why Modulated DSC? An overview and summary of advantages and disadvantages relative to traditional DSC. TA Instruments 2005;1:1–8.

doi:10.1017/CBO9781107415324.004.

[205] Strabala KW. The Effects of Combined Compression and Aging on the Properties of Glassy Polycarbonate 2009.

[206] Surana R, Pyne A, Rani M, Suryanarayanan R. Measurement of enthalpic relaxation by differential scanning calorimetry - Effect of experimental conditions. Thermochim Acta 2005;433:173–82. doi:10.1016/j.tca.2005.02.014.

[207] Hay JN. The physical ageing of amorphous and crystalline polymers. Pure Appl Chem 1995;67:1855–8. doi:10.1351/pac199567111855.

[208] Cowie J, Ferguson R. Physical aging studies in poly (vinylmethyl ether). I. Enthalpy relaxation as a function of aging temperature. Macromolecules 1989:2307–12. doi:10.1021/ma00195a053.

[209] Spectrophotometer n.d. http://cnx.org/content/m34601/1.1/Picture 1.png (accessed April 7, 2014).

[210] Förster H. UV / VIS Spectroscopy 2004:337–426. doi:10.1007/b94239.

[211] Campbell D, Pethrick RA, White JR. Polymer Characterization: Physical Techniques, 2nd Edition. CRC Press; 2000.

[212] Ultraviolet-Visible (UV-Vis) Spectroscopy | Analytical Chemistry | PharmaXChange.info n.d. http://pharmaxchange.info/press/2011/12/ultraviolet-visible-uv-vis-spectroscopy-principle/ (accessed March 14, 2014).

[213] cmperkinelmerlambda35uv_visspectrometer n.d. https://equipment.lboro.ac.uk/search/item/577/perkin-elmer-lambda-35.html?q=uv-vis (accessed April 6, 2016).

[214] Wang L, Kamal M, Rey A. Light transmission and haze of polyethylene blown thin films. Polym Eng Sci 2001;41.

[215] National A, Occupational S, Eye EP, Devices FP. American National Standard Occupational and Educational Personal Eye and Face 2014:1–67.

[216] Nakai K, Yokoyama T. Uniaxial Compressive Response and Constitutive Modeling of Selected Polymers Over a Wide Range of Strain Rates. J Dyn Behav Mater 2015;1:15–27. doi:10.1007/s40870-015-0003-9.

[217] Hughes F, Prudom A, Swallowe G. The high strain-rate behaviour of three molecular weights of polyethylene examined with a magnesium alloy split-Hopkinson pressure bar . n.d.;44.

[218] Bucknall CB, Sims B, Mk B. Cavitation of Rubber Particles Dispersed in a Rigid Polymer Matrix n.d.

[219] Milliman H. Structure–property evaluation of trisilanolphenyl POSS®/polysulfone composites as a guide to POSS melt blending. J Appl … 2012;125:2914–9. doi:10.1002/app.

[220] Prządka D, Jęczalik J, Andrzejewska E, Marciniec B, Dutkiewicz M, Szłapka M. Novel hybrid polyurethane/POSS materials via bulk polymerization. React Funct Polym 2013;73:114–21. doi:10.1016/j.reactfunctpolym.2012.09.006.

[221] Jansen JA. Fractographic Characterisation Of Polycarbonate Failure Modes 2004.

[222] Fan JT, Weerheijm J, Sluys LJ. Dynamic compressive mechanical response of a soft polymer material. Mater Des 2015;79:73–85. doi:10.1016/j.matdes.2015.04.035.

[223] Thomas S, Rouxel D, Ponnamma D, editors. Spectroscopy of polymer nanocomposites. 2016.

[224] Boundless. Specific Heat and Heat Capacity 2016. https://www.boundless.com/chemistry/textbooks/boundless-chemistry-textbook/thermochemistry-6/calorimetry-60/specific-heat-and-heat-capacity-282-1442/ (accessed May 11, 2016).

[225] Differential Scanning Calorimetry (DSC) theory | Particle Analytical n.d. http://particle.dk/methods-analytical-laboratory/dsc-differential-scanning-calorimetry/dsc-theory/ (accessed May 11, 2016).

[226] K.P.Menard. Dynamic Mechanical Analysis: A Practical Introduction. CRC Press; 1999.

[227] Mulliken AD, Boyce MC. Mechanics of the rate-dependent elastic–plastic deformation of glassy polymers from low to high strain rates. Int J Solids Struct 2006;43:1331–56. doi:10.1016/j.ijsolstr.2005.04.016.

[228] Paton CA, Hashemi S. Plane-stress essential work of ductile fracture for polycarbonate. J Mater Sci 1992;27:2279–90. doi:10.1007/BF01105033.

[229] Odegard GM, Bandyopadhyay A. Physical aging of epoxy polymers and their composites. J Polym Sci Part B Polym Phys 2011;49:1695–716. doi:10.1002/polb.22384.

Appendix

An investigation into the differences between polycarbonate grades

Three polycarbonate grades under different names but reported to be of the same grade were used in this project. The grades will be referred to as PC1, PC2 and PC3 from this point forward.

It was found that the PC2 control had better tensile properties than the original polycarbonate grade, PC1. However, the DMA results of PC2 differed from the PC1 based samples and so PC1 was again used to synthesise nanocomposites samples. Once the PC1 was finished, PC3 was used instead as PC1 was no longer available to purchase. PC3/TSP-POSS nanocomposites were used in the remainder of the research including UV-Vis, physical aging and SHPB testing, as well as re-testing morphological, tensile and viscoelastic properties. It was again found that the viscoelastic and tensile properties of PC3/TSP-POSS nanocomposites differed to the PC1 and PC2 nanocomposites. The results presented in this thesis are from nanocomposites created using PC3, as a complete set of results from all characterisation and experimental techniques have been gathered for this grade.

An investigation was carried out to determine the reason for the differences between the three polycarbonate grades. This involved using techniques such as gel permeation chromatography (GPC) to measure the molecular weight of the polycarbonate grades, thermogravimetric analysis (TGA) to identify the presence of any additional constituents in the polymers such as plasticisers etc. and the measurement of the melt flow index (MFI) to compare the flow properties of the polycarbonate grades.

Overall, PC3 has the best balance of viscoelastic properties and performs consistently over the three DMA experiments. The T_g of PC3 is most affected by the addition of POSS where it decreases. This could be because it has the highest T_g out of all PC grades tested as measured from the *tanδ* peak. The storage modulus is retained over the glass transition and when subjected to increasing frequencies. The viscoelastic properties of PC1 are relatively unaffected although the storage modulus decreases with the addition of TSP-POSS over the glass transition. The addition of TSP-POSS actually decreases the storage modulus of PC1 and decreases its energy dissipation capabilities. The addition of TSP-POSS to PC2 did not produce any noteworthy effects.

The investigation did not determine, however, what could have caused the differences between nanocomposites synthesised from different polycarbonate grades as in the end, after all processing had taken place, there was little difference between the molecular weight, thermal degradation behaviour and melt flow index values of the compression moulded samples (see figures 84-85 and table 12).

It was found that the time between DMA calibration and testing varied between polycarbonate grades. This could explain the differences between the polycarbonate grades and could mean that the DMA results of PC1- and PC2-based nanocomposites are less accurate than those made from PC3.

The investigation did reveal, however, that there is some polymer degradation occurring during the processing of all polycarbonate grades. This is shown by the difference in derivative weight (see figure 85) between the resin samples and the compression moulded samples; the derivative weight decreases during processing suggesting that something that was present in the polycarbonate resins, such as a plasticiser, has degraded or been removed or simply that the polymer has degraded. However, the molecular weight of the all the polymer grades is the same pre- and post-testing, as shown by figure 84, which contains the results from the GPC experiments. The peak between roughly *logM* = 4 and 5 represents the polymer molecular weight and it can be seen that this is identical for all polycarbonate grades and does not change during processing. The peaks at the lower *logM* values represent smaller molecules e.g. plasticisers, and it is clear that these change in shape and intensity during processing. The samples had a slight yellow tint which was more noticeable as the sample thickness increased. This could be due moisture present in the samples which undergo hydrolysis at the high processing temperatures. Hydrolysis can have a detrimental effect on the final properties of the nanocomposite samples and may go towards explaining some of the anomalous results found in the research. It could also be due to some degradation of additional molecules such as plasticisers. Zhao and Schiraldi also synthesised TSP-POSS/polycarbonate nanocomposites and found that the samples had a slight yellow tint after compression moulding. Moreover, they stated that different polycarbonate grades can contain proprietary additives which could subtly alter the interactions between the polymer and POSS. Perhaps this is what occurred in our research.

a

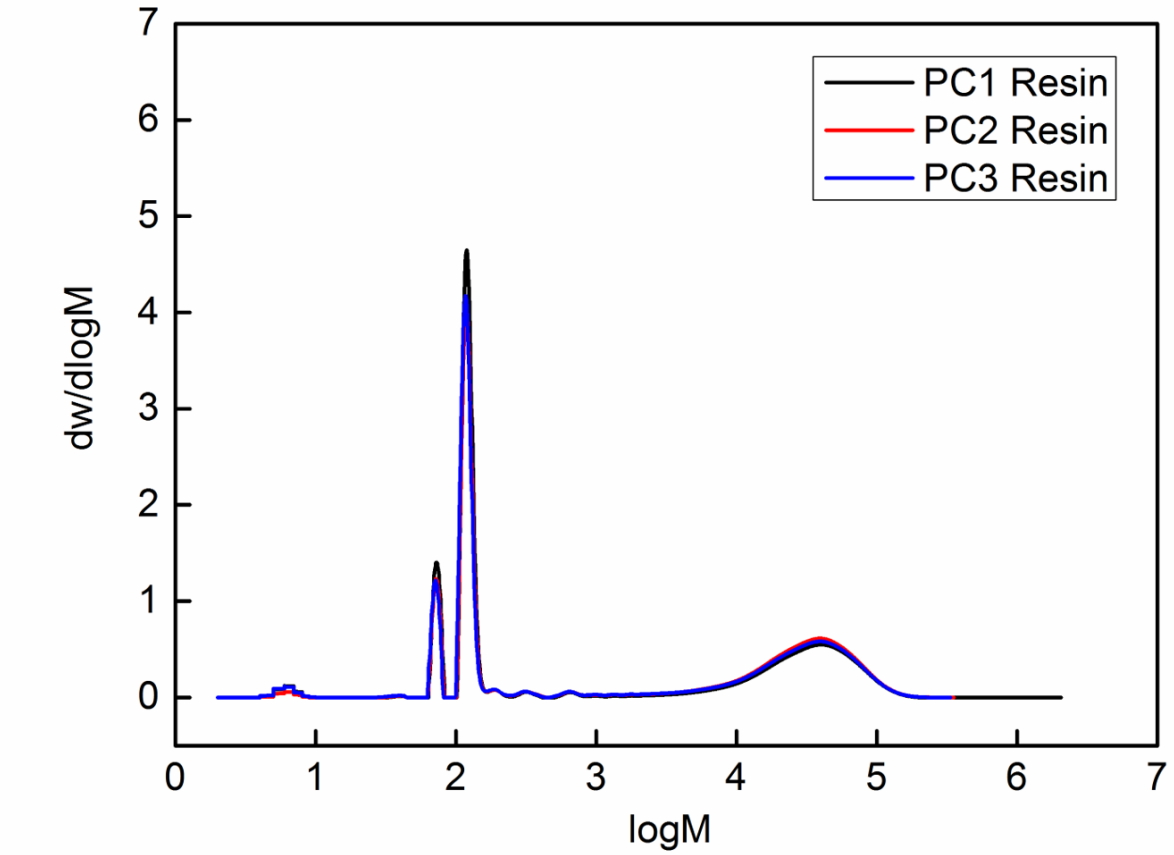
PC1 Resin
PC2 Resin
PC3 Resin
dw/dlogM
logM
0
1
2
3
4
5
6
7

b

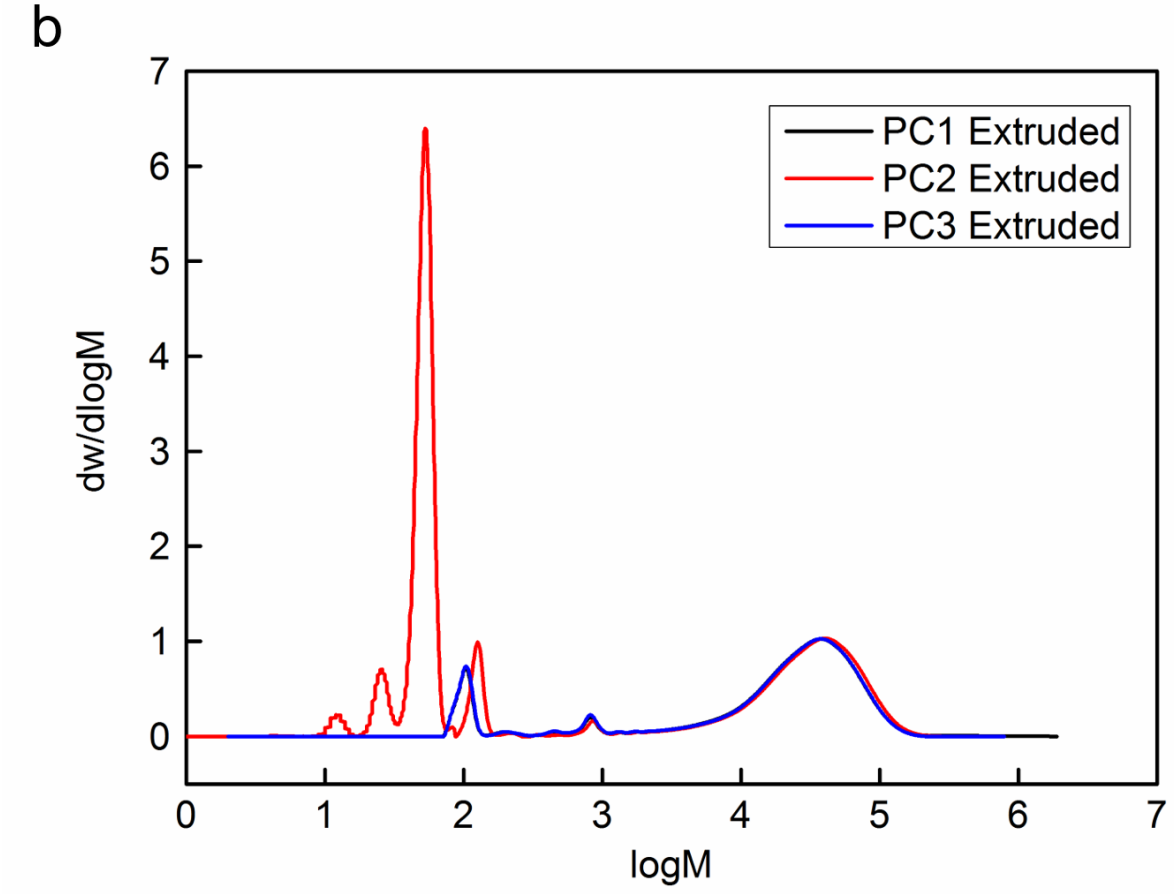
PC1 Extruded
PC2 Extruded
PC3 Extruded
dw/dlogM
logM
0
1
2
3
4
5
6
7

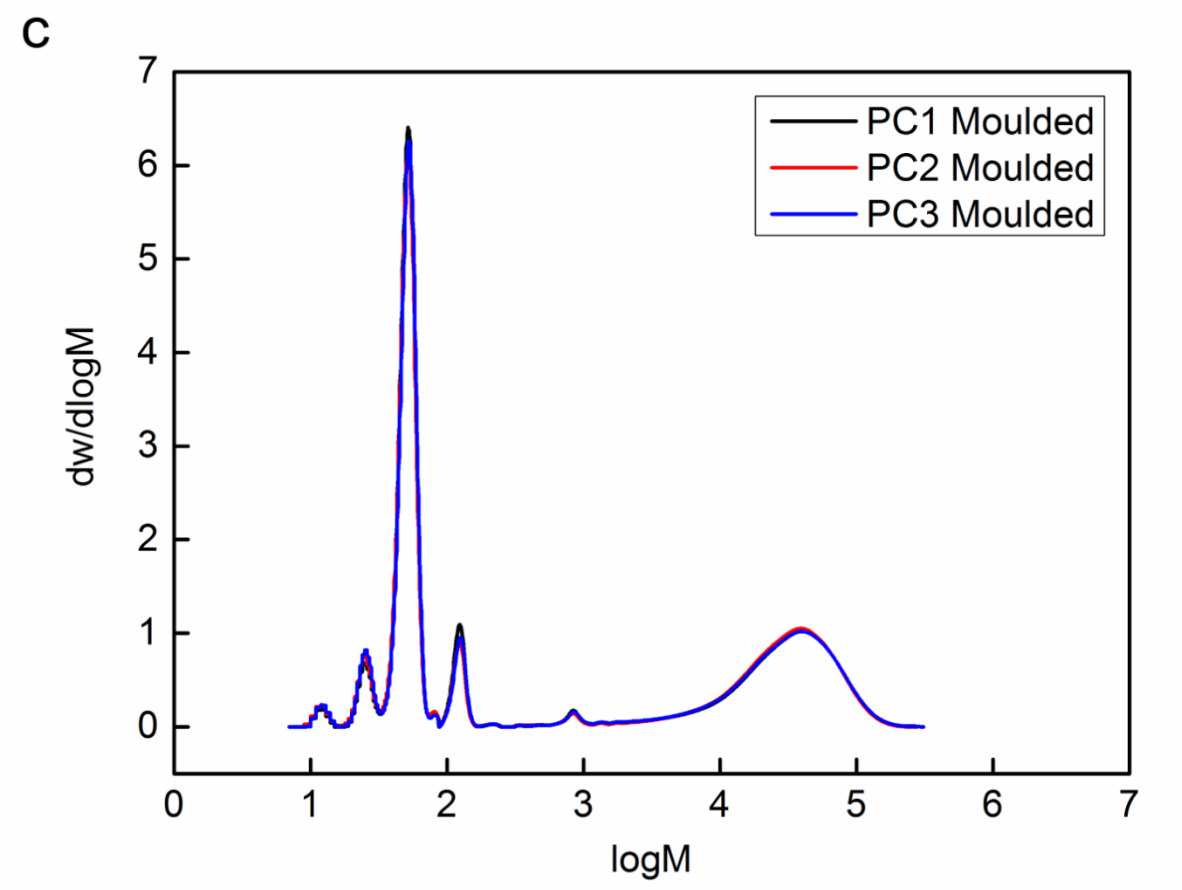

Figure 84 Graphs of dw/dlogM against logM for a) PC1, b) PC2 and c) PC3 in resin, extruded and moulded form obtained from GPC data

a

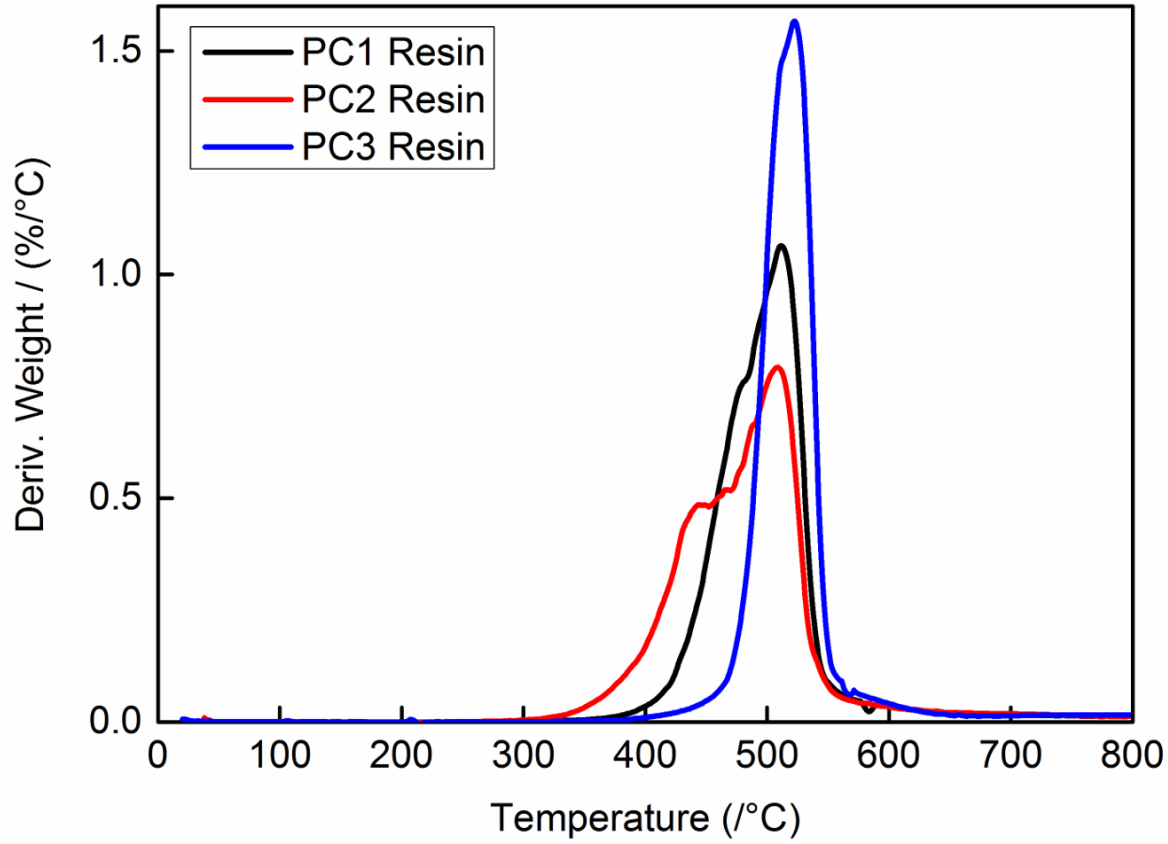
PC1 Resin
PC2 Resin
PC3 Resin
Deriv. Weight / (%/°C)
Temperature (/°C)
0.0
0.5
1.0
1.5
0
100
200
300
400
500
600
700
800

b

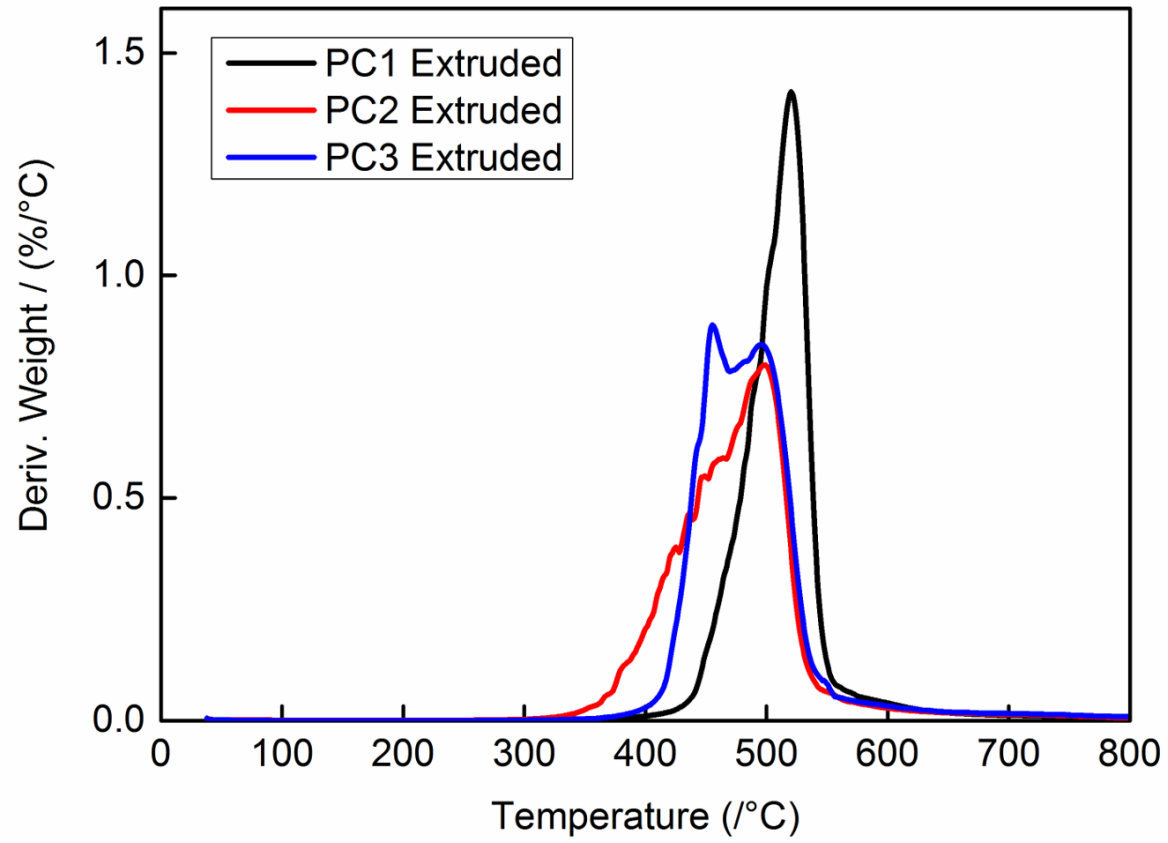
PC1 Extruded
PC2 Extruded
PC3 Extruded
Deriv. Weight / (%/°C)
Temperature (/°C)
0.0
0.5
1.0
1.5
0
100
200
300
400
500
600
700
800

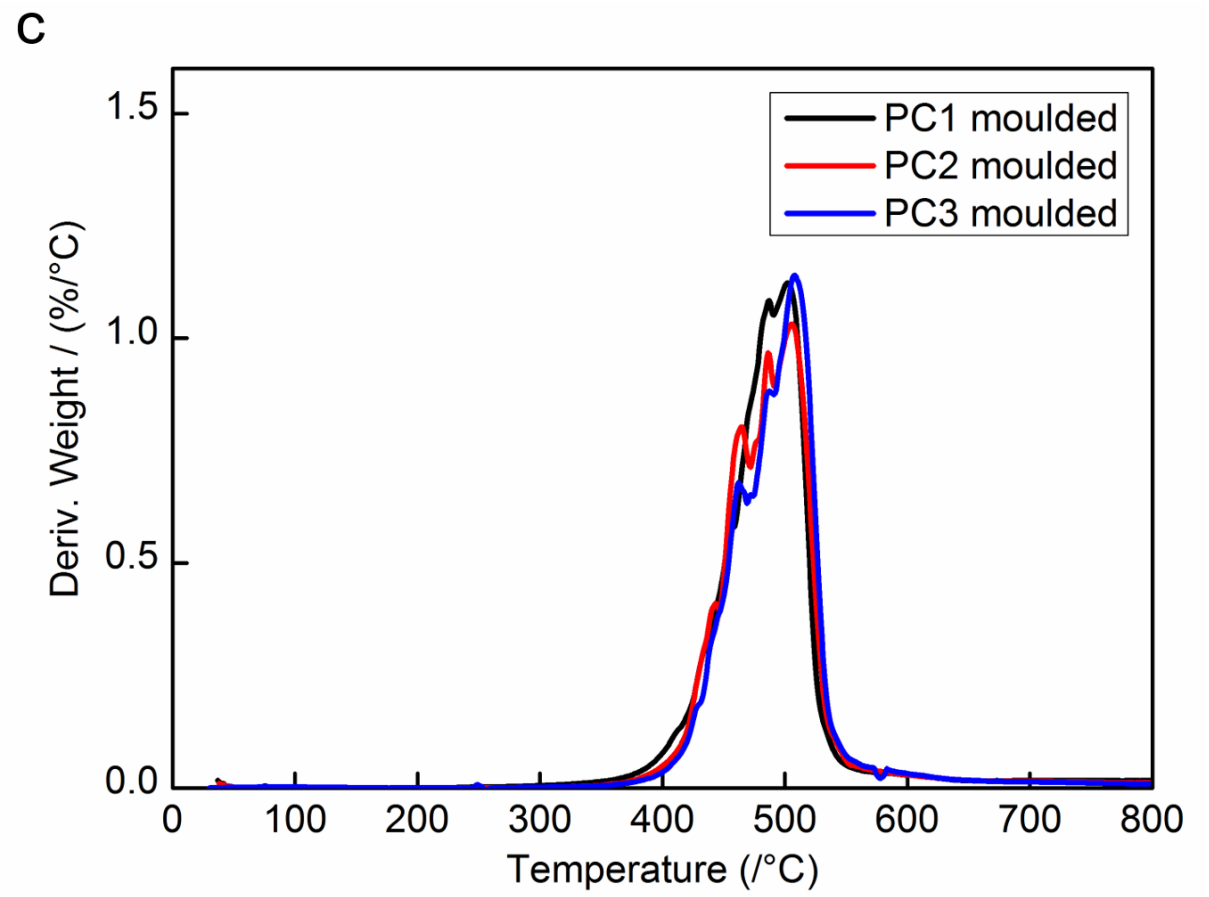

Figure 85 Derivative weight curves of the three polycarbonate grades in a) resin and b) extruded, c) moulded form obtained from TGA analysis

PC Grade	Melt Flow Rate (g/10min)
PC3	36.110
PC1	30.379
PC2	34.912

Table 12 MFI values of the three polycarbonate grades